



HAL
open science

Study of dehydrogenation properties of metallic borohydrides for hydrogen storage

Parviz Hajiyev

► **To cite this version:**

Parviz Hajiyev. Study of dehydrogenation properties of metallic borohydrides for hydrogen storage. Materials Science [cond-mat.mtrl-sci]. Université Grenoble Alpes [2020-..], 2020. English. NNT : 2020GRALY003 . tel-02939130

HAL Id: tel-02939130

<https://theses.hal.science/tel-02939130>

Submitted on 15 Sep 2020

HAL is a multi-disciplinary open access archive for the deposit and dissemination of scientific research documents, whether they are published or not. The documents may come from teaching and research institutions in France or abroad, or from public or private research centers.

L'archive ouverte pluridisciplinaire **HAL**, est destinée au dépôt et à la diffusion de documents scientifiques de niveau recherche, publiés ou non, émanant des établissements d'enseignement et de recherche français ou étrangers, des laboratoires publics ou privés.

THÈSE

Pour obtenir le grade de

DOCTEUR DE L'UNIVERSITE GRENOBLE ALPES

Spécialité : **Physique des Matériaux**

Arrêté ministériel : 25 mai 2016

Présentée par

« Parviz HAJIYEV »

Thèse dirigée par **François RIEUTORD**, Directeur de Recherche, **Institut de recherche interdisciplinaire de Grenoble (IRIG-CEA)**, et codirigée par **Vasile IOSUB**, Ingénieur de Recherche, **Laboratoire d'Innovation pour les Technologies des Energies Nouvelles (LITEN - CEA)**

préparée au sein du **Laboratoire d'Innovation pour les Technologies des Energies Nouvelles (LITEN - CEA)** dans l'**Ecole Doctorale de Physique - GRENOBLE**

Etude des propriétés de déshydrogénation des borohydrures métalliques pour le stockage de l'hydrogène

Thèse soutenue publiquement le « **22 Janvier 2020** », devant le jury composé de :

M. Olivier ISNARD

Professeur, Directeur de l'Ecole Doctorale de Physique de Grenoble, Président

M. Yaroslav FILINCHUK

Professeur, Institute of Condensed Matter and Nanosciences (IMCN) Université Catholique de Louvain (UCL), Rapporteur

M. Umit DEMIRCI

Professeur, Département de Chimie de l'Université de Montpellier, Rapporteur

M. Michel LATROCHE

Directeur de Recherche, l'Institut de Chimie et des Matériaux Paris-Est (CNRS), Membre

M. Michel BARDET

Directeur de Recherche, Institut de recherche interdisciplinaire de Grenoble (IRIG-CEA), Membre



"You are not a drop in the ocean, you are the entire ocean in a drop"

Mevlana Rumi

"Science without religion is lame, religion without science is blind."

Albert Einstein

"Any sufficiently advanced technology is indistinguishable from magic."

Arthur C. Clarke

I dedicate this thesis work to my family who supported me unconditionally in every step of my life.

Bu tezis işini həyatımın hər addımında məni sonuna qədər şərtsiz bir şəkildə dəstəkləyən ailəmə həsr edirəm.

Acknowledgements

This thesis project was a test of my physiological endurance more than my technical competences and knowledge of science. Maybe that is what a PhD supposed to be.

I didn't have that romanticized mentor-student relationship during my thesis but I didn't succeed in this endeavor solely on my own. Sometimes the best help one can give you is a boost of motivation. My supervisors almost at every opportunity expressed their confidence in my ability to carry the task. According to my peers, most PhD students are not as lucky. So in hindsight, the persistent positive encouragement of my supervisors was the key to my success.

I'd like to thank to my thesis director Francois Rieutord for enabling the smooth continuation of my activities however he can, guiding me to the right expert and the equipment whenever my research activities arrived at an impasse.

I am grateful to Michel Bardet for his always friendly and accommodating approach to my problems, for teaching me how to use solid state NMR which without it the quality of my scientific arguments and the success of this thesis work would have been questionable.

I shared the same office for three years with my supervisor Vasile Iosub, a luxury most PhD students don't have. I thank him for tolerating my spontaneous interruptions regardless whether the topic of the question was scientific, personal or anything in between. I express my gratitude for his patience and willingness to solve my problems. I think number one priority of scientists is to preserve their child-like curiosity for topics and issues outside of their field of expertise. So I thank Vasile for not shying away from my lunch-time discussion topics, continuing to teach, listen and challenge my views in a very productive manner and more importantly I thank him for being a friend.

I'd like to thank to Philippe Capron for giving me all the resources and the freedom to perform my research activities, for taking special interest in my progress and doing everything in his capacity to remove the barriers impeding my activities. Above everything else, during the times of uncertainty, I found his support and assurances were an important much-needed boost of motivation. I get to enjoy continuing my activities here in LITEN after my PhD. Many colleagues and friends expressed the rarity of this opportunity. So I am thankful to Philippe for giving me this valuable opportunity as well.

Majority of my difficulties during my research activities in the lab were small, forgettable and not easily definable. I am very grateful for energetic and helpful support of my colleagues Isabelle Rougeaux and Jerome Delmas for swiftly overcoming most of these difficulties.

I am convinced that a healthy psychology is the most important factor for a successful completion of a thesis work. This wouldn't have been possible without my like-minded friends and most importantly without my girlfriend who constantly radiated with positive energy and made my life both inside and outside CEA a beautiful memory.

Acknowledgements	3
Abstract	7
Résumé	9
Abbreviations	11
I. State of the art	13
I.1. Introduction	13
I.2. Hydrogen economy	13
I.2.1. Bigger Picture	15
I.3. Physical hydrogen storage	16
I.3.1. Compressed hydrogen	16
I.3.2. Liquefied hydrogen	16
I.3.3. Hydrogen in porous compound	17
I.4. Chemical hydrogen storage	17
I.4.1. Hydrogen containing gases	18
I.4.2. Liquid organic hydrogen carriers	19
I.4.3. Solid-state hydrogen storage	19
I.4.3.1. Metal hydrides	19
I.4.3.2. Complex hydrides	21
I.4.3.3. Metal amides	21
I.4.3.4. Ammonia Borane	21
I.4.3.5. Metal amidoboranes	24
I.4.3.6. Metal borohydrides	25
I.4.3.7. Metal borohydride derivatives	28
I.4.3.8. Composite Reactive hydrides	31
I.4.3.9. Hydrolysis	32
I.4.3.10. Direct hydrogenation catalysts	33
I.4.3.11. Frustrated Lewis Pairs	34
I.5. Conclusion	35
II. Methodology	38
II.1. Crystallographic analysis	38
II.1.1. Powder X-ray diffraction	39
II.2. Thermodynamic analysis	40
II.2.1. Differential Scanning Calorimetry - Thermogravimetry	40

II.2.2.	Sievert type volumetry.....	40
II.3.	Spectroscopic analysis	41
II.3.1.	Mass Spectrometry.....	42
II.3.2.	Raman and Infra-red Spectroscopy	42
II.3.3.	Nuclear Magnetic Resonance Spectroscopy	43
II.4.	Synthesis process	45
II.4.1.	Ball-milling.....	45
II.4.2.	Review of mechanochemical synthesis of metal borohydrides.....	47
II.4.3.	Review of solvothermal synthesis of metal borohydrides.....	48
II.4.4.	Solvothermal synthesis equipment.....	55
III.	Synthesis and characterization of ammine zinc borohydrides.....	60
III.1.	Objective.....	60
III.2.	Literature review on synthesis of zinc borohydride solvates.....	60
III.3.	Road to scalable synthesis	62
III.3.1.	Synthesis procedure.....	64
III.4.	Experimental results	65
III.4.1.	Crystallographic analysis.....	65
III.4.2.	Thermodynamic analysis.....	66
III.4.3.	Spectroscopic analysis	70
III.5.	Discussion of results	74
III.6.	Conclusions	81
III.7.	Appendix.....	82
IV.	Optimizing hydrogen storage capacity of Zn-B-N-H compounds.....	95
IV.1.	Objective.....	95
IV.2.	Ammonium metal borohydrides.....	95
IV.2.1.	Ammonium Zinc borohydride	95
IV.2.1.1.	Crystallographic analysis.....	96
IV.2.1.2.	Raman analysis	97
IV.2.1.3.	Thermodynamic analysis.....	98
IV.2.2.	Overview of ammonium metal borohydrides	101
IV.3.	Ammonia borane destabilization	103
IV.4.	Ammine zinc borohydride – Ammonia borane complex.....	107
IV.4.1.	Metal Amidoboranes	112

IV.4.2.	Zinc amidoborane.....	113
IV.5.	Hydrogen storage capacity of Zn-B-N-H system.....	115
IV.6.	Conclusions.....	118
IV.7.	Appendix.....	119
V.	Mg-B-N-H system and exploration of reversibility.....	122
V.1.	Drawback of Zn-B-N-H system as practical hydrogen storage system	122
V.2.	Objective.....	123
V.3.	Synthesis of Mg-B-N-H compounds	123
V.4.	Hydrogen storage properties of Mg-B-N-H system	131
V.5.	Regeneration of spent $M(\text{BNH}_x)_m$ fuel	134
V.5.1.	Direct hydrogenation of $M(\text{BNH}_x)_m$	135
V.5.2.	Metal recovery from $M(\text{BNH}_x)_m$	136
V.5.3.	Full regeneration of $\text{Mg}(\text{BNH}_x)_2$	137
V.5.3.1.	B-N bond cleavage	137
V.5.3.2.	B-F bond reduction.....	139
V.6.	Conclusion.....	143
V.7.	Appendix.....	145
VI.	General Conclusions and Perspectives	150
VII.	Résumé détaillé des chapitres	153
VII.1.	Chapitre I - L'état de l'art	153
VII.2.	Chapitre II - Méthodologie.....	155
VII.3.	Chapitre III - Synthèse et caractérisation de borohydrures d'amines de zinc	155
VII.4.	Chapitre IV - Optimiser la capacité d'hydrogène des composés Zn-B-N-H.....	156
VII.5.	Chapitre V - Système Mg-B-N-H et exploration de la réversibilité	156
References.....		159

Abstract

This thesis work is dedicated to the exploration of metal borohydride compounds and their derivatives as a family of materials that can potentially enable solid-state storage of hydrogen, with high gravimetric capacity (>10wt%) and moderate desorption temperatures (<150°C). The candidate materials are ammine metal borohydrides, $A_xM(BH_4)_{m+x}(NH_3)_n$ where A is alkali metal, M any other metal (for example Zn, Al, Mg), m is the oxidation state of M, n is the number of neutral ammonia adducts and $x=0-2$. These materials contain positively ($N-H^{\delta+}$) and negatively ($B-H^{\delta-}$) charged hydrogens in their structure, upon heating the electrostatic attraction between these oppositely charged hydrogens, their combination and release as a hydrogen molecule is the main dehydrogenation process. The major challenges preventing the application of these materials are the lack of straight-forward synthesis process to obtain desired composition, precise control of dehydrogenation properties based on the chemical formula and the rehydrogenation of spent fuel.

High electronegativity metal borohydrides are stabilized by combining them with alkali metal borohydrides. By adhering to the same logic, we explored the potential of ammonium cation $[NH_4]^+$ as pseudo-alkali cation that can also participate in decomposition of $Zn(BH_4)_2$ and increase its theoretical hydrogen capacity. So, we synthesized ammonium zinc borohydride $(NH_4)Zn(BH_4)_3$ for the first time. However, the compound was not stable at room temperature and its thermal decomposition released a lot of diborane and borazine gases.

In literature, the typical synthesis process involves salt metathesis reaction using ball-milling or solvothermal approaches to obtain metal borohydride, followed by exposure to ammonia gas. To bypass this multi-step approach we developed liquid ammonia synthesis process that directly enables the formation of $AZn(BH_4)_3(NH_3)_2$. The technique allowed us to synthesize $LiZn(BH_4)_3(NH_3)_2$ and $KZn(BH_4)_3(NH_3)_2$ for the first time. By combining the known compounds from literature $Zn(BH_4)_2(NH_3)_2$ and $NaZn(BH_4)_3(NH_3)_2$, we obtained a unique set of compounds that have zinc cation sharing its coordination sphere with two borohydride and two ammonia molecules. We determined that monometallic and bimetallic compounds have different dehydrogenation reactions. The presence of an alkali cation with lower polarizing power than zinc cation in the structure is more detrimental to the purity of released hydrogen. Use of zinc chloride precursors results in chloride anion substitution of borohydride sites in $AZn(BH_4)_3(NH_3)_2$ which also increases ammonia impurity. Chloride anion substitution is eliminated by using ZnF_2 precursor which also enables the filtration of the main phase from ammonia insoluble alkali fluoride byproduct. Hydrogen capacity and the purity can be improved by adding ammonia borane (NH_3BH_3). $ZnCl_2-8NaZn(BH_4)_3(NH_3)_2-20NH_3BH_3$ mixture releases 10 wt% pure hydrogen, which is highest performance for Zn-B-N-H system. This performance comes at the cost of thermal stability which lower the dehydrogenation temperature too much making the mixture essentially unstable at room temperature. Therefore, we explored Mg-B-N-H system instead which have higher thermal stability. We observed that magnesium metal (or magnesium

hydride) in liquid ammonia can react with ammonia borane to form magnesium amidoboranes $\text{Mg}(\text{NH}_2\text{BH}_3)_2(\text{NH}_3)_3$ type compounds. This reaction even under 67 bar hydrogen pressure cannot be forced to form borohydride phases. Since magnesium amidoboranes is a type destabilized ammonia borane we continued our efforts for synthesis of $\text{Mg}(\text{BH}_4)_2(\text{NH}_3)_6$ phase. Synthesis of these compounds with MgF_2 precursors were not possible; instead, the reaction of MgH_2 with $\text{L}\cdot\text{BH}_3$ (L = triethylamine) in liquid ammonia was successful. The hydrogen storage properties of amorphous $\text{Li}_2\text{Mg}(\text{BH}_4)_4(\text{NH}_3)_2$ was the most attractive with at least 10 wt% hydrogen capacity and high hydrogen purity.

Résumé

Ce travail de thèse a été consacré à l'exploration des composés à base de borohydrures métalliques et de leurs dérivés en tant que matériaux prometteurs pour le stockage de l'hydrogène à l'état solide, avec des capacités massiques théoriques élevées (> 10 wt%) et des températures de désorption modérées (< 150 °C). Les candidats potentiels sont les borohydrures métalliques complexés avec l'ammoniac, $A_xM(BH_4)_{m+x}(NH_3)_n$ où A – métal alcalin, M tout autre métal (par exemple Zn, Al, Mg), m – le degré d'oxydation de M, n – nombre de molécules d'ammoniac et $x = 0-2$. Ces composés contiennent des atomes d'hydrogène chargés positivement (N-H $^{\delta+}$) et négativement (B-H $^{\delta-}$). Le processus de déshydrogénation est basé principalement sur l'attraction électrostatique entre ces atomes d'hydrogène à charge opposée, leur combinaison et libération sous forme de molécule d'hydrogène.

Les borohydrures métalliques à haute électronégativité sont stabilisés en les combinant avec des cations métalliques alcalins. En suivant la même approche, nous avons exploré le potentiel du cation ammonium $[NH_4]^+$ en tant que cation pseudo-alcalin pouvant également participer à la décomposition du $Zn(BH_4)_2$ et augmenter sa capacité théorique en hydrogène. Nous avons donc synthétisé pour la première fois le borohydrure d'ammonium et de zinc $(NH_4)Zn(BH_4)_3$. Cependant, le composé n'est pas stable à la température ambiante et sa décomposition thermique libère beaucoup de gaz tels que le diborane ou la borazine.

Dans la littérature, le processus de synthèse typique implique une réaction de métathèse de sels utilisant des techniques de broyage à billes ou la méthode solvothermale pour obtenir d'abord le borohydrure métallique, suivi par une exposition à l'ammoniac gazeux. Pour contourner cette approche en plusieurs étapes, nous avons développé un procédé de synthèse d'ammoniac liquide qui permet directement la formation de $AZn(BH_4)_3(NH_3)_2$. La technique nous a permis de synthétiser les composés $LiZn(BH_4)_3(NH_3)_2$ et $KZn(BH_4)_3(NH_3)_2$ pour la première fois. Avec les composés déjà connus, $Zn(BH_4)_2(NH_3)_2$ et $NaZn(BH_4)_3(NH_3)_2$, nous avons obtenu un ensemble unique de composés dont le cation zinc partage sa sphère de coordination avec deux BH_4 et deux NH_3 . Nous avons déterminé ainsi que les composés monométalliques et bimétalliques ont des réactions de déshydrogénation différentes. La présence d'un cation alcalin avec un pouvoir polarisant inférieur à celui du zinc dans la structure nuit davantage à la pureté de l'hydrogène libéré. L'utilisation de précurseurs de chlorure de zinc entraîne la substitution par l'anion chlorure de sites borohydrures dans $AZn(BH_4)_3(NH_3)_2$, ce qui augmente également les impuretés d'ammoniac. La substitution par l'anion chlorure est éliminée en utilisant un précurseur de ZnF_2 qui permet également la filtration de la phase principale à partir du sous-produit de fluorure alcalin, insoluble dans l'ammoniac. La capacité en hydrogène et la pureté peuvent être améliorées en ajoutant du borazane (NH_3BH_3). Le mélange $ZnCl_2-8NaZn(BH_4)_3(NH_3)_2-20NH_3BH_3$ libère 10 wt% d'hydrogène pur, ce qui représente la meilleure performance pour le système Zn-B-N-H.

Nous avons également exploré le système Mg-B-N-H, qui présente une stabilité thermique supérieure. Nous avons observé que le magnésium métallique (ou l'hydruure de magnésium)

dans l'ammoniac liquide peut réagir avec le borazane pour former des composés de type amidoboranes de magnésium $\text{Mg}(\text{NH}_2\text{BH}_3)_2(\text{NH}_3)_3$. Même sous une pression d'hydrogène de 67bar, la formation des phases borohydrure n'a pas été possible. Comme l'amidoborane de magnésium est une sorte de borazane déstabilisé, nous avons poursuivi nos efforts afin de synthétiser le composé $\text{Mg}(\text{BH}_4)_2(\text{NH}_3)_6$. La réaction de MgH_2 avec le $\text{L}\cdot\text{BH}_3$ (L= triéthylamine) dans l'ammoniac liquide a réussi. Parmi ces composés, les propriétés de stockage d'hydrogène de $\text{Li}_2\text{Mg}(\text{BH}_4)_4(\text{NH}_3)_2$ amorphe sont les plus attractives, avec une capacité en hydrogène d'au moins 10 wt% et une pureté élevée.

Abbreviations

RT – room temperature

MB – metal borohydride

AMB – ammine metal borohydride

AB – ammonia borane

XRD – x-ray diffraction

DCS – differential scanning calorimetry

TG – thermogravimetry

TPD – sievert type volumetry

MS – mass spectrometry

IR – infra-red

Et₂O – diethyl ether

THF – tetrahydrofuran

DMS – dimethyl sulfide

TMA – trimethyl amine

TEA – triethyl amine

L – organic solvent, adduct

A – alkali metal

M – any other metal

X – halogen atom

PTFE – Polytetrafluoroethylene (Teflon)



Chapter I

State of the art



I. State of the art

I.1. Introduction

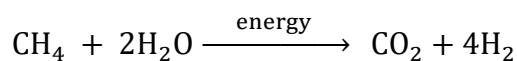
The energy consumption is directly related to global economic disparity since e.g. top 20% of world population consumes more than twice the energy of bottom 80%. It is not a coincidence that gross domestic product of any country correlates with its energy consumption level [1]. Increasing world population and its desire to live a wealthier lifestyle will inevitably increase our energy demand. While the energy needs of the world increase faster and faster, as of 2019, the renewable energy sources account for only 4.5% of global demand, still remaining behind nuclear and hydrothermal sources. The good news is that more than 60% (and increasing) of net new energy addition is from the renewable sources. However this is the primary energy source which means by the time it is treated, distributed, delivered and converted to usable form like electricity or car fuel, the process incurs a lot of efficiency losses [2].

In terms of the cost of electricity generation, the renewable energy generation technologies like solar cells and wind turbines are already cost competitive with conventional fossil fuel sources in many regions of the world. However, the biggest hurdle to their faster adoption is the mismatch between demand and supply of electricity. This problem has been dubbed as ‘the duck curve’ problem, illustrating a rough duck shape due to daily imbalance of peak electricity demand and renewable energy production [3]. Beyond the daily scale these imbalances exist on longer scales such as monthly, seasonal and annual timeframes. The solution is energy storage technologies.

The supercapacitor and battery technologies have matured enough to become economically viable for electromobility and short-term energy storage applications. However, there is a fundamental limitation of how much energy can be stored using these technologies due to their low gravimetric energy capacity. Therefore, for long-term and large-scale energy storage the only options are hydrogen, pumped hydro and compressed air storage (Figure I-1). Among them hydrogen storage is the only one that is not limited by available geographical features (mountains, rivers and deep underground caves) of the country [4].

I.2. Hydrogen economy

The energy released from burning hydrogen gas is 142MJ/kg, the highest of any known fuel. However, hydrogen gas H₂ in its natural state does not exist in nature in large quantities. Hence, it needs to be produced. Therefore, sometimes hydrogen is referred to as an “energy carrier”. Currently, in industrial scale, hydrogen is generated during steam reforming process of methane gas in two steps through formation of syngas which further reacts with water. The general reaction is:



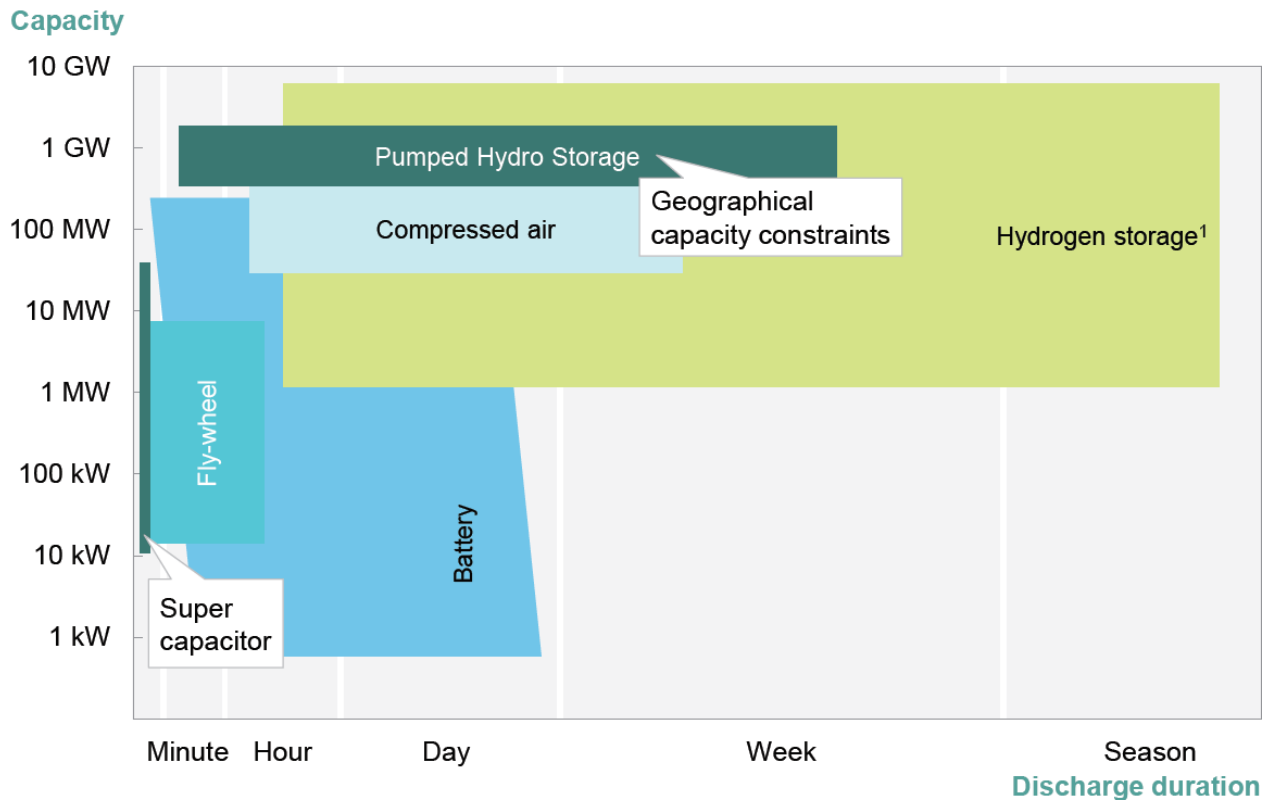
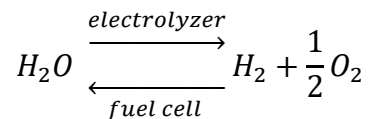


Figure I-1: The energy storage technologies, from ref. [3]

Roughly, 96% of all hydrogen gas currently produced is from fossil fuel sources and most of it is consumed for petrochemical feedstocks. The rest (4%) is produced by electrolysis which is the cleanest and renewable source of hydrogen [5]. The source of electricity must also be clean and renewable for this process to remain sustainable. Thus, combining cheap renewable electricity when it is not needed, the excess electricity can be turned into hydrogen and distributed, stored for use in the future.



Ideally the fuel cell can perform both water splitting and combination reactions. Decades long intensive research on technologies such as alkaline, polymer electrolyte membrane (PEM), solid oxide fuel cell and electrolyzers have enabled commercial companies that can sustain their business activities. However, one major hurdle that prevents global adoption of hydrogen cycle is the storage and the distribution problem.

Although hydrogen gas has the highest gravimetric energy capacity due to its very low density its volumetric energy capacity is not so impressive 0.12MJ/L compared to conventional fuel such as diesel at 38.6 MJ/L [6]. Hence, the need to store hydrogen in denser medium have become very important. Currently, there are two main approaches to alleviate this drawback:

- 1) forcing more and more hydrogen molecules into a fixed volume container or
- 2) storing hydrogen atoms as part of other chemical compounds that can be readily turned into hydrogen gas when needed.

We will distinguish these two approaches as physical and chemical storage of hydrogen.

1.2.1. Bigger Picture

We will introduce the major concepts and the types of storage options in detail in the following sections. However, before these discussions, we can look at the hydrogen cycle on the larger scale. Any excess renewable electricity generated on an unusually sunny or windy day needs to be stored and converted back to electricity when needed for example on a still cloudy day. As a mature energy storage technology, batteries have low energy density however the excess electrical energy is directly stored as chemical energy and converted back to electricity with close to 99.9% efficiency per cycle. On the other hand, despite its potential to be globally scalable energy storage system, the hydrogen cycle is crippled with number of energy conversion steps and their efficiency levels (Figure I-2). These steps include electrolysis, separation, purification, compression, heating, cooling, hydrogenation, dehydrogenation, transportation, combustion etc. Nevertheless, the major advantage of the hydrogen rich fuels compared to batteries is that they can be used either as a hydrogen carrier or directly as carbon neutral fuels (for example: aviation applications).

Direct electrochemical synthesis of hydrogen rich fuels that can be converted back to electricity using corresponding fuel cells is an interesting approach to minimize these conversion steps. Prominent examples would be direct ammonia or alcohol fuel cell (and electrolyzer) technologies [7],[8]. Electrochemical synthesis of ammonia relies on $N_2 + 3 H_2O \rightarrow 2 NH_3 + 3/2 O_2$ reaction while direct ammonia solid oxide fuel cells have already high efficiency demonstration projects.

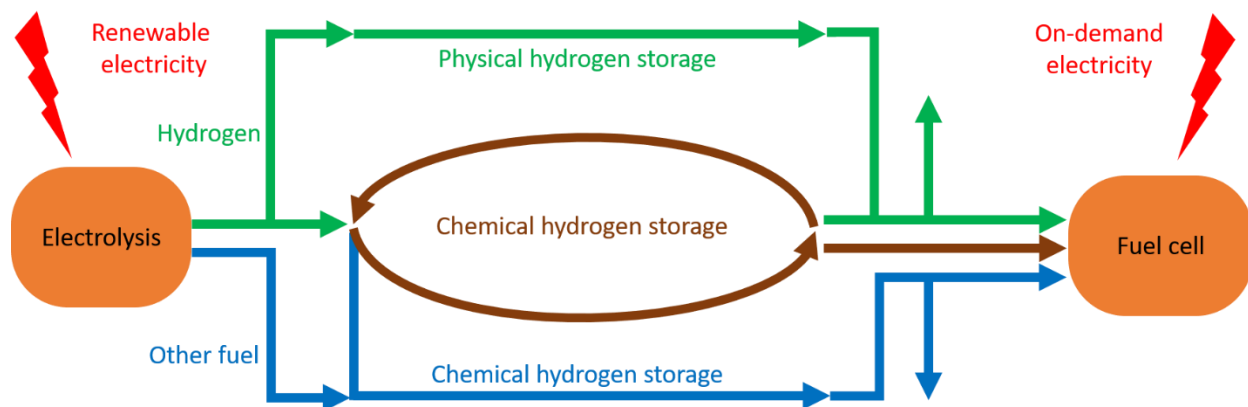


Figure I-2: Global view of various hydrogen storage approaches. Ends of the arrows indicate energy conversion steps. The colours indicate various energy carriers, green – hydrogen, brown – chemical storage by conversion from or to hydrogen, blue – hydrogen rich energy carrier (fuel)

Combined with the ease of storage, the existing distribution and transportation

infrastructure, ammonia is indeed a promising energy carrier [9]. This approach describes hydrogen cycles without the presence of hydrogen gas at any conversion stage.

I.3. Physical hydrogen storage

In physical storage, hydrogen is stored as densely packed hydrogen molecules (H_2). To achieve this, liquefaction and compression of the gas to high pressures are two main techniques that are used.

I.3.1. Compressed hydrogen

Electrolyzers usually produce hydrogen in 30-40bar pressure range without compromising too much their efficiency [10]. Hydrogen is typically compressed using a reciprocating pump which is a flat metal piston that moves back and forth, hence compresses the hydrogen gas into smaller volume. These pumps allow pressure increase up to 350-700 bar [11].

Compressed hydrogen can be stored in steel tanks up to 200 bar, but this system has very low capacity due to heavy weight of the steel container. Better alternative is lighter aluminum tanks which also has lower permeability to hydrogen gas compared to steel. To further increase the storage pressure up to 700 bar, the carbon fiber tanks are utilized with aluminum liner [12]. These tanks are already commercialized in hydrogen passenger cars such as Toyota Mirai. Under these conditions volumetric energy density of hydrogen gas increases up to 5.5MJ/L [13].

When real gases compress, they (usually) experience an increase in temperature. This is due to the fact that unlike simplified model of ideal gases, the real gases are not point particles and they have forces that interact on each other. However, the increase in temperature would only happen if the initial temperature of the compressed gas is above its inversion temperature. For hydrogen, this temperature is $-77\text{ }^\circ\text{C}$. So, compressing the hydrogen to high pressures at room temperature increases its temperature. However, once this high pressure gas is passed through a heat exchanger and cooled down using liquid nitrogen, series of expansions further decrease its temperature until liquefaction is achieved [14].

I.3.2. Liquefied hydrogen

Liquefied hydrogen is mostly developed and used as a rocket propellant. Under 33 K and 13 bar (critical temperature and pressure conditions) hydrogen becomes liquid. However to remain a liquid under 1 atmosphere, it needs to be cooled down to 20 K [15]. Normally, this liquefied hydrogen can be stored in heavily insulated pressurized vessels. Even under the best insulation conditions less than 2% daily boil-off cannot be prevented [16] and requires special storage environment since the flammability limits of hydrogen in air has a very wide range (4% to 75%) under 1 atmosphere [17].

If the spins of two hydrogen nuclei in H_2 molecule are parallel it is referred to as orthohydrogen while if the spins are antiparallel it is known as parahydrogen. At room temperature hydrogen gas is mostly in orthohydrogen state. However, when liquefied, these orthohydrogen molecules slowly undergo an exothermal transition and turn into parahydrogen molecules. This transition generates heat and speeds up the boil-off process

in liquefied hydrogen. Hence for long term storage all hydrogen must be intentionally turned into parahydrogen molecules before liquefaction. Repeated cooling to 20K and few degrees warming with the help of iron oxide or activated carbon catalysts up to 99% of hydrogen molecules can be turned into parahydrogen [18].

After liquefaction, despite the considerable improvement in volumetric energy density to 10MJ/L, it is still far behind common fuels such as liquefied natural gas (20.2 MJ/L) or diesel [6]. Hence this techniques remains challenging and prohibitively expensive for commercial applications.

I.3.3. Hydrogen in porous compound

Various Van der Waals interactions between hydrogen molecules can also be observed between hydrogen and other molecules. These interactions are usually weak (10-100meV) and at high temperatures can be easily overcome by thermal vibrations. However, at low temperatures these interactions become strong enough to bind a hydrogen molecule to a particular surface. This is known as physisorption process. To maximize the amount of hydrogen stored through this approach it is important to choose a host material that has lowest mass but highest internal surface area and pore volume. These requirements dictate the choice of host structure. At medium pressures, the adhesion to surface of the open pores facilitates the hydrogen storage process. However, with increasing hydrogen pressure ($P > 30\text{bar}$) gas molecules are forced into the porous volume, essentially liquefying it at “milder” conditions [19]. Besides porous carbon compounds the most popular host compounds are metal organic frames (MOF). They can be synthesized from transition metals (or oxides) and organic molecules that link them in periodic structure leaving variable size of porous volume in the crystalline structure. Metals or organic linkers can provide various chemical functionality resulting in infinitely large possibilities to design a MOF for specific applications such as gas storage, gas separation and catalysis [20].

At liquid nitrogen temperatures (77 K) and below 200 bar, storage of hydrogen in porous medium enables a playing ground that cannot be reached by liquefied or compressed hydrogen processes [21]. Indeed at 77 K, under the same hydrogen pressure conditions it is possible to store several times more hydrogen in tanks filled with porous compounds compared to an empty tank. However, this advantage is quickly lost once the temperature is increased to ambient conditions. This approach is too expensive for pressures above 200 bar [22]. Below this pressure improving the volumetric capacity of the system using porous compounds is only achieved at the cost of the lost gravimetric capacity. To minimize this penalty on gravimetric capacity, active research continues in synthesizing cheap, light porous materials with adequate surface area and pore distribution.

I.4. Chemical hydrogen storage

Chemical storage of hydrogen refers to any medium that contain hydrogen atoms except in its H_2 form. Unlike physisorption, the energy of interaction in chemisorption between hydrogen atom and the host compound are high enough to dissociate the H_2 molecule. There is another type of interaction that is in between physisorption and chemisorption in its

binding energy range, it is referred as quasi molecular Kubas-type interactions. In this interaction, bonding strength of hydrogen atoms in H₂ molecules is weakened due to the charge transfer from bonding orbital of H₂ molecule to the transition metal cation or H₂ molecule is polarized in strong electric field generated by the transition metal cation [23].

Many chemical compounds that include hydrogen atoms in high quantity are of interest. However, compared to the hydrogen gas, the higher density of the new hydrogen containing molecule enables a hydrogen storage medium with better volumetric hydrogen capacity at the expense of the gravimetric capacity. The list of important selection criteria for good hydrogen storage materials starts with the ease of hydrogenation (adding hydrogen) or dehydrogenation (removing hydrogen) reactions of these compounds. In other words, the strength of chemisorption must be not too strong or too weak in order not to lose too much energy to hydrogenation or dehydrogenation process.

I.4.1. Hydrogen containing gases

Due to their high gravimetric hydrogen capacity, light organic molecules such as methane (CH₄ – 24 wt%), ammonia (NH₃ – 17 wt%), diborane (B₂H₆ – 22 wt%) attract the attention. Unlike water (H₂O – 11 wt%), most of these compounds are toxic and dangerous gases at ambient conditions. Nevertheless, high pressure and low temperature conditions for liquefaction of these gases are much milder than those for hydrogen gas. Liquefied natural gas (LNG) and ammonia are most attractive candidates since these gases are already produced and transported globally at large scale and has established competitive commodities market. To remain liquid at 1 atmosphere while LNG requires cooling CH₄ down to -162°C, ammonia only requires -33°C.

Besides cooling and compression processes, another source of energy loss comes in the form of thermo-catalysis (cracking) of these light molecules to release the hydrogen. As I mentioned in previous section, steam reforming is a popular choice of CH₄ cracking that requires 950-1100°C and 100 bar conditions in the presence of nickel catalyst. Additionally, steam reforming of methane releases a lot of carbon dioxide defeating the image of hydrogen as renewable energy carrier. CO₂ sequestration and direct thermo-catalysis (pyrolysis) of methane (CH₄ → C + 2H₂) are proposed solutions for transition period to green hydrogen economy [24].

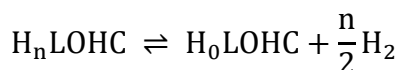
Ammonia is on the other hand a carbon free source of hydrogen. Despite occurring naturally in nature, in high concentration it is toxic but not very combustible in air. Since most of produced hydrogen globally is used for ammonia production, this offers a chance for circular hydrogen economy around ammonia. The production (Haber-Bosch process), transportation and storage of ammonia are well established industrial processes while efficient cracking of ammonia and purification of produced hydrogen are topics of intensive investigation. Synthesis and decomposition of ammonia is based on $N_2 + 3H_2 \rightleftharpoons 2NH_3$ reversible reaction where the enthalpy of conversion is -92.4 kJ/mol. However, in reality a catalyst is needed to enable the multi-step decomposition of the ammonia. The most active catalyst is ruthenium and other catalysts based on nickel, cobalt, iron are being developed.

The basic rule for catalyst is to follow Sabatier rule, where chemisorption interaction of ammonia on catalyst surface is not too strong or too weak to enable sufficient decomposition of ammonia but also fast enough desorption of species from the catalyst surface not to block the active catalyst sites (poisoning of catalyst) [25].

I.4.2. Liquid organic hydrogen carriers

Liquid organic hydrogen carriers (LOHC) are larger organic compounds that have high hydrogen capacity. As evident from their name they remain in liquid state within the temperature window required for transportation, distribution and ideally for their hydrogenation / dehydrogenation processes.

During the last century, the global energy infrastructure is built to handle, transport and distribute the flammable, liquid and gaseous chemicals like oil and natural gas. For successful transition to the hydrogen economy in financially and economically sustainable manner, it is crucial that we can utilize existing global energy infrastructure. Hence, this is the main advantage of LOHCs compared to liquefied and high-pressure hydrogen storage that require enormous infrastructure investments. The common cheapest LOHCs are methanol followed by dibenzyltoluene and toluene[26]. Typical (de/re)hydrogenation reaction is expressed as:



Dehydrogenation is endothermic and the enthalpy of dehydrogenation in 40-70 kJ/mol range is preferred in order to have a stable compound at ambient conditions but not too stable to facilitate dehydrogenation easily. Platinum or palladium catalyst are utilized for dehydrogenation in 150-450 °C and 10 bar conditions. On the other hand, the hydrogenation is typically done in the presence of ruthenium or nickel catalyst under 100-250 °C and 10-50 bar hydrogen pressure conditions [27].

I.4.3. Solid-state hydrogen storage

For chemical storage options of hydrogen, we already presented gaseous and liquid compounds; equally significant research topic is the solid compounds with high density. Solid state hydrogen storage compounds are equivalent of coal in hydrogen fuel cycle. In the following sections, various type of compounds, their general hydrogen storage properties, advantages and disadvantages will be discussed.

I.4.3.1. Metal hydrides

Metal hydrides consists of metal cation (M^{m+}) and negatively charged hydrogen anion (H^- aka hydride). Typical formation reaction is through chemisorption and direct dissociation of hydrogen gas on the metal surface $M + x/2 H_2 \rightleftharpoons MH_x$. Metal hydrides have fully reversible hydrogen storage property and excellent volumetric hydrogen capacity which unfortunately comes at an extreme penalty to their gravimetric hydrogen capacity. As any chemical reaction, the concentration of precursors (ratio of metal to hydride phase, pressure of hydrogen), the enthalpy and entropy of the hydrogenation (or dehydrogenation) reaction determine the equilibrium point at a given temperature. This means in the ideal case, the

pressure of hydrogen reaches a plateau where additional hydrogen molecules prefer to react with metal to form more hydride phase (Figure I-3a). This equilibrium pressure plotted vs the temperature can provide the enthalpy and the entropy values for the hydrogenation reaction (Figure I-3b) [28].

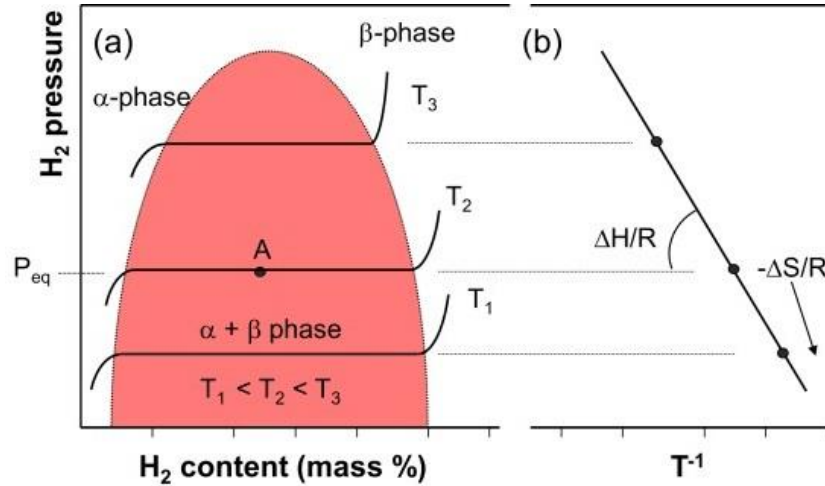


Figure I-3: a) Pressure Composition Isotherm (PCI) plot b) Van't Hoff plot of ideal metal hydride. [Figure taken from Ref.28]

Since the entropy of hydrogen gas is very high compared to metal or hydride phase, the entropy change of the hydrogenation reaction is mostly the same for all hydrides. So $T_{eq} = \Delta H / \Delta S$ equation is used to estimate the temperature needed for desorption of hydrogen under 1 atmosphere. In practice however, the required temperature and pressure can be far from the ideal values due to the kinetic activation barriers.

Magnesium hydride (MgH_2) held the spotlight as a promising metal hydride with 7.7 wt% hydrogen capacity, moderate hydrogen reversibility and relative abundance of magnesium source. Hydrogenation of magnesium $Mg + H_2 \rightleftharpoons MgH_2$ is exothermic with enthalpy value of 75.3 kJ/mol. However, the dehydrogenation process requires heating the hydride up to 300 °C due to challenges associated with low kinetics of dehydrogenation and high endothermic enthalpy. Alloying is the main technique used to modify crystalline structure, unit cell parameters of the metal hosts, which modify the associated energy barriers to hydrogen dissociation, diffusion into the host structure and hydride formation. For magnesium, alloying with transition metals such as iron and nickel allows the formation of Mg_2NiH_4 and Mg_2FeH_6 with more favorable dehydrogenation properties [29].

AlH_3 (alane) is another interesting hydride with 10.1 wt% hydrogen capacity and global abundance of aluminum source. It is thermodynamically unstable at room temperature, however kinetically stabilized from dehydrogenation: $AlH_3 \rightarrow Al + 3/2 H_2$. It can decompose in 60-200 °C temperature range; however, direct rehydrogenation of aluminum requires extremely high pressures of 25000 bar [30], [31]. Reaction of alkali hydrides with aluminum hydrides results in formation of complex hydrides such as $LiAlH_4$ and $NaAlH_4$,

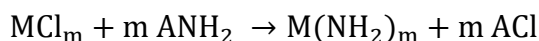
referred to as alanates. TiCl_3 doped NaAlH_4 relaunched the interest in complex hydrides due to its high, reversible hydrogen capacity compared to known metal hydrides. It can be rehydrogenated under 170 °C and 150 bar conditions with reversible 4.2 wt% capacity [32].

1.4.3.2. Complex hydrides

To improve the low gravimetric capacity of metal hydrides, light weight hydrides were synthesized that constitutes from metal cation and complex anion such as borohydride $[\text{BH}_4]^-$, amide $[\text{NH}_2]^-$ and alanate $[\text{AlH}_4]^-$. Though, unlike metal hydrides most of these compounds displayed complex multistep hydrogenation and dehydrogenation reactions. Subsequently, the kinetic and thermodynamic energy barriers build-up with each step making the complex hydrides usually too stable. Hence, their dehydrogenation process requires high temperatures, meanwhile partial or negligible rehydrogenation necessitates extreme hydrogen pressure and temperature conditions. Synthesis of these compounds required development of chemical routes and in-depth characterization of each compounds was necessary to build theories on characteristics of certain family of materials. In the following sections, we will focus on the state of the art about major groups of complex hydride materials and their properties.

1.4.3.3. Metal amides

Metal amides consist of metal cation M^{m+} and amide anion $[\text{NH}_2]^-$. Alkali amides ANH_2 are synthesized by reaction of alkali metal with ammonia in the presence of ferric nitrate $\text{Fe}(\text{NO}_3)_3$ catalyst. Transition metal amides can be synthesized by salt metathesis reaction between metal chloride and alkali amide:



Although, due to their lower gravimetric hydrogen capacity of transition metal amides, mostly light alkali and alkali earth amides were investigated as potential reversible hydrogen storage materials [33]. Lithium amide and hydride mixture can dehydrogenate reversibly at temperature below 430 °C in two steps through following reaction:

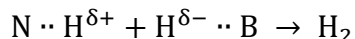


which yields theoretical hydrogen capacity of 10.4 wt%. Second part of the reaction has lower enthalpy hence it can reversibly hydrogenate up to 5.5 wt% (without the excess LiH phase) under 30 bar pressure in 255-285 °C temperature range [34]. This temperature range can be lowered, and kinetics can be improved with the help of catalysts such as TiCl_3 . Lithium amide is known to decompose exothermally into Li_2NH and release ammonia. However in good contact with LiH the mixture dehydrogenates before ammonia can be generated [35]. Another $8\text{LiH} - 3\text{Mg}(\text{NH}_2)_2$ mixture was found to rehydrogenated at 200 °C under 10 bar with reversible dehydrogenation at 150 °C with capacity of 5.5 wt% [36].

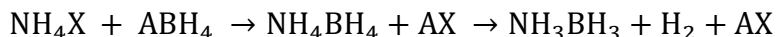
1.4.3.4. Ammonia Borane

Ammonia borane NH_3BH_3 has theoretical hydrogen capacity of 19.4 wt%. Due to the existence of protic hydrogen atoms in its NH_3 group and hydridic hydrogen atoms in BH_3

group, the electrostatic attraction between this oppositely charged hydrogen atoms facilitate combination and productions of hydrogen gas through dihydrogen elimination reaction:



Ammonia borane is mainly synthesized by metathesis reaction between ammonium salt and alkali borohydride in an organic solvent:



However, ammonium borohydride NH_4BH_4 is not stable above $-40^\circ C$, hence it dehydrogenates into NH_3BH_3 . Another synthesis approach is base displacement reaction where strong base ammonia replaces the weak base (L) in $L \cdot BH_3$ in organic solvent. $L \cdot BH_3$ in general is prepared by reacting diborane gas (B_2H_6) with electron pair donating solvents.

In practice, ammonia borane might release up to 13 wt % hydrogen under $200^\circ C$. Upon heating at constant rate, around $\sim 90^\circ C$ ammonia borane melts which is immediately followed by first exothermal dehydrogenation step releasing roughly 1 mole of H_2 . This turns the compounds in amorphous polymeric structure consisting of various combination of $[-H_2B = NH_2-]$ molecular unit. Upon melting, ammonia borane starts to foam and experiences volumetric expansion of up to 12 times. Second step of the decomposition process turns this molecular unit into $[-HB \equiv NH-]$; however, on its own it is not enough to explain the BNH_x final byproduct at $200^\circ C$ (where $0 < x < 2$). Various polymeric decomposition byproducts are generated, common ones are depicted in Figure I-4.

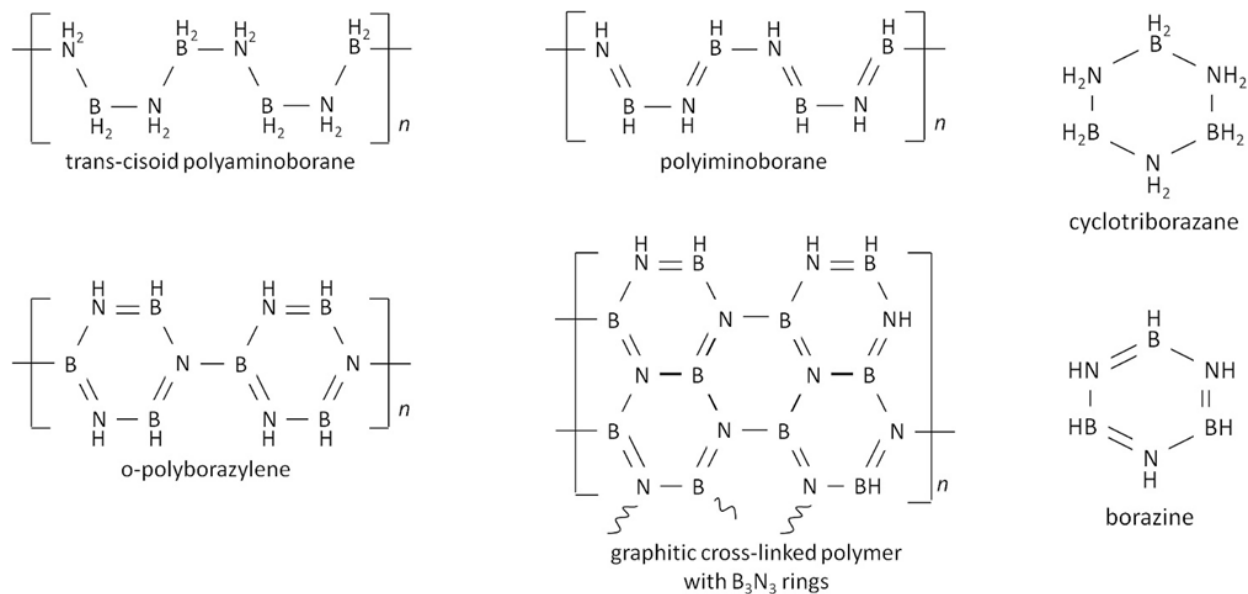


Figure I-4: Various common polymeric B-N-H by-products of thermal decomposition of ammonia borane (figure taken from reference [37]).

The main drawback of ammonia borane is that the released hydrogen is mostly accompanied by ammonia, diborane, borazine type impurities gases. The second decomposition step is

mostly dominated by borazine B₃N₃H₆ gas. The amount of released impurities is difficult to quantify and their amount change depending on the synthesis technique, the purity of ammonia borane and the heating rate during decomposition [37].

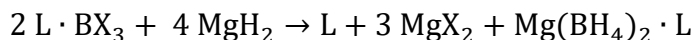
Direct rehydrogenation of ammonia borane spent fuel is not possible. Due to the very high entropy increase associated with the release of at least 2 mole hydrogen during decomposition of ammonia borane, the pressure values required for direct rehydrogenation of ammonia borane is extreme. However, there is a valid rationale for chemical regeneration of the spent fuel byproducts back to ammonia borane. Mainly because it could be cheaper compared to Schlesinger process that is used for production of sodium borohydride precursor for synthesis of ammonia borane [38]. The rehydrogenation process needs to take into account the sources of hydridic and protic hydrogen atoms required to reconstruct the ammonia borane. Among the polymeric decomposition byproducts of ammonia borane only the polyborazylene (Figure I-4) can be directly regenerated back to NH₃BH₃ using hydrazine in liquid ammonia solution. However, it is not possible to purposefully steer the ammonia borane decomposition to yield 100% polyborazylene. Hence, this methods always delivers partial regeneration of spent fuel [39]. Other polymeric by-products are difficult to regenerate mainly due to their limited solubility in organic solvents. Additionally, hydrazine is an expensive chemical and in its anhydrous form, it is basically an explosive rocket fuel. Unless a cheaper synthesis process for hydrazine is not developed the regeneration of ammonia borane through this approach is not cost effective. Hence, to bypass the limitations of hydrazine approach, the ammonia borane regeneration using common and cheap chemicals remains an attractive alternative [40]. The proposed multistep process consists of mainly three steps:

- 1) Digestion: addition of H⁺ through a reaction of the byproducts with strong hydrogen halide acid HX which form halogenated BX₃ species. Various acids and their mixture with metal halides as strong Lewis acids were investigated to improve the yield of BX₃ generation.

BCl₃ for example is a gas at ambient conditions however it can be trapped in Lewis base solvents (L) through formation of complex such as L·BCl₃. Among the best performance is AlCl₃-HCl-CS₂ superacid/solvent mixture that achieved 90 % conversion yield under 40 bar HCl pressure at 80 °C [41].

- 2) Reduction: addition of H⁻ species, the halogen species in BX₃ are replaced with hydrides (aka hydrodehalogenation).

Most effective hydrodehalogenation reactions are with metal hydrides such as NaH or MgH₂:



The kinetics of this reaction improves with the choice of weaker Lewis base (L). Hence, without the coordinating solvent kinetics of the reaction is reported to be much higher [42]. The main issue with this approach is that it simply shifts the problem of rehydrogenation to costly hydride materials. Hence, direct hydrogenation with molecular hydrogen is more attractive approach. Direct hydrodehalogenation of BX₃

into diborane gas through $BX_3 + 3 H_2 \rightarrow \frac{1}{2} B_2H_6 + 3 HX$ reaction is not thermodynamically possible. However, $L \cdot BX_3$ hydrogenation to $L \cdot BH_3$ is thermodynamically allowed if $L \cdot HX$ complex is also stable. Nevertheless, the conditions for the reaction:



to take place are extreme (1000-4000 bar at 180-250°C temperature range for $L = NMe_3$ trimethylamine) [43]. Nonetheless, it was demonstrated that using weaker base in $L \cdot BX_3$ improves the hydro dehalogenation conditions provided that this weaker base can still form stable $L \cdot HX$ complex [42]. Additionally, use of hydrodehalogenation catalyst such as Ni_3B helped to drastically soften the experimental condition. Triethylamine complex $NEt_3 \cdot BCl_3$ only in the presence of this catalyst, at 160 °C under 60 bar hydrogen pressure after 48 hours saturates and yield $NEt_3 \cdot BH_2Cl / NEt_3 \cdot BH_3$ mixture in 70%/30% ratio [41].

Ni_3B , elemental nickel and palladium unlike most precious-metal-based catalysts are found to be very resistant to halide or amine poisoning. Nevertheless, for hydrodehalogenation of BCl_3 , it was proposed that $N-CH_2$ groups of NEt_3 plays an important role as the activation of hydrogen molecule on Ni_3B catalyst surface [44].

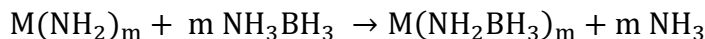
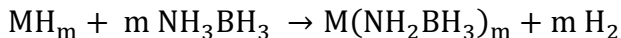
3) Ammoniation: displacement of coordinating solvent (L) with ammonia.

It is important that L chosen in previous steps is not a stronger Lewis base than ammonia for successful base displacement reaction. Higher temperatures in liquid ammonia can speed up this displacement reaction [41].

Under isothermal conditions at temperatures below 100 °C, ammonia borane can remain stable for a certain amount of time referred as the induction period. This period becomes longer with the lower temperature. In the end of the induction period, ammonia borane molecules overcome the dihydrogen bonding stabilization, expand in volume and become more mobile. This results in very quick exothermal decomposition. In the presence of transition and alkali earth metal chlorides [45], ammonia borane can be destabilized much easily, the induction period becomes much shorter and the dehydrogenation starts at lower temperatures. The degree of destabilization increases with the higher electronegativity of metal in the metal chloride [46]. Hence, for example $PdCl_2$ and $CuCl_2$ cause excessive destabilization which makes ammonia borane unstable at room temperature. Pure metal additives do not display same destabilization behavior. With metal chlorides additives, the metal cation being Lewis acid attracts the NH_3 group (Lewis base), after partial dehydrogenation and partially reduced of metal cations form $M \cdots NH_2BH_2$ species. This $M \cdots NH_2BH_2$ species act as Lewis acid and further facilitate ammonia borane decomposition [47]. With metal chloride additives, the amount of released ammonia or borazine impurities are decreased but not completely suppressed.

1.4.3.5. *Metal amidoboranes*

A common modification of ammonia borane is replacement of a protic hydrogen with metal cation that forms $M(NH_2BH_3)_m$ phase. Typical synthesis process is based on ball-milling or solvothermal synthesis of metal hydride (or metal amides) with ammonia borane:



where compounds for $M = \text{Li, Na, K, Mg, Ca, Y, Sr, Al}$ have been reported in the literature. The polarity and the stability of dihydrogen bonds in these compounds can be modified by tuning the electronegativity (replacement) of the metal cations. All metal amidoboranes are a type of destabilized ammonia borane which means they decompose at temperatures below 90°C . This is due the role of metal cation for transferring the $\text{H}^{\delta+}$ from ammonia to $\text{H}^{\delta-}$ of the borane group that facilitates dihydrogen elimination process. Metal cations with smaller ionic radius and higher electronegativity are more active in this process. The main advantage compared to pristine ammonia borane is purer decomposition process that releases only ammonia impurity (no diborane or borazine gases) [48].

1.4.3.6. Metal borohydrides

Metal borohydrides are described with general chemical formula of $\text{M}(\text{BH}_4)_m$. Borohydride anion makes ionic bonds with alkali and alkali earth metals while covalent type bond is preferred with transition metal cations. Light alkali borohydrides are especially interesting, e.g. LiBH_4 has a theoretical gravimetric hydrogen capacity of 18.5 wt% while retaining volumetric energy density (43.4 MJ/L) higher than that of diesel. However, alkali borohydrides are too stable and do not release hydrogen unless they are heated to temperatures above 400°C which is not acceptable temperature range for many applications.

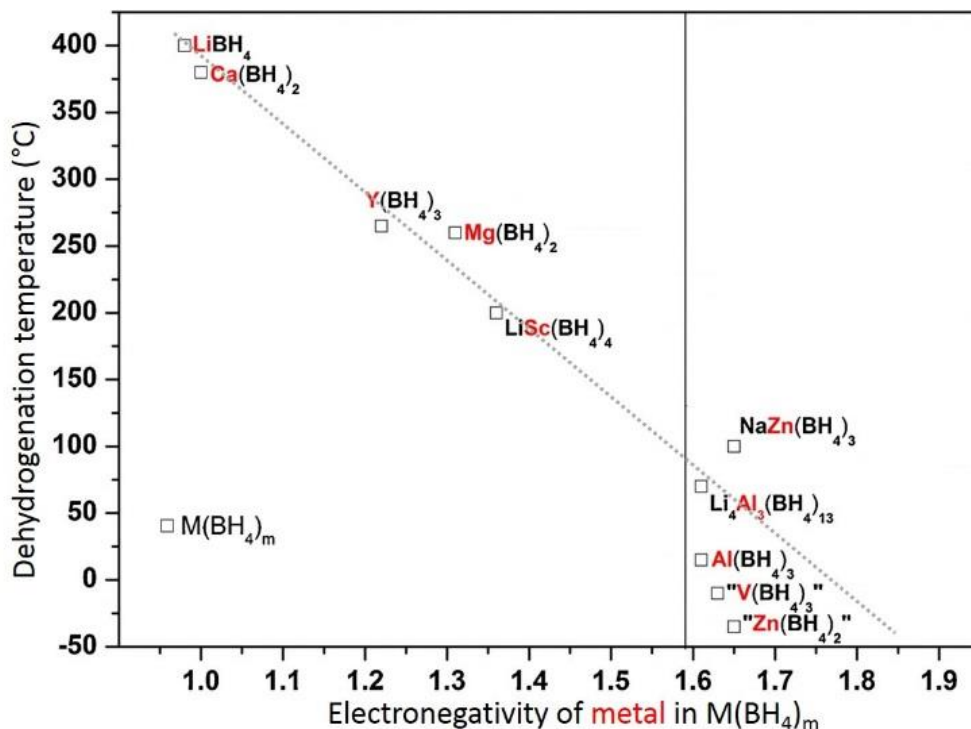
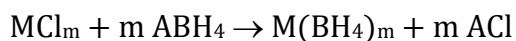


Figure I-5: Linear relationship between dehydrogenation temperature and electronegativity of the metal in metal borohydride. Figure adopted from ref.[50]

Stability of metal borohydrides can be tuned by changing the metal cation, the linear relationship between enthalpy of formation and Pauling electronegativity of the cation (χ_M) has been demonstrated [49]. Increasing the χ_M destabilizes the metal borohydrides, while choosing a cation with electronegativity higher than 1.6 results in unstable metal borohydrides at room temperature (RT) [50]. Destabilized metal borohydrides exhibit lowered decomposition and dehydrogenation temperature. Unfortunately, the decomposition of these metal borohydrides is also accompanied by release of diborane (B_2H_6) which is toxic and explosive gas [50]. The properties of the metal borohydride can be modified through combination with an alkali borohydride forming a bimetallic borohydrides, $A_xM(BH_4)_{m+x}$ (where A is alkali cation). Bimetallic borohydrides are first observed as a by-product of synthesis process.

Metal borohydrides are usually obtained through a salt metathesis reaction between metal chloride and alkali (Li or Na) borohydride:



The typical synthesis process is either a mechanochemical (dry ball-milling) synthesis or solvothermal synthesis using solvents such as tetrahydrofuran (THF), diethyl ether (Et_2O) or dimethyl sulphide (DMS). Combination of both techniques (solvent assisted ball-milling) is also used to manage advantages and disadvantages of each technique and improve the yield of the synthesis process.

The synthesis of bimetallic borohydrides is solely done by dry or solvent assisted ball milling. Nevertheless, the possibility of solvothermal synthesis of bimetallic borohydrides has been demonstrated through the use of the bulky organic cations and weakly coordinating anions [51],[52]. However, the solvent assisted metathesis reaction described above only results in formation of separate monometallic borohydride phases. This is presumed to be due to the bimetallic phase being thermodynamically less stable than monometallic phases. Additionally, the complete removal of typical solvents used for synthesis such as THF, Et_2O and DMS has proven to be difficult for some compounds due to the strong coordination of these solvent molecules to the metal cation resulting in formation of metal borohydride solvates $M(BH_4)_m(solvent)_n$. We will discuss the synthesis process in detail in Chapter 2.

Compared to metal hydrides, the reversible hydrogenation of metal borohydrides is a one of their major drawbacks. Upon decomposition, metal borohydrides decompose into elemental metal, boron, metal hydride or metal boride phases [53], [54]. Mixture and different ratios of these phases can be obtained depending on the dehydrogenation reaction conditions.

With 14.9wt% gravimetric hydrogen capacity magnesium borohydride is one of the most studied compounds. The enthalpy of decomposition reaction from $MgBH_4$ to MgB_2 is calculated to be 38.6 kJ/(mol H_2) which corresponds to dehydrogenation under 1 bar and 73 °C conditions. However, this cannot be achieved in practice due to the formation of

intermediate phases [55]. Magnesium borohydride decomposes in three steps upon heating to 530 °C, after first dehydrogenation step MgH_2 and $\text{Mg}(\text{B}_n\text{H}_n)$ type intermediate phase form (Figure I-6a). Then MgH_2 phase after further dehydrogenation to Mg reacts with $\text{Mg}(\text{B}_n\text{H}_n)$ phase to finally decompose into MgB_2 :

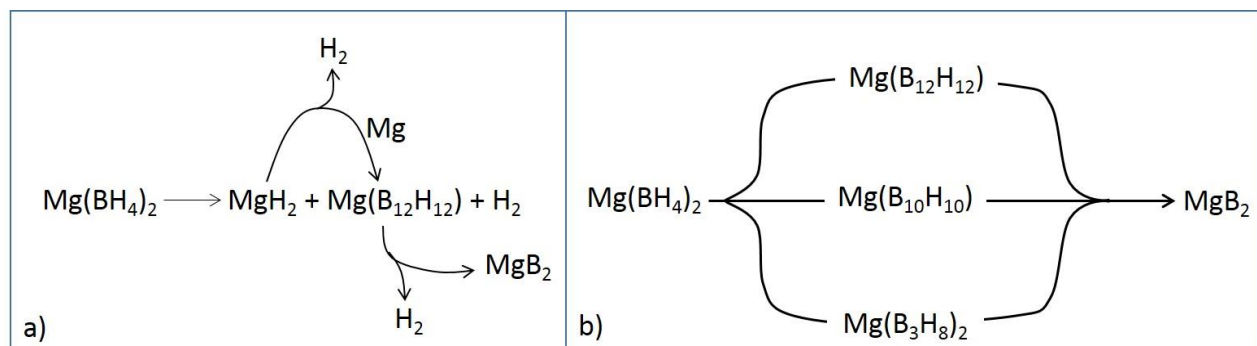


Figure I-6: a) typical decomposition reactions of magnesium borohydride b) competition of different complex borohydride intermediate phases

The issue with metal boride phase is that it is very stable compound. Hence, for example direct rehydrogenation of MgB_2 back to $\text{Mg}(\text{BH}_4)_2$ requires 950 bar at 400 °C for 108 hours to reach 75 % yield. Low kinetics of the hydrogenation of intermediate $\text{Mg}(\text{B}_{12}\text{H}_{12})$ phase is proposed to be the main barrier [56]. When decomposition process is conducted at 200 °C, $\text{Mg}(\text{B}_{12}\text{H}_{12})$ intermediate is instead mostly replaced with $\text{Mg}(\text{B}_3\text{H}_8)_2$ phase (Figure I-6b). This intermediate phase can be hydrogenated back to $\text{Mg}(\text{BH}_4)_2$ under 120 bar at 250 °C in 48 hours. It was observed that directly synthesized $\text{Mg}(\text{B}_3\text{H}_8)_2 \cdot 2\text{THF}$ complex when mixed with MgH_2 can be rehydrogenated under even milder conditions, at 200 °C under 50 bar hydrogen back to $\text{Mg}(\text{BH}_4)_2$ phase. Without the hydride phase $\text{Mg}(\text{B}_3\text{H}_8)_2 \cdot 2\text{THF}$ can only transform into $\text{Mg}(\text{B}_{10}\text{H}_{10})$ and $\text{Mg}(\text{B}_{12}\text{H}_{12})$ phases [57]. The effect of THF adduct was further investigated with different solvents. $\text{Mg}(\text{BH}_4)_2 \cdot n(\text{solvent})$ solvates were kept at 180 °C under inert atmosphere for 24 hours followed by ^{11}B NMR analysis in THF/ D_2O solution. Among solvates with DMS, Et_2O , triethylamine, diglyme, dimethoxy ethane and THF, it was found that THF resulted in highest degree of transformation of $[\text{BH}_4]^-$ species to intermediate species such as $[\text{B}_{10}\text{H}_{10}]^{2-}$, $[\text{B}_3\text{H}_8]^-$ and $[\text{B}_{12}\text{H}_{12}]^{2-}$, while pure $\text{Mg}(\text{BH}_4)_2$ had the lowest degree of transformation. Solvent adducts are believed to modify the coordination environment as well as electron density distribution around Mg^{2+} cation leading to modification of the activation energy to dehydrogenation [58]. Even the chemically inert MgB_2 phase once ball-milled with THF enables the hydrogenation back to $\text{Mg}(\text{BH}_4)_2$ under “milder” 700 bar and 300 °C conditions. Although no direct association of THF molecules with the MgB_2 phase was observed, ball-milled MgB_2 became pyrophoric indicating chemical activity. This pyrophoric phase was suggested to contain small amounts of Mg/MgH_2 based phases. This idea was further supported by the improved hydrogenation of MgB_2 phases ball-milled in THF with Mg or MgH_2 additives [59].

1.4.3.7. *Metal borohydride derivatives*

There are mainly two types of modification of metal borohydrides; first one is the combination with an alkali metal borohydride forming a bimetallic borohydrides, $A_xM(BH_4)_{m+x}$ (where A is alkali cation, $x = 0; 1; 2$). First reported such compound is $LiK(BH_4)_2$ [60]. The main observation is the stabilization of high electronegativity “unstable” metal borohydride by inclusion of alkali borohydrides in the structure (Figure I-5). The crystal structure typically rearranges as alkali cations countered by complex anions centred around high electronegativity metal cation such as $[Zn(BH_4)_3]^-$ and $[Zn_2(BH_4)_5]^-$ anions in $NaZn(BH_4)_3$ and $Na_2Zn(BH_4)_5$ compounds [61]. Based on the ability and tendency of metals such as Mg, Mn and Zn to substitute each other, trimetallic compounds were also reported [62]. Upon heating multimetallic borohydrides dissociate into their individual metal borohydrides and decompose independently. Hence, this type of modifications does not help with the release of toxic diborane impurities during decomposition process.

The second modification technique is possibly inspired from metal borohydride solvates $M(BH_4)_m(solvent)_n$. The idea is to replace the solvent molecules with light organic molecules that can participate in, modify and improve the dehydrogenation process of the metal borohydride. The choice of nitrogen containing light organic molecules are attractive. Because, similar to ammonia borane, these molecules with the presence of protic hydrogen in their structure provide an advantage for facilitating dihydrogen elimination reaction ($N\cdots H^{\delta+} + H^{\delta-}\cdots B \rightarrow H_2$) with the hydridic hydrogen in borohydride anions. Additionally, these molecules can increase the theoretical hydrogen capacity of the associated metal borohydride.

Some popular adducts to metal borohydrides include hydrazine (N_2H_4), ammonia borane and ammonia. Anhydrous hydrazine besides being hazardous and expensive, does not provide compelling advantage due to its presence as an impurity in the released hydrogen from metal borohydride hydrazinates [63],[64].

Ammonia borane metal borohydrides $M(BH_4)_m(NH_3BH_3)_n$ were mostly synthesized by ball-milling ammonia borane with corresponding metal borohydride. Compounds with Li, Ca, Mg, Al metals were reported where typically BH_3 group of ammonia borane coordinates to the metal cation together with BH_4 groups. Li and Ca compounds decompose by dissociating where at low temperature ammonia borane component decomposes followed by metal borohydride component at higher temperatures [65]. Both Mg and Al compounds melt before decomposition process and unlike Li and Ca compounds they decompose in two consequent steps between 50-150 °C range. Similar to ammonia borane decomposition, the first decomposition step mostly releases hydrogen while second step is accompanied by release of ammonia, diborane and borazine impurities. The polarizing power of the metal cation defines the degree of modification to the reaction between ammonia and borohydride groups in M-B-N-H systems. Higher polarizability (higher electronegativity and smaller ionic

radius) allows the coordination of ammonia borane to the metal cation, this was attributed to the lack of reaction between ammonia borane and ABH_4 where $A = Na; K; Rb; Cs$ [66]. The melting before decomposition ensures homogeneity, prevents the dissociation into different phases and guarantees the presence of metal cation in the presence of $N \cdot H^{\delta+} + H^{\delta-} \cdot B$ dihydrogen elimination reaction. Similar to catalytic decomposition of ammonia borane in the presence of high electronegativity metal chlorides, $Al(BH_4)_3(NH_3BH_3)$ complex behaves as destabilized ammonia borane and the presence of metal cation although improves, does not completely solve the release of borazine, diborane type impurities [67].

The most popular adducts to metal borohydrides is the ammonia molecule. Typically, a reaction of metal borohydrides with ammonia gas results in formation of ammine metal borohydrides, $M(BH_4)_m(NH_3)_n$. Unlike the previously discussed metal borohydride derivatives, the ammoniated version of almost every known metal borohydride was reported, except for ABH_4 where $A = Na; K; Rb$ which does not react with ammonia gas. Number of borohydride groups bonded to metal cation is fixed by its oxidation number. However, the number of ammonia adducts in the structure can be modified since ammonia is a neutral molecules. This provided a further degree of freedom for exploring the chemistry of M-B-N-H system.

Under ambient ammonia atmosphere, saturation of metal borohydride reaction with ammonia results in varying number of ammonia adducts from 1 in $LiBH_4NH_3$ to 8 in $Zr(BH_4)_4(NH_3)_8$ [68],[69]. To understand this, we can look at ammine metal chlorides $MCl_m(NH_3)_n$ which start with up to $n=8$ ammonia adducts at low temperatures and release the ammonia gas in steps and achieve a new stability plateau at $n = 6; 4; 2; 1; 0$ at various temperatures [70]. Similarly, ammine metal borohydrides upon heating release ammonia as long as the decomposition temperature of $M(BH_4)_m(NH_3)_n$ phase is above the next de-ammoniation plateau. At certain temperature and the n/m ratio, the dihydrogen elimination reaction becomes more favourable over de-ammoniation reaction. This behaviour is easily observed for stable low electronegativity metal borohydride. High electronegativity metal borohydrides ($\chi > 1.6$) on the other hand, experience stabilization upon reaction with ammonia (Figure I-7). Due to the preference of ammonia molecules for coordinating to high electronegativity metal cation they can physically separate metal cation and shield it from a reduction attack of the borohydride anions [71]. Hence, the synthesis of high electronegativity ammine metal borohydrides requires the initial synthesis and stabilization of metal borohydride either at low temperature or in a solvent that is weaker Lewis base than ammonia.

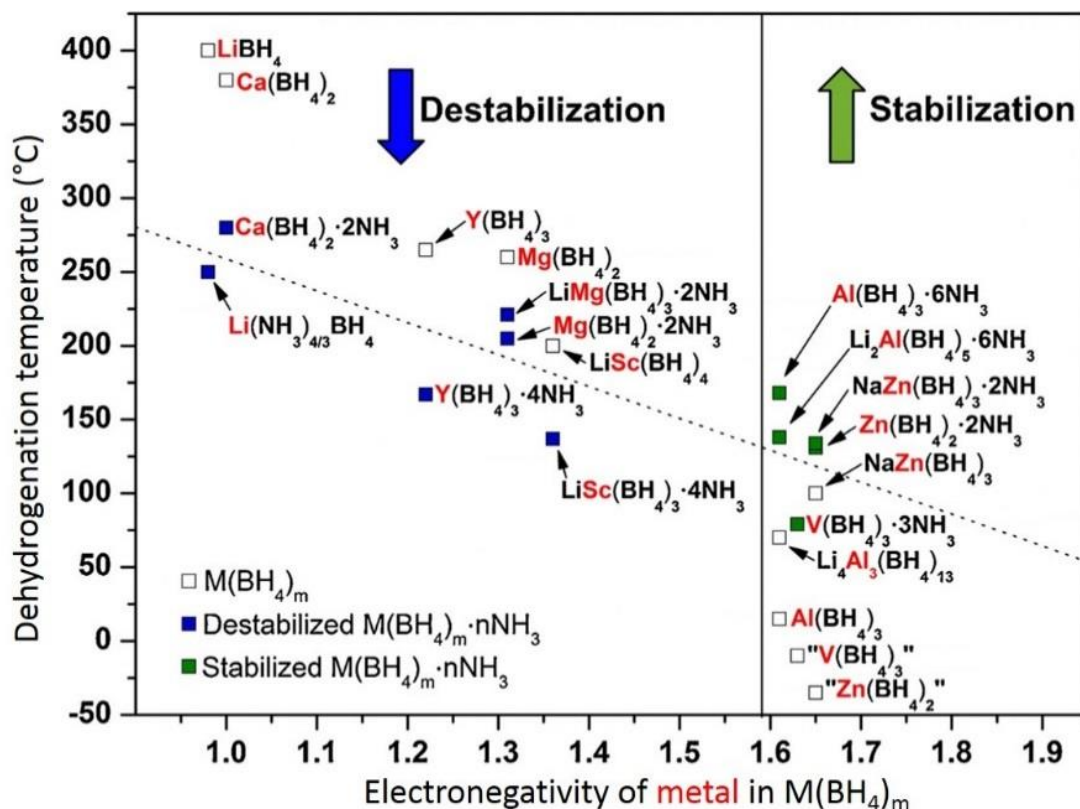


Figure I-7: The linear correlation of dehydrogenation temperature of ammine metal borohydrides to the electronegativity of the metal cation. Figure taken from ref.[50]

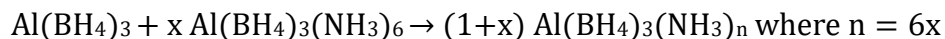
An important advantage of ammine metal borohydrides is the complete suppression of diborane, borazine type impurities by ammonia adduct [50]. However, similarly the main drawback is the release of ammonia impurity. This drawback is somewhat mitigated by exploring the ammoniates of bimetallic borohydrides and modifying the number of ammonia adducts. Through the years, few notable compounds were discovered:

Compound	Dehydrogenation peak (°C)	H ₂ capacity at T<250°C (wt%)	Purity (mol%)	Type of modification	Ref.
Zn(BH ₄) ₂ (NH ₃) ₂	128 at 5K/min	8.9	100	Decreasing the NH ₃ adducts	[72]
Al(BH ₄) ₃ (NH ₃) ₃	113 at 5K/min	13.7	99		[73]
Li ₂ Al(BH ₄) ₄ (NH ₃) ₆	138 at 10K/min	15.5	97	Alkali borohydride	[74]
LiMg(BH ₄) ₃ (NH ₃) ₂	221 at 5K/min	10.0	99	Both	[75]
Li ₂ Ti(BH ₄) ₅ (NH ₃) ₅	105 at 5K/min	15.8	100	Both	[76]

Among these compounds, Zn(BH₄)₂(NH₃)₂ and Li₂Ti(BH₄)₅(NH₃)₅ compounds were reported with LiCl by-product due to the limitation of the synthesis technique. Typically, ammonia saturated metal chloride MCl_m(NH₃)_n (n=6 for ZnCl₂ and 5 for TiCl₂) heated to

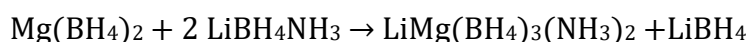
reduce the number of ammonia adducts to desired value then ball-milled with stoichiometric or excess amount of LiBH₄. Excess amount of LiBH₄ in some cases results in formation of bimetallic phases.

Al(BH₄)₃ is a pyrophoric liquid at room temperature and boils at 44°C [77]. Its reaction with ammonia gas results in formation of solid Al(BH₄)₃(NH₃)₆. Hence, reaction of Al(BH₄)₃ gas with Al(BH₄)₃(NH₃)₆ solid in various ratios allows to control the number of ammonia adducts:



Similar strategy was also employed for ball-milling the pure manganese borohydride with its ammoniated version Mn(BH₄)(NH₃)₆ in order to obtain the desired amount of ammonia adducts [78].

The reaction of magnesium borohydride with ammonia yields Mg(BH₄)₂(NH₃)₆. Reduced ammonia adduct version Mg(BH₄)₂(NH₃)₂ is obtained by heat treatment under vacuum at 120°C for 4 hours [79]. This is due to the fact that unlike all the compounds mentioned up to now, Mg(BH₄)₂(NH₃)₆ can release up to 4 ammonia molecules before dehydrogenation starts above 135 °C. Other lower electronegativity compounds such as Ca(BH₄)₂(NH₃)₆ and LiBH₄NH₃ does not dehydrogenate until all the ammonia molecules are desorbed completely [80],[68]. This is explained by weaker coordination strength of ammonia to Li⁺ and Ca²⁺ cations while having strong coordination bond with cations such as Mg²⁺, Al³⁺, Zn²⁺ [72]. LiMg(BH₄)₃(NH₃)₂ is also synthesized by ball-milling ammine lithium borohydride with pure magnesium borohydride:



Assuming that synthesis of the precursors are also not straight-forward, it is obvious that simplified synthesis approach for obtaining desired A_xM(BH₄)_{m+x}(NH₃)_n is needed.

The dehydrogenation process in all ammine metal borohydrides is exothermic which means their direct rehydrogenation is thermodynamically not feasible and chemical regeneration routes need to be developed. The main decomposition by-products include mainly M(BNH_x)_m type amorphous phases.

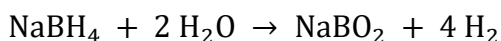
1.4.3.8. Composite Reactive hydrides

Dehydrogenation process in all the compounds discussed so far (except metal hydrides) takes place through multiple competing reactions. By combining different types of hydride materials, a new dehydrogenation reaction pathway can be created that essentially destabilizes both compounds. The destabilization of various metal borohydrides, amines and alanates mainly through reaction with light metals, metal hydrides and chlorides were investigated. The problem with this composites is the lack of theoretical models to follow for designing better composites. Nevertheless, by trial and error approach several interesting

composites were identified [28]. These composites mostly suffer from same irreversible hydrogenation problems as individual hydrides that constitute them. Nevertheless, among them we have already mentioned reversible hydrogenation of $\text{Mg}(\text{NH}_2)_2\text{-LiH}$ composite in previous section. A more popular type of destabilization is by reaction with water.

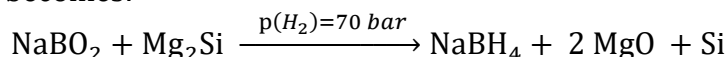
1.4.3.9. Hydrolysis

Most popular hydrolysis compounds are NaBH_4 and ammonia borane. Similar to decomposition of ammonia borane, the protic hydrogens of water like to react with hydridic hydrogens of borohydride group. Most metal borohydrides undergo exothermal reaction with water. NaBH_4 on the other hand can be stabilized in very basic solutions. Hence, by utilizing metal-based catalyst:



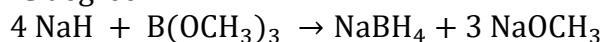
This reaction theoretically can deliver 10.8 wt% hydrogen. However, in practice to prevent spontaneous hydrolysis of the borohydride species NaOH is added to the water. In reality, excess amount (more than 2 mole) of water is also needed to fully solubilize NaBH_4 and prevent the precipitation of NaBO_2 byproduct on catalyst surface that can hinder its performance [81]. Another challenge is related to the regeneration of spent sodium metaborate (NaBO_2) byproduct back to sodium borohydride.

Sodium metaborate can be reduced with MgH_2 at 550 °C under 70 bar of hydrogen pressure and can be converted into NaBH_4 and MgO with high yield. When Mg_2Si is used instead of MgH_2 , the reaction becomes:

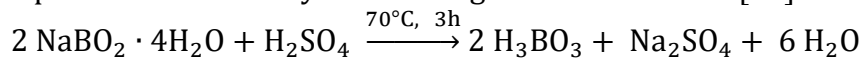


Magnesium silicide is much cheaper alternative to magnesium hydride; nevertheless, the experimental conditions remain very energy intensive [82]. This reaction is further improved by ball-milling of Mg_2Si with $\text{NaBO}_2 \cdot 2\text{H}_2\text{O}$ derived from heat treatment of hydrolysis byproduct $\text{NaBO}_2 \cdot 4\text{H}_2\text{O}$ at 54 °C. This approach does not require any high temperature or high hydrogen pressure and manages to recycle the water molecules in $\text{NaBO}_2 \cdot 2\text{H}_2\text{O}$ as a hydrogen source [83]. However, as the mechanochemical synthesis is not industrially scalable technique, the amount of regenerated sodium metaborate will be limited by this approach.

Industrial synthesis of sodium borohydride involves a reaction between sodium hydride and trimethyl borate at 250 °C degree:



This process is known as Brown-Schlesinger process [84]. Trimethyl borate on the other hand is prepared by reaction of boric acid (H_3BO_3) with methanol in the presence of H_2SO_4 as a catalyst [85]. Hence, the conversion of $\text{NaBO}_2 \cdot 4\text{H}_2\text{O}$ hydrolysis byproduct directly to boric acid is proposed as industrially scalable regeneration method [86]:

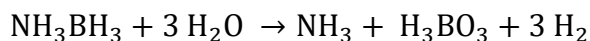


All these reactions still rely on reduction of trimethyl borate by NaH species which is prepared by energy intensive electrolysis of NaCl into Na metal that is then reacted with hydrogen obtained from steam reforming. Hence direct reduction of sodium borate by simple and abundant chemical such as methane is more desirable solution:



However, the temperature required for Gibbs free energy of the reaction to be negative is well above 2000°C. Hence, other energy sources such as plasma are required to drive the reaction to completion [38].

Another popular hydrolysis compound is ammonia borane. Like NaBH₄, ammonia borane despite being stable in basic solution decomposes through hydrolysis in the presence of metal catalysts. There are two competing hydrolysis reaction:



Equilibrium between boric acid and ammonium hydroxyborate species exists which is sensitive to temperature and the pH of the solution. Acidic species can be made dominant byproduct by lowering the pH of the solution which is important for the regeneration of the spent fuel [87]. As can be seen from the hydrolysis reactions only hydridic hydrogens in ammonia borane participate in hydrolysis reaction leaving behind NH₃ species in water. This reduces the effective hydrogen capacity of the system. Another drawback is the release of ammonia gas alongside hydrogen depending on the water amount [37].

1.4.3.10. Direct hydrogenation catalysts

As an alternative to chemical regeneration routes for many compounds, it is also important to discuss the importance of catalysts for direct hydrogenation of spent fuels. M-B-N-H compounds after exothermal dehydrogenation cannot react with hydrogen directly because the enthalpy and the entropy of the reaction does not allow it. Even if the thermodynamics would allow it, the barrier to kinetic activation is still a major hurdle. Part of this energy barrier comes from the dissociation of hydrogen molecules in order to facilitate the rehydrogenation reaction. Metal catalyst that can form hydride phase can easily dissociate the hydrogen molecules, then dissociated hydrogen atoms can diffuse through the surface of the catalyst and reach the host compound that the catalyst is mounted on. This process is known as catalyst “spill-over” effect [88]. The hydrogen “spill-over” effect has even been employed for increasing the hydrogen capacity of MOF compounds [89]. The smaller the size of the catalyst the shorter the distance that hydrogen atoms need to diffuse to reach the host, hence this effect is even prevalent in nanocatalysts. Additionally, kinetic improvement in hydrogenation of palladium or transition metal doped magnesium was also explained by this effect [90]. Typical catalysts include Pt, Pd, TiF₃, LaNi₅, Ni₃B and other transition metals.

Good contact between the catalyst and the host is very important. Additionally, the catalyst loading must to be kept to minimum since they are much dense than the host compounds. Once the hydrogenation is complete these catalyst become a dead weight until the next hydrogenation cycle unless they can also participate in the dehydrogenation process. Even worse, poisoning of the catalyst by dehydrogenation byproduct is more probably. This necessitates an easy extraction technique for the catalyst once they participate in the hydrogenation process. As opposed to heavy nanocatalyst the extraction would be much easier with light and bulky organic molecules that can perform the same task.

1.4.3.11. Frustrated Lewis Pairs

In Lewis classification of molecules, the electron pair donating molecule is a base while electron pair acceptor is an acid. When Brønsted acids and bases react, they neutralize each other and form water. Lewis acids and bases on the other hand neutralize each other by forming Lewis acid/base adduct (like NH_3BH_3). Although this simple model can explain most of the chemical reactions, it was observed that due to steric effects some bulky acids and bases cannot form Lewis acid/base adducts.

By incorporating the Lewis acid and Lewis base species into the same host molecule that sterically prevented them from quenching each other, Gregory *et al* managed to synthesize an organic molecule $((\text{C}_6\text{H}_2\text{Me}_3)_2\text{PH}(\text{C}_6\text{F}_4)\text{BH}(\text{C}_6\text{F}_5)_2)$ that can contain both hydridic and protic species (referred as zwitterionic salt) [91]. These molecules are shown to remain as monomers in solution and do not form agglomerates due to steric effects hence referred as intramolecular “frustrated Lewis pairs” (FLP). Despite the expectation that this compounds may lose hydrogen spontaneously, they were stable in air and moisture and only released hydrogen when heated to 150°C :

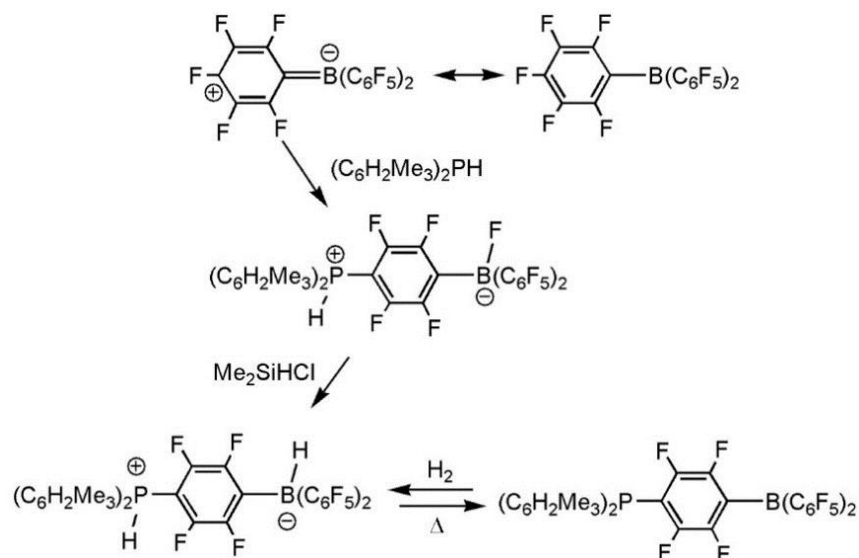
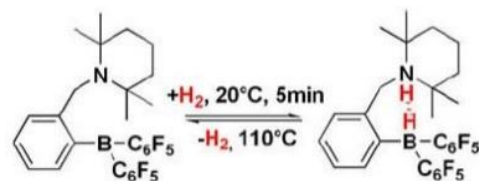


Figure I-8; Synthesis and reversible hydrogenation of $(\text{C}_6\text{H}_2\text{Me}_3)_2\text{PH}(\text{C}_6\text{F}_4)\text{BH}(\text{C}_6\text{F}_5)_2$.
Figure taken from Ref.[91]

More interestingly this dehydrogenated FLP was found to react with hydrogen rapidly at ambient temperature by splitting (heterolytic cleavage) molecular hydrogen (Figure I-8). Similarly, mixtures of Lewis acid/base pairs such as $\text{P}(\text{t-Bu})_3$ (Tri-tert-butylphosphine) and $\text{B}(\text{Ph})_3$ (Triphenylborane) in solution can form non-covalent coordination through their ligands. This is a type of intermolecular FLP. In these compounds acidic (phosphorus) and basic (boron) centers approach but are blocked from forming a covalent bond due to steric limitations. However, hydrogen molecule can enter the space between $\text{P}\cdots\text{B}$ centers and it can split between these two donor and acceptor sites. Hence, similar to hydrogenation of

compounds using transition metal complexes, FLPs can be used as metal free catalyst by splitting the hydrogen, transferring proton and hydride onto the host substrate [92].

By changing the ligands bonded to B or P center the strength of their acid or base nature can be controlled. It was observed that combined strength of Lewis acidity and basicity is required for hydrogen splitting by FLPs. Similarly, using bulky amine and boranes, $N\cdots B$ compounds such as *ansa*-animoborane FLP were also synthesized that can reversible activate hydrogen and release it under 150°C [93]. There are also Lewis acid/base pairs that does not form stable adducts nevertheless upon reaction with hydrogen can perform heterolytic cleavage of hydrogen. These compound such as $[\text{C}_6\text{H}_3\text{Me}_2\text{N}][\text{B}(\text{C}_6\text{F}_5)_3]$ are referred as “hidden” FLPs [94]. Despite being a young research field, the ability of FLPs as metal free hydrogenation catalyst of various compounds for hydrogen storage applications will continue to increase [95].



I.5. Conclusion

In this chapter, we discussed the importance and the role of hydrogen storage in enabling the transition of global energy cycle to renewable sources. We explored the types of materials that enable the physical and chemical hydrogen storage technologies. Among them higher density chemical storage compounds remain attractive medium for hydrogen storage due to their combined theoretically high volumetric and gravimetric capacity values. In Figure I-9, we can see that liquid ammonia, ammonia borane, light metal borohydrides and

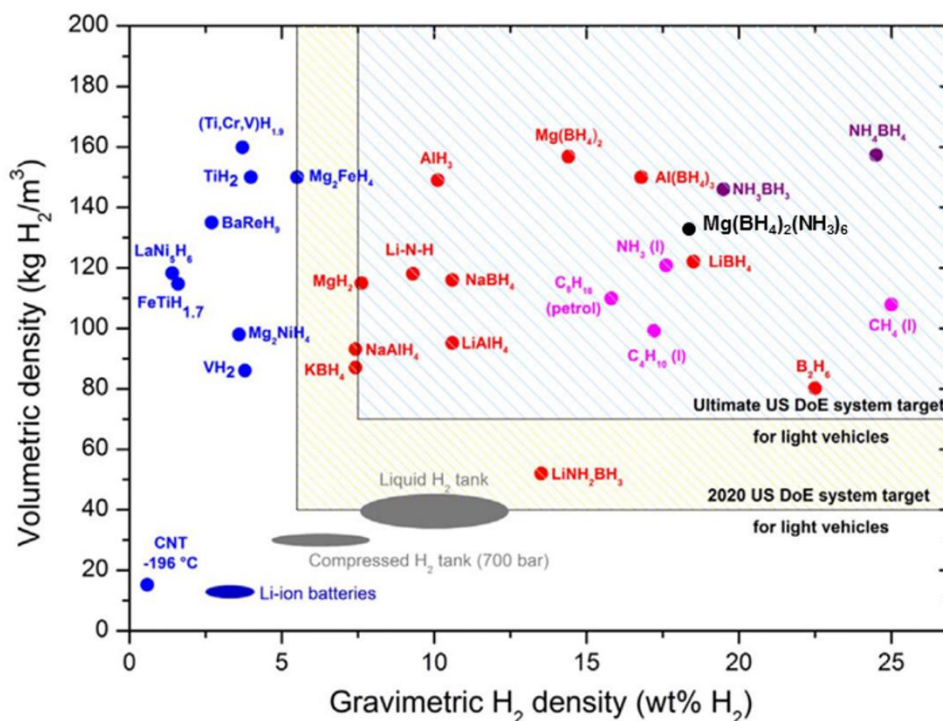


Figure I-9: $\text{Mg}(\text{BH}_4)_2(\text{NH}_3)_6$ compound added to figure taken from reference [4]

their ammoniates are among the compounds that can potentially fulfil the hydrogen capacity requirements defined by US Department of Energy for mobile application based on hydrogen fuel cells. Excluding liquid ammonia, the rest of these compounds are based on M-B-N-H system.

Hence, in this thesis, our focus will be on M-B-N-H compounds in order to understand what kind of concessions needs to be made to realize experimental hydrogen capacity as close as possible to the theoretical values. Some of these concessions come from the other requirements such as the released hydrogen purity and the dehydrogenation temperature. The practical hydrogen capacity, the purity and the dehydrogenation temperature of a given M-B-N-H compound are interconnected and this connection can only be understood by revealing the role of each atom in the structure and their interaction during the dehydrogenation process. Thus, by employing various characterization techniques we will strive to unravel the intricacy of these interactions.

Another major challenge is the difficulty, the high cost and the lack of scalability of the synthesis processes needed to enable the development of practical technologies based on M-B-N-H compounds. Thus, we will focus on developing better and simpler synthesis approaches that will address these shortcomings.

Finally, potentially biggest drawback preventing the practical applications of M-B-N-H compounds is the absence of reversible hydrogenation routes of the spent fuel. This step is crucial to achieve the cost minimization and the sustainability. As mentioned previously direct hydrogenation of spent fuel is improbable, however, chemical routes will be explored for full regeneration process.



Chapter II

Methodology



II. Methodology

In this chapter, short descriptions and experimental conditions for common characterization techniques of M-B-N-H type compounds will be provided. Then, various synthesis approaches of these compounds described in the literature will be summarized followed by the procedures and the equipment utilized during this thesis work.

II.1. Crystallographic analysis

Electron, neutron and x-ray diffraction are the main techniques that can provide crystallographic information on the compounds. X-rays interact with the electrons of the atom while neutron are only scattered by its nuclei. Conversely, electron scattering can be influenced by both electrons and the nuclei of the atoms. Each technique has its advantages and disadvantages.

Electron diffraction requires a Transmission Electron Microscope (TEM) and time-consuming sample preparations since the sample has to be electron transparent (very thin). It has advantages of focusing the electron beam on a nanometer sized crystallites. Obtaining crystal symmetry information on this scale combined with high resolution imaging TEM can be very powerful technique for specific applications. However, it has limited accuracy for calculation of unit cell parameters and the atomic positions compared to neutron and x-ray diffraction. For these experiments unless the nanocrystallites in the samples can be grown big enough for single crystal diffraction experiments, the typical sample is in powder form.

As the atomic number increases so does its number of electrons, hence heavier atoms scatter more strongly the x-rays than light atoms. On the other hand, neutron scattering cross-section is almost random and does not show any correlation with the atomic number. Hence, different isotopes can have wildly different neutron scattering power. Although ^1H scatters neutron very strongly, the big part of this scattering is incoherent (becomes flat background noise in diffraction experiments). This deficiency can be overcome with increasing the flux of neutrons source or accumulation time during the diffraction analysis. A much better approach is to synthesize the deuterated samples using ^2H which has lower ratio of incoherent to coherent scattering coefficient. Light elements such as alkali metals, boron, nitrogen and others are often used to synthesize hydrogen storage materials with high gravimetric capacity. Unfortunately, ^6Li and ^{10}B isotopes are neutron absorbing elements. Non-enriched samples contain 7.5 % ^6Li and 20 % ^{10}B . This means that for accurate neutron diffraction analysis, the samples have to be prepared using ^7Li and ^{11}B isotopes.

Atomic nuclei being much smaller than neutron wavelength act as point scattering sources, while electron density cloud being comparable to x-ray wavelength are not point sources. This translates into a decrease in x-ray scattering power with increasing scattering angle (atomic scattering factor). This problem can be partially eliminated by increasing the intensity of the x-ray source. On the other hand, neutron are scattered equally in all scattering angles. The diffraction information at high scattering angles is important for precise determination of the atomic positions in the crystal structure. Neutron diffraction does not suffer from intensity loss at higher scattering angles; consequently, precise

experimental determination of the hydrogen atom positions becomes possible. A popular hydrogen storage material, NH_3BH_3 had a disputed crystalline structure for a long time because X-ray diffraction (XRD) analysis can only see scattered x-rays from boron and nitrogen atoms and hydrogen atoms are essentially transparent to it. Using neutron diffraction, not only hydrogen atoms provide extra diffraction information, but due to the higher contrast in neutron scattering between boron and nitrogen atoms, their atomic position in crystal structure became distinct and clear. This allowed accurate measurement of B-H and N-H bonding lengths in ammonia borane [96].

A popular source of x-rays is the synchrotron radiation that allows production of high flux beam with tunable wavelength. The large 2D x-ray detectors in synchrotron facilities can provide almost instantaneous data acquisition, making it ideal for in-situ dehydrogenation or hydrogenation experiments under varying temperature and hydrogen pressure conditions. Besides XRD measurements, x-ray near edge absorption spectroscopy (XANES) can be performed to study the oxidation state of the heavy atoms and their atomic neighborhood in hydride complexes. Small angle x-ray (SAXS) and neutron scattering (SANS) measurements can provide the information regarding size and distribution of hydride phases and the catalyst additives. Finally, an atom being mostly an empty space, neutrons can penetrate much deeper into the heavy materials before they encounter a nuclei to scatter off. This allows tomography and internal imaging of pressurized hydrogen containers, as well as evolution of dehydrogenated phases in these containers [97]. Nevertheless, neutron experiments require fission or spallation sources and therefore their access is generally limited to few researchers. Hence, the main advantage of XRD measurements is its ease of use in laboratory conditions, minimal sample preparation requirements and the fast data processing options for identification of known phases, especially for powder samples.

II.1.1. Powder X-ray diffraction

The typical Powder X-ray Diffraction (XRD) experiment is performed using Bruker D8. A special XRD sample holder is used due to the air sensitive (possible pyrophoric) nature of the hydrogen storage materials. The sample holder has a silicon substrate that suppresses background noise in $2\theta=20-120^\circ$ range for Cu $K\alpha$ wavelength (1.5406 Å). The sample holder is prepared in glovebox and it is sealed using Teflon O-ring and 8 μm thick polyimide (Kapton) film that is transparent to x-rays.

For known crystalline phases, EVA database is used to identify them. High resolution measurements are performed to analyze the unknown phases. Phase analysis was performed using the structure models (crystal information file - cif) taken from the databases (Crystallography Open Database) or literature. Possible solutions to unit cell type and parameters were determined using DICVOL and the most likely space group symmetry was determined by CHEKCELL software. Le Bail fit analysis using HighScore software was performed to fit standard peak shape parameters and Chebyshev polynomial of 15th order for background signal. The unit cell parameters were calculated for each compound with reasonable accuracy (goodness of fit below 0.01). The standard deviation in unit cell volume

is calculated by manually changing unit cell parameters until the goodness of fit started to increase. Rietveld refinement analysis was performed using both HighScore and FullProf programs.

II.2. Thermodynamic analysis

Various hydrogen storage materials discussed in Chapter 1 require the thermal energy as the main energy source to release the hydrogen gas. Hence, investigation of thermodynamic parameters such as the heat and the kinetics of de/rehydrogenation reactions, mass loss corresponding to volatile decomposition products, types of gases that are released and the quantification of the amount of each released gas necessitate multiple characterization equipment to provide a full picture.

II.2.1. Differential Scanning Calorimetry - Thermogravimetry

Differential Scanning Calorimetry (DSC) and Thermogravimetry (TG) experiments usually are performed together using Setaram Sensys Evo. DSC provides the heat flow information that can help to explain various phase transition events such as melting, boiling, decomposition reactions etc. Simultaneously performed TG experiment provides mass loss information which coincides with each phase transition. This extra information for example helps to differentiate the melting process from endothermal decomposition process.

Typically, 15-30mg of powder is transferred to an aluminum crucible in glovebox and sealed with a perforated aluminum cap. The cap restricts the sample exposure to air during the transfer from glovebox. A small hole on the cap helps to avoid built-up of overpressure during the decomposition process. The typical experiment is performed under 20ml/min He flow and the samples is heated up to 500°C with the rate of 2°C/min.

II.2.2. Sievert type volumetry

Gravimetric analysis can provide a complete picture of the decomposition process if only one type of volatile species is released. In all the other cases, the TG result needs to be complemented with a volumetric analysis to provide a more quantitative assessment. Hence, by decomposing the sample under similar conditions to TG in a precisely known reservoir volume (V_r) and measuring the increase in pressure (ΔP) we can calculate the mole amount (n) of various gases. Compressibility factor (Z) for real gases is used to take into account the intermolecular attraction of gas molecules and their molecular volume:

$$\Delta P_{\text{TPD}} = \left(\frac{RT_r}{V_r} \right) \sum_i (n_i Z_i)$$

$$\Delta m_{\text{TG}} = \left(\frac{m_{\text{TG}}}{m_{\text{TPD}}} \right) \sum_i (n_i M_i)$$

In these equations, Δm_{TG} is the weight loss measured by TG while m_{TG} is the initial mass of the powder, similarly m_{TPD} is the initial mass of the same sample powder used in volumetric measurement, n_i and M_i are the molar quantity and the molar mass of the gas i released during decomposition. Since there are two independent equations, the molar quantity of

only up to two different gas mixtures can be quantified by solving these equations. Theoretically, by changing the reservoir temperature (T_r) or volume more independent equations can be obtained to solve for more than one impurity gases. The compressibility factor $Z_i(T, P)$ for gases depends on the pressure and the temperature. Hence, care must be given to use correct compressibility factor for chosen experimental conditions. For example, compressibility factor of hydrogen and ammonia under 1 bar and 25 °C conditions are $Z(\text{H}_2) = 1.0006$ and $Z(\text{NH}_3) = 0.98946$.

The volumetric decomposition experiments (Temperature Programmed Desorption – TPD) are conducted using Setaram PCT Pro. Typically, 100-200mg of powder is loaded into the steel sample holder in glovebox, sealed and connected to the machine. This steel reactor is certified up to 200 bar pressure and sealed using copper rings that can handle up to 250 °C temperature without risking the hydrogen leakage. Sample and the system is purged several times with helium gas and evacuated to achieve lowest possible vacuum. Then, the large reservoir ($V_r = 1\text{L}$) and the sample holder are filled with 1 bar hydrogen to obtain similar decomposition conditions as in TG experiments. The pressure, sample and reservoir temperature values are typically recorded with time interval range of 1-100s depending on the kinetics and total duration of the decomposition reaction. Once the data acquisition is started, the sample holder is dynamically heated up to 250 °C with external electrical heating element (average heating rate in 25°C/min). Precise volume calibration in volumetric measurements is very important for improving the accuracy of the calculation, especially for hydrogenation experiments that can be performed with hydrogen pressures up to 50 bar. The “dead volume” is referred to any volume that is outside the known PCT Pro internal volume. This volume is usually minimized by filling the empty areas of the sample holder as much as possible with steel pieces that fit tightly. The rest of the dead volume is calibrated using helium gas, which has closest real gas properties to hydrogen. This procedure is performed both at initial and final sample temperatures of the typical experiment since the calibration process is temperature sensitive.

The molar quantity calculations using TPD and TG experiments are only possible if the nature of the volatile decomposition product are known. For an unknown or new compounds, the qualitative analysis of the volatile species needs to be performed beforehand. Additionally, to identify amorphous phases in synthesized samples or in decomposition by-products spectroscopic analysis tools are necessary.

II.3. Spectroscopic analysis

The various spectroscopy experiments can be performed in transmission mode as absorption spectroscopy or in reflection mode as emission spectroscopy. As a general description, a spectroscopic analysis concerns the interaction of an electromagnetic radiation with the matter. The energy of the excitation source determines the type of the interaction. X-rays have high enough energy to excite the electrons from core shells of the atoms. Ionizing radiation (x-ray and ultraviolet) can also eject electrons from the atom creating photoelectrons which can be used to study surface chemical composition of samples, oxidation state of the atoms (XPS). For ultraviolet/visible light, due to lower energy,

only outer shell electrons of the atoms can be excited. The visible/infrared radiation can induce vibration of atoms in the molecular compounds.

For elemental analysis, atomic spectroscopy techniques require an extra energy source for vaporization, atomization and ionization of the samples. This energy source could be flame, laser, plasma, electric arc and others. Since hydrogen storage materials release volatile gases upon heating, it is possible to combine DSC-TG assembly with Mass Spectrometry (MS) to analyze the nature of the released gases. Most of these techniques provide a qualitative information on the analyzed sample. However, calibration and quantitative analysis is also possible. For example, inductively coupled plasma atomic emission spectroscopy ICP-AES can provide precise elemental concentrations in a given sample. For this analysis the sample needs to be prepared by digestion in aqueous acidic solution. It is also widely used for characterization of hydrogen storage materials in order to verify the purity of the synthesized compounds, especially for poorly crystalline samples or samples that might contain amorphous phases [79]. Unfortunately, ICP-AES technique is not the suited for quantification of nitrogen atoms. For that purpose, ion chromatography is used to quantify nitrogen content by analyzing the diffusion of $[\text{NH}_4]^+$ cations through an ion exchange membrane [98].

II.3.1. Mass Spectrometry

Mass Spectrometry (MS) ionizes a molecule by bombarding it with electron beam. This process splits the molecule to its fragments that will have various mass and charge values. These ionized species are further accelerated by electric field and to separate them, a magnetic field deflects them onto an electron multiplier detector. The signal detected for each species is integrated for various mass-to-charge ratios which provides a unique chemical fingerprint that can identify each molecule.

A typical ATG-MS study is conducted by Netzsch STA 449 - QMS 403C equipment under 20ml/min Ar flow and heating rate of 10 °C/min. Sample preparation was carried similar to DSC-TG experiments.

II.3.2. Raman and Infra-red Spectroscopy

As the excitation source, Raman spectroscopy employs a laser beam with wavelength in visible range of the spectrum. While infra-red (IR) spectroscopy scans through a certain range of frequencies in infra-red region. Both Raman and IR spectroscopy techniques probe the vibrational frequencies of various atomic bonds in the molecule. Despite this, they can provide complementary information to each other. Generally strong intensity IR peaks are weak in Raman spectroscopy and vice versa. This is mainly due to the fact that in a Raman active vibrational mode the molecule must experience polarizability change during the vibration while IR active modes require dipole change. Depending on the symmetry of the molecule Raman and IR active vibrational modes can be mutually exclusive.

Raman spectroscopy experiments were conducted by confocal Raman microscope (Renishaw) using airtight sample holder with a thin glass window transparent to 633 nm

red laser. In some cases, the sample holder was precooled to 5°C and wide beam spot is used to avoid the decomposition of the sample due to local laser heating.

FTIR measurements were performed using Bruker Vertex 70 in Attenuated Total Reflection (ATR) mode. A constant flow of nitrogen in the close vicinity of the sample is used to limit its exposure to air for the duration of the experiment.

II.3.3. Nuclear Magnetic Resonance Spectroscopy

Neutrons and protons forming the nuclei have a $\frac{1}{2}$ spin. Due to the internal structure of quarks that form them, the lowest energy state for a proton and a neutron is when they have parallel (not anti-parallel) spins. Spins of all the protons and neutrons in the nuclei adds up to overall spin value S . Therefore, atoms with even number of both neutrons and protons have spin $S=0$, therefore no NMR signal. On the other hand, the nuclei with $S=1/2$ is called dipolar while those with $S>1/2$ are known as quadrupolar nuclei. The magnetic dipole moment (μ) of atom represented as $\mu = \gamma S$, where γ is the gyromagnetic constant. For a given nuclei with spin number S , there is an associated magnetic quantum number m which only take values in $-S, S+1, \dots, S-1, S$. Hence, any nucleus has $2S+1$ angular magnetic states where each has magnetic momentum of $\mu = \gamma S = \gamma \hbar m$. The energy of each state depends on the applied magnetic field strength, $E = -\mu B = \gamma \hbar m B$. Hence, in the absence of magnetic field $B = 0$, these states have same energy levels (degenerate).

Under non-zero magnetic field, spins prefer to occupy lower energy states. This creates a net magnetization vector parallel to magnetic field. If this vector is not exactly parallel to B , it will precess around it with frequency $\nu_L = \gamma B / 2\pi$ (Larmor frequency). This precession does not affect the population of energy states. However, the population can be disturbed by electromagnetic excitation that has frequency matching to ν_L (usually in radio frequency range of electromagnetic spectrum). The electric coils are used to generate radio frequency (RF) pulse that induce rotation of magnetization vector and change its angle versus B . Length (time), and strength of the pulse define this angle. Magnetization vector will precess and decay towards equilibrium (parallel to B) while emitting RF signal that is detected in electric coils as NMR signal. This decaying signal acquisition is referred as Free Induction Decay (FID).

The electrons around the nucleus also have spins and magnetic moment which in general serves to minimize the applied external magnetic field by generating their own magnetic field in the opposite direction. This effect is known as “shielding”. Hence to achieve the resonance with nucleus, the ν_{RF} needs to be decreased due to lower effective magnetic field. This shift in resonance frequency is known as chemical shift. When electron density around the nucleus have high symmetry due to bonding geometry with neighboring atoms, we obtain “isotropic” chemical shift. However, if the symmetry is low the electron density will depend on the orientation of the molecule in the magnetic field. This “anisotropic” effect takes care of itself in solution, where the molecules rapidly tumble in random directions which results in averaging out of anisotropic NMR interactions. However, in solid-state NMR the molecular orientations are fixed. Hence, the anisotropic interactions can only be

suppressed by magic angle spinning (MAS). In MAS NMR the samples are spun around at several kilohertz at an angle that cancels anisotropic chemical shift signals. This angle is usually $\sim 54.74^\circ$ but $\sim 30.6^\circ$ is also used to minimize quadrupole interactions.

The effective magnetic field on the nuclei can also be affected by magnetic fields of neighboring nuclei. This spin-spin coupling effect results in splitting of chemical shift peaks. In solids, the dipole-dipole interactions of nuclei (direct dipolar coupling) broadens the chemical shift signal while nuclei with $S > 1/2$ have further broadening due to quadrupole interactions. An example to dipolar coupling would be proton bonded to carbon atoms. This coupling can be removed (decoupled) by continuously irradiating the protons.

The dipolar coupling of nuclei can be used to further probe the chemical environment through multichannel pulse sequence. In this sequence, one atom is irradiated by 90° pulse (that flips the magnetization vector 90°) followed by FID acquisition while the coupled atoms are continuously decoupled. This sequence is repeated several times for accumulation of signal. In between each sequence a relaxation time is needed for excited spins to return to equilibrium. There are two types of spin relaxation mechanisms: spin-lattice (longitudinal) and spin-spin (transverse). Spin-lattice relaxation (T_1) is the time needed to achieve full magnetization once the magnetic external field is applied. Spin-spin relaxation (T_2) is the time needed for the magnetization vector to decay from 90° to 0° versus external magnetic field. Inhomogeneity in magnetic field has an extra contribution resulting in T_2' , referred as the dephasing time. Any anisotropy in the system also changes T_1 and T_2 . A known pulse sequences are applied to measure these values.

For ammine metal borohydride compounds, we are interested in NMR spectra of hydrogen, boron and nitrogen atoms. NMR active ^{15}N isotope of nitrogen has a very low abundance, hence requires isotopic enrichment to increase the NMR signal. On the other hand, ^{11}B with 80% abundance suffers from lower spectral resolution due to quadrupolar effects. The double resonance experiments with proton decoupling $\text{B}^{11}\{-\text{H}^1\}$ helps to boost the signal intensity and suppresses signal broadening due to heteronuclear dipolar coupling. Hence, boron atoms directly bonded to protons benefit most from this effect. Strength of the quadrupolar interaction due to half-integer nucleus ($S = 3/2$) depends on the degree of the distortion of boron atomic site compared to the cubic symmetry. Boron sites with higher symmetry have small quadrupolar coupling constant which minimizes the distortion to usual Gaussian NMR signal. This effect results in broadening of the peaks which can be minimized by increasing the strength of the magnetic field [99]. Alternatively to get rid of the quadrupolar broadening, in order to obtain isotropic spectrum 2D ^{11}B multi-quantum (MQ) MAS experiments can be performed [100].

High-resolution solid-state ^{11}B and ^1H NMR spectra were recorded with a 4 mm Bruker CPMAS probe head on a Bruker AVANCE III DSX 500 spectrometer with an 11.74 T magnet operating at 160.4 MHz for the ^{11}B , and 500.18 MHz for the ^1H . The 4 mm (92 μL) diameter cylindrical double bearing rotors made of zirconia were used with specific airtight Teflon inserts which were filled inside glovebox with the sample powder. Experimental referencing,

calibration, and setup were done using solid powder NaBH_4 , its chemical shift was set to -42.06 ppm relative to the primary standard, liquid $\text{F}_3\text{B}\cdot\text{O}(\text{C}_2\text{H}_5)_2$ (where $\delta_{(11\text{B})}$ is set to 0.00 ppm). The probe exhibits a small, but manageable background ^{11}B signal due to boron nitride in the stators. The Hahn echo pulse sequence was generally effective at suppressing the background signal. ^1H NMR signals were acquired either with direct excitation or Hahn echos. Proton decoupling was applied during the acquisition of the FIDs. MAS spinning frequencies was generally set to 12 kHz. Data was processed using TopSpin 3.6 software.

II.4. Synthesis process

All the precursors, the chemicals and the solvents necessary for synthesis of highly energetic materials need to be kept free from oxygen and more importantly water. This introduces a lot of practical challenges from handling of the chemicals to performing the synthesis in air-free manner. The main tool necessary for storage and handling of these chemicals is glovebox. It is kept at slight overpressure of inert atmosphere which is continuously circulated through a water and oxygen scrubbing system. Typically, large amount of organic solvents cannot be handled inside the glovebox unless it is specifically adapted for this purposes.

II.4.1. Ball-milling

Ball-milling has been used for grinding the particle size of powder, alloying of the metals and providing mechanical energy source to enable chemical reaction (mechanochemical synthesis). Due to the high centrifugal forces involved in operational conditions of the ball-mills, they are usually limited to the laboratory or pilot scales. However, on these small scales, they have several advantages over solvent based chemical routes with higher reaction yield, lower reaction time and solvent free synthesis which amounts to efficient use of chemicals and energy [101].

The popular choice of materials for ball-mill pot and the balls are stainless steel, zirconia and tungsten carbide. A material with hardness sufficiently higher than the milled compound needs to be chosen. The number of balls in the pot needs to be in certain range (typically fills one third of the pot) to provide the optimum collision trajectory and frequency. The amount of energy delivered to milled material depends on the rotation speed, mass ratio of the balls to the milled material (ball-to-powder ratio), the milling time, the milling atmosphere and the temperature. Due to the complexity of the milling process, it is not possible to predict the necessary milling parameters for any system. However, by trying a range of parameters for a desired milling reaction, a synthesis recipe can be developed.

Higher yield of the reaction is generally achieved with higher milling rotation and time. However, if the powder does not coat the surface of the balls and the walls of the pot (ductile or brittle materials), the kinetic energy is wasted to wear and tear of the equipment, resulting also in contamination of the milled material. This effect is intensified (up to 7 times) for solvent assisted milling processes [101]. Hence, just enough milling rotation and time is needed to achieve desired yield of the reaction while preventing the contamination and the decomposition of the milled material. The decomposition of the compounds can happen due

to high temperatures in the milling pot which can be prevented by active cooling using water chiller or by regularly pausing the rotation and giving time for the heat dissipation from the system.

In mechanochemical synthesis, the temperature is the main factor that drives the exothermal self-sustaining reactions. During milling process, the kinetic energy acquired between consequent collisions is transferred as thermal energy onto the walls, the balls themselves and the powder that is crushed in the collision of the two. Nevertheless, the balls can reach much higher temperatures in range of 100-600°C depending on the milling conditions [102]. The temperature of the balls increases with:

- higher rotation speed of the planetary mill
- lower surface to mass ratio of the balls (bigger diameter)
- lower thermal conductivity of the inert gas
- lower gas pressure in the pot.

Ductile materials will stick and form a layer on the walls of the pot, while brittle materials will mostly remain free in the pot. In the former case, due to less interaction between the balls and the milled material, the temperature of the balls will be higher as the milled material will not participate in the heat dissipation process. This of course assumes that thermal conductivity of the milled material is higher than that of the inert gas in the pot. Hence the choice of inert gas in the pot is also important due to different thermal conductivity of gases (at 300 K and 1 bar) [103]:

Gas	Thermal conductivity (mW/Km)
Hydrogen	186.6
Helium	155.7
Nitrogen	26.0
Ammonia	25.1
Argon	17.7

Table 1: Thermal conductivity of common gases used in mechanochemical syntheses of hydrogen storage materials

Depending on the milling rotation and time, a fixed amount of energy needs to be delivered to the milled material to “ignite” the exothermal reaction. Keeping all the other milling parameters constant, the ignition time (the milling time required for ignition) decreases with increasing ball-to-powder ratio, ball diameter and density.

In a typical mechanochemical synthesis, 50 of 10 mm diameter steel balls (or 400 of 5 mm diameters balls) were transferred into ball-mill pot with total 125ml of volume. The typical ball-to-powder ratio is usually kept as 35 or 70. The ball-mill pot is sealed in the glovebox and connected to Retsch Emax milling machine. Typical rotation speed was selected in 300 to 500 rpm range. Every 2 mins the rotation was paused for 2 minutes to avoid over-heating of the balls. Retsch Emax is not a planetary ball-mill, nevertheless it works on a similar principle (Figure II-1). The main advantage of this machine is the integrated temperature sensor and the active cooling systems through the walls of the milling pot. Internal cooling

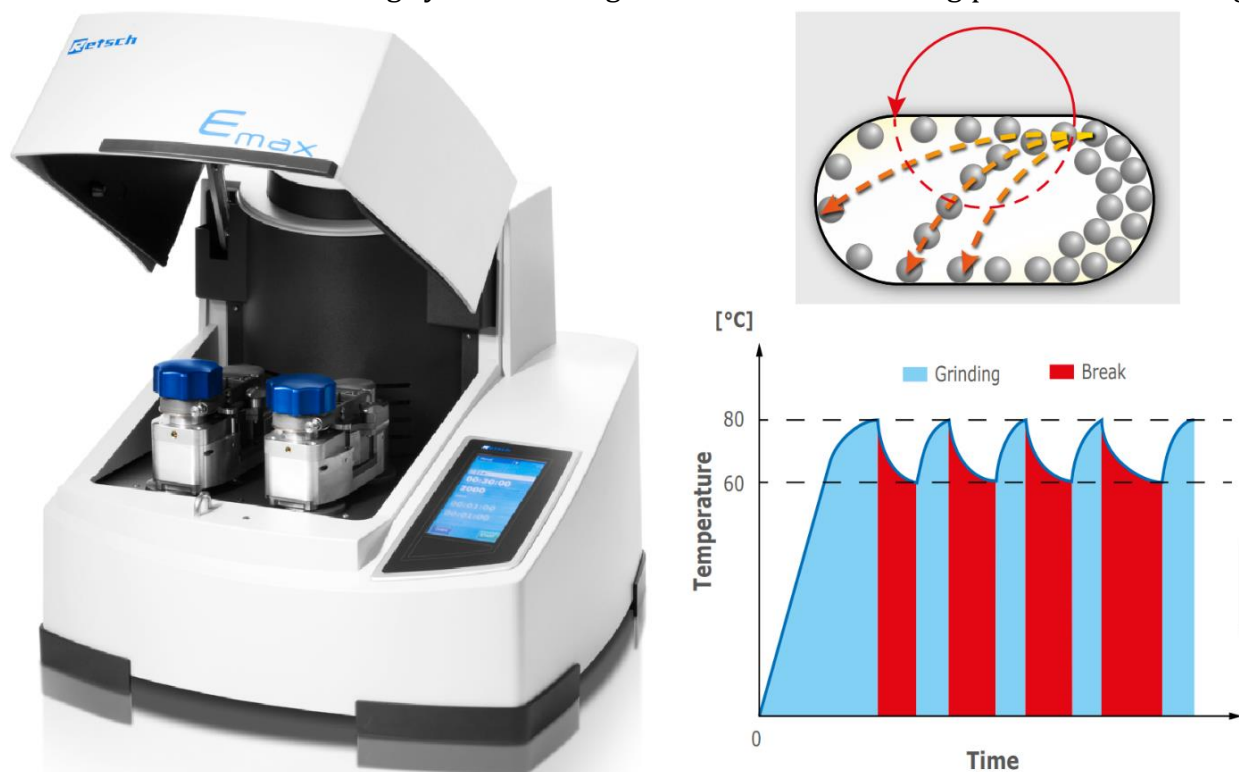
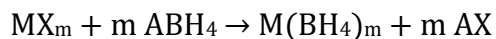


Figure II-1: Retsch Emax, diagram of the ball trajectory during the temperature-controlled milling process

system can be enhanced by external chiller as well enabling synthesis below room temperature down to 5°C. Temperature sensors allow the control of synthesis process in a predefined temperature window to avoid sample heating and unintentional decomposition.

II.4.2. Review of mechanochemical synthesis of metal borohydrides

A typical synthesis reaction in mechanochemical synthesis is the salt metathesis reaction, in ideal case it can be written as:



, where X = F, Cl, Br, I and A = Li; Na; K; Ca. However, in reality formation of bimetallic phases $\text{A}_n\text{M}(\text{BH}_4)_{m+n}$, complex salts $\text{A}_n\text{MX}_{n+m}$ as well as mixed anionic compounds $\text{MCl}_n(\text{BH}_4)_{m-n}$ are possible. The choice of metal fluoride precursor lowers the kinetics of the metathesis reaction which might slow the decomposition of metal borohydride phase at milling

temperatures as shown for $\text{Ti}(\text{BH}_4)_3$ intermediate phase [104]. However, fluoride precursor might also completely prevent the formation of the metal borohydride phase as shown for YF_3 [105].

Most metal borohydrides are synthesized using corresponding metal chloride precursors. Hence, to claim that anion substitution with metal fluoride, bromide or iodide precursors does not occur would be a statistically skewed analysis. Nevertheless, a ball-milling study with $\text{Ca}(\text{BH}_4)_2\text{-CaX}_2$ mixtures showed that unlike CaCl_2 no anion substitution occurs with CaF_2 or CaBr_2 precursors [106]. It is difficult to generalize this result as well, however it is safe to assume that similar substitution will be easier with halides that have similar ionic radius to $[\text{BH}_4]^-$ (Table 2). Fluoride anions are too small to replace $[\text{BH}_4]^-$ anion but they may replace H^- anion. However, $\text{H}^- \rightarrow \text{F}^-$ substitution process is only achieved by mechanochemical reaction of $[\text{BH}_4]^-$ groups with $[\text{BF}_4]^-$ groups [107]. Metal fluoride precursors have similar properties to metal hydrides hence they are also used for destabilization of other complex hydride compounds. However, due to the significantly higher electronegativity difference, they form more stable decomposition byproducts such BF_3 [108].

Anions	Ionic radius [\AA]	Cations	Ionic radius [\AA]
F^-	1,33	Li^+	0,76
H^-	1,40	Na^+	1,02
Cl^-	1,84	$[\text{NH}_4]^+$	1,37
$[\text{BH}_4]^-$	1,94	K^+	1,38
Br^-	1,96		
I^-	2,20		
$[\text{BF}_4]^-$	2,32		

Table 2: Ionic radii of common anions and cations involved in synthesis process of metal borohydrides and their derivatives

II.4.3. Review of solvothermal synthesis of metal borohydrides

Solvothermal synthesis typically refers to the reaction of precursors in a non-aqueous solvent at high temperatures and pressures. However, in literature this term also used for the choice of 1 atmosphere pressure and room temperature conditions. In this thesis, I will adopt this meaning of the term referring to any synthesis in organic non-aqueous solvent under any pressure and temperature conditions.

Alkali borohydrides similar to other hydrides are used as reduction agents in organic chemistry. This limits the number of possible solvents that are stable with alkali borohydrides. As commercially most available sources of borohydride, NaBH_4 tend to react strongly with protic solvents, hence polar aprotic solvents are needed to solvate the ionic alkali borohydrides. For a successful metathesis reaction in an organic solvent, at least the metal chloride or the alkali borohydride must be adequately soluble in it. In the table below the solubility values of several precursors and byproducts in common organic solvents are listed:

	LiBH ₄	NaBH ₄	KBH ₄	LiCl	NaCl	KCl	NaF
Methanol	reaction	16.4 g/ 100 ml	0.56 g/ 100ml	43,9 g/ 100 g	1,39 g/ 100 g		0,4 g/ 100 g
Ethanol	44 g/ 100g	4g/ 100g	0.25 g/ 100ml	24,5 g/ 100 g	0,07 g/ 100 g		0,1 g/ 100 g
Et ₂ O	4,28 g/ 100 g	Insoluble	Insoluble	0.6 mg /100g	Insoluble		
THF	28 g/ 100 g	0.1 g/ 100 g	Insoluble	4.3 g/ 100g			
Dioxane	0.3 g/ 100 g		Insoluble	2.7 g/ 100g			
DMF		18 g/ 100 g	1,2 g/ 100 g	11 g/ 100g	0,04 g/ 100g	0,05 g/ 100 g	0.2 mg/ 100 g
Isopropylamine	1.27M	6 g/ 100 g	Insoluble				
Dimethyl sulphoxide			7,6 g/ 100 g		0,5 g/ 100 g		
Liquid ammonia	30,4 g/ 100 g @ 0°C	104 g/ 100 g @ -33°C	20 g/ 100 g @ 10°C	1,41 g/ 100 g @ 0°C	12,9 g/ 100g @ 0°C	0,13 g/ 100g @ 0°C	0,35g/ 100g

Table 3: Solubility values are given for temperature range of 25-30°C unless otherwise stated, some of the values are taken from references [109], [110].

Since most of the metal chlorides are not soluble in the solvents listed in Table 3, it is important to choose the solvent with highest alkali borohydride solubility.

In general, the equilibrium of any chemical reaction in any medium depends on temperature and the concentration (of the precursors and the products). For solvothermal synthesis, this reaction medium is the chosen solvent, and the concentration of the solutes depends on the solubility of the precursors and the products. If at least one of the final products is not a precipitate or a volatile gas hence remains soluble in the selected solvent, this reaction will not reach to the completion (rather an equilibrium). For example, Et₂O despite having good solubility for LiBH₄ when reacted with MgCl₂ in 2:1 ratio yields Li_xMgCl_y(BH₄)_{3-y}·Et₂O type complex solvate phase. On the other hand, MgCl₂ reaction with NaBH₄ results in formation of the only soluble product in diethyl ether which is Mg(BH₄)·Et₂O. NaCl byproduct is not soluble in Et₂O hence contamination of the main phase with chloride anions is also avoided. However NaBH₄ is also nearly insoluble in Et₂O hence without the assistance of mechanochemical ball-milling the yield of this reaction remains very low [111].

Amine solvents such as isopropylamine are interesting to avoid sodium chloride contamination of the main phase since they can solvate NaBH₄ while NaCl remains insoluble. Although, precise 1:2 ratio of MgCl₂:NaBH₄ reaction delivers Mg(BH₄)₂ solvates with 70%

yield, it is mainly contaminated with NaBH₄ phase. Nevertheless, a contamination with NaCl phase was also observed which was speculated to be due to the precipitation of NaCl on the surface of MgL₆Cl₂ solvate phase [111]. To synthesize a pure metal borohydride with high yield using metathesis reaction, ideally only M(BH₄)_m phase must be insoluble in a chosen solvent.

The contamination with chloride phases can be circumvented by using MgH₂ or Mg(C₄H₉)₂ (butyl magnesium or MgBu₂) type precursors instead of MgCl₂. The reaction of metal hydrides with borane complexes L·BH₃ where L = THF; TEA; DMS is based on nucleophilic addition mechanism:

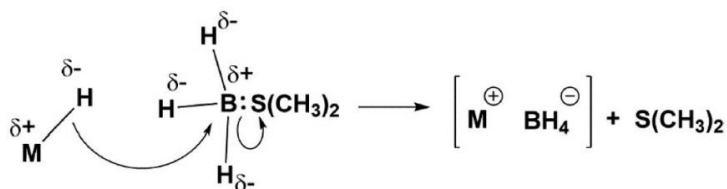
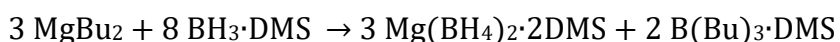


Figure II-2: Mechanism describing the nucleophilic addition reaction between metal hydride and dimethyl sulphide borane complex, figure taken from reference [112]

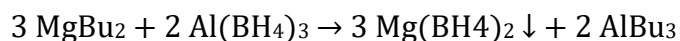
This reaction only takes place if the M-H bond is ionic or polar-covalent type. These reactions result in formation of metal borohydride solvates with 85-95% yield range with high purity. Despite being an efficient synthesis technique it is only applicable for alkali or alkali earth borohydrides since other metals cannot form stable ionic or polar-covalent metal hydride phases [112].

Similarly, borane complexes can also be reacted with organometallic precursors:



This reaction when conducted in large excess of BH₃·DMS is reported to yield pure Mg(BH₄)₂·2DMS precipitate. While B(Bu)₃·DMS byproduct is soluble in toluene and can be removed from it, the preparation of unsolvated Mg(BH₄)₂ phase requires dynamic vacuum of 10⁻⁵ mbar at 75 °C for 13 hours to remove all DMS [113].

The only example of direct synthesis of unsolvated magnesium borohydrides is based on:



reaction which achieves 85% yield thanks to the poor solubility of Mg(BH₄)₂ in toluene as opposed to Al(BH₄)₃ as well as MgBu₂ and AlBu₃ precursors. While MgBu₂ is a commercial product, toluene solution of Al(BH₄)₃ needs to be prepared by metatheses reaction of AlCl₃ and LiBH₄. Due to the high volatility of pure Al(BH₄)₃ it is distilled away from the LiCl precipitate as toluene solution. After its reaction with butylmagnesium, pure unsolvated Mg(BH₄) is precipitated due to the non-coordinating property of toluene unlike strong Lewis base (donor) solvents mentioned up to now [113]. Nevertheless, this technique is not applicable to other metal borohydride synthesis. This is mainly due to fact that the metal

alkyl precursors similar to MgBu_2 are either unstable for other metals or they are not commercially available. Additionally, $\text{Al}(\text{BH}_4)_3$ is a very volatile and explosive compound in contact with air which limits its value proposition.

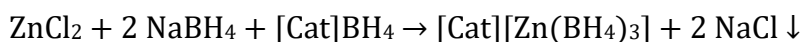
Obviously, the main disadvantage of solvothermal synthesis of metal borohydrides involves the formation of solvate phases $\text{M}(\text{BH}_4)_m(\text{L})_n$ where L is a strong Lewis base (electron donor solvent molecule). The usual approach to remove the solvent adducts is to heat the solvate phase under high dynamic vacuum. The ease of removing the solvent without decomposing the $\text{M}(\text{BH}_4)_m$ phase determines the popular choices such as Me_2S and Et_2O . This task becomes even more difficult with higher electronegativity metal borohydrides since their decomposition temperatures are lower, making it challenging to obtain unsolvated high electronegativity metal borohydrides through solvothermal routes [114]. Even for low electronegativity metal borohydrides, theoretically possible synthesis routes do not guaranty experimental success as explored solvothermal approaches to unsolvated pure $\text{Y}(\text{BH}_4)_3$. Although, YCl_3 and LiBH_4 metathesis reactions in THF was confirmed to deliver yttrium borohydride solvate, nevertheless it was not possible to dissociate THF ligands without decomposing the $\text{Y}(\text{BH}_4)_3$ phase. Alternatively, solvothermal reactions of YCl_3 , YF_3 , YH_3 , $\text{Y}(\text{OC}_4\text{H}_9)_3$ type precursors in various non-coordinating solvents like toluene, dichloromethane, n-hexane did not produce the desired product [105]. Later, YCl_3 and LiBH_4 metathesis reaction performed in 2M of $\text{DMS}\cdot\text{BH}_3$ complex in toluene to obtain a $\text{Y}(\text{BH}_4)_3\cdot\text{DMS}$ solvate which was then solubilized in large quantity of DMS solvent (1g powder in 20ml of solvent) to filtrate the LiCl precipitate. Finally, the DMS ligands were possible to remove from the solvate at 50°C under dynamic vacuum [115]. The reaction of YH_3 with excess $\text{DMS}\cdot\text{BH}_3$ complex in toluene followed by solvent extraction also yielded pure unsolvated $\text{Y}(\text{BH}_4)_3$ [112]. Hence, despite its unpleasantly strong smell and low solubility, dimethyl sulfide remains a popular solvent for synthesis of pure unsolvated metal borohydrides.

The solvates of metal borohydrides tend to yield oily greasy compounds (sometimes dry crystalline as well) that are not suitable for studying the dehydrogenation properties of the corresponding metal borohydride. Solvent ligands can stabilize the metal borohydride and result in decomposition at higher temperature. Additionally, released hydrogen will be contaminated by solvent and its decomposition byproducts. Conversely, the advantage of the solvothermal synthesis is the ability to filtrate alkali halide byproducts. Contrary to solvent adducts, the alkali halide byproducts does not influence thermodynamic properties of the metal borohydride [46]. Nevertheless, if not removed from the main phase both solvent adduct, and the alkali halides becomes “dead weight” which decrease the effective hydrogen capacity of the metal borohydride phase.

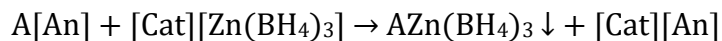
Although mechanochemical synthesis allows rapid screening of possible metal borohydride compounds, the separation of alkali halide from the main phase is not possible. Therefore, solvent assisted mechanochemical synthesis can combine the advantages of both techniques. After ball-milling, the borohydride phase remains in solution while alkali halide by-product precipitates. The right choice of solvent is important to facilitate sufficient solubility and at

the same time to avoid irreversible solvate formation. In case of low solubility, mechanochemical synthesis product mixtures can be purified by solvent extraction technique that recycles the small quantity of solvent (Soxhlet extraction). Due to the substantial density difference between metal borohydride and alkali halide phases, it is tempting to separate them by floating the light phase (or sinking the heavy phase) in an inert non-coordinating solvent mixture with the suitable density. However, in practice this technique fails due to intergrown micro-crystallites of metal borohydride and alkali halides that constitute the aggregate particles of the final product [105].

The mechanochemical synthesis of bimetallic borohydrides $A_xM(BH_4)_{x+m}$ is rather easily controlled by stoichiometry of the precursors. In solvothermal synthesis, the thermodynamically most stable phase tend to dominate. The stoichiometry of alkali borohydride only minimizes the halide substitution or the alkali borohydride contamination of the main phase. Hence, obtaining alkali halide free bimetallic borohydrides are difficult in unsolvated form. This problem can be bypassed by making the metal borohydride phase soluble in non-coordinating, non-polar solvents via complex formation with bulky cations and anions. For example:



In this reaction $[Cat]^+$ is bulky cation such as $[nBu_4N]^+$, together with $[Zn(BH_4)_3]^-$ bulky counter anion, $[Cat][Zn(BH_4)_3]$ becomes soluble in solvents such CH_2Cl_2 , $CHCl_3$, or toluene leaving behind $NaCl$ sediment. Once the alkali halides are filtrated from the solution it can be reacted with alkali salts of bulky anions $[An]^-$ such as BARF, $[B\{3,5-(CF_3)_2C_6H_3\}_4]^-$ [51]:



Bimetallic phase precipitates leaving the soluble salt of $[Cat][An]$ in CH_2Cl_2 . Unfortunately, $[Cat][M(BH_4)_{m+1}]$ type compounds cannot be turned into pure $M(BH_4)_m$. For example $[nBu_4N][Al(BH_4)_3]$ is stable up to $90^\circ C$ and decomposes exothermally around $150^\circ C$ releasing impurity gases such as butane besides hydrogen [116]. Nevertheless this technique is very powerful for the synthesis of pure unsolvated bimetallic borohydrides as demonstrated for a series of $AY(BH_4)_4$ compounds for all the member of alkali metals (A) [52]. Even thermodynamically unstable compounds such as $LiZn(BH_4)_3$, $LiY(BH_4)_4$ that are not possible to synthesize by mechanochemical approach, were successfully synthesized by this technique. Upon synthesis, these compounds proceeded by gradual decomposition at room temperature. Unfortunately, prohibitively expensive cost of bulky cation and anion salts limits the use case of this synthesis process to the laboratory scale.

As a conclusion, synthesis of high electronegativity transition metal borohydrides due to the lack of precursors in their metal hydride or organometallic form, limits their synthesis to metathesis reaction by mechanochemical or solvothermal routes using polar aprotic solvents. Solvent assisted mechanochemical synthesis allows the formation of metal borohydride solvates and alkali halide filtration. Due to the significant affinity of transition metals to polar coordinating solvents, in most cases they cannot be removed below

decomposition temperatures of the metal borohydride phase. Additionally, solvent adducts stabilize high electronegativity metal borohydrides hence their synthesis in unsolvated form might require cooling below room temperature. Nevertheless, described problems are not of concern, if the goal is to synthesize ammine metal borohydrides. We have already discussed the advantages of ammoniation of high electronegativity metal borohydrides in Chapter 1. Henceforth, I will only focus on their synthesis. The main synthesis approach for ammine metal borohydrides involves two steps:

- first, metal borohydride phase is synthesized by mechanochemical or solvothermal routes,
- then, it is exposed to ammonia atmosphere to form ammine metal borohydride.

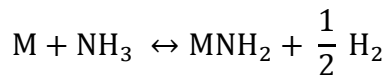
As long as the solvent adduct is a weaker Lewis base than the ammonia, exposure of the metal borohydride the solvate (or solution) to the ammonia atmosphere will yield ammine metal borohydride (base displacement reaction). Alternative approach is to perform mechanochemical synthesis under ammonia atmosphere [117].

Liquid ammonia can also be used as a solvent for the direct synthesis of ammine metal borohydrides. In fact, a report from 1956 demonstrates synthesis of $\text{Co}(\text{BH}_4)_3(\text{NH}_3)_6$ and $\text{Cr}(\text{BH}_4)_3(\text{NH}_3)_6$ in liquid ammonia. The metathesis reaction between metal fluoride and NaBH_4 precursors were performed in temperature range of -45°C to -65°C . The choice of metal fluoride precursors was necessary to obtain ammonia insoluble (almost insoluble, Table 3) NaF byproduct as opposed to ammonia soluble ammine metal borohydrides. Soxhlet type extraction of the main phase was performed to obtain pure phase. The challenge with this synthesis process was keeping various parts of the borosilicate glass reactor at necessary low temperature and avoid evaporation of the ammonia [118]. Another patent from 1958 presents an electrochemical synthesis approach of pure $\text{Mg}(\text{BH}_4)_2(\text{NH}_3)_6$ and $\text{Ca}(\text{BH}_4)_2(\text{NH}_3)_6$ compounds using Mg or Ca metal anode and mercury anode submerged into liquid ammonia solution of NaBH_4 . Synthesis was performed at -33°C in glass electrolysis cell. Upon oxidation M^{2+} cations dissolved into the electrolyte reacting with $[\text{BH}_4]^-$ species, while mercury cathode forms NaHg amalgam. This study also indicates drop in ionic conductivity of the electrolyte due to solubility of $\text{Mg}(\text{BH}_4)_2$ in liquid ammonia [119]. A more recent 2015 study synthesized $\text{Fe}(\text{BH}_4)_2(\text{NH}_3)_6$ and $\text{Co}(\text{BH}_4)_2(\text{NH}_3)_6$ compounds for the first time by metathesis reaction of metal chloride with LiBH_4 in liquid ammonia at -50°C . Notably the main phases were accompanied by $\text{M}(\text{NH}_3)_6\text{Cl}_2$ and $\text{M}(\text{NH}_3)_6(\text{Cl}_x\text{BH}_{4-x})_2$ type byproducts [71].

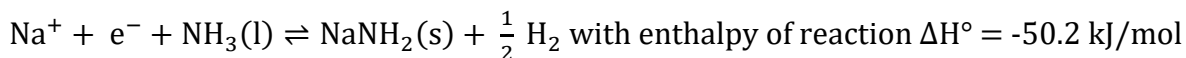
Ammonia can liquefy below -33.35°C under 1 atmosphere. Liquid ammonia is one of the few non-aqueous solvents that is amphiprotic (both proton donor and acceptor), hence very similar to water. Although much weaker than water, ammonia can self-ionize into: $2\text{NH}_3 \leftrightarrow \text{NH}_4^+ + \text{NH}_2^-$. Ammonia is more basic than water due to higher stability of ammonium cations compared to hydronium cations in water. A particularly unique ability of liquid ammonia is solubility of alkali and alkali earth metals as dissolved electron and metal cation [120]:



This solution becomes a very strong reducing agent and can even reduce chemically inert compounds such as polytetrafluoroethylene (PTFE) [121]. Remarkably, alkali metal solution is even stable at room temperature for long time thanks to the equilibrium of another reaction:



In fact, an infrared spectroscopy (at 1356nm wavelength) study demonstrated this equilibrium using liquid ammonia solution of NaNH₂ under varying hydrogen pressure:



The concentration of the electrons was measured by the absorption of the IR signal. Hence, it was observed that the dissolved electron concentration increased proportionally with the square root of the applied hydrogen pressure. The equilibrium constant of the reaction was calculated to be 3×10^9 [122].

Ammonium salts NH₄X make the liquid ammonia more acidic while alkali amides ANH₂ more basic. Interestingly, if sufficient amount of NH₄NO₃ is dissolved in liquid ammonia (0.83 mol%) the vapor pressure of the solution (aka Divers' solution) can be decreased down to 400 mbar at 0 °C (less than 1bar at 25°C). Unlike other alkali or alkali earth metals, Mg metal is sparingly soluble in liquid ammonia. Hence NH₄I ammonoacidic catalyst is necessary for the formation of Mg(NH₂)₂ phase in liquid ammonia [123].

At a given temperature, the solubility of metal halide increases in relationship of F<Cl<Br<I. Ammonium salts are in general most soluble in liquid ammonia. Ammonia is a stronger Lewis base than water. Just like the formation of metal chloride hydrates, the chlorides of magnesium, calcium, zinc, manganese, nickel, copper, iron form ammoniates M(NH₃)_nCl_m that are insoluble in liquid ammonia. The number of coordinated ammonia molecules can range from 10 to 1 depending on the oxidation number of the metal cation and nature of the halide anion (typical number is 6). Metal halides with +4, +5 or +6 oxidation number of metal such as TiCl₄, ZrCl₄, VF₅, NbF₅ and WCl₆ upon reaction with ammonia undergo ammonolysis and form M(NH₂)_nX_{m-n} type ammoniates [124]. Alkali and alkali earth fluorides including NH₄F are generally known as insoluble in liquid ammonia [125]. However, a 1952 U.S. Air Force report published 1.9mg/100g solubility for NH₄F in liquid ammonia [126].

Due to low solubility of many inorganic compounds in liquid ammonia compared to water, the synthesis products might be poorly crystalline or amorphous. However, the solubility shortcomings of the ammonia can be overcome under supercritical conditions:

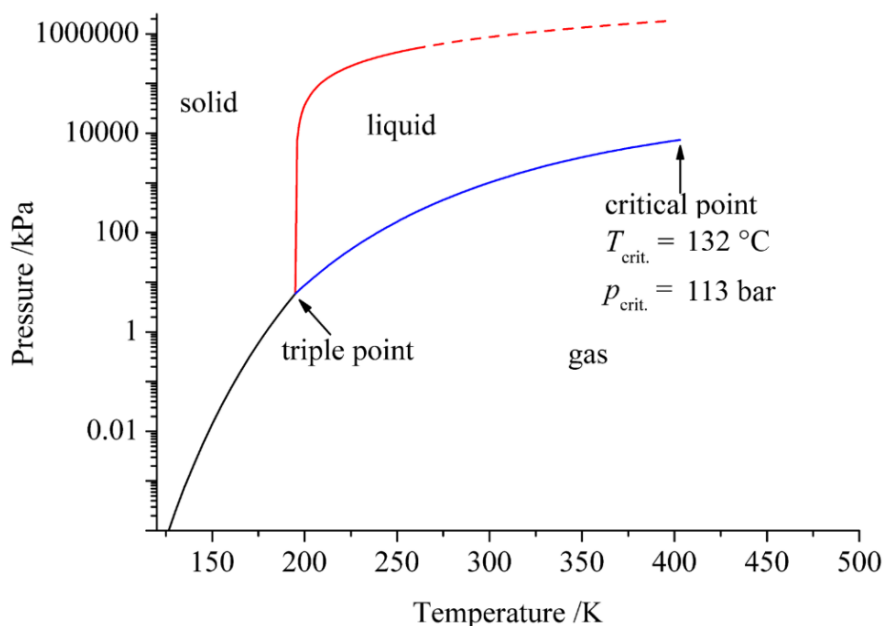


Figure II-3: Pressure-temperature diagram of ammonia (figure from reference [127])

Unfortunately, as can be seen from Figure II-3, the supercritical ammonia requires a reaction vessel (autoclave) that can withstand at least 113 bar pressure at 132 °C. These conditions are particularly useful for single crystal growth. Even below supercritical conditions increased temperature and pressure guarantees improved solubility of inorganic ionic solids [127].

II.4.4. Solvothermal synthesis equipment

Air sensitive precursors were always stored in glovebox which have below 0.5 ppm oxygen or water and filled with inert Ar gas. The common organic solvents were kept in glovebox as well. When possible, anhydrous precursors and solvents were purchased for use in synthesis. For solvents when anhydrous option was not available, they were frozen by liquid nitrogen under dynamic vacuum, or Ar was bubbled through a submerged needle in the solvent for a few hours to remove solvated gases such as oxygen. Molecular sieves were further utilized to remove solvated water molecules in the organic solvent. For solid precursors when anhydrous option was not available, they were dried under dynamic vacuum while being heated to 100°C for at least 24 hours before transfer into the glovebox.

The precursor mass was usually measured and transferred into the either glass (borosilicate) or stainless steel (Swagelok) reactors. Gloveboxes cannot handle too much solvent unless they are specifically designed for this purpose. Hence, the synthesis reactions has been always performed outside the glovebox in air-free manner. The transfer of solvents or precursors into the reactor, filtration, solvent extraction processes require the use of Schlenk line. I had the joy of building my Schlenk line since there was none available in the beginning of the thesis project. Main component is the Schlenk manifold made from glass:

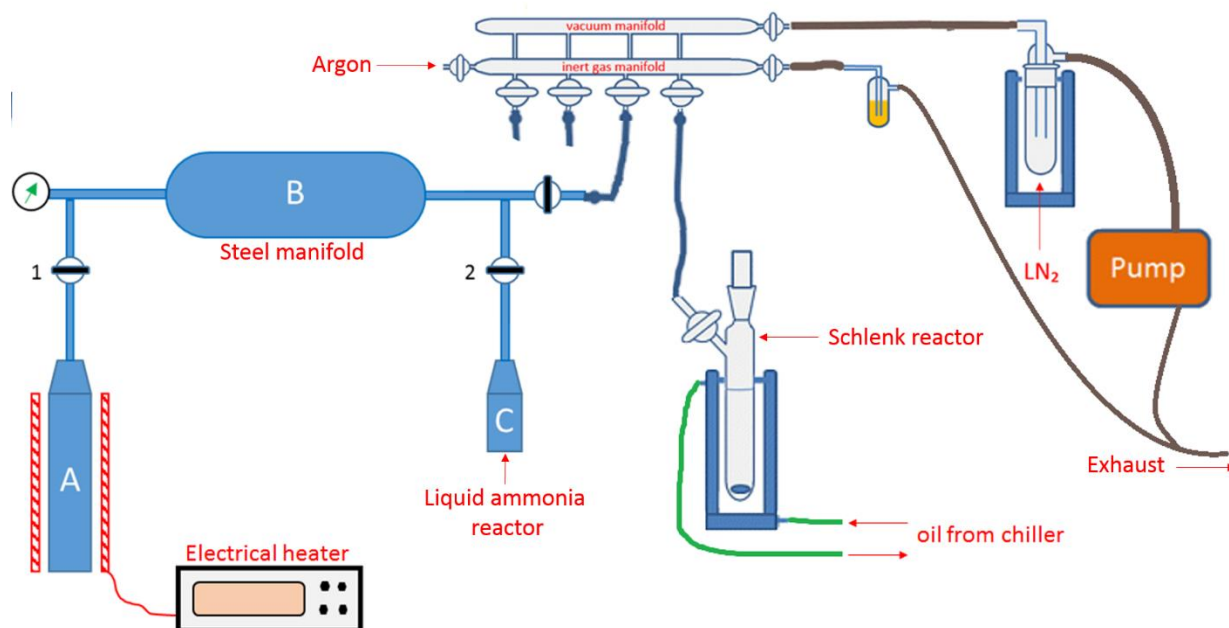


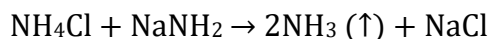
Figure II-4: Diagram of the Schlenk line and Ammonia reactor assembly

It consists of two tubes and several valves that connected to both and allows seamless switching between them. “Inert gas manifold” is connected to argon or nitrogen line from one end and the air is prevented from entering to this manifold by keeping the inert gas overpressure. This is achieved by bubbling the excess gas continuously through a silicone oil. The “vacuum manifold” is connected to vacuum pump with cold trap in between. The cold trap is usually cooled by liquid nitrogen to recover the solvents used in synthesis process. The lubrication oils or plastic components of the typical pumps are easily degraded by organic solvents, so the cold trap also serves an important role for protecting the most expensive component of the Schlenk line. The alternative approach is to use diaphragm pumps which cannot achieve as high vacuum levels as the other pumps but are chemically resistant to many organic solvents. The choice of the plastic tubing to connect these various components of the Schlenk line is important to maintain high vacuum and low air contamination. Some consideration to be taken into account are their chemical resistance to the organic solvents, silicone oil and low air permeability. To maintain high vacuum, all glass joints need to be lubricated with vacuum grease. Care also needs to be taken for not contaminating the synthesis process if the grease is soluble in chosen solvent (such as THF and hexane).

As discussed in previous section, $M(\text{BH}_4)_m(\text{NH}_3)_n$ type compounds were synthesized by metathesis reaction in an organic solvent using a glass reactor followed by exposure to ammonia gas at room temperature. Alternatively, direct synthesis in liquid ammonia was performed at temperature below -33°C . In all cases, an ammonia bottle is directly connected to Schlenk line and used as the ammonia source in the synthesis processes. These bottles are commercially available in which anhydrous ammonia remains liquefied under 10 bar vapor

pressure at room temperature. Due to strict safety regulations of CEA-LITEN, purchase of such a bottle or its use as ammonia gas in glass Schlenk reactor was not permitted. So, I had to find an alternative approach to this restriction.

The solution was to generate the anhydrous ammonia needed for each synthesis. Most examples with ammonia generation reactions in literature included formation of water alongside ammonia. Hence, after certain exploration I decided to test following reaction:



The easiest way to verify this reaction was to perform TG-DSC analysis:

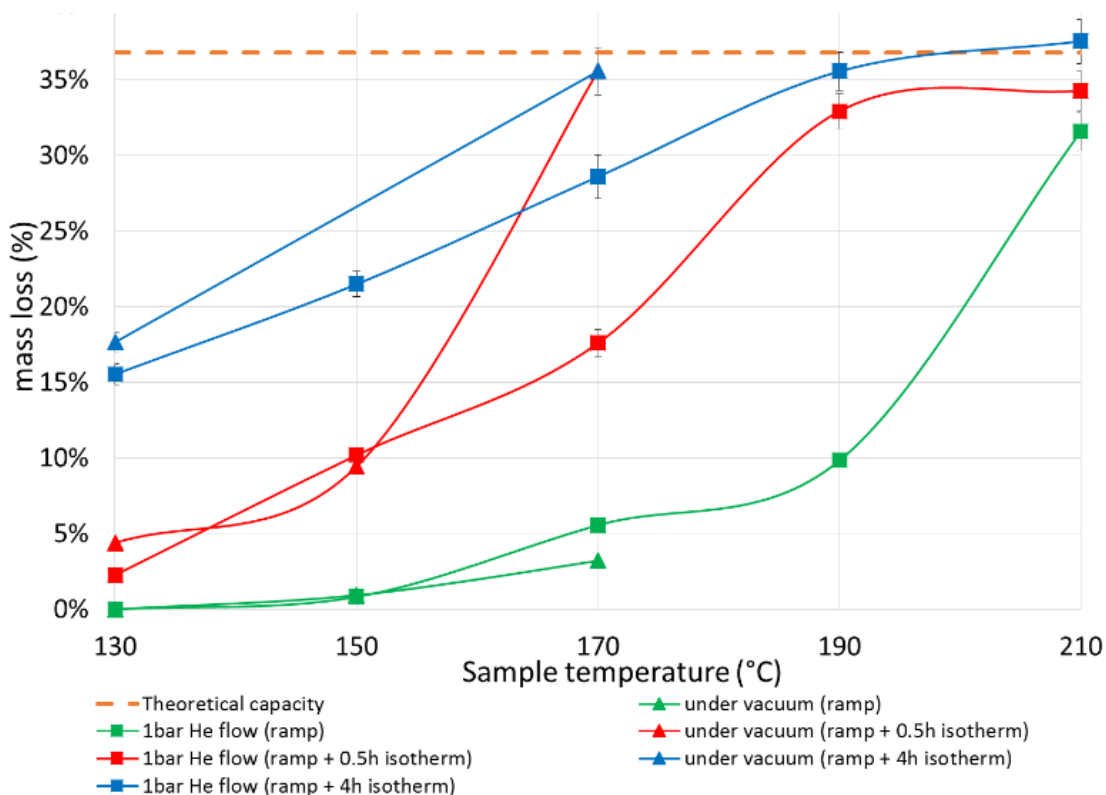


Figure II-5: TG result of NH_4Cl – NaNH_2 mixture heated $10^\circ\text{C}/\text{min}$ (ramp) then held at the certain temperature up to 4 hours (isotherm). The dashed orange line represents the theoretical ammonia capacity of the mixture, $\sim 37\text{wt}\%$.

Thermogravimetric analysis indicated that dynamic heating of the reaction mixture to 170°C and keeping there for less than 15 minutes resulted in weight loss corresponding to theoretical ammonia capacity (Figure II-5). Alternatively, under 1 bar inert atmosphere reaction mixture can be heated to 200°C dynamically to release most of the ammonia gas. However, since NH_4Cl can decompose into ammonia and hydrogen chloride while NaNH_2 can generate ammonia and hydrogen upon heating, it was important to verify that the mixture of these compounds upon heating will only release anhydrous ammonia and most importantly not hydrogen. Hence, MS experiment was performed to verify the purity of the released ammonia gas:

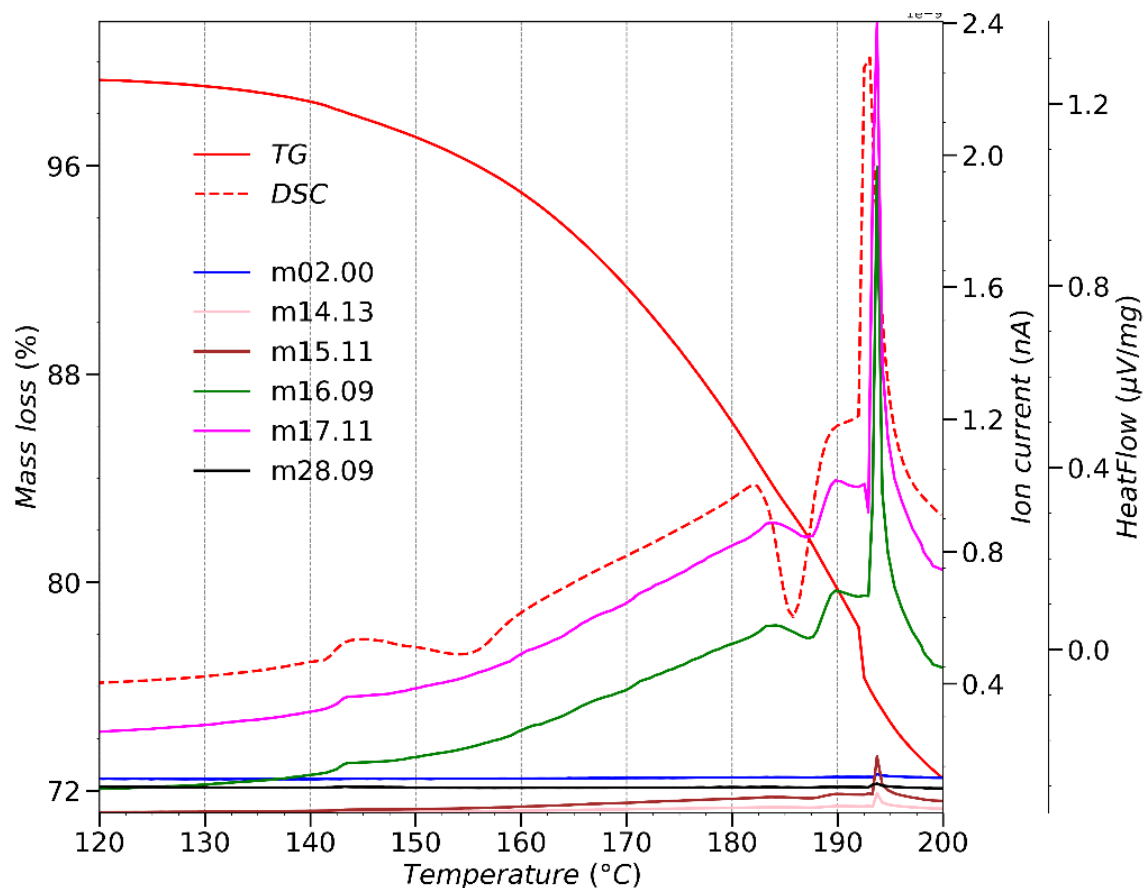


Figure II-6: DSC-TG-MS study of released gases from $\text{NH}_4\text{Cl}-\text{NaNH}_2$ reaction mixture

MS analysis confirmed the generation of only ammonia ($m/e = 16, 17$) while no signal was detected for hydrogen ($m/e = 2$) or hydrogen chloride ($m/e = 36$). Hence, the reaction mixture was proven to generate predictable amount of pure anhydrous ammonia.

To prevent any possibility of unintentional ammonia leakage, a stainless-steel manifold was built from Swagelok parts that can withstand 60 bar pressures and connected to Schlenk line (Figure II-4). During a typical liquid ammonia synthesis, 1:1 premixed $\text{NH}_4\text{Cl}-\text{NaNH}_2$ powder would be weighed and transferred into the A reactor. It was heated by electric heater and generated ammonia would be stored in larger volume of reactor B. For a typical liquid ammonia synthesis, reactor C containing the precursors cooled down by liquid nitrogen and ammonia condensed into it. The valve 2 closed and the reactor C heated up to desired reaction temperature. Typical synthesis process was conducted either at RT or at 60°C (the temperature is limited by 60 bar safety limit of Swagelok reactor and the ammonia vapor pressure, for example at 98°C ammonia vapor pressure can reach 51.2bar [128]).



Chapter III

Synthesis and characterization of ammine
zinc borohydrides



III. Synthesis and characterization of ammine zinc borohydrides

III.1. Objective

One of the two goals of the work described in this chapter is to obtain most economically scalable synthesis approach for pure $\text{Zn}(\text{BH}_4)_2(\text{NH}_3)_2$. As we discussed in Chapter 1, it has one of the lowest ammonia impurity levels among ammine metal borohydrides with reasonable hydrogen capacity that can be released without the need to exceed suitable temperature range for PEM fuel cell system (150°C). Second goal is to use related compounds to $\text{Zn}(\text{BH}_4)_2(\text{NH}_3)_2$ as a test bed for studying various factors that might affect the decomposition process and the hydrogenation properties of ammine metal borohydrides. Instead of comparing many different ammine metal borohydrides, the objective is to focus on a system that can exclude the effects of various synthesis approaches, different crystalline structures, number of ammonia adducts, electronegativity changes of the central metal cations and other impurity phases.

III.2. Literature review on synthesis of zinc borohydride solvates

The reaction of ZnCl_2 and LiBH_4 (or NaBH_4) in 1:2 ratio in Et_2O solvent results in formation of $\text{Li}_y\text{ZnCl}_{x+y}(\text{BH}_4)_{2-x}$ type equilibrium phase. Despite LiCl byproduct being almost insoluble in Et_2O , the equilibrium phase is obtained due to solubility of LiCl in the presence of $\text{Zn}(\text{BH}_4)_2$ as $\text{LiZnCl}(\text{BH}_4)_2$ species. ZnBr_2 and ZnI_2 precursors result in formation LiBr or LiI byproducts that are more soluble in ether than LiCl . Nevertheless, chloride-free $\text{Li}_2\text{Zn}(\text{BH}_4)_4 \cdot 3\text{Et}_2\text{O}$ solvate can be obtained by using LiBH_4 in excess (in 1:4 molar ratio) [129].

In contrast to lithium borohydride, NaBH_4 is insoluble in Et_2O . Nevertheless, due to slight solubility of ZnCl_2 in ether the reaction does take place in excess of NaBH_4 although much slowly, resulting in formation of bimetallic borohydride phase:



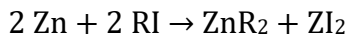
By contrast this reaction is much faster in THF. $\text{NaZn}(\text{BH}_4)_3 \cdot 3\text{Et}_2\text{O}$ and $\text{NaZn}(\text{BH}_4)_3 \cdot 4\text{THF}$ type solvates can be extracted from the solutions. Contrary to ZnCl_2 , zinc bromide and iodide precursors do not react with NaBH_4 in Et_2O . Unlike the THF solvate, the ether solvate can be desolvated under dynamic vacuum at 30°C within 9 hours to give white powder [130]. However recently, $\text{NaZn}(\text{BH}_4)_3 \cdot n\text{THF}$ solvate is also reported to be successfully desolvated under dynamic vacuum at RT within 36 hours [131].

KBH_4 is not soluble in both THF and Et_2O . Its reaction with ZnCl_2 in ether even in 1:10 ratio does not yield $\text{KZn}(\text{BH}_4)_3$ phase instead the main product is $\text{K}_2\text{Zn}_3(\text{BH}_4)_8$ solvate. ZnBr_2 also yields the same complex borohydride phase [130].

In fact, synthesis of pure $\text{Zn}(\text{BH}_4)_2$ solvate phase requires specific precursors and reaction conditions. Schlesinger et al first reported formation of zinc borohydride in ether. This was achieved by allowing the suspension of ZnH_2 in diethyl ether to absorb the diborane gas. The elemental analysis showed the formation of $\text{Zn}(\text{BH}_4)_2$. They prepared ZnH_2 as a precipitate in ether through the reaction of dimethylzinc $\text{Zn}(\text{CH}_3)_2$ with lithium alanates LiAlH_4 . White

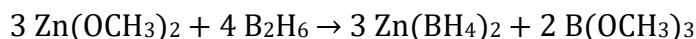
non-volatile ZnH_2 is reported to be stable in air, but gradually turned grey becoming pyrophoric in the matter of days [132].

Organozinc ZnR_2 (where $\text{R} = \text{CH}_3$ or C_2H_5) compounds are synthesized by disproportionation reaction of powder metallic zinc with ethyl or methyl iodide (RI):



Dimethyl zinc is volatile compound with disagreeable odor. Both organozinc compounds are pyrophoric in contact with air especially diethyl zinc. Both compounds react with diborane gas to form $\text{Zn}(\text{BH}_4)_2$ however self-igniting pyrophoric nature of the precursors and ethylborane byproduct are a major drawback.

A relatively safer alternative is a reaction between zinc methoxide and the diborane gas:



However, the preparation of zinc methoxide precursor still involves exothermal reaction between ZnR_2 and dry methanol while the main byproduct of the reaction is ethane or methane gas [133]. Although synthesis of pure zinc borohydride is possible with expensive organometallic precursors of zinc, needless to say that the rewards outweigh the risks.

Obtained $\text{Zn}(\text{BH}_4)_2 \cdot 2\text{Et}_2\text{O}$ solvate easily turns into oily $\text{Zn}(\text{BH}_4)_2 \cdot \text{Et}_2\text{O}$ which is stable up to 60°C under dynamic vacuum. Nevertheless, removal of last ether adduct results in rapid decomposition of pure $\text{Zn}(\text{BH}_4)_2$. Crystalline $\text{Zn}(\text{BH}_4)_2 \cdot 2\text{THF}$ solvate can be obtained at RT and melts at 67°C . Stronger Lewis bases such as Pyridine (NC_5H_5 , Py), Trimethylamine ($\text{N}(\text{CH}_3)_3$, TMA) and ammonia (NH_3) can displace Et_2O or THF adducts in the solvate. By these approaches, the crystalline solvates of $\text{Zn}(\text{BH}_4)_2 \cdot 2\text{Py}$, $\text{Zn}(\text{BH}_4)_2 \cdot 2\text{TMA}$ and $\text{Zn}(\text{BH}_4)_2 \cdot 4\text{NH}_3$ were reportedly prepared. No crystalline information was provided for these powders, the main characterization was performed using elemental analysis. Although, the behavior of $[\text{BH}_4]^-$ anion as pseudo-halide similar to the Cl^- anion in $\text{Zn}(\text{NH}_3)_2\text{Cl}_2$ is discussed, the solvate nevertheless identified as $\text{Zn}(\text{BH}_4)_2 \cdot 4\text{NH}_3$ [133]. More recently, Gu et al successfully synthesized $\text{Zn}(\text{BH}_4)_2 \cdot 2\text{NH}_3$ and resolved its crystal structure by synchrotron XRD analysis. The main phase together with LiCl byproduct is obtained by mechanochemical synthesis between $\text{Zn}(\text{NH}_3)_2\text{Cl}_2$ and LiBH_4 . Zinc chloride initially was exposed to 1 bar of ammonia atmosphere for 24 hour to obtain fully saturated $\text{Zn}(\text{NH}_3)_6\text{Cl}_2$ complex. Then it was heated to 150°C under inert atmosphere to decompose the salt into $\text{Zn}(\text{NH}_3)_2\text{Cl}_2$ [72].

Similar to solvothermal synthesis of zinc borohydride, mechanochemical synthesis through metathesis reaction of zinc chloride and alkali borohydrides results in formation of several bimetallic borohydrides such $\text{LiZn}_2(\text{BH}_4)_5$, $\text{NaZn}_2(\text{BH}_4)_5$, $\text{NaZn}(\text{BH}_4)_3$ [61], as well as mixtures of $\text{KZn}(\text{BH}_4)_3$ and $\text{K}_2\text{Zn}(\text{BH}_4)_x\text{Cl}_{4-x}$ with $\text{K}_3\text{Zn}(\text{BH}_4)_x\text{Cl}_{5-x}$ impurities [134]. All of these compounds are also contaminated with corresponding alkali halide or complex halide $\text{A}_x\text{ZnX}_{2+x}$ phases. However, THF assisted ball-milling of $\text{ZnCl}_2:\text{NaBH}_4$ in 1:3 ratio results in precipitation of NaCl byproduct from the $\text{NaZn}(\text{BH}_4)_3 \cdot n\text{THF}$ solution. After NaCl filtration,

subsequent treatment of this solution with ammonia atmosphere precipitated white $\text{NaZn}(\text{BH}_4)_3 \cdot 2\text{NH}_3$ powder in THF [131].

III.3. Road to scalable synthesis

To achieve potential industrial applications of ammine metal borohydrides as solid hydrogen storage materials, their dependency on mechanochemical synthesis must be alleviated. As discussed in detail in previous section, all the recent synthesis of zinc borohydrides and even their ammoniates used ball-milling as a major part of the synthesis process. Studies from the 1950-1970 period, focused on mostly solvothermal synthesis. $\text{NaZn}(\text{BH}_4)_3$ synthesis in Et_2O required longer time compared to THF. And obtained solvates from both solvents were reportedly desolvated under dynamic vacuum at RT.

Similar to reaction in ether, at RT we did not observe any reaction between ZnCl_2 and NaBH_4 in dimethyl sulfide (DMS). Conversely, it was rather easy to obtain THF solution of $\text{NaZn}(\text{BH}_4)_3$ and filtrate NaCl byproducts. However, despite several tries of desolvation under dynamic vacuum at 10-50°C temperature range, it was not possible to obtain dry $\text{NaZn}(\text{BH}_4)_3$ without decomposing it. Upon initial evaporation of excess THF the transparent oily product was obtained, this product had a melting point of 30-40°C. Even at lower temperature after long evaporation time, the sticky powder like compound could be obtained. However, XRD analysis indicated this powder to be a mixture of possibly several solvate phases. The color would slowly turn grey indicating the reduction of zinc and decomposition of the solvate phase even at RT. Xia et al reported THF assisted ball-milling of $\text{NaZn}(\text{BH}_4)_3$ and its successful desolvation under dynamic vacuum [131]. Even though we reproduced the exact synthesis process, we were not successful in desolvation of the $\text{NaZn}(\text{BH}_4)_3 \cdot n\text{THF}$ solvate. Additionally, the color of THF solution of $\text{NaZn}(\text{BH}_4)_3$ obtained from mechanochemical synthesis would turn noticeably grey after a day. These observation are consistent with literature which suggested possible light sensitivity of solvates [133] and the decomposition of $\text{NaZn}(\text{BH}_4)_3 \cdot 2\text{THF}$ solvate into $\text{NaBH}_4 + \text{Zn}(\text{BH}_4)_2 \cdot 2\text{THF}$ above -25°C while $\text{NaZn}(\text{BH}_4)_3 \cdot \text{Et}_2\text{O}$ solvate remaining stable up to 25°C. Hence, synthesis of unsolvated $\text{NaZn}(\text{BH}_4)_3$ would be much easier with DMS or Et_2O assisted ball-milling since the kinetics of the metathesis reaction is slower in these solvents unlike THF.

For solvothermal synthesis of $\text{NaZn}(\text{BH}_4)_3 \cdot 2\text{NH}_3$ we needed the ammonia precursor. Hence first logical approach was to react $\text{NaZn}(\text{BH}_4)_3 \cdot 2\text{THF}$ with 0.4M ammonia solution in THF. Although complete evaporation of the solvent was possible, the obtained product was amorphous. Ammonia solution in THF was purchased from Sigma Aldrich and did not claim to be anhydrous. Hence, we tried to synthesize our own anhydrous THF ammonia solution. Without liquid ammonia bottle, the only approach was the reaction of NaNH_2 and NH_4Cl precursors in THF, however this reaction had very low kinetics. Nevertheless, introduction of ZnCl_2 into this mixture very quickly delivered $\text{Zn}(\text{NH}_3)_2\text{Cl}_2$ and NaCl . This was an unexpected result since reaction of anhydrous zinc chloride with ammonia gas results in formation of $\text{Zn}(\text{NH}_3)_6\text{Cl}_2$ and only by heating it at 150°C under Ar flow $\text{Zn}(\text{NH}_3)_2\text{Cl}_2$ can be obtained [72]. However, since both $\text{Zn}(\text{NH}_3)_2\text{Cl}_2$ and NaCl are insoluble in THF, facile separation of two salts is not possible. However, we managed to prepare pure $\text{Zn}(\text{NH}_3)_2\text{Cl}_2$

from both aqueous and THF solutions of ammonia. This is similar to leaching of zinc metal as $\text{Zn}(\text{NH}_3)_2\text{Cl}_2$ from aqueous ammonium chloride solutions [135]. Reactions of $\text{Zn}(\text{NH}_3)_2\text{Cl}_2$ in THF with sodium borohydrides in 1:3 molar ratio delivered amorphous products. However, together with the ease of solvent evaporation and the observation of corresponding NaCl byproduct in XRD analysis indicated partially successful reaction.

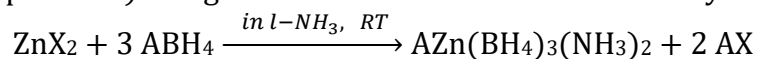
After building the ammonia reactor described in Chapter 2, through the reaction of $\text{NaZn}(\text{BH}_4)_3 \cdot n\text{THF}$ solvate with ammonia gas, the crystalline $\text{NaZn}(\text{BH}_4)_3 \cdot 2\text{NH}_3$ was successfully recovered. Mikhaeva et al by performing elemental analysis reported that for the chloride-free $\text{NaZn}(\text{BH}_4)_3 \cdot n\text{THF}$, molar ratio of ZnCl_2 and NaBH_4 precursors must be at least 1:4 [129]. Xia et al reported 1:3 molar ratio for pure $\text{NaZn}(\text{BH}_4)_3 \cdot n\text{THF}$, however while reproducing this result significant contamination of the main phase with NaBH_4 could be observed. Upon closer inspection of the article, the reported precursor masses translated into 1:2.5 molar ratio. Additionally, in-situ XRD measurement from the same work shows the formation of NaCl phase at 150°C that is absent in the main phase at RT. This indicates that reported $\text{NaZn}(\text{BH}_4)_3$ phase has significant chloride contamination [131].

Solvothermal synthesis technique using liquid ammonia as a solvent enables direct formation of $\text{A}_x\text{M}(\text{BH}_4)_{m+x}(\text{NH}_3)_n$ type materials in a single step without the need for ball-milling and other organic solvents. This synthesis technique bypasses the formation step of a metal borohydrides and jumps directly to ammine metal borohydride phase. We have discussed in detail the advantages of liquid ammonia synthesis in Chapter 2. As a summary, a typical liquid ammonia synthesis setup involves a glass reactor of Schlenk line which cannot withstand pressure above 1 bar, hence all the ammonia reactions need to be conducted either at RT as a gas or below -33°C as a liquid [136]. The reaction with ammonia gas cannot exploit solvent properties of ammonia. Some reactions simply cannot be performed due to lower solubility of precursors in other conventional solvents such as THF or DMS. The reaction at -33°C is severely limited in terms of kinetics of the reaction in liquid ammonia as well as lowered solubility. On the other hand, the stainless-steel synthesis setup that we built (Chapter 2) from Swagelok® parts can withstand reasonable vapor pressures of ammonia (up to 60 bar) for synthesis well above RT. Hence, it does not suffer from any of the disadvantages described above.

As a summary, the two-step synthesis of ammine metal borohydrides in literature includes the formation and the stabilization of metal borohydrides by ball-milling or as a solvate followed by reaction with ammonia gas. If we pursued this approach for synthesis of various ammine zinc borohydrides, isolation of known $\text{LiZn}_2(\text{BH}_4)_5$, $\text{Li}_2\text{Zn}(\text{BH}_4)_4 \cdot \text{Et}_2\text{O}$, $\text{NaZn}(\text{BH}_4)_3$, $\text{NaZn}_2(\text{BH}_4)_5$, $\text{NaZn}(\text{BH}_4)_3 \cdot \text{THF}$, $\text{KZn}(\text{BH}_4)_3$ and $\text{K}_2\text{Zn}(\text{BH}_4)_x\text{Cl}_{4-x}$ phases and their reaction with ammonia gas would create ammoniated main phase and disproportionate alkali borohydride phases. Utilizing liquid ammonia synthesis technique allowed the synthesis of various ammine zinc borohydride compounds with similar crystalline structure and enabled us to investigate the factors that control the release of ammonia impurity during dehydrogenation process.

III.3.1. Synthesis procedure

The typical synthesis process was conducted in liquid ammonia at RT under 10 bar (ammonia partial pressure) using a stainless-steel reactor. The ideal synthesis reaction is:



where A = Li; Na; K and X = Cl; F. At standard ambient temperature and pressure conditions, 500 ml of ammonia gas is condensed into small (10 ml) stainless steel reactor containing 300 mg of ZnCl₂ (or 230 mg of ZnF₂) and corresponding amount of alkali borohydride precursors and mixed at 350 rpm using magnetic bar. The typical synthesis duration of 24 hours is sufficient for LiZn(BH₄)₃(NH₃)₂ and NaZn(BH₄)₃(NH₃)₂ compounds while KZn(BH₄)₃(NH₃)₂ compounds require up to one week due to lower reactivity. The complete evaporation of ammonia solvent is more difficult for LiZn(BH₄)₃(NH₃)₂ compound which requires up to 24 hours under dynamic vacuum.

Surprisingly, the synthesis of pure mono-metallic Zn(BH₄)₂(NH₃)₂ in liquid ammonia although possible is not very reproducible. Instead, formation of bimetallic phase is preferred even with ABH₄:ZnCl₂ ratio of 2:1 or lower, where [BH₄]⁻ sites in the main phase are substituted with Cl⁻ anions to compensate for the deficiency of ABH₄. This effect will be discussed in detail. Lowering (increasing) the synthesis temperature suppresses (enhances) the anion substitution effect to a certain degree at the cost of lowered reactivity.

Hence, synthesis of Zn(BH₄)₂(NH₃)₂ is performed in two steps. Initially, Zn(NH₃)₂Cl₂ precursor is prepared by introducing ZnCl₂ into 35 wt% aqueous ammonia or ammonia in THF solutions. The second step is the reaction of this precursor with LiBH₄ in 2:1 ratio in THF using the Schlenk reactor. However, the kinetics of the reaction is rather slow and requires at least 10 day for complete reaction and delivers a product with poor crystallinity. The evaporation and complete removal of THF from the final product requires at least 48 hours under dynamic vacuum. In all cases white powder needs to be obtained, any grey color indicates the partial decomposition and reduction of zinc precursor. Hence, for this study we chose to also reproduce the synthesis process described in reference [72]. Zn(NH₃)₂Cl₂ precursor ball-milled with 2 mole of LiBH₄ in Retsch Emax. Ball-mill jar of 125 ml was filled with 30 steel ball (10 mm diameter) and the precursor added in ball-to-powder ratio of 155. The rotation speed was set to 500 rpm and pause steps to 2-minute interval while the ball-milling jar was cooled actively to 10°C. The total duration of the synthesis was 2.5 hours.

Dry white powders were stored under inert argon filled glass containers inside a refrigerator at 5 °C. The samples are referred by their respective chemical formulas in the rest of this chapter. Anhydrous ZnCl₂(99.995%), NaBH₄ (99.99%), KBH₄ (98%), NH₄Cl (99.5%) and NaNH₂ (98%) were purchased from Sigma Aldrich while LiBH₄ (95%) from Fluka and ZnF₂ (95%) from Acros Organics. Anhydrous ammonia gas is generated by heating the NaNH₂–NH₄Cl mixture to 150°C. The precursors and products are handled in air-free manner under high purity argon atmosphere of glovebox and Schlenk line. Various characterization techniques and procedures utilized for analysis of synthesized compounds are described in Chapter 2.

III.4. Experimental results

Four different ammine zinc borohydride compounds were synthesized. As mentioned before, $\text{Zn}(\text{BH}_4)_2(\text{NH}_3)_2$ and $\text{NaZn}(\text{BH}_4)_3(\text{NH}_3)_2$ have been previously reported while we were able to synthesize $\text{LiZn}(\text{BH}_4)_3(\text{NH}_3)_2$ and $\text{KZn}(\text{BH}_4)_3(\text{NH}_3)_2$ compounds for the first time. Among these compounds, $\text{LiZn}(\text{BH}_4)_3(\text{NH}_3)_2$ has the highest theoretical hydrogen capacity (12 wt%). For all the compounds, achieving these theoretical capacities is only possible if ammonia impurity release is completely suppressed and solid by-products of the decomposition reaction do not contain any hydrogen atoms.

III.4.1. Crystallographic analysis

XRD analysis of $\text{AZn}(\text{BH}_4)_3(\text{NH}_3)_2$ compounds revealed that they all have same orthorhombic unit cell structure with $\text{P2}_1\text{nb}$ symmetry, as previously identified for $\text{NaZn}(\text{BH}_4)_3(\text{NH}_3)_2$ compound [131] (Figures III-S1–S6 in Appendix section below). As it can be seen from Figure III-1 (green line), for $\text{AZn}(\text{BH}_4)_3(\text{NH}_3)_2$ compounds synthesized with ZnCl_2 precursor, the potassium compound has the smallest unit cell volume while the lithium compound has the biggest unit cell volume. As the ranking of alkali cation ionic radii is $r(\text{K}^+) > r(\text{Na}^+) > r(\text{Li}^+)$, the only possible explanation for inverse relationship in unit cell volume was that the impact of anion substitution effect ($[\text{BH}_4]^- \rightarrow \text{Cl}^-$) dominating over the cation replacement effect. Since ionic radius of Cl^- is smaller than that of $[\text{BH}_4]^-$, this means that the degree of anion substitution increases as we move from lithium to potassium compound.

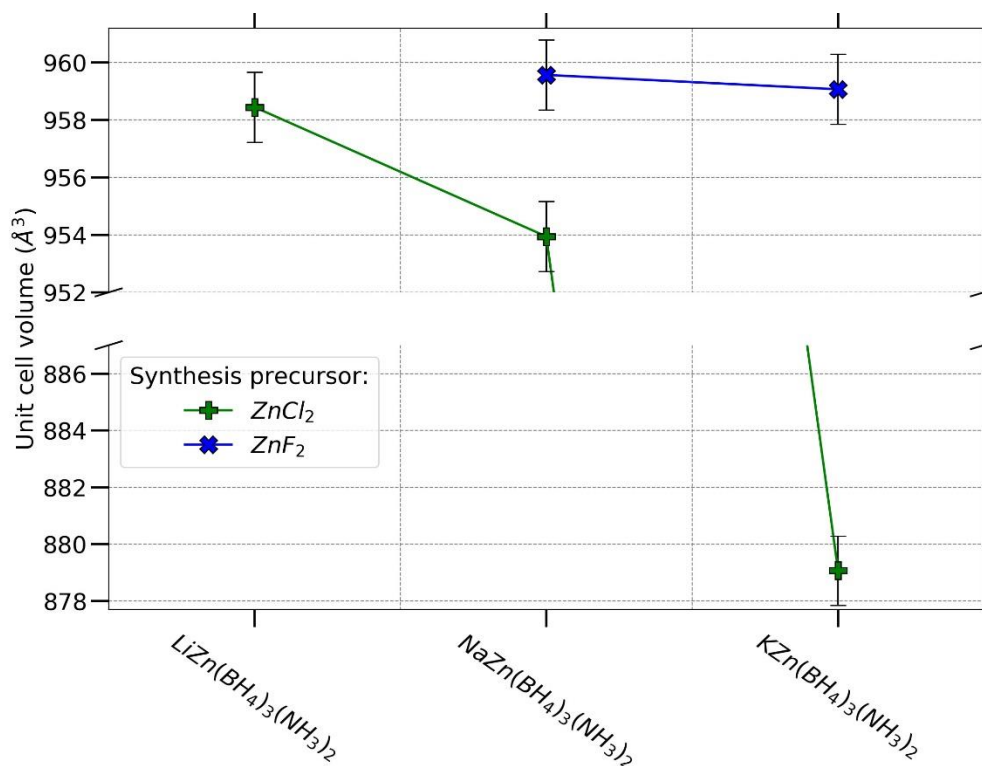
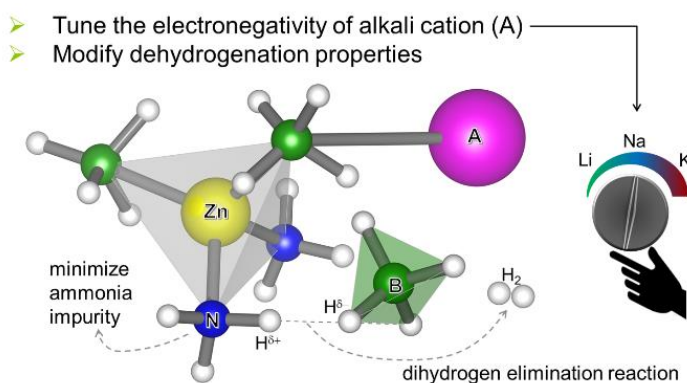


Figure III-1: Unit cell volume comparison for all bimetallic AZB compounds synthesized from ZnCl_2 and ZnF_2 precursors

To confirm this hypothesis and eliminate the anion substitution effect, $\text{NaZn}(\text{BH}_4)_3(\text{NH}_3)_2$ and $\text{KZn}(\text{BH}_4)_3(\text{NH}_3)_2$ compounds were synthesized using ZnF_2 precursors since F^- anions are too small to replace $[\text{BH}_4]^-$ anions. As expected, both compounds respectively showed 0.6 % and 9.2 % unit cell volume increase to $\sim 960 \text{ \AA}^3$. It was not possible to synthesize $\text{LiZn}(\text{BH}_4)_3(\text{NH}_3)_2$ compound with ZnF_2 precursor. Curiously, even in the absence of anion substitution, $\text{KZn}(\text{BH}_4)_3(\text{NH}_3)_2$ still does not have detectably larger unit cell volume than $\text{NaZn}(\text{BH}_4)_3(\text{NH}_3)_2$ (blue line in Figure III-1). One explanation is that crystallographic site for alkali cation in $\text{AZn}(\text{BH}_4)_3(\text{NH}_3)_2$ is big enough even for K^+ cation, hence no change in unit cell volume. Another possibility is due to existence of potentially higher amount of alkali cation vacancies in $\text{KZn}(\text{BH}_4)_3(\text{NH}_3)_2$ compared to $\text{NaZn}(\text{BH}_4)_3(\text{NH}_3)_2$, this assumption is supported by our Rietveld refinement analysis as well (Figures III-S1–S6). Further studies using synchrotron powder diffraction experiments on pure samples will be necessary to assess the validity of this assumption.

Although the $\text{Zn}(\text{BH}_4)_2(\text{NH}_3)_2$ compound has different crystalline structure (P2_1 space group) [72], on atomic level it is still very similar to bimetallic compounds. In all of these ammine zinc borohydride compounds zinc seats in the center of the tetrahedra and coordinates by two ammonia as well as two borohydride ligands. Therefore on the scale of



the unit cell, a bimetallic phase consists of this zinc tetrahedra with an additional alkali borohydride in its vicinity, $\text{AZn}(\text{BH}_4)_3(\text{NH}_3)_2 = \text{Zn}(\text{BH}_4)_2(\text{NH}_3)_2 + \text{ABH}_4$.

In AMBs, the ammonia molecules in general prefer to coordinate to higher electronegativity metals, while the borohydride anions prefer to bond with lower electronegativity metals.

The hypothesis for this study is that introducing an alkali cation in close proximity of zinc tetrahedra and tuning its electronegativity will enable the fine control of the bonding lengths and strengths which should affect the decomposition process.

Unlike comparing various ammine metal borohydrides to each other, this set of zinc compounds provides a unique opportunity to study dehydrogenation reactions independent of the effect of different crystalline structures while introducing a new control mechanism (replacing = tuning electronegativity of alkali cation) in order to understand the dehydrogenation process of AMBs.

III.4.2. Thermodynamic analysis

DSC-TG-MS coupled characterization system allows one to identify at which temperature range which gaseous species are released and how much corresponding weight is lost. All

zinc compounds upon heating decompose in two steps: a broad shallow endothermic peak quickly followed by sharp exothermic peak (Figures III-S8–S13). The endothermic process is reported to correspond to melting process [72] while the sharp exothermic peak can be explained by “dihydrogen elimination” process. The on-set and off-set temperatures of both endothermic and exothermic peaks of all compounds are plotted in Figure III-2. The first observation is that the thermal stabilization of compounds is mainly due to the Cl⁻ anion substitution which is confirmed in the literature [134]. This result might have bigger implications since most ammine metal borohydrides reported in literature are synthesized with metal chloride precursors. Extra care must be taken for compounds where crystalline phases of an ammine metal chloride is same with its borohydride counterpart. On the other hand, the effect of alkali cation replacement on decomposition temperature is almost negligible. For all the AZn(BH₄)₃(NH₃)₂ compounds, the main weight loss is due to exothermic decomposition process which happens in 110-140°C temperature range. The lower stability of Zn(BH₄)₂(NH₃)₂ compared to bimetallic compounds indicates a possibly different decomposition reaction pathway due to the absence of an alkali cation.

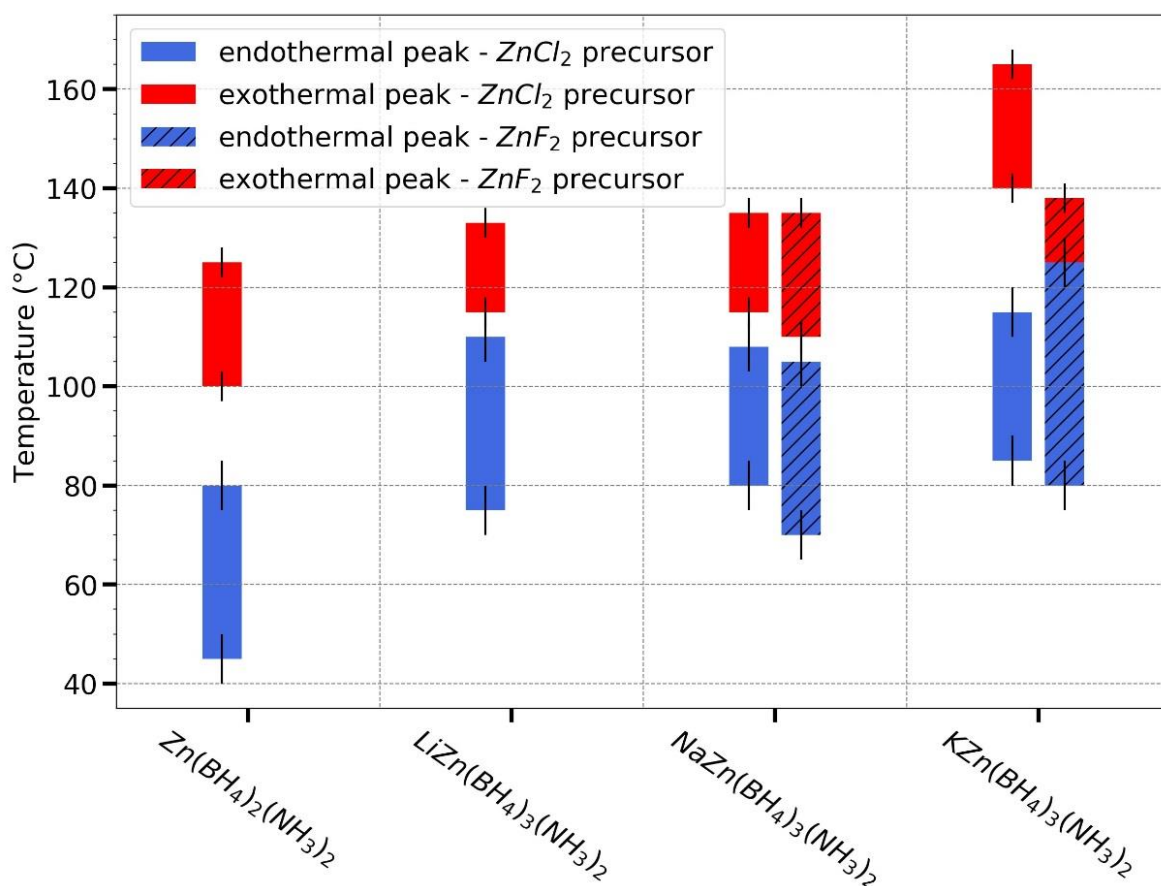


Figure III-2: On-set and off-set temperatures (bottom and top of the bar) of endothermic (blue) and exothermic (red) peaks for the compounds synthesized with ZnCl₂ precursors (solid fill) and ZnF₂ precursor (dashed fill). The heating rate is 2°C/min.

The notable exception to the decomposition behavior of bimetallic compounds is $\text{KZn}(\text{BH}_4)_3(\text{NH}_3)_2$ compound synthesized with ZnCl_2 precursor. It has sufficiently resolved peaks and a clear mass loss corresponding to the endothermic peak (Figure III-3). More precisely this peak can be associated with the melting triggered ammonia evaporation process. The area below the MS signal (m/e signal 2 for H_2 and 17 for NH_3), the total charge detected for each gas can be semi-quantitatively correlated to the amount of each released gas (under same experimental conditions such as same equipment, same heating rate and similar sample mass). However, this parameter is not precise enough for quantification of each released gas amount.

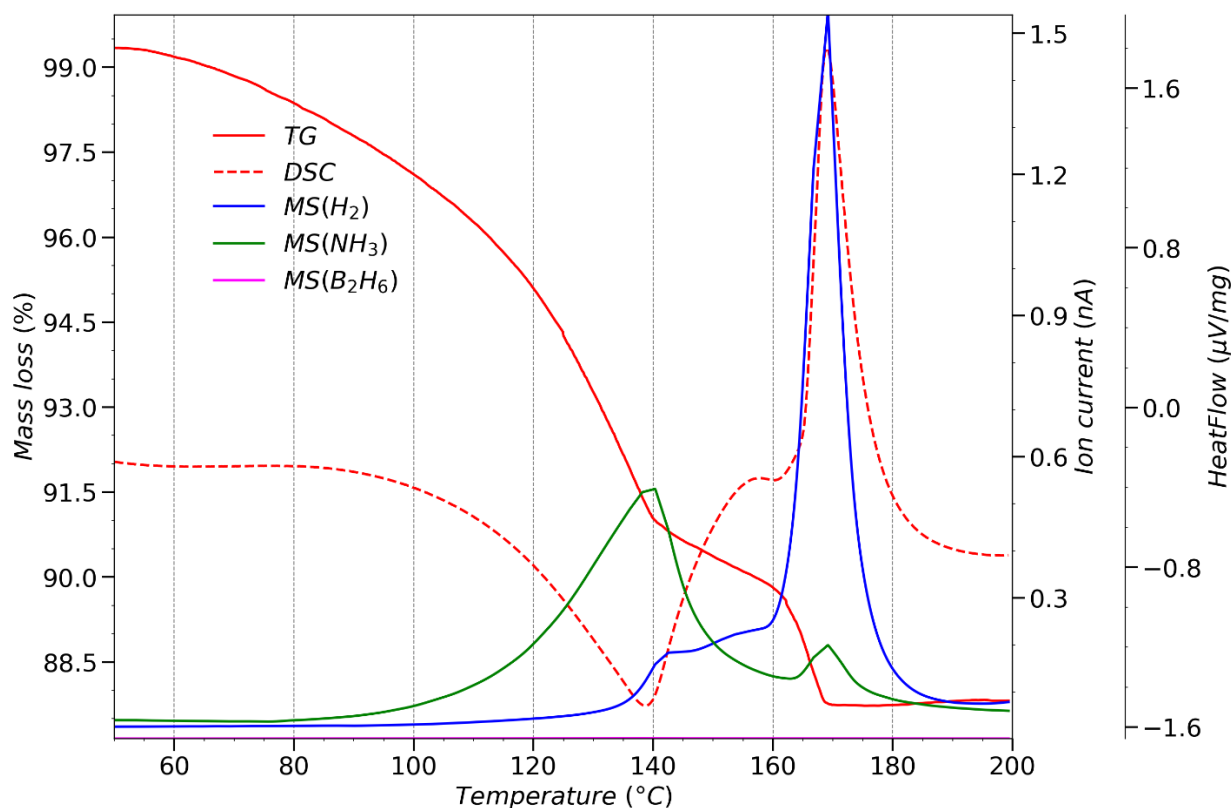


Figure III-3: DSC-TG-MS analysis of $\text{KZn}(\text{BH}_4)_3(\text{NH}_3)_2$ compound synthesized by ZnCl_2 precursor ($10^\circ\text{C}/\text{min}$ heating rate)

On the other hand, the released ammonia quantity can be more precisely calculated by combining gravimetric (TG) and Sievert-type volumetric temperature-programmed desorption (TPD) analysis as discussed in Chapter 2. TPD experiments are conducted under 1bar of hydrogen pressure to maintain similar pressure condition to TG (under 1bar of Ar flow) for the decomposition reaction (TG and TPD results for $\text{LiZn}(\text{BH}_4)_3(\text{NH}_3)_2$ are shown as an example in Figure III-4b).

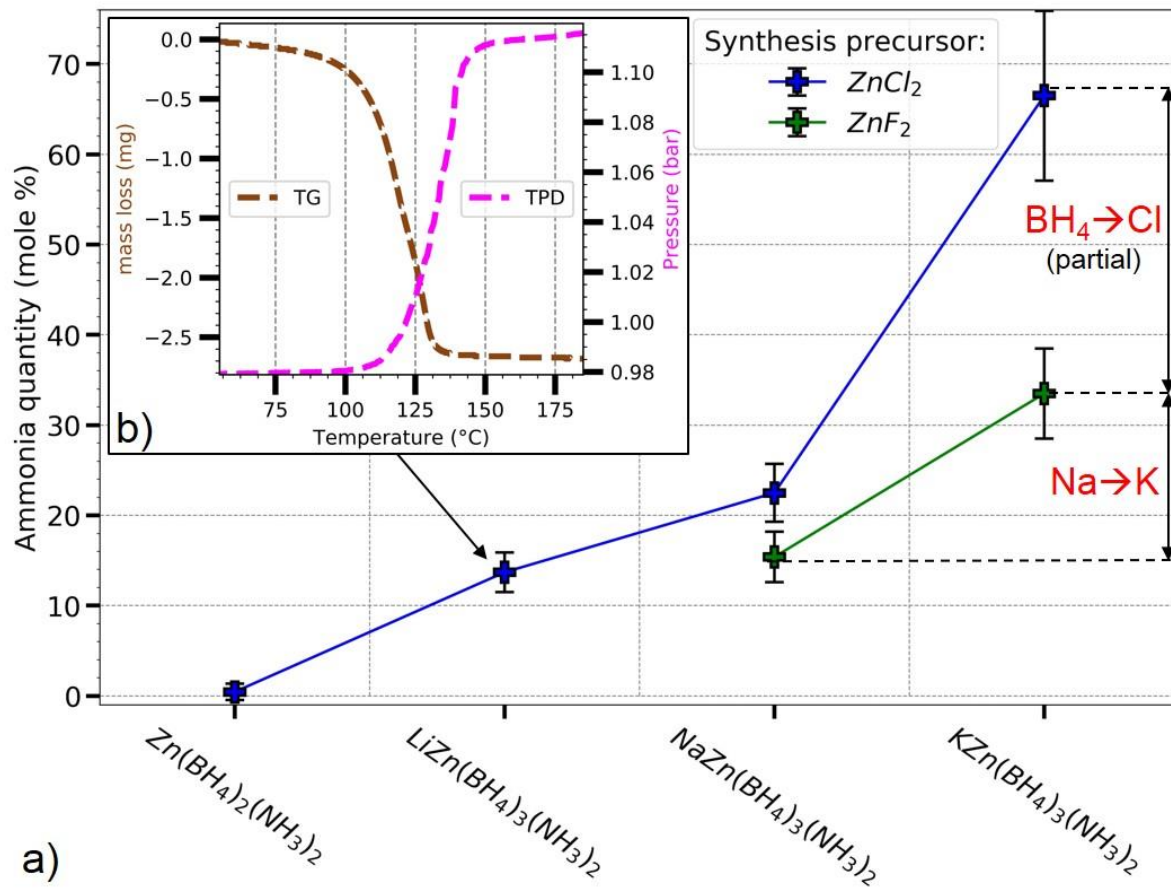


Figure III-4: a) Calculated quantity of ammonia per 100 mole of H₂ released for each compounds synthesized with ZnCl₂ (solid-green) and ZnF₂ (solid-blue) precursors b) TG (dashed-cyan) and TPD (dashed-magenta) measurements of LiZn(BH₄)₃(NH₃)₂ compound (25°C/min and 10°C/min heating rate, respectively)

The prerequisite for this calculation is the existence of only one type of impurity gas alongside the hydrogen which is confirmed by MS analysis. The mole percentage of released ammonia was calculated and plotted for all compounds (Figure III-4a). The result indicates that the ammonia release from ammine zinc borohydride compounds increases with decreasing average cation electronegativity. Since the compounds synthesized with ZnF₂ precursor do not have any anion substitution (green line in Figure III-4a), the replacement of Na⁺ with K⁺ in AZn(BH₄)₃(NH₃)₂ results in doubling of ammonia mole percentage. The partial substitution of certain [BH₄]⁻ sites with Cl⁻ anions in KZn(BH₄)₃(NH₃)₂ results in further doubling of ammonia mole percentage. NaZn(BH₄)₃(NH₃)₂ compounds have lower degree of anion substitution compared to potassium compound (Figure III-1). Clearly, the degree of Cl⁻ anion substitution correlates well with the released ammonia impurity amount. Hence, the released amount of ammonia between NaZn(BH₄)₃(NH₃)₂ compounds synthesized with fluoride and chloride precursors is also lower compared to potassium compounds.

The presence of lower electronegativity cation in the vicinity of Zn tetrahedra, increases ammonia release. The monometallic $\text{Zn}(\text{BH}_4)_2(\text{NH}_3)_2$ synthesized in THF released at least ~ 8 mol % ammonia (not included in the figure). Since MS analysis of this sample showed no THF release, we can assume chloride anion substitution is the main reason for observed ammonia release. This value despite being better than those of $\text{LiZn}(\text{BH}_4)_3(\text{NH}_3)_2$ (~ 13 mol %), due to the significantly heavier molar mass of ammonia, it still constitutes 40wt% of released gasses which is far from required hydrogen purity for fuel cell applications. On the other hand, $\text{Zn}(\text{BH}_4)_2(\text{NH}_3)_2$ synthesized by ball-milling releases almost pure hydrogen (~ 0.4 mole % ammonia which is smaller than experimental precision). However, with ball-milling duration less than 2.5 hours, the ammonia release remains high. This is due to insufficient reaction to replace all the chlorides in $\text{Zn}(\text{NH}_3)_2\text{Cl}_2$ with borohydride groups. XRD analysis alone is not enough to confirm the anion substitution $\text{ZnCl}_2:\text{LiBH}_4$ synthesis due to very close LiCl and LiBH_4 unit cell parameters. The yield of the solvothermal synthesis in THF can also be improved with longer synthesis duration or higher stoichiometry of LiBH_4 . However, with synthesis already lasting at least 10 days we did not pursue this approach.

III.4.3. Spectroscopic analysis

To confirm the purity of synthesized phases and to eliminate the possibility of unwanted phases affecting the decomposition reaction of the compounds, solid-state B^{11} NMR and Raman spectroscopic analysis were performed for each compound. Spectroscopic techniques are also powerful for identifying amorphous phases that might not be visible in XRD analysis.

Solvothermal synthesis of metal borohydrides in THF is known to produce ammonia borane type impurities in addition to the main phase[136]. Therefore, it was important to ensure the absence of NH_3BH_3 or any other boron phase except alkali halides in our samples. Figure III-5 shows Raman spectra of zinc compounds as well as NH_3BH_3 as a reference. The N-H and B-H stretching modes are common in all of these compounds. However, more importantly unlike ammonia borane, B-N stretching mode (780 cm^{-1}) is absent in ammine zinc borohydride compounds. Additionally, they all have a strong vibrational mode present at $\sim 420\text{ cm}^{-1}$ which has been previously attributed to Zn-B stretching mode in zinc borohydride compounds [137],[138]. It was also reported that formation of NH_3BH_3 phase was negligible for Zn compared to other transition metal borohydrides [136] during solvothermal synthesis in THF. This finding also aligns well with our results and confirms the purity of our zinc compounds.

Splitting of B-H stretching peaks in ammonia borane is assigned as asymmetric stretching mode for higher frequency region and symmetric stretching mode for the lower frequency peak [139]. $\text{Zn}(\text{BH}_4)_2(\text{NH}_3)_2$ has similar splitting in B-H stretching vibrational modes which previously reported in metal borohydrides as the evidence of bidentate (two M-H-B bridges)

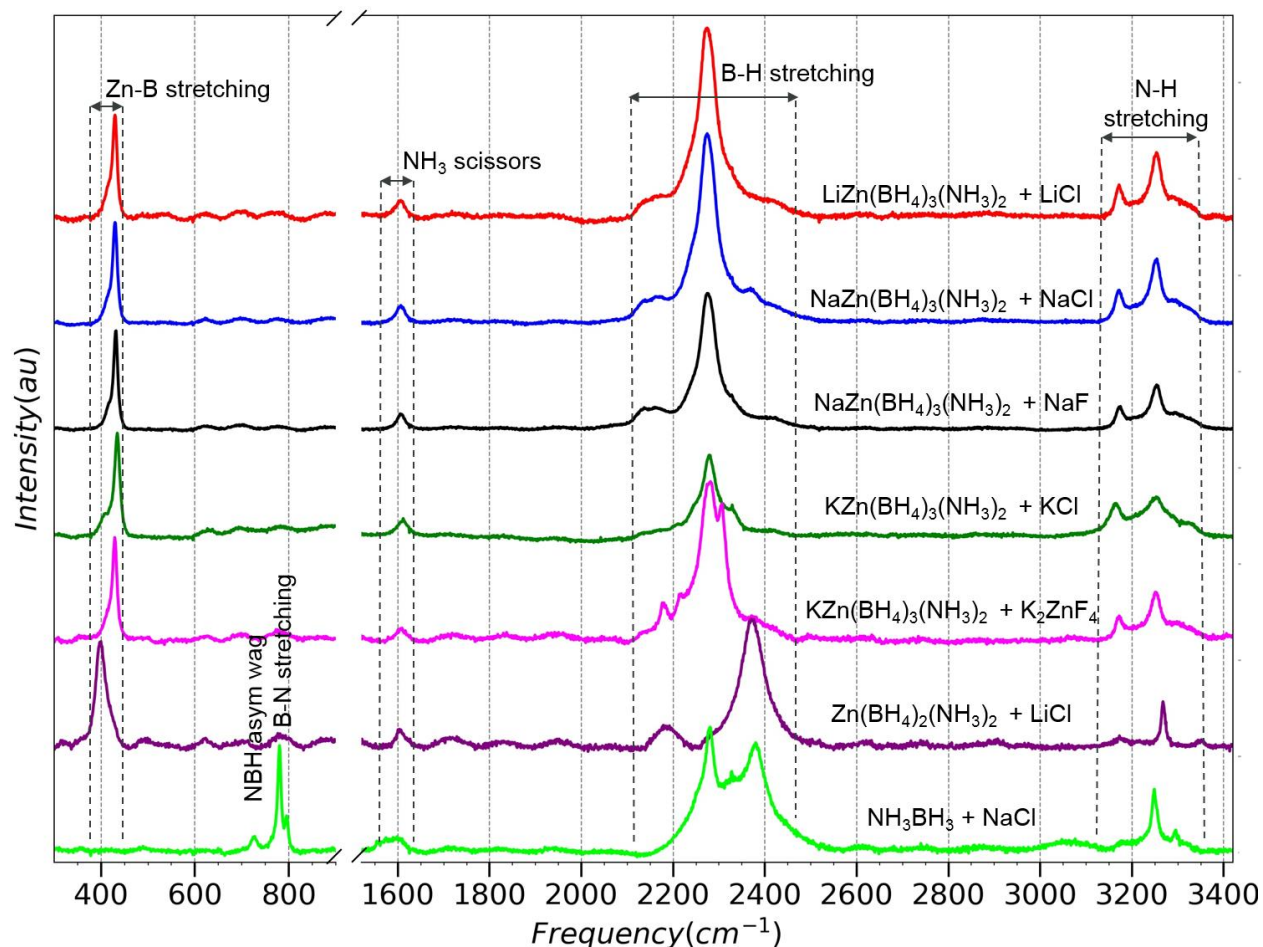


Figure III-5: Raman spectra of all the AZB compounds as well NH_3BH_3 .

and tridentate (three M-H-B bridges) bonding structure [140]. As evidence to the presence of $[\text{M}(\text{BH}_4)_m]^{m+}$ complex anions in the structure the higher frequency peaks are tentatively attributed to outward stretching B-H bond while lower frequency peaks to inwards stretching modes [67]. The intensity ratio of these peaks are used to differentiate between bidentate and tridentate structure [137]. By applying same logic, it is possible to conclude that $\text{Zn}(\text{BH}_4)_2(\text{NH}_3)_2$ has monodentate structure. This is also supported by vibrational frequency of the main peak being in the $2300\text{-}2450\text{ cm}^{-1}$ range. Same argument is applicable for bimetallic $\text{AZn}(\text{BH}_4)_3(\text{NH}_3)_2$ compounds as well, however the main peak is shifted to $2200\text{-}2350\text{ cm}^{-1}$ range. For tetrahedral geometry of metal cation, this range is attributed to ionic structure similar to $\text{Mg}(\text{BH}_4)_2$ [141]. The peak center of 2280 cm^{-1} corresponds exactly to the value reported for $\text{Mg}(\text{BH}_4)_3(\text{NH}_3)_6$. Conversely, splitting of B-H vibrational modes in $\text{Li}_2\text{Mg}(\text{BH}_4)_4(\text{NH}_3)_6$ is attributed to formation of $[\text{Li}_2(\text{BH}_4)_4]^{2-}$ complex anion [142]. The explanation agrees well with $\text{AZn}(\text{BH}_4)_3(\text{NH}_3)_2$ compounds since no complex anion exists in the structure. For alkali borohydrides (except LiBH_4) increasing cation size ascribed to B-H bond lengthening. This translates to lowering of vibrational frequency for stretching mode [141]. Hence, lower frequency of Zn-B stretching mode tells us that Zn-B bonding length is

longer in monometallic $\text{Zn}(\text{BH}_4)_2(\text{NH}_3)_2$ compared to bimetallic $\text{NaZn}(\text{BH}_4)_3(\text{NH}_3)_2$, which is confirmed by crystal structure (2.28 Å vs 2.12 Å) (supplementary information from references [131] and [72]). Changes in multiples of N-H stretching modes are also ascribed to local symmetry change of M-NH₃ group in the crystalline structure [68]. As a conclusion, Raman spectra of ammine zinc borohydrides compounds reveal that despite the presence of same zinc tetrahedra in all the compounds, various bonding energies in monometallic and bimetallic compounds are distinctly different and not much affected by the nature of alkali cation.

Similar to Raman spectroscopy, solid-state boron NMR is used for determining amorphous boron phases as well. However, much more additional information can be obtained using NMR spectroscopy. $\text{Zn}(\text{BH}_4)_2(\text{NH}_3)_2$ has a single peak at 42.9 ppm (Figure III-S) which corresponds to single type of boron site namely boron atoms which are the ligands of Zn tetrahedra. Conversely, all $\text{AZn}(\text{BH}_4)_3(\text{NH}_3)_2$ compounds show two distinct chemical sites for boron atoms within the structure. For $\text{LiZn}(\text{BH}_4)_2(\text{NH}_3)_2$ higher intensity peak is at 37.9 ppm while lower intensity peak is at 36.4 ppm. These values are exactly same $\text{NaZn}(\text{BH}_4)_2(\text{NH}_3)_2$ and $\text{KZn}(\text{BH}_4)_2(\text{NH}_3)_2$ compounds synthesized with ZnF_2 precursor (Figure III-S) indicating negligible changes in chemical shifts due to the differences in electronegativity of alkali cations. On the other hand, the chemical shift due to the Cl⁻ anion

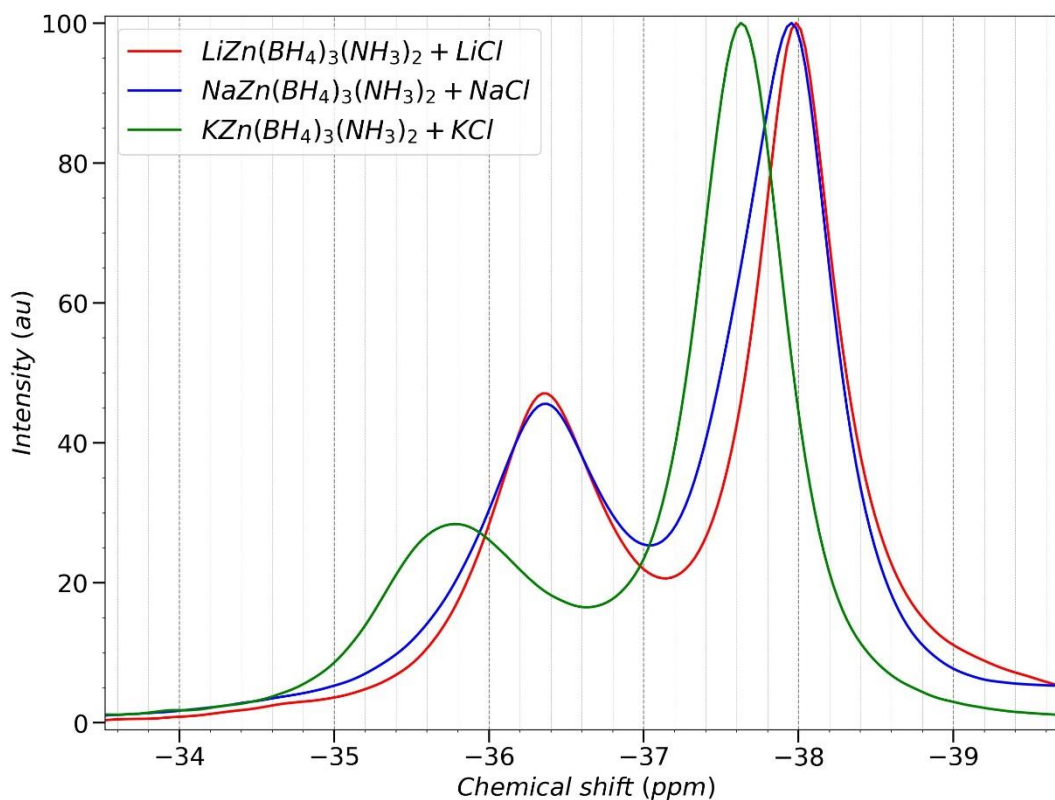


Figure III-6: ¹¹B MAS NMR spectra of bimetallic AZB compounds synthesized with ZnCl_2 precursors

substitution is much higher which shows a high correlation to the unit cell volume change (Figure III-6). This is expected since the bonding lengths within the compound will change proportional to unit cell volume. Additionally, the electronegativity difference between chloride and boron atoms occupying the same crystallographic sites is much bigger than electronegativity changes of alkali cations.

The double peak can be explained from the crystalline structure of bimetallic compounds (Figure III-S) where two boron sites (B2 and B3) which constitute the edges of the zinc tetrahedra are close to both alkali cation and zinc cation while the third boron site (B1) has longest bonding lengths with both cations. Hence, the ratio of the areas of NMR peaks should ideally be 0.5, provided Cl⁻ anion substitution process has no preferential boron site. This can be confirmed by fitting the peaks with pseudo-Voigt profile, resolving the peaks and looking at the ratio of the area of two ¹¹B MAS NMR peaks. In Figure III-7, the area ratio of two peaks is plotted for each AZn(BH₄)₃(NH₃)₂ compound. The ratio for NaZn(BH₄)₃(NH₃)₂ and KZn(BH₄)₃(NH₃)₂ compounds synthesized with fluoride precursors is in range of 0.75-0.80. Taking these values as reference, it can be observed that for AZB compounds synthesized with ZnCl₂ precursors, the area ratio drops as we move from lithium towards potassium compound. This result reveals that chloride anions likes to substitute B1 boron site more preferentially instead of the boron sites that constitute the corners of zinc tetrahedra.

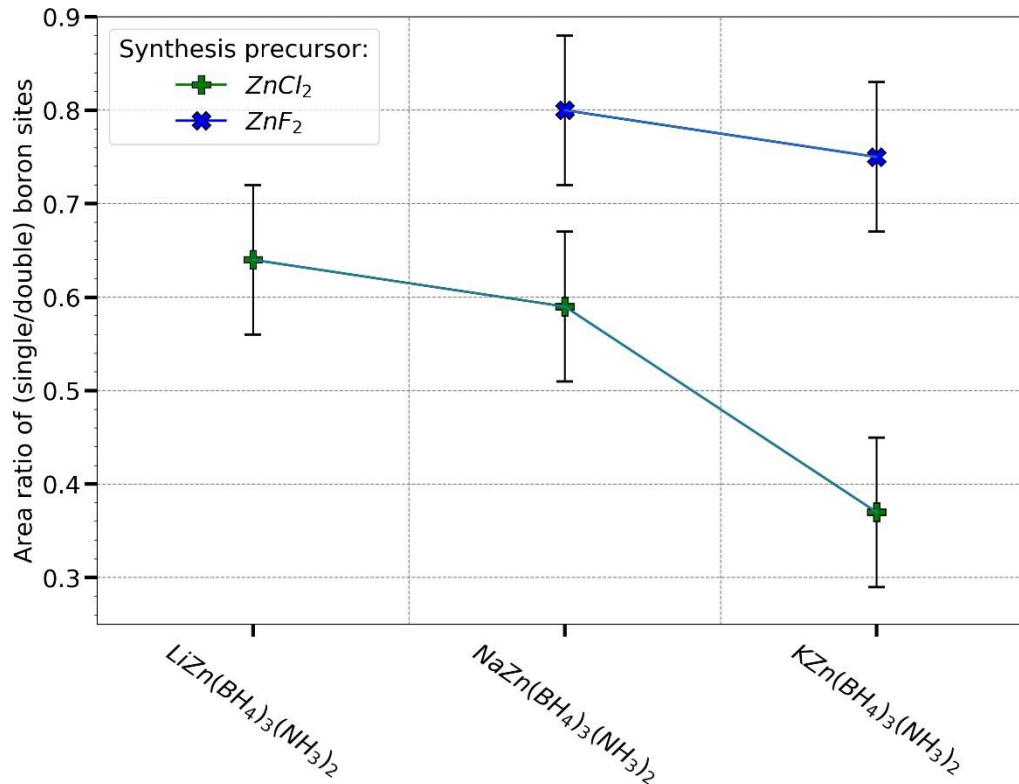


Figure III-7: ¹¹B MAS NMR peak area ratio of single and double boron sites

Although fluoride anion cannot substitute borohydride anion as a whole, it may substitute the hydrides that constitute it. To that end, we analyzed ^1H MAS NMR of ammine zinc borohydride compounds. Precision of these spectra are lower compared to ^{11}B NMR spectra due to strong and broad background signal. Nevertheless, normalizing the spectra for the peak at ~ 0 ppm, we can see that with increasing anion substitution in $\text{AZn}(\text{BH}_4)_3(\text{NH}_3)_2$ the peak at 3.8 ppm decreases. Additionally, $\text{Zn}(\text{BH}_4)_2(\text{NH}_3)_2$ despite broader peaks has lower signal compared to even $\text{KZn}(\text{BH}_4)_{3-x}\text{Cl}_x(\text{NH}_3)_2$. Previously, the chemical shift of liquid ammonia is assigned as 0.03–0.08 ppm [143]. With this knowledge we can safely assign the 3.8 ppm hydrogens bonded to boron atoms. Since, $\text{NaZn}(\text{BH}_4)_3(\text{NH}_3)_2$ and $\text{KZn}(\text{BH}_4)_3(\text{NH}_3)_2$ compounds synthesized with fluoride precursors has higher peak than $\text{LiZn}(\text{BH}_4)_3(\text{NH}_3)_2$ compound we can conclude that fluoride anion substitution of hydrides is non-existent.

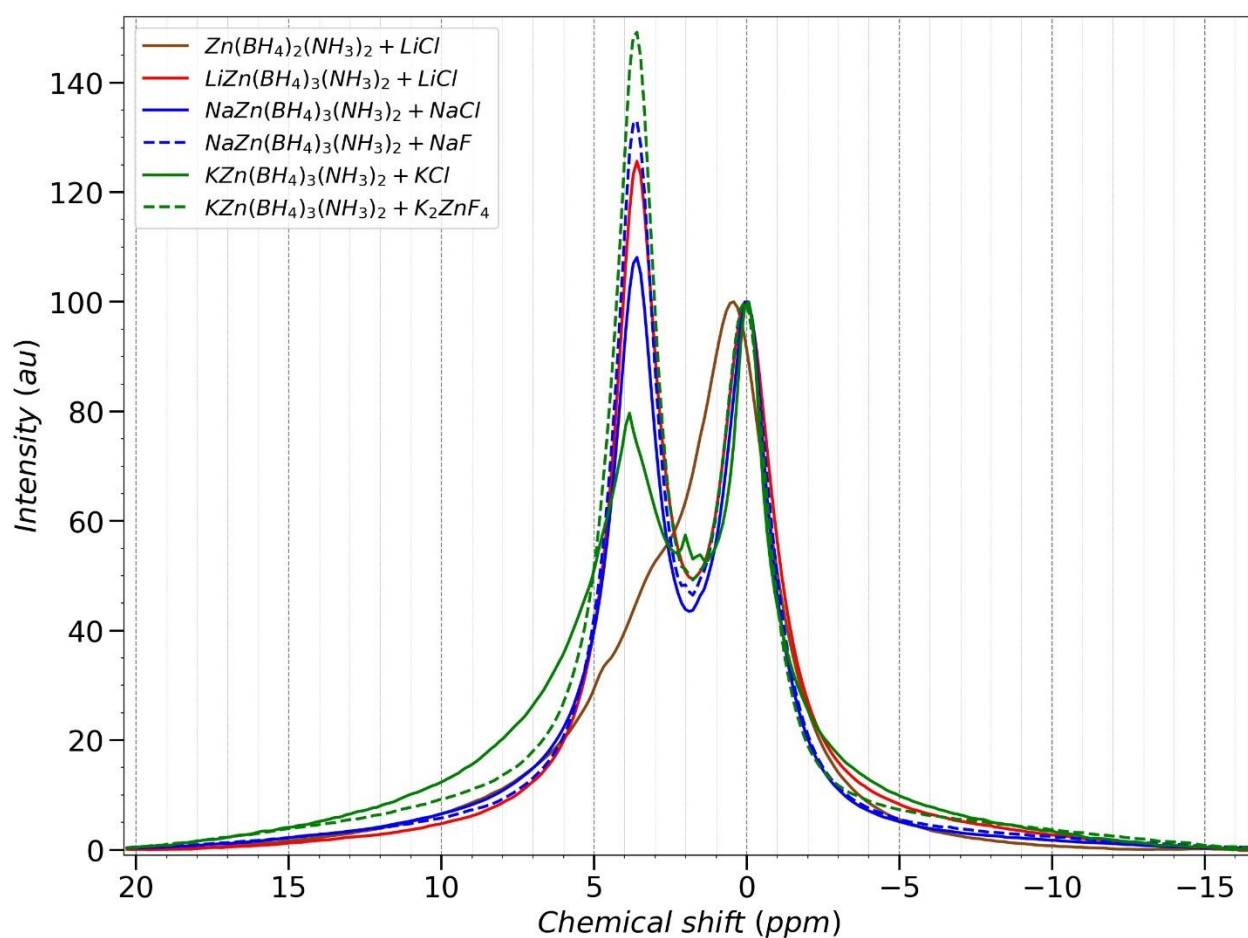


Figure III- 8: ^1H MAS NMR spectra of all ammine zinc borohydride compounds

III.5. Discussion of results

We have demonstrated the efficiency of room-temperature liquid ammonia synthesis for preparation of various bimetallic ammine zinc borohydrides. The formation of bimetallic borohydrides by solvothermal means were thought to be improbable. All the reported bimetallic AMBs are synthesized using mechanical ball-milling. Hence, their thermodynamic

or kinetically limited stabilization was an open question. However, AZB compounds showed higher preference for the formation of bimetallic compounds in liquid ammonia rather than the formation of monometallic ammine zinc borohydride. In fact, $\text{LiZn}(\text{BH}_4)_3(\text{NH}_3)_2$ is the ideal example for demonstrating the sensitivity of synthesis technique and conditions in order to obtain the desired compound. Despite being more stable than $\text{Zn}(\text{BH}_4)_2(\text{NH}_3)_2$, $\text{LiZn}(\text{BH}_4)_3(\text{NH}_3)_2$ phase cannot be obtained neither by ball-milling $\text{Zn}(\text{NH}_3)_2\text{Cl}_2$ and LiBH_4 [72] nor by solvothermal synthesis in organic solvents. Additionally, ball-milling ZnCl_2 and LiBH_4 precursors results in formation of $\text{LiZn}_2(\text{BH}_4)_5$ phase since $\text{LiZn}(\text{BH}_4)_3$ is unstable. Without stabilizing $\text{LiZn}(\text{BH}_4)_3$, the reaction with ammonia gas is also not possible. Hence the only route to $\text{LiZn}(\text{BH}_4)_3(\text{NH}_3)_2$ formation is direct synthesis using liquid ammonia as a solvent. $\text{KZn}(\text{BH}_4)_3(\text{NH}_3)$ with major chloride substitution requires a reaction between ZnF_2 and KBH_4 . We tried to replicate this reaction in THF assisted ball-milling, after several attempts with different ball-to-powder ratio, and synthesis duration at 500rpm no evidence of reactions between the precursors could be observed. Hence, the only option is liquid ammonia synthesis.

The dehydrogenation properties and ammonia impurity release from various ammine metal borohydrides have been previously studied by varying the ammonia to borohydride ratio in the compound [n/m ratio in $\text{A}_x\text{M}(\text{BH}_4)_m(\text{NH}_3)_n$] [144], [145]. The results showed that ammonia release is minimized if the number of NH_3 molecules within the crystalline structure is lower than borohydride anions ($n/m < 1$) [78]. Moreover, for $n/m > 1$ ratios decomposition processes can be in few steps with first steps mostly releasing pure ammonia until compounds achieve a favorable n/m ratio for the dihydrogen elimination reaction. The number of ammonia adducts in $\text{M}(\text{BH}_4)_m(\text{NH}_3)_n$ is thought to correspond to its complex chloride phase $\text{MCl}_m(\text{NH}_3)_n$. Despite the fact that ZnCl_2 likes to take up to 6 ammonia adducts just like most transition metal chlorides, ammine zinc borohydride compounds are unique for their natural preference of two ammonia adducts which translates into $n/m \leq 1$ for all AZBs.

As shown in the literature, ammine metal borohydrides have various low symmetry crystalline structures that change with the number of coordinating ammonia molecules as well. Additionally, the systematic comparison of the dehydrogenation properties between monometallic and bimetallic version of a chosen ammine metal borohydride and the role of alkali cations within the structure had not been performed due to the limited number of known bimetallic compounds [108] [48]. Therefore, having the same zinc tetrahedra in all ammine zinc borohydride compounds allowed us to perform unique characterization study which is less dependent (possible independent) of crystalline structure. In this study, identical crystallographic structure of $\text{AZn}(\text{BH}_4)_3(\text{NH}_3)_2$ compounds allowed us to replace alkali cation from Li^+ to Na^+ to K^+ without modifying zinc tetrahedral building block. Hence, the main observation is that the introduction of an alkali cation in the vicinity of this

tetrahedra increases the released ammonia impurity during decomposition. Lower alkali cation electronegativity corresponds to more ammonia impurity (Figure III-4a).

We have also successfully demonstrated that chloride anion substitution of borohydride sites has major effect on the ammonia impurity release as well as the decomposition temperature of ammine metal borohydrides. Figure III-3 clearly illustrates melting induced ammonia release in $\text{KZn}(\text{BH}_4)_{3-x}\text{Cl}_x(\text{NH}_3)_2$. Once enough borohydride sites around given ammonia molecules are replaced by chloride anions, the evaporation of excess ammonia in the structure will happen until a favorable stoichiometric ratio of ammonia to borohydride molecules (n/m ratio) is achieved for dihydrogen elimination reaction. Hence, due to the anion substitution the real n/m ratio is higher than $2/3$. On the other hand, almost no ammonia impurity is released from $\text{Zn}(\text{BH}_4)_2(\text{NH}_3)_2$ compound (Figure III-4a) despite the fact that its n/m ratio is exactly 1. Therefore, it is safe to conclude that n/m ratio alone is not a reliable parameter for predicting ammonia impurity release from ammine metal borohydrides without considering other factors that control decomposition process.

Increase in ammonia release due to anion substitution has important implications given the fact that most ammine metal borohydride compounds are synthesized using corresponding MCl_m precursors. Therefore, the degree of ammonia release from certain compounds needs to be taken into account together with their tendency for chloride substitution. We have shown that synthesis using metal fluoride precursor is a good way to eliminate anion substitution effect, provided that the reactivity of MF_m precursor with corresponding alkali borohydride is high enough.

Thermal decomposition byproducts of bimetallic $\text{A}_x\text{Zn}(\text{BH}_4)_{2+x}$ compounds synthesized by mechanochemical route are mainly Zn, B_2H_6 , H_2 and AlCl . Unlike alkali halide byproduct complex halides $\text{A}_x\text{ZnX}_{2+x}$ may participate in this decomposition reaction [61], [134]. However, another study did not observe similar reaction of $\text{A}_x\text{ZnX}_{2+x}$ during decomposition process [137]. $\text{Zn}(\text{BH}_4)_2(\text{NH}_3)_2$ is speculated to decompose through formation of Zn and $\text{Zn}(\text{BNH})_2$ type solid byproducts while releasing almost pure hydrogen gas. Boron and nitrogen containing decomposition byproducts are usually amorphous at the same time very difficult to quantitatively characterize by spectroscopic techniques as well [72]. However, main crystalline decomposition byproducts of $\text{NaZn}(\text{BH}_4)_3(\text{NH}_3)_2$ are mainly Zn and very small amount of NaBH_4 as observed with XRD analysis. The rest is amorphous BN or possibly $\text{Zn}(\text{BNH})_2$. If $\text{NaZn}(\text{BH}_4)_3(\text{NH}_3)_2$ can be assumed to be $\text{NaBH}_4 + \text{Zn}(\text{BH}_4)_2(\text{NH}_3)_2$, the decomposition process essentially should not release any ammonia if the additional mole of NaBH_4 does not participate in the decomposition process. Since this is not the case, it can be concluded that NaBH_4 disrupts the decomposition process of $\text{Zn}(\text{BH}_4)_2(\text{NH}_3)_2$. This is also evident from the difference in decomposition temperature of $\text{Zn}(\text{BH}_4)_2(\text{NH}_3)_2$ and $\text{AZn}(\text{BH}_4)_3(\text{NH}_3)_2$ compounds.

Computational studies identified various decomposition pathways that ammine metal borohydrides take upon heating. Direct dihydrogen elimination process in a given ammine

metal borohydride depends on relative charge of H atoms in BH_4 and NH_3 molecules (Brader charge) as well as local geometry of hydrogen bond network. Despite being energetically more favorable in ammine metal borohydride compounds with higher metal electronegativity, dihydrogen elimination reaction alone does not explain the whole dehydrogenation process. These compounds also benefit from $[\text{B}_2\text{H}_7]^-$ formation that might react with NH_3 to form NH_3BH_3 intermediate species and rerelease more hydrogen [146].

Tang et al compared the dehydrogenation properties of ball-milled $\text{M}(\text{BH}_4)_m\text{-Al}(\text{BH}_4)_3(\text{NH}_3)_6$ mixtures to that of pristine $\text{Al}(\text{BH}_4)_3(\text{NH}_3)_6$ where $\text{M} = \text{Li, Na, K, Ca, Mg}$. The main result of this study is that with higher polarizing power of the M^{m+} cation, the lower the decomposition temperature and less ammonia impurity was released. MS study of selectively deuterated mixtures of $\text{M}(\text{BD}_4)_m\text{-Al}(\text{BH}_4)_3(\text{NH}_3)_6$ showed the initial release of HD gas while $\text{M}(\text{BH}_4)_m\text{-Al}(\text{BD}_4)_3(\text{NH}_3)_6$ mixture released H_2 gas. This confirmed that unlike in pristine $\text{Al}(\text{BH}_4)_3(\text{NH}_3)_6$ in the presence of $\text{M}(\text{BH}_4)_m$ its hydridic hydrogen reacted first with the protic hydrogens of ammonia molecules coordinated to aluminum cation. The polarizing power of cations in MCl_m additives also slightly decreased decomposition temperature of $\text{Al}(\text{BH}_4)_3(\text{NH}_3)_6$, however compared to $\text{M}(\text{BH}_4)_m$ additives the effect was much weaker and almost negligible [147].

Polarizing power of a cation is, simply put, its ability to polarize and deform the corresponding anion. It is usually calculated as Z/r^2 where Z is the charge of the cation while r is the Shannon ionic radius that considers coordination number (CN) of an atom in crystalline structure [148]. Similarly, unlike Pauling electronegativity, the more precise estimation of electronegativity are provided by Li and Xue taking into account the coordination environment of the ions [149]. The electronegativity values of the selected cations discussed in this chapter are plotted versus their polarizing power in Figure III-9, assuming fixed $\text{CN}=6$ for all atoms. Polarizing power of cations explains why KBH_4 is stable in water while LiBH_4 hydrolyzes and $\text{Al}(\text{BH}_4)_3$ reacts explosively. On the contrary, the polarizing power of $[\text{Al}(\text{NH}_3)_6]^{3+}$ complex cation in $\text{Al}(\text{BH}_4)_3(\text{NH}_3)_6$ roughly equals to 0.1 (the radius measured as 5.45\AA from cif file of $\text{Li}_2\text{Al}(\text{BH}_4)_5(\text{NH}_3)_6$, from ref.[74]). From Figure III-9 we can see that despite having different electronegativity values, polarizing power of Mg^{2+} and Zn^{2+} cations are very similar. Excluding this fact, for the remainder of this discussion we can use electronegativity and polarizing power concepts interchangeably due to overall positive correlation between the two.

In $\text{M}(\text{BH}_4)_m$ the lower electronegativity of M means higher ionic character of the bond with borohydride group and corresponding increase of negative (Brader) charge on hydridic hydrogens of $\text{B-H}^\delta-$. While lower electronegativity in $[\text{M}(\text{NH}_3)_n]^{m+}$ system means lower partial positive charge on $\text{N-H}^\delta+$ [146]. Therefore, in $\text{M}(\text{BH}_4)_m/\text{Al}(\text{BH}_4)_3(\text{NH}_3)_6$ mixtures the dihydrogen elimination reaction is favored with increased partial charges of hydrogens in $\text{M-B-H}^\delta-\cdots\text{H}^\delta+-\text{N-Al}$ bonds. This explanation does not work for ammine zinc borohydride compounds since the coordination sphere of Zn^{2+} is not completely occupied with ammonia adducts unlike in $\text{Al}(\text{BH}_4)_3(\text{NH}_3)_6$. Zinc cation polarizes the hydrogens in both

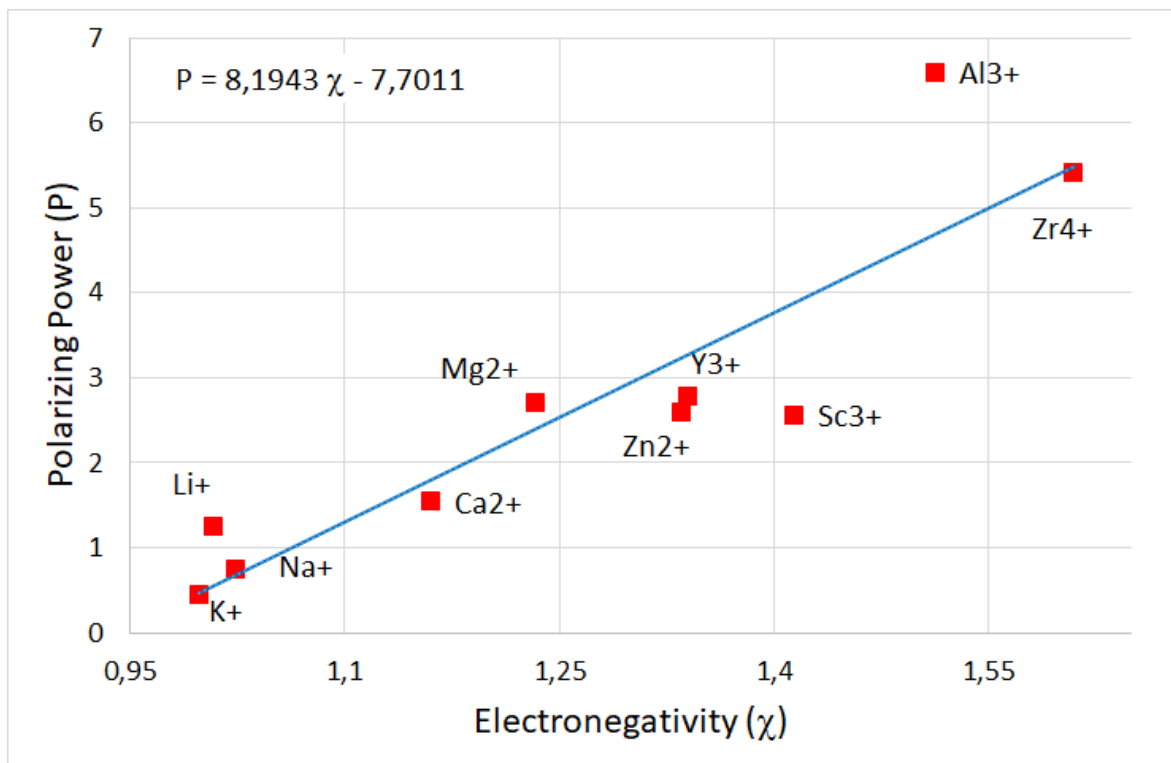


Figure III-9: Polarizing power of various cations vs their Li-Xue electronegativity

borohydride and ammonia ligands. In fact, Guo et al decreased the number of ammonia adducts in $\text{Al}(\text{BH}_4)_3(\text{NH}_3)_6$ step-wise by ball-milling it with $\text{Al}(\text{BH}_4)_3$ in various mixtures. This opened the coordination sphere of the Al^{3+} to BH_4 groups as well, resulting in distinct decrease of peak dehydrogenation temperature from 170°C to 110°C with almost pure hydrogen release at $n/m = 1$. Above this ratio $\text{Al}(\text{BH}_4)_3(\text{NH}_3)_n$ compound released ammonia while below it released diborane [73].

Recently, Chen et al reported computational analysis of $\text{Zn}(\text{BH}_4)_2(\text{NH}_3)_2$ decomposition process. The authors propose that unlike other ammine metal borohydrides direct dihydrogen elimination reaction could be less likely in $\text{Zn}(\text{BH}_4)_2(\text{NH}_3)_2$. This is explained by mismatch between the calculated energy barrier for dihydrogen elimination and the decomposition temperature. According to calculations, after the melting induced amorphization process in $\text{Zn}(\text{BH}_4)_2(\text{NH}_3)_2$, Zn^{2+} cation actively participate in H_2 release process through formation of intermediate species such as NH_3BH_3 and $[\text{B}_2\text{H}_7]^-$ by extracting a hydride H^- from $[\text{BH}_4]^-$ anions and forming Zn-H ionic bond. Furthermore, NH_3 participates in overall decomposition process through formation of $[\text{NH}_4]^+$ cation which reacts with $[\text{BH}_4]^-$ anions to release more hydrogen [150]. The authors did not investigate $\text{NaZn}(\text{BH}_4)_2(\text{NH}_3)_2$ compound, however as our results indicate the effect of alkali cation on these decomposition pathways is not negligible.

Another study focused on the properties of similar set of materials, namely $\text{Mg}(\text{BH}_4)_2(\text{NH}_3)_2$ and $\text{LiMg}(\text{BH}_4)_3(\text{NH}_3)_2$. The main differences between these materials and ammine zinc borohydrides are lower electronegativity of Mg^{2+} compared to Zn^{2+} (despite having similar

polarizing power) and change in coordination environment of Mg^{2+} once $LiBH_4$ is incorporated into $Mg(BH_4)_2(NH_3)_2$. Similar to zinc compounds, the dehydrogenation process takes place beyond melting temperature. But unlike $LiZn(BH_4)_3(NH_3)_2$, incorporation of $LiBH_4$ into the $Mg(BH_4)_2(NH_3)_2$ structure results in suppression of NH_3 impurity release. This is explained using DFT calculations as the ammonia vacancy formation and diffusion energy barriers being higher in bimetallic compound which prevents release of NH_3 molecules [151].

$AZn(BH_4)_3(NH_3)_2$ can be thought as $Zn(BH_4)_3(NH_3)_2 + ABH_4$, especially after melting process. This means above described decomposition process for $Zn(BH_4)_3(NH_3)_2$ will likely take place and will be affected by the presence of an alkali cation and an extra borohydride anion. Lower electronegativity cation will attract more the borohydride anions, causing a higher degree of disruption to the dehydrogenation reactions facilitated by zinc cation. Interestingly, in the original work for $NaZn(BH_4)_3(NH_3)_2$ compound the addition of $1/3 ZnCl_2$ resulted in complete suppression of NH_3 impurity from this compound at the cost of decreased hydrogen capacity [131]. Essentially, the additional $1/3$ mole Zn^{2+} sites neutralized the disruption of 1 mole Na^+ sites. The role of $ZnCl_2$ is explained as an additive that stabilizes the NH_3 molecules through formation of $Zn(NH_3)_2Cl_2$ phase, changes the decomposition pathways and promotes dihydrogen elimination reaction [152]. Further computational analysis are required to understand what type of decomposition reactions need to be supported or suppressed to minimize the NH_3 release during the decomposition process.

Various additives were tried to suppress the released ammonia from $NaZn(BH_4)_3(NH_3)_2$ (Figure III-10). The mixture was prepared by mortar mixing and the effect of additives was analyzed by integrating the total charge registered for ammonia and hydrogen ($m/e = 17$ and 2 , respectively) in MS and defining the relative hydrogen purity as charge ratio $Q(NH_3)/Q(H_2)$. This method is not as precise as TPD-TG calculation method to provide the exact molar ratio of ammonia impurities. However, by performing MS measurements under similar conditions, relative quantification is possible for following changes in hydrogen purity between different samples. $1/3$ mole of ZnF_2 slightly decreases the ammonia impurity of $NaZn(BH_4)_3(NH_3)_2$ considering the precision of the method it is negligible. On the other hand, addition of $1/3$ mole $ZnCl_2$ can almost completely suppress ammonia release. This can be achieved by optimizing molar ratio of $ZnCl_2$ additive. Hydrogen purity of neat $NaZn(BH_4)_3(NH_3)_2$ can also be improved by addition of 1 mole MgH_2 and $LiBH_4$, both compounds increase the concentration of hydridic hydrogens and by polarizing the $B-H^{\delta-}$ and $N-H^{\delta+}$ bonds and modifying the partial charges (δ) of hydridic and protic hydrogens. This result is similar to $M(BH_4)_n-Al(BH_4)_3(NH_3)_6$ discussed above. $Mg(BH_4)_2$ with highest cation polarization showed highest improvement in hydrogen purity of $Al(BH_4)_3(NH_3)_6$. The complex cation $[Al(NH_3)_6]^{3+}$ had polarization power lower than Na^+ (0.1 vs 1). Direct application of this concept to $NaZn(BH_4)_3(NH_3)_2$ is difficult since Zn^{2+} cation is bonded

directly to both BH_4 and NH_3 group. Despite the difference in electronegativity the polarization power of Zn^{2+} is similar to Mg^{2+} and higher than that of Li^+ . Hence, improvement of hydrogen purity by MgH_2 and LiBH_4 is similar to destabilization of Reactive Composite Hydrides, simply enabling new decomposition pathways and requiring computational studies to explain in detail.

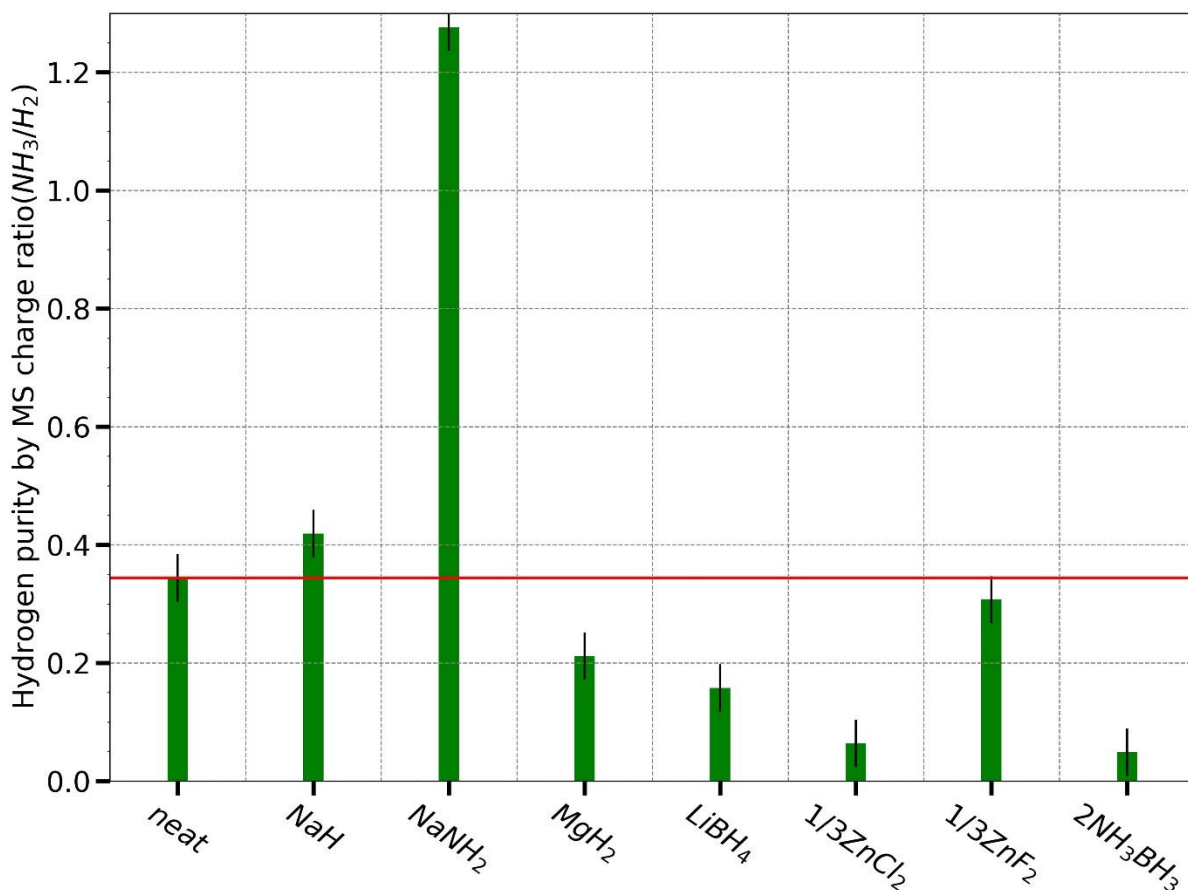
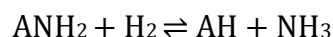


Figure III-10: Relative quantification parameter, MS charge ratio for hydrogen and ammonia (0 means pure hydrogen release) in neat $\text{NaZn}(\text{BH}_4)_2(\text{NH}_3)_2$ and with additives (molar ratio and the chemical formula provided in x-axis)

Interestingly, NaH slightly worsen the hydrogen purity of $\text{NaZn}(\text{BH}_4)_3(\text{NH}_3)_2$ while NaNH_2 is the worst additive (Figure III-10). Since the polarization power of Na^+ cation is irrelevant in these examples we need a different hypothesis. This might shine light into why $\text{AZn}(\text{BH}_4)_3(\text{NH}_3)_2$ compounds release ammonia contrary to $\text{Zn}(\text{BH}_4)_2(\text{NH}_3)_2$. Equilibrium reaction between hydrogen and ammonia over alkali amides and alkali metal (hydrides) is well known [122]. By applying hydrogen pressure to alkali amides ammonia gas can be generated:



It was shown that reaction enthalpy is smallest for KNH_2 and highest for LiNH_2 . Additionally, under similar experimental conditions ammonia equilibrium concentration is higher for KNH_2 compared to LiNH_2 [153]. In another study, at 100°C under 5 bar of hydrogen flow over ANH_2 the yield of the ammonia generation reaction was 0%, 13.8%, 78.8% for $A = \text{Li}, \text{Na}, \text{K}$ [154]. Although decomposition of $\text{AZn}(\text{BH}_4)_3(\text{NH}_3)_2$ were performed under 1 bar, due to the sharp and very exothermal decomposition process the local heating of the sample might reach much higher temperatures. And disproportionation reaction would generate ammonia by forcing ANH_2 intermediate species to consume hydrogen produced by dihydrogen elimination reaction. By this assumption, ammonia impurity in this compounds will increase with increasing heating rate and hydrogen pressure. Our ammonia impurity results shown in Figure III-4a support this hypothesis with highest ammonia being released with $\text{KZn}(\text{BH}_4)_3(\text{NH}_3)_2$ while lowest for $\text{LiZn}(\text{BH}_4)_3(\text{NH}_3)_2$. The experimental evidence to the presence of alkali amide intermediate phase could possibly be observed in in-situ XRD or NMR studies. However, due to highly exothermal and fast kinetics of $\text{AZn}(\text{BH}_4)_3(\text{NH}_3)_2$ decomposition, ANH_2 might be a transient phase and difficult to observe.

III.6. Conclusions

A new synthesis technique was developed based on liquid ammonia as a solvent which enabled direct and single step synthesis of various ammine zinc borohydride compounds. The compounds synthesized with ZnCl_2 precursors showed partial substitution of borohydride anions with chloride anions. Upon use of ZnF_2 precursors this anion substitution effect was completely eliminated. Four ammine zinc borohydride compounds were synthesized. Among those, two are reported for the first time in this work, namely $\text{LiZn}(\text{BH}_4)_3(\text{NH}_3)_2$ and $\text{KZn}(\text{BH}_4)_3(\text{NH}_3)_2$ compounds.

The zinc tetrahedra with two borohydride and two ammonia ligands forms the basis of all the reported compounds. A bimetallic $\text{AZn}(\text{BH}_4)_3(\text{NH}_3)_2$ where $A = \text{Li}; \text{Na}; \text{K}$ on atomic level is a combination of monometallic $\text{Zn}(\text{BH}_4)_2(\text{NH}_3)_2$ (Zn tetrahedra) and ABH_4 . For compounds with partial chloride anion substitution, this atomic environment is more likely to look like $\text{AZn}(\text{BH}_4)_{3-x}\text{Cl}_x(\text{NH}_3)_2 = \text{Zn}(\text{BH}_4)_2(\text{NH}_3)_2 + \text{ACl}$ due to preferential boron site for chloride substitution. The presence of an additional alkali borohydride in the vicinity of this tetrahedra and the ability to tune the electronegativity of alkali cation by replacing it from lithium to potassium provided a unique set of compounds to study the dehydrogenation process as well as the release of unwanted ammonia impurity. Hence, the lower alkali cation electronegativity and the higher chloride anion substitution effects independently result in more ammonia impurity release during decomposition process.

III.7. Appendix

All XRD samples were measured at RT using air-tight samples holder and with $\lambda = 1.54\text{\AA}$ wavelength. CIF file for $\text{Zn}(\text{BH}_4)_2(\text{NH}_3)_2$ is taken from reference [72] and for bimetallic compounds from reference [131]. Atomic displacement parameter B_{iso} was set to 1 for all the atoms.

For all samples synthesized with ZnCl_2 precursors, during Rietveld refinement chloride atoms introduced at the same atomic positions as boron atoms. The chloride anion substitution were performed for all boron sites at the same time. Following refinement order applied: chloride anion occupancy $\text{Occ}(\text{Cl})$ (occupancy of boron sites adjusted manually accordingly as $1 - \text{Occ}(\text{Cl})$), boron (and corresponding chloride) atomic positions, zinc atomic positions, nitrogen atomic position and finally alkali cation (if exists) atomic positions.

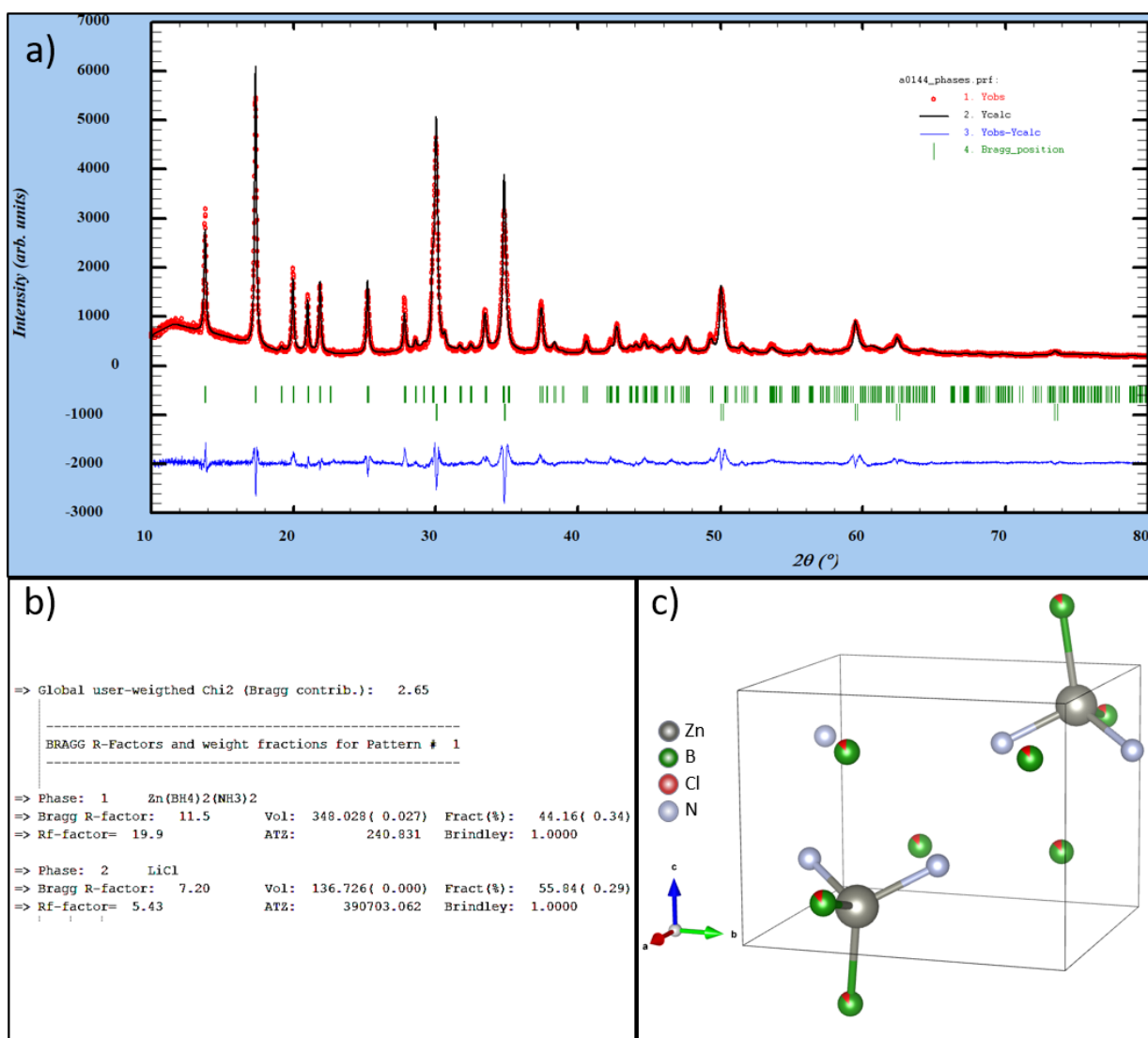


Figure III-S1: a) Rietveld refinement of XRD data for $\text{Zn}([\text{BH}_4]_{0.89}\text{Cl}_{0.11})_2(\text{NH}_3)_2 + \text{LiCl}$. b) Refinement quality and yield calculation for each phase from (.sum) file c) Unit cell visualization based on refinement data.

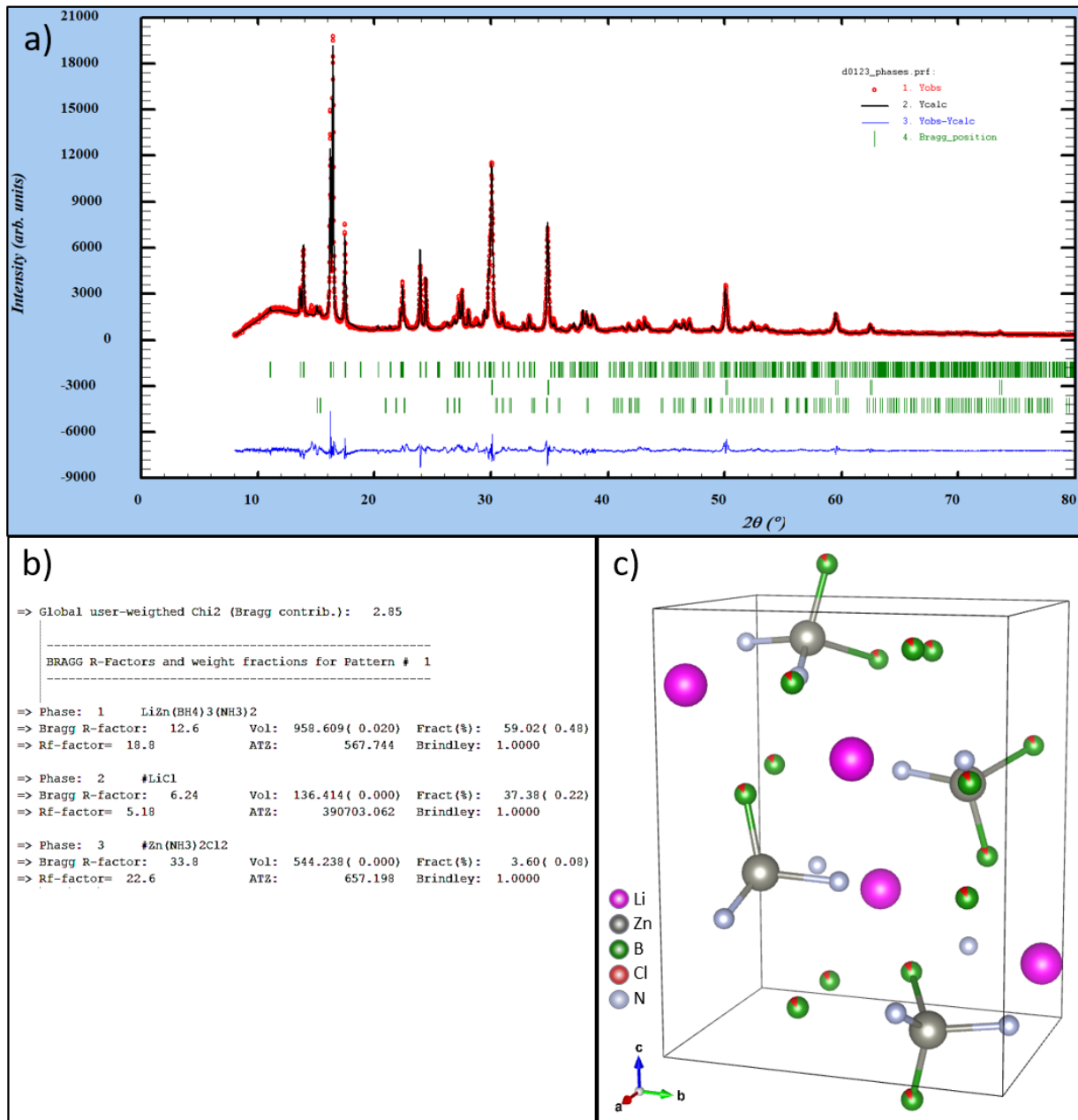


Figure III-S2: a) Rietveld refinement of XRD data for $\text{LiZn}([\text{BH}_4]_{0.87}\text{Cl}_{0.13})_3(\text{NH}_3)_2 + \text{LiCl} + \text{Zn}(\text{NH}_3)_2\text{Cl}_2$. b) Refinement quality and yield calculation for each phase from (.sum) file c) Unit cell visualization based on refinement data.

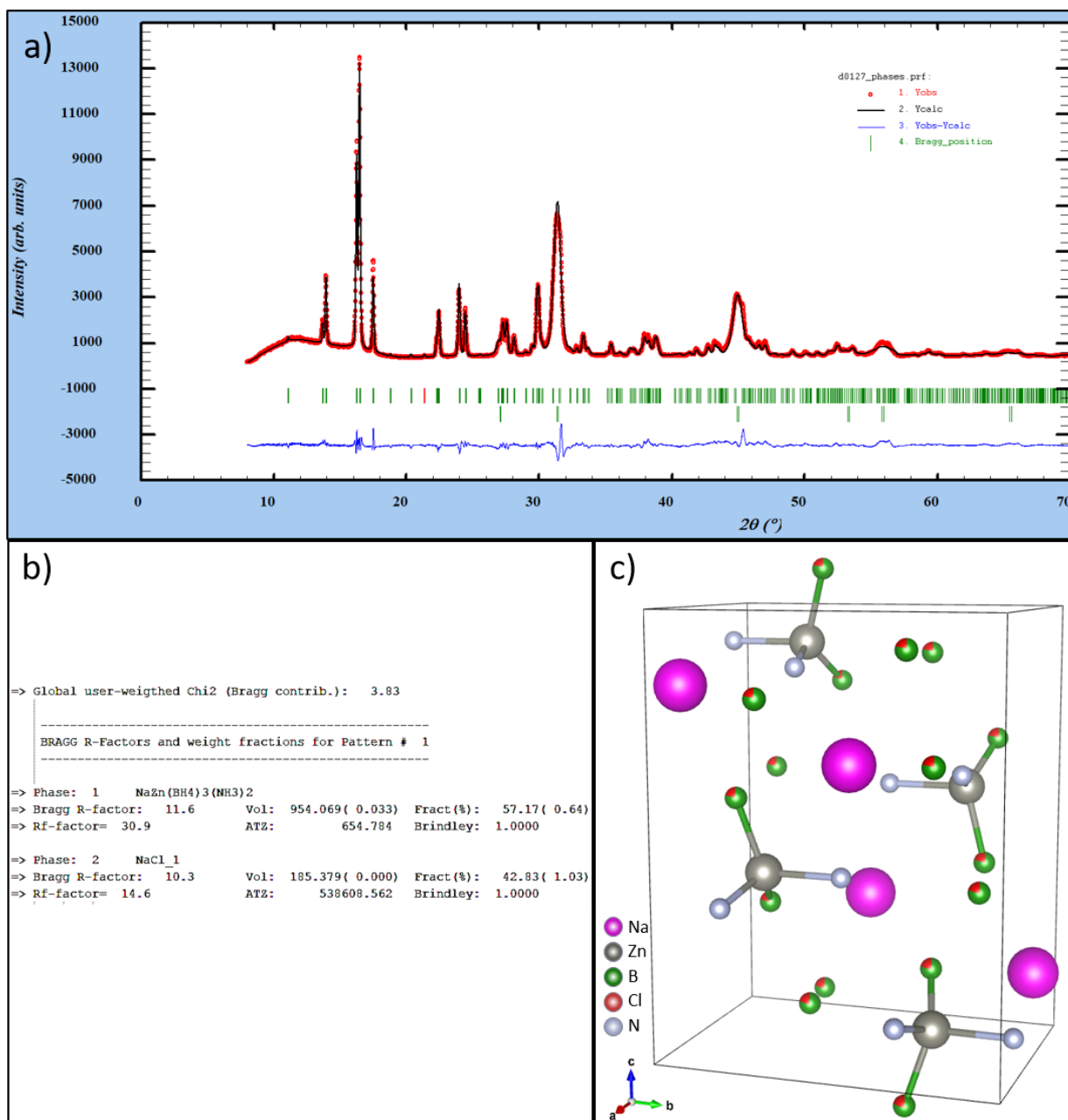


Figure III-S3: a) Rietveld refinement of XRD data for $\text{NaZn}([\text{BH}_4]_{0.8}\text{Cl}_{0.2})_3(\text{NH}_3)_2 + \text{NaCl}$ sample. b) Refinement quality and yield calculation for each phase from (.sum) file c) Unit cell visualization based on refinement data.

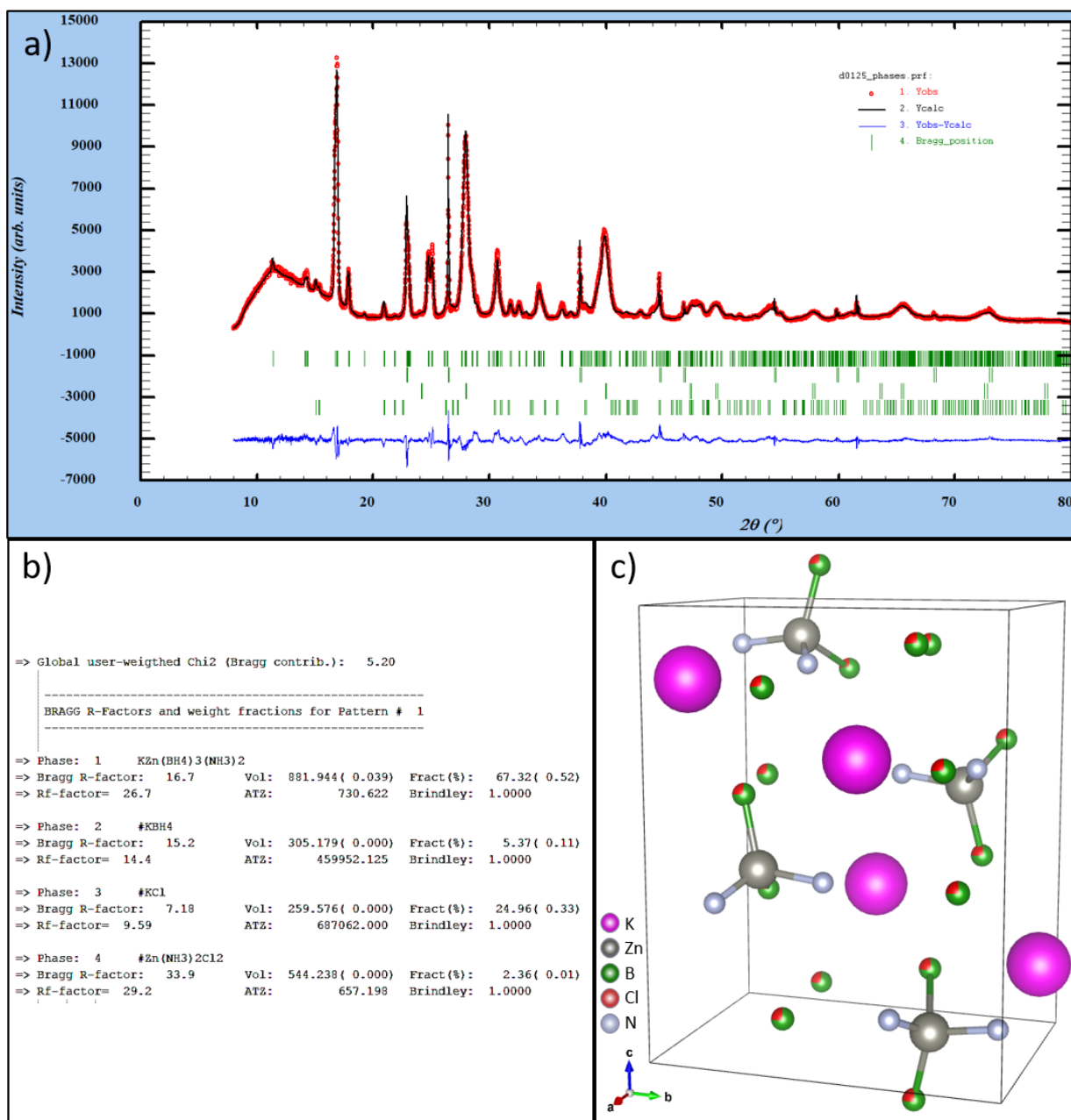


Figure III-S4: a) Rietveld refinement of XRD data for $KZn([BH_4]_{0.76}Cl_{0.24})_3(NH_3)_2 + KBH_4 + KCl + Zn(NH_3)_2Cl_2$ sample. b) Refinement quality and yield calculation for each phase from (.sum) file c) Unit cell visualization based on refinement data.

Compounds synthesized with $ZnCl_2$ precursors as expected shows increasing degree of anion substitution from $Zn(BH_4)_2(NH_3)_2$ to $KZn(BH_4)_3(NH_3)_2$. This is in agreement with stoichiometric ratio of the precursors and the NMR studies. Although our NMR results showed preferential sites for chloride anion substitution we could not reliably apply this model during our Rietveld refinement analysis.

For bimetallic samples synthesized with ZnF_2 , knowing that no anion substitution exists alkali cation vacancy model was explored. The vacancies in borohydride anion sites were also introduced to preserve the electroneutrality. The vacancies were distributed equally among three boron sites. Although ^{11}B NMR peak ratio in Figure SIII-7 might indicate that vacancies also prefer B1 site over B2 and B3. Following refinement order was applied: alkali cation occupancy $\text{Occ}(\text{A})$ (occupancy of boron sites adjusted manually accordingly as $1 - \text{Occ}(\text{A})/3$), then boron, zinc, nitrogen and finally alkali cation atomic positions.

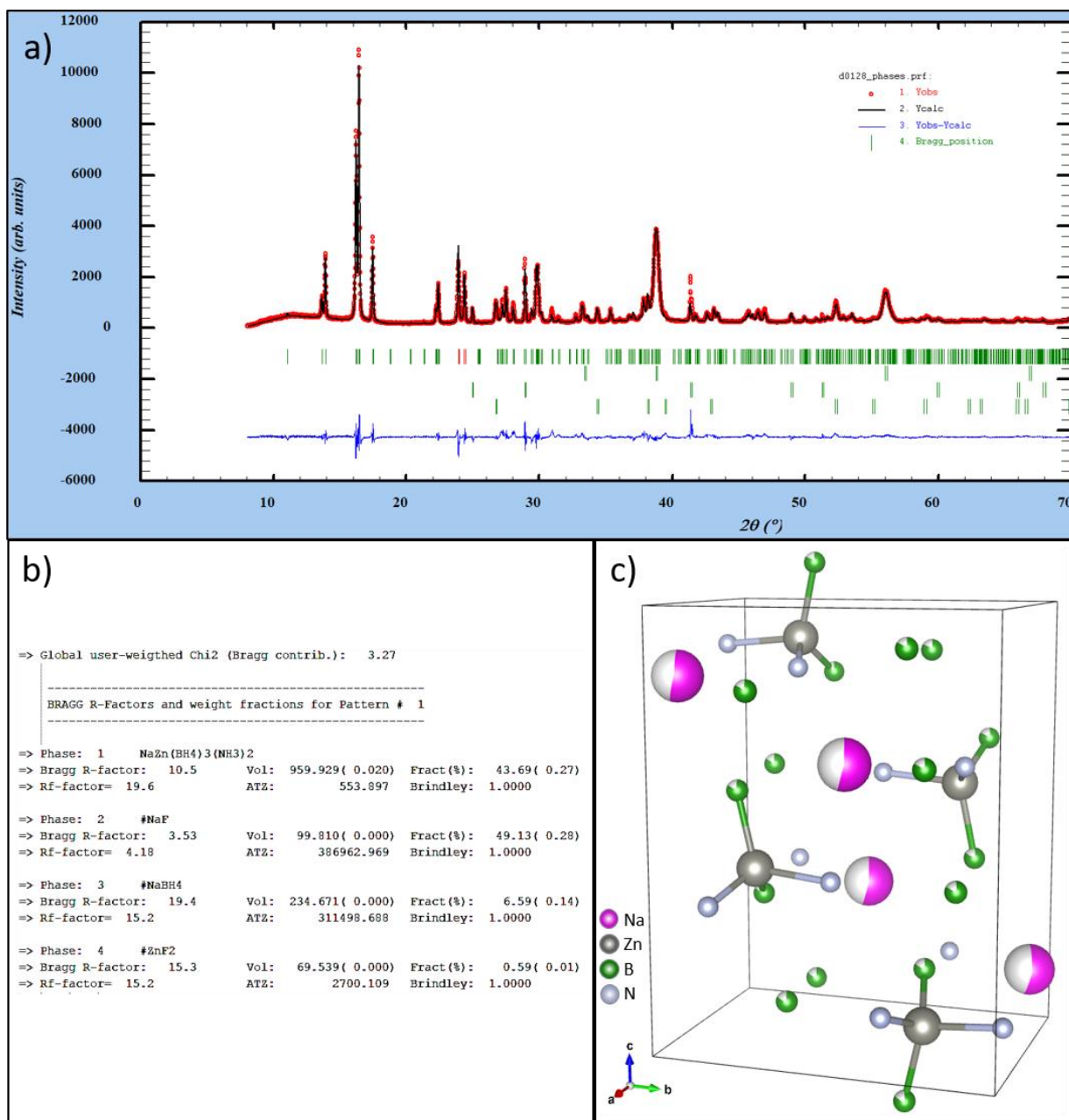


Figure III-S5: a) Rietveld refinement of XRD data for $\text{Na}_{0.55}\text{Zn}(\text{BH}_4)_{2.55}(\text{NH}_3)_2 + \text{NaF} + \text{NaBH}_4 + \text{ZnF}_2$ sample. b) Refinement quality and yield calculation for each phase from (.sum) file c) Unit cell visualization based on refinement data.

It is important to mention that the alkali cation partial occupancy model is supported by synthesis data. $\text{NaZn}(\text{BH}_4)_3(\text{NH}_3)_2$ compound in order to be synthesized without excess unreacted precursors the stoichiometric ratio of $\text{ZnF}_2:\text{NaBH}_4$ had to be 1:2.3 instead of expected 1:3. This could also be explained by formation of $\text{Na}_{1-x}\text{Zn}(\text{BH}_4)_{3-x}(\text{NH}_3)_2$ main phase.

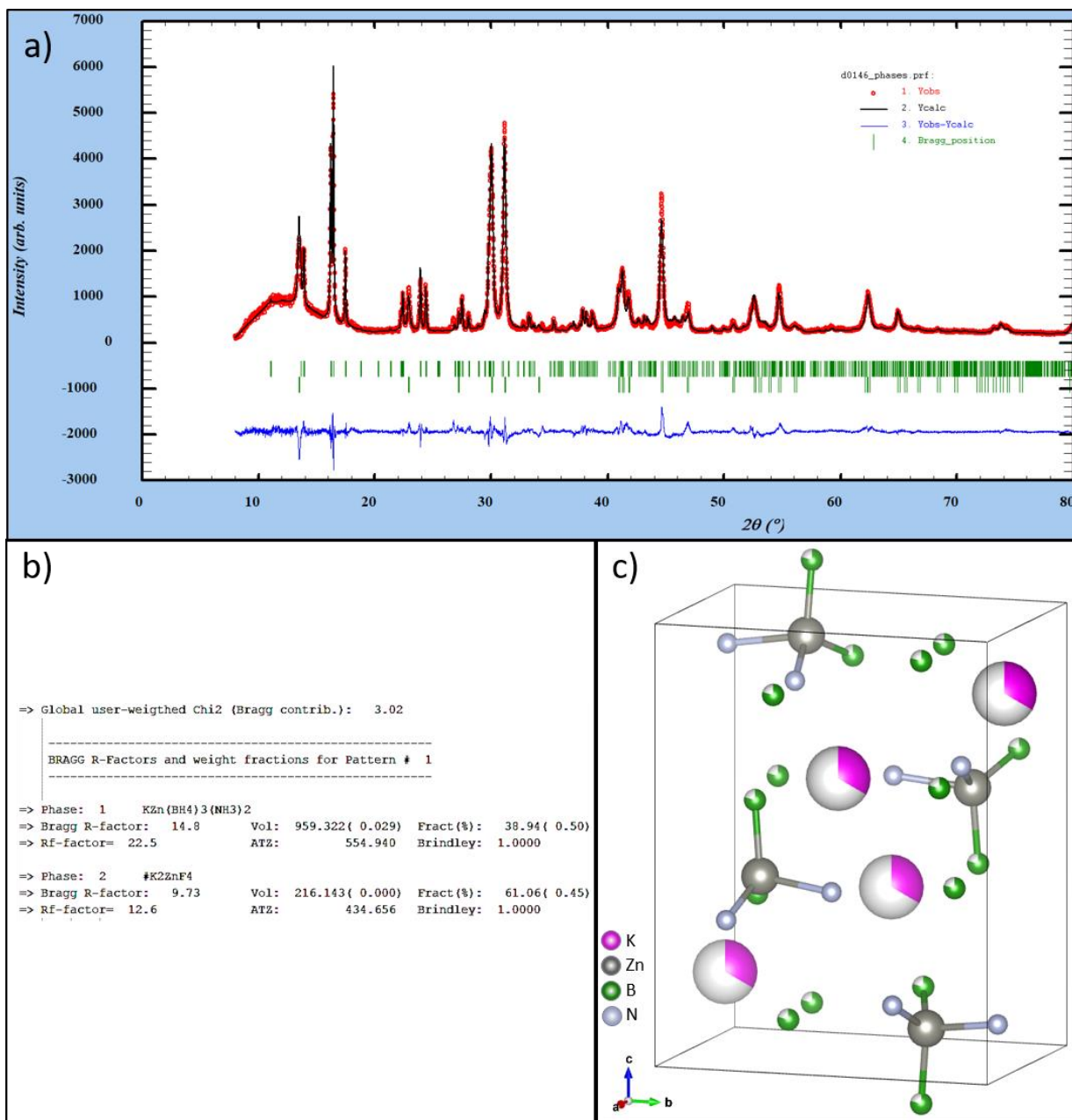


Figure III-S6: Rietveld refinement of XRD data for $\text{K}_{0.33}\text{Zn}(\text{BH}_4)_{2.33}(\text{NH}_3)_2 + \text{K}_2\text{ZnF}_4$ sample. b) Refinement quality and yield calculation for each phase from (.sum) file c) Unit cell visualization based on refinement data.

Similarly, to synthesize $\text{KZn}(\text{BH}_4)_3(\text{NH}_3)_2$ compound with minimal excess unreacted precursors the stoichiometric ratio of $\text{ZnF}_2:\text{KBH}_4$ had to be 1:1.2 instead of theoretical 1:1.5. This could also be explained by formation of $\text{K}_{1-x}\text{Zn}(\text{BH}_4)_{3-x}(\text{NH}_3)_2$ type main phase. Another reason for alkali cation vacancy model was born from the inability to perform Rietveld refinement without this assumption. XRD diffractogram of $\text{KZn}(\text{BH}_4)_3(\text{NH}_3)_2 + \text{K}_2\text{ZnF}_4$ powder was refined without this assumption (Figure III-S7a). Global Chi and Bragg factor values obtained were worse compared to Figure III-S6b. Additionally, “zinc tetrahedra” was distorted beyond the definition of tetrahedron as a result of the refinement process (Figure III-S7b).

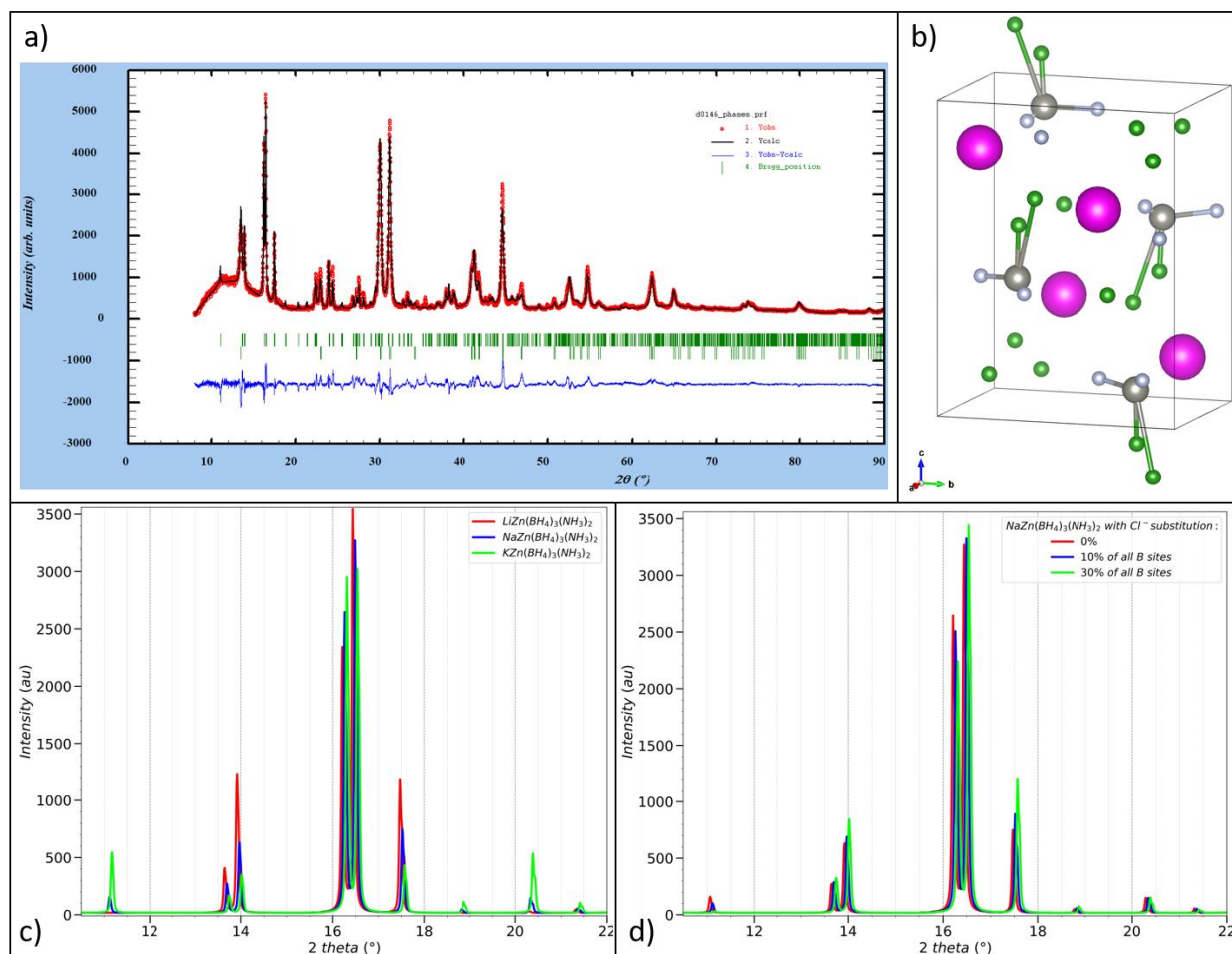


Figure III-S7: a) simulated XRD pattern for various $\text{AZn}(\text{BH}_4)_3(\text{NH}_3)_2$ for $A=\text{Li}; \text{Na}; \text{K}$ while keeping the atomic positions fixed (small 2θ is introduced for better visibility) b) simulated XRD pattern for various $\text{NaZn}([\text{BH}_4]_{1-x}\text{Cl}_x)_3(\text{NH}_3)_2$ for $x=0; 0.1; 0.3$ c) Rietveld refinement attempt of $\text{KZn}(\text{BH}_4)_3(\text{NH}_3)_2 + \text{K}_2\text{ZnF}_4$ without partial alkali cation occupancy; Global Chi = 4.12; main phase Bragg factor = 20.1 d) Unit cell visualization based on refinement data.

Simulated XRD pattern for various $\text{AZn}(\text{BH}_4)_3(\text{NH}_3)_2$ (Figure III-S7c) showed that the peaks at $2\theta \sim 11^\circ$ and 20.5° are highest for $A=\text{K}$ and lowest for $A=\text{Li}$. Similarly, simulated XRD pattern for various $\text{NaZn}([\text{BH}_4]_{1-x}\text{Cl}_x)_3(\text{NH}_3)_2$ (Figure III-S7d) showed that the peak at

$2\theta \sim 11^\circ$ decreases with increasing degree of chloride anion substitution. In our attempts to perform Rietveld refinement without these two approaches the peak at $2\theta \sim 11^\circ$ always displayed a mismatch in intensity between calculated and experimental pattern.

Better quality XRD measurements needs to be performed on the pure main phase samples in order to build any reliable conclusions. It is worthy to note that more mobile alkali cations might also have higher thermal displacement coefficient (B_{iso}) eliminating the need (partially) for the cation vacancy. This can be an indication of ionic conductivity in these compounds.

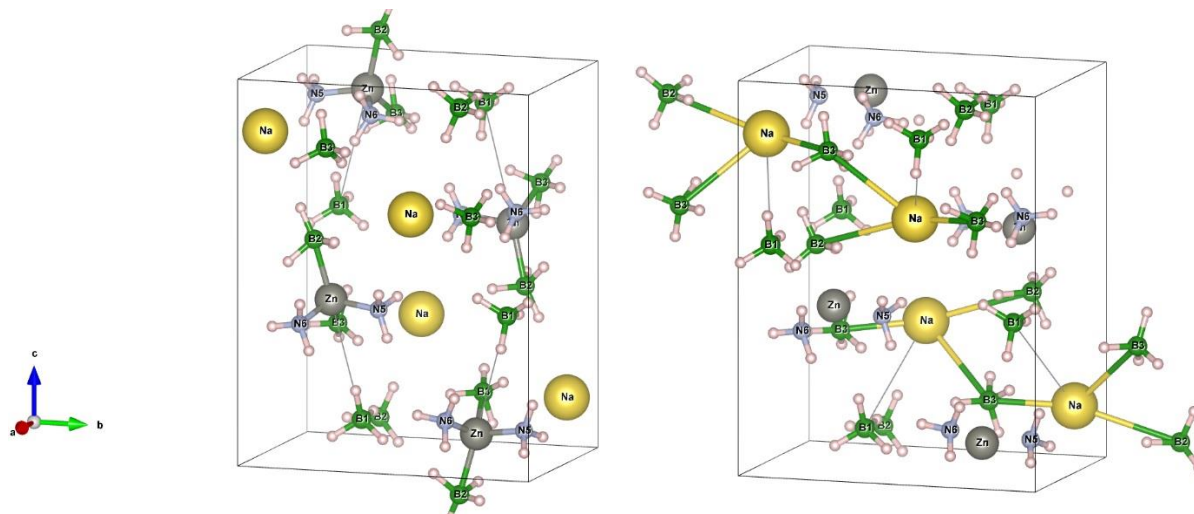


Figure III-S8: Unit cell environment of $\text{NaZn}(\text{BH}_4)_3(\text{NH}_3)_2$ compound, where both cations are closer to B2 and B3 and farther from B1 atoms a) Zn-B_{2,3} bond length 2.1-2.3 (cylinder), Zn-B1 bond length 4.1-4.3Å (line) b) Na-B_{2,3} bond length 3.6-3.7 (cylinder), Na-B1 bond length 4.4-4.5Å (line)

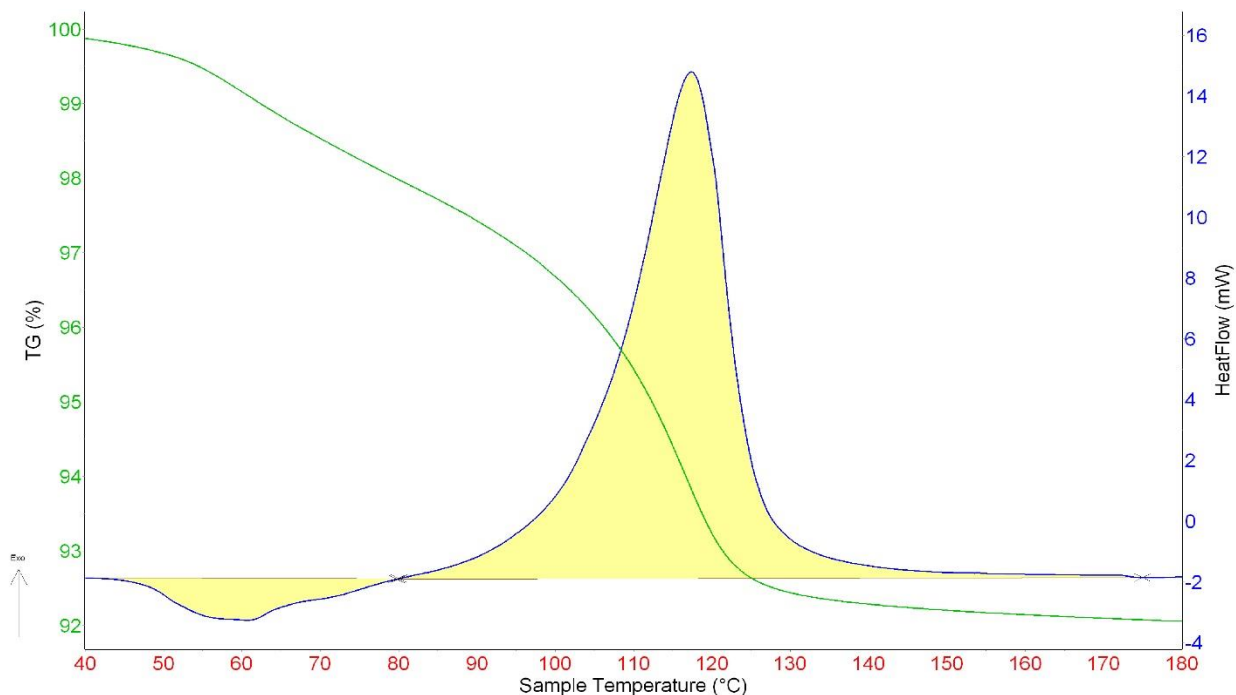


Figure III-S9: DSC-TGA result of $\text{Zn}(\text{BH}_4)_2(\text{NH}_3)_2 + \text{LiCl}$ sample measured under helium flow and 2°C min^{-1} heating rate

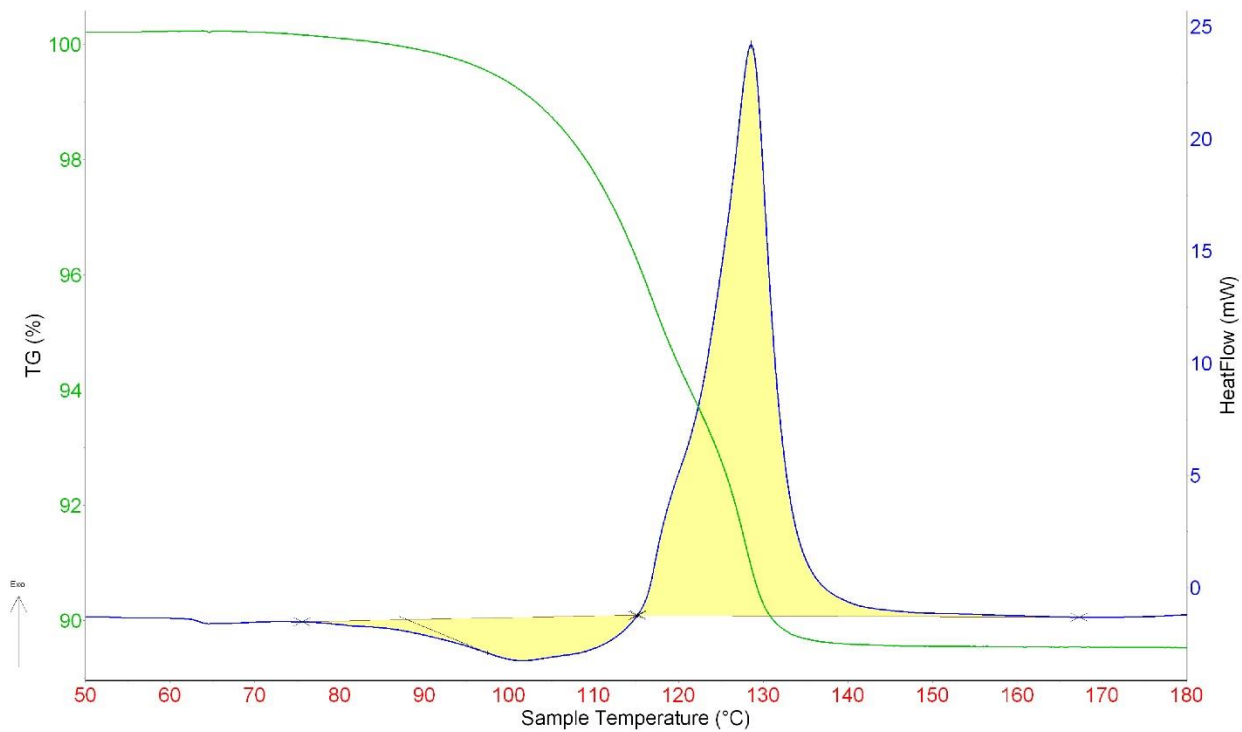


Figure III-S10: DSC-TGA result of $\text{LiZn}(\text{BH}_4)_2(\text{NH}_3)_2 + \text{LiCl}$ sample measured under helium flow and 2°C min^{-1} heating rate

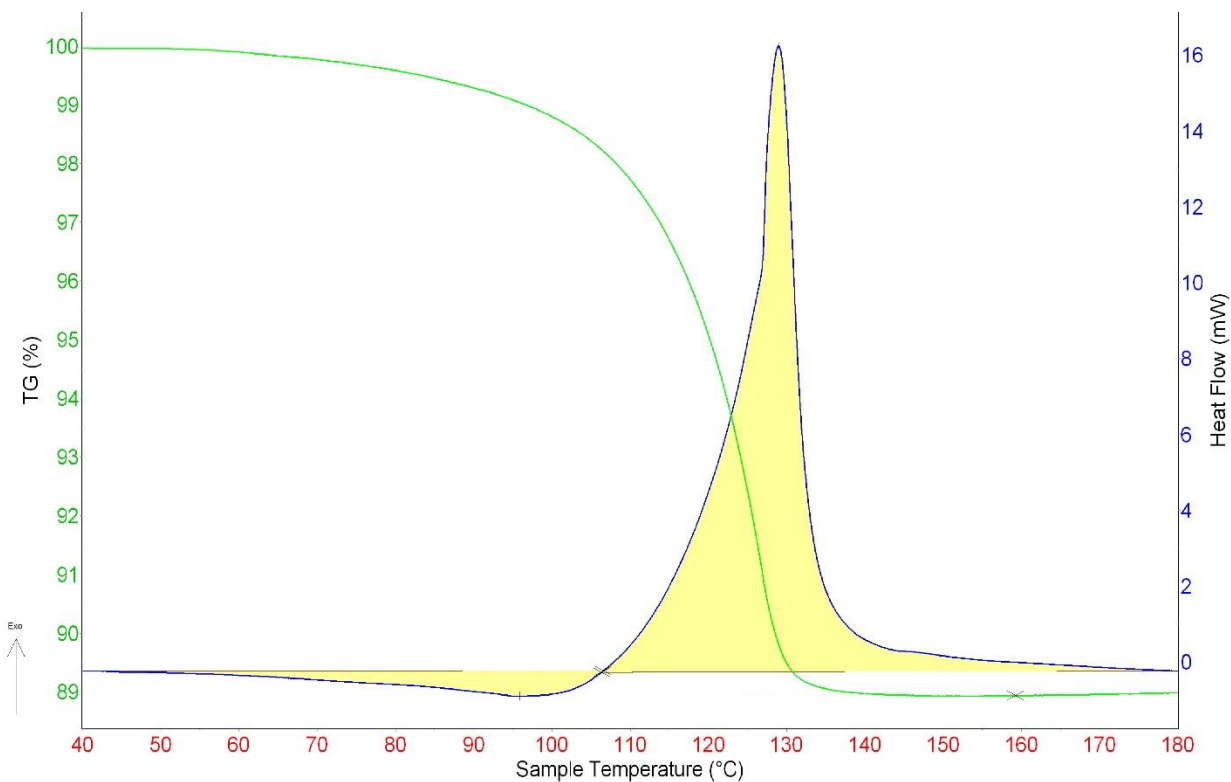


Figure III-S7: DSC-TGA result of $\text{NaZn}(\text{BH}_4)_2(\text{NH}_3)_2 + \text{NaCl}$ sample measured under helium flow and $2^{\circ}\text{C min}^{-1}$ heating rate

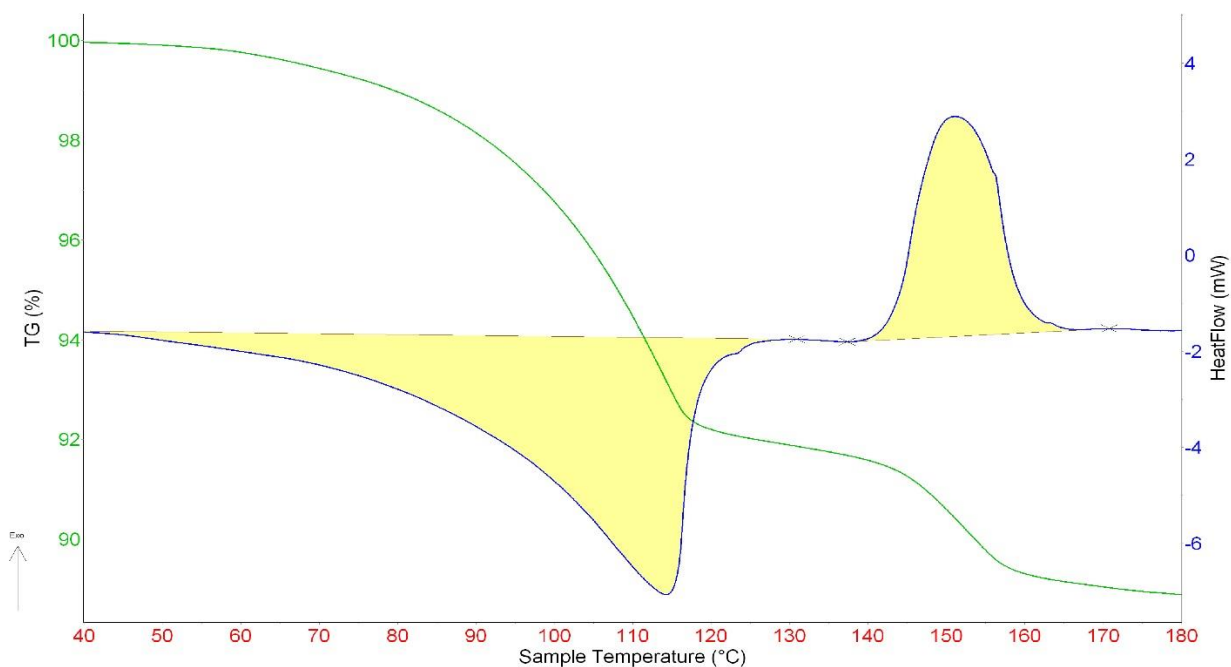


Figure III-S8: DSC-TGA result of $\text{KZn}(\text{BH}_4)_2(\text{NH}_3)_2 + \text{KCl}$ sample measured under helium flow and $2^{\circ}\text{C min}^{-1}$ heating rate

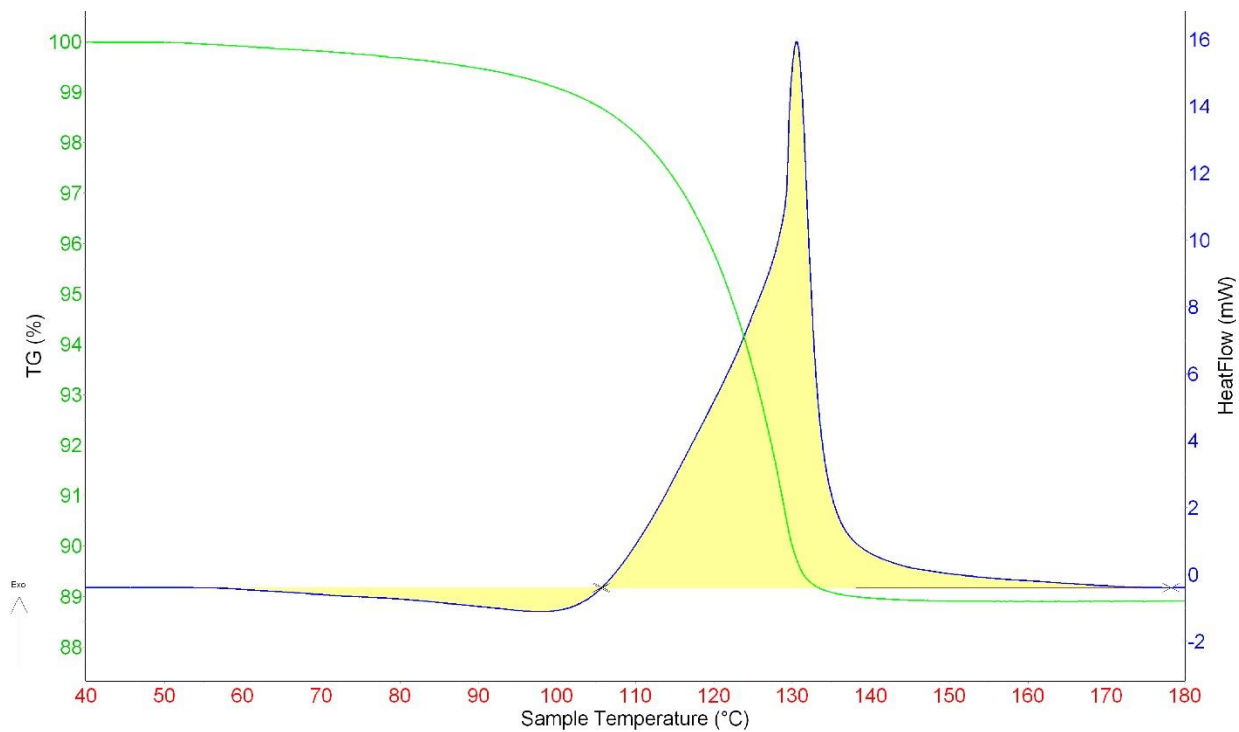


Figure III-S13: DSC-TGA result of $\text{NaZn}(\text{BH}_4)_2(\text{NH}_3)_2 + \text{NaF}$ sample measured under helium flow and 2°C min^{-1} heating rate

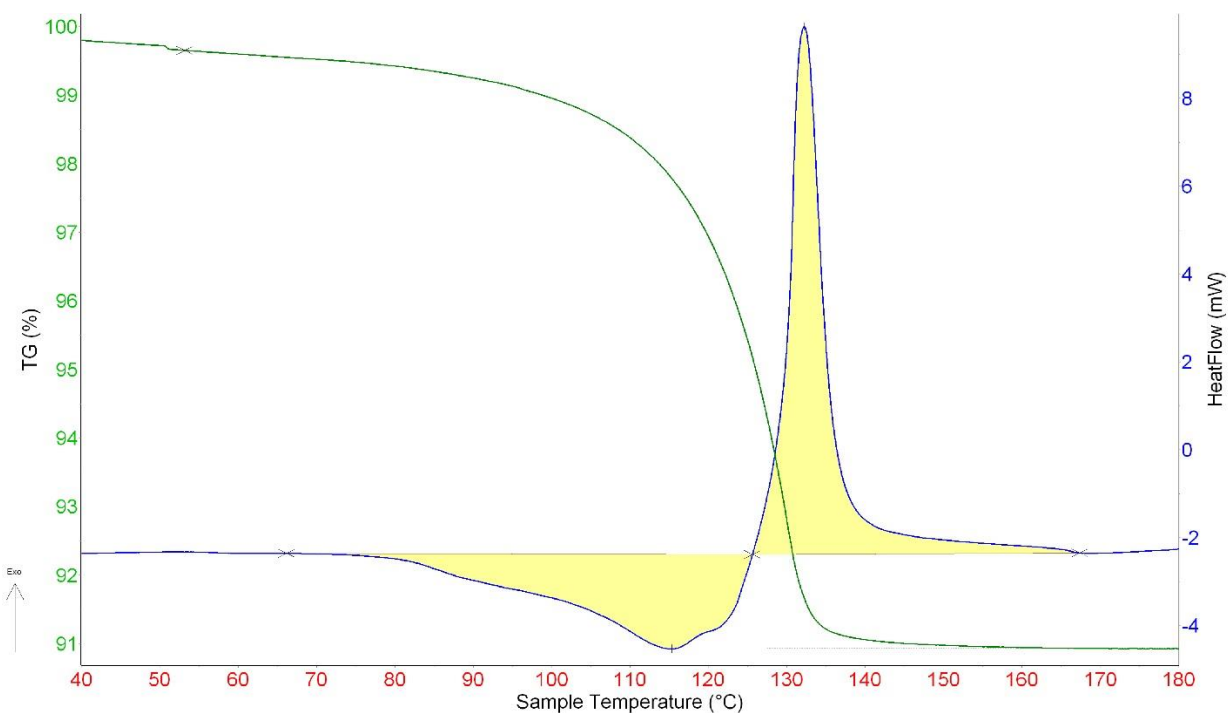


Figure III-S14: DSC-TGA result of $\text{KZn}(\text{BH}_4)_2(\text{NH}_3)_2 + \text{K}_2\text{ZnF}_4$ sample measured under helium flow and 2°C min^{-1} heating rate

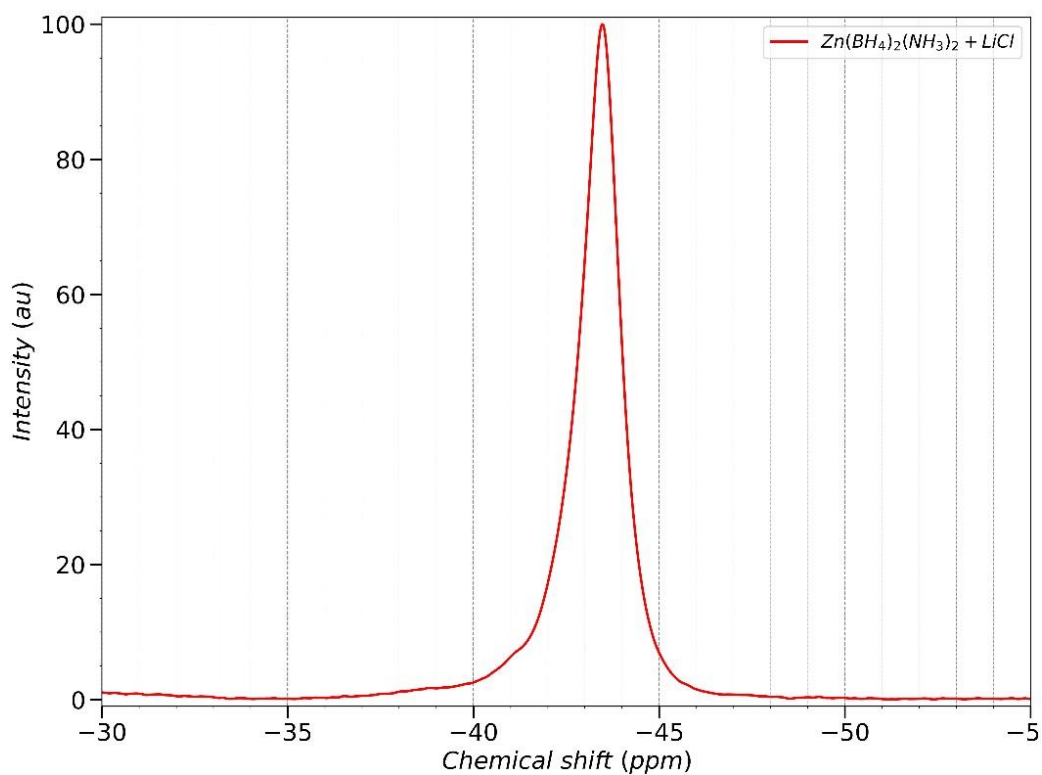


Figure III-S15: ^{11}B MAS NMR spectrum of $\text{Zn}(\text{BH}_4)_2(\text{NH}_3)_2 + \text{LiCl}$ sample

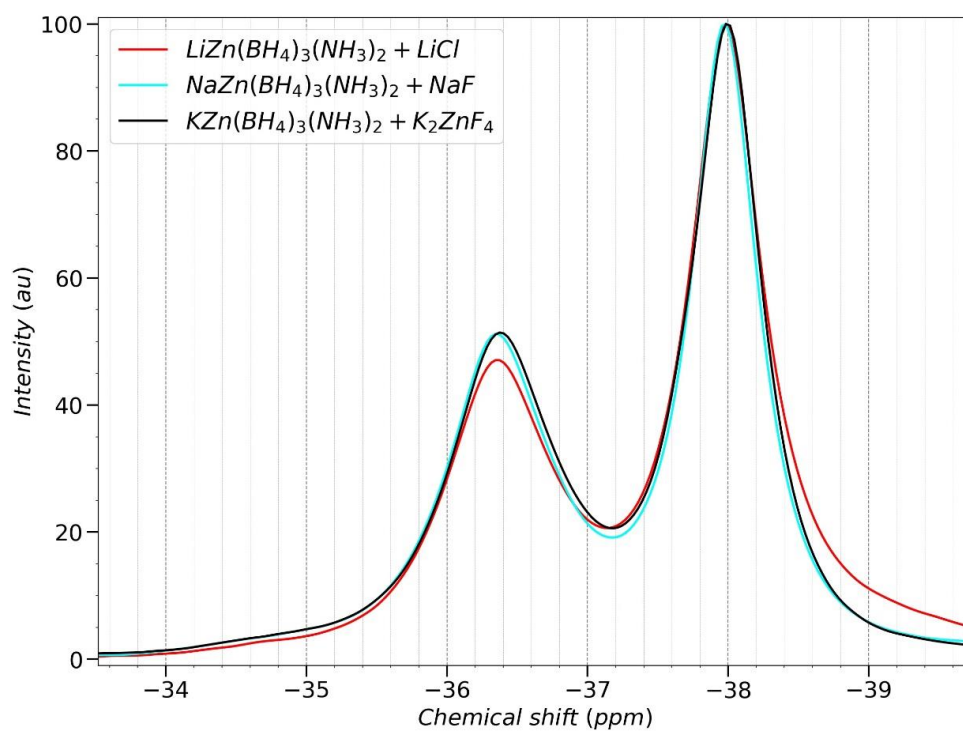


Figure III-S16: ^{11}B MAS NMR spectra of bimetallic AZB compounds synthesized with ZnF_2 precursors



Chapter IV

Optimizing hydrogen storage capacity of Zn-B-N-H compounds



IV. Optimizing hydrogen storage capacity of Zn-B-N-H compounds

IV.1. Objective

In this Chapter, we will focus on improving the hydrogen storage capacity of Zn-B-N-H system and explore all the possible hydrogen storage compounds and mixtures that can be formed from these atoms: $\text{NH}_4\text{Zn}(\text{BH}_4)_3$, $\text{Zn}(\text{BH}_4)_2(\text{NH}_3)_2$, $\text{Zn}(\text{NH}_2\text{BH}_3)_2$ and others. Building on the results and the understanding of ammine zinc borohydride materials and their scalable synthesis technique presented in Chapter 3, in this chapter we will discuss their experimental hydrogen capacity and the approaches that can be utilized to improve this capacity on the material level.

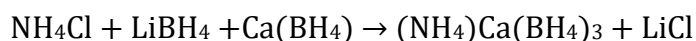
IV.2. Ammonium metal borohydrides

For a given M-B-N-H system, the highest theoretical hydrogen capacity can be achieved in ammonium metal borohydride $(\text{NH}_4)_n\text{M}(\text{BH}_4)_{m+n}$ type structure due to their hydrogen bond saturation level compared to ammine metal borohydride $\text{M}(\text{BH}_4)_m(\text{NH}_3)_n$ or metal amidoboranes $\text{M}(\text{NH}_2\text{BH}_3)_m(\text{NH}_3)_n$.

Ammonium metal borohydrides can be seen as molecular mixture of NH_4BH_4 and $\text{M}(\text{BH}_4)_m$ compounds. Unfortunately, NH_4BH_4 despite having highest known theoretical hydrogen capacity of 24.5 wt%, it decomposes rapidly above -20°C into NH_3BH_3 and releases a mole of hydrogen [118]. Hence, the $(\text{NH}_4)_n\text{M}(\text{BH}_4)_{m+n}$ can be seen as $\text{M}(\text{BH}_4)_m$ stabilized NH_4BH_4 or as a bimetallic borohydride $\text{A}_n\text{M}(\text{BH}_4)_{m+n}$ where instead of the alkali cation we use $\text{A}=[\text{NH}_4]^+$ complex cation. The latter approach is more intuitive since the stabilization of high electronegativity metal borohydrides by alkali borohydrides is already known.

First ammonium borohydride compound, $\text{NH}_4\text{Ca}(\text{BH}_4)_3$ was reported in a study that screened perovskite-type bimetallic borohydrides [155]. Goldschmidt tolerance factor is used to predict the stability of various AMX_3 type perovskite compounds where $\text{A} = \text{Li}^+, \text{Na}^+, \text{K}^+, [\text{NH}_4]^+$ and $\text{X} = \text{Cl}^-, \text{Br}^-, [\text{BH}_4]^-, \text{I}^-$.

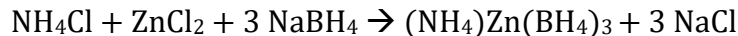
$\text{NH}_4\text{Ca}(\text{BH}_4)_3$ was first synthesized by mechanochemical synthesis:



For chloride free synthesis, ball-mill jar was precooled to -30°C and filled with NH_4BH_4 and $\text{Ca}(\text{BH}_4)_2$, however this approach had low yield due to heating of the jar to 40°C before the end of synthesis. Same synthesis with ether is used to stabilize NH_4BH_4 , but despite the high yield the obtained product was a type of ether solvate. Upon heating $(\text{NH}_4)\text{Ca}(\text{BH}_4)_3$ turns into $\text{Ca}(\text{BH}_4)_3 \cdot \text{NH}_3\text{BH}_3$ intermediate phase at around 110°C while releasing a mole of hydrogen. Above 130°C ammonia borane adduct decomposes completely releasing more hydrogen and some ammonia gas. This leaves behind partially chloride substituted calcium borohydride [156].

IV.2.1. Ammonium Zinc borohydride

To explore other ammonium metal borohydride compounds, we performed the following mechanochemical synthesis reaction:



Initial synthesis at RT resulted in formation of grey powder indicating reduction of the zinc. Hence the synthesis was repeated at 10°C with active cooling, 2 minutes ball-milling with 2 minutes pause to avoid heating of the sample. An hour of synthesis at 500 rpm was sufficient to form NaCl byproduct and unknown crystalline phase. Typical ball-to-powder ration of 155 was chosen for 30 steel balls with 10 mm diameter as a final synthesis recipe. The recovered powder was white, and it was stored below 10°C for further characterization.

IV.2.1.1. Crystallographic analysis

XRD analysis indicated a crystalline phase that was rapidly becoming amorphous at RT (Figure IV-1). Despite our efforts to perform an XRD analysis below 10°C, the long-term stability of the crystalline phase could not be achieved to obtain high precision diffractogram. In fact, even after keeping at 5°C in the refrigerator, the crystallinity of the main phase is lost after few days.

The intensity decay and consequent skewed intensity ratio between lower and higher 2θ peaks was partially circumvented by accumulating all the signal during several fast consequent measurements. The rate of decay of the peaks indicates the presence of a single phase. Possible phases derived from known compounds such as $(\text{NH}_4)\text{Ca}(\text{BH}_4)_3$, $\text{NaZn}(\text{BH}_4)_3$, $\text{LiZn}_2(\text{BH}_4)_5$, $\text{K}_2\text{Zn}(\text{BH}_4)_4$ as well complex zinc halides were tried. Nevertheless, no match could be identified. Hence, the direct identification of the unknown phase was the only approach.

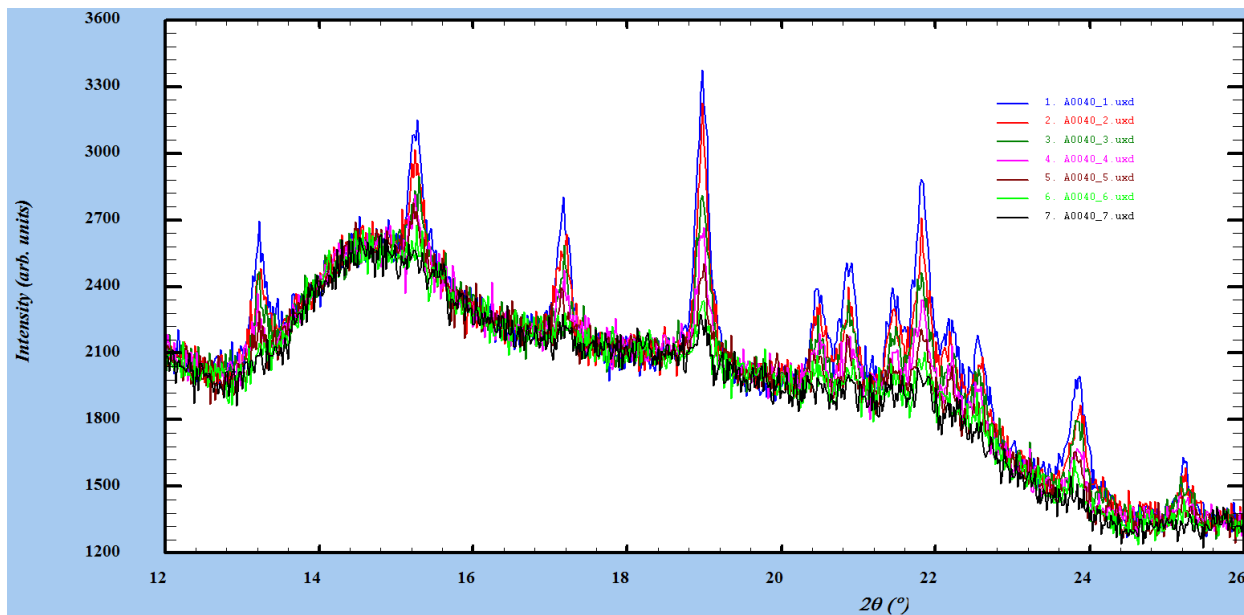


Figure IV-1: The XRD measurement at RT of $\text{NH}_4\text{Zn}(\text{BH}_4)_3$ measured continuously each taking 15mins. Within 1h sample has lost its crystallinity.

DICVOL software identified the only match as the monoclinic unit cell. CHECKCELL software minimized the best fitting space group to only $\text{P2}_1/\text{c}$. Using FullProf WinPLOTR Le Bail profile matching was performed and the best unit cell parameters were fit as $a=12.090\text{\AA}$

$b=11.484\text{\AA}$ $c=9.507\text{\AA}$ $\beta=104.720^\circ$ (Figure IV-2). Then, using the FOX (Free Objects for Crystallography) software Monte-Carlo optimization was performed to find the best positions of the atoms in the unit cell. Alongside the Zn cation, BH_4 and NH_4 tetrahedra were introduced to the model with fixed B-H bond length of 1.141\AA and N-H bond length of 1.1\AA .

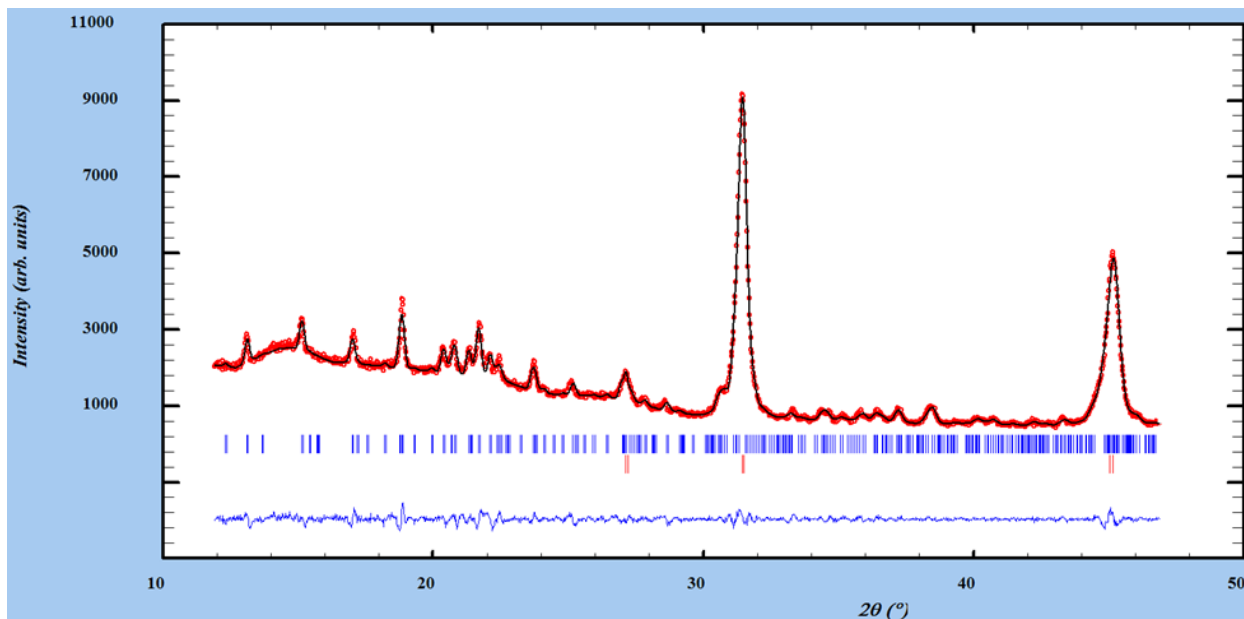


Figure IV-2: Le Bail Profile match analysis of $(\text{NH}_4)\text{Zn}(\text{BH}_4)_3$ phase (blue) and Rietveld analysis of $\text{Na}(\text{BH}_4)_x\text{Cl}_{1-x}$ phase (red)

These values were taken from reference [155] cif file for $(\text{NH}_4)\text{Ca}(\text{BH}_4)_3$. Unfortunately, the FOX simulation could not provide a satisfying solution to the structure and atomic positions. Hence, further structural analysis efforts were eventually abandoned. Needless to say, a higher quality diffractogram obtained at low temperature preferably with high resolution synchrotron diffraction measurements would be necessary to fully resolve the crystalline structure of this compound. Our XRD data were not of sufficient quality for phase identification further complicated by perturbed peak intensities.

IV.2.1.2. Raman analysis

Raman spectroscopic analysis was performed to understand the bonding structure of the $(\text{NH}_4)\text{Zn}(\text{BH}_4)_3$. The spectroscopic analysis is performed by precooling the metallic sample holder to below RT. This minimized the local heating of the sample by laser spot during 15 to 45 minutes long signal accumulation. As can be seen from Figure IV-3, its Raman spectrum is surprisingly similar to that of $\text{NaZn}(\text{BH}_4)_3$. The only difference is small peaks in $3100\text{--}3300\text{ cm}^{-1}$ range that correspond to N-H stretching vibrational modes similar to ammonia borane and $\text{NaZn}(\text{BH}_4)_3(\text{NH}_3)_2$ compounds. Upon amorphization the Raman active modes of the $(\text{NH}_4)\text{Zn}(\text{BH}_4)_3$ phase are also lost. This also indicates that the similar Raman peaks are not coming from $\text{NaZn}(\text{BH}_4)_3$ impurity phase since it is stable at RT for much longer duration (up to days vs an hour). Laser induced decomposition of $\text{NaZn}(\text{BH}_4)_3$ is also accompanied by formation of new Raman peaks presumably corresponding to intermediate decomposition

phases.

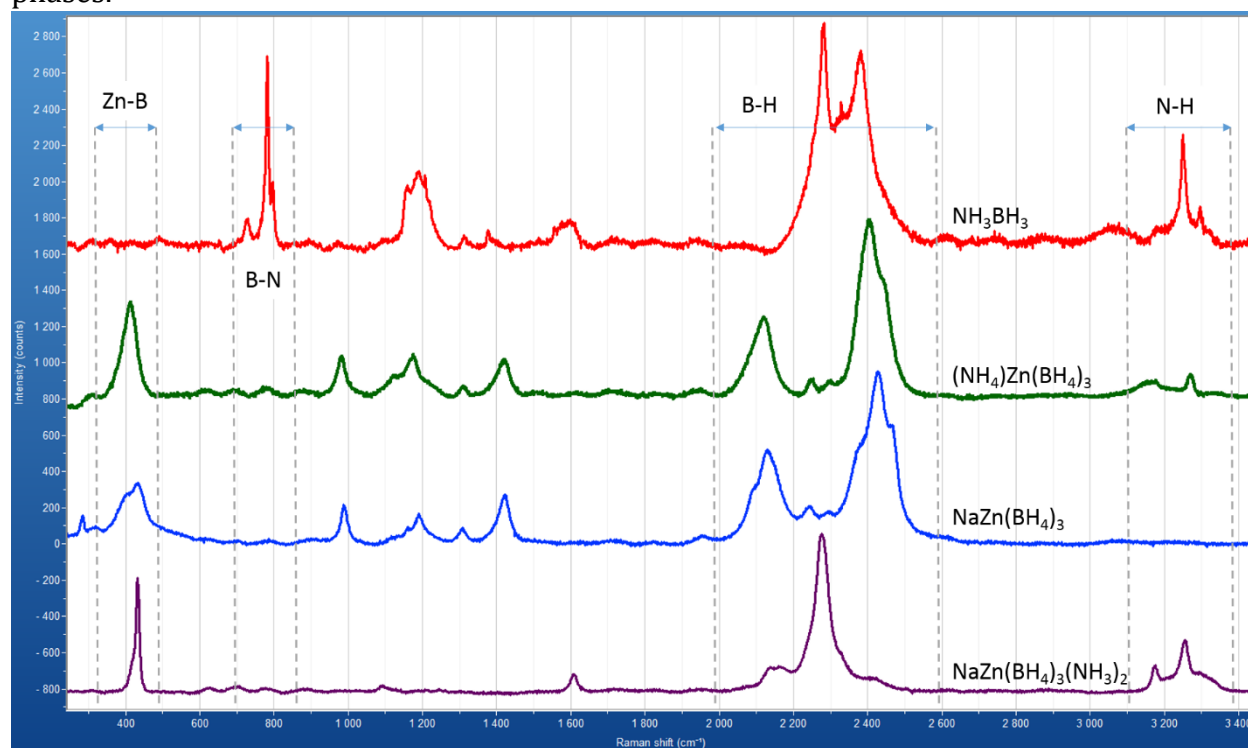


Figure IV-3: Raman spectra of NH_3BH_3 (red), $\text{NH}_4\text{Zn}(\text{BH}_4)_3$ (green), $\text{NaZn}(\text{BH}_4)_3$ (blue) and $\text{NaZn}(\text{BH}_4)_3(\text{NH}_3)_2$ (purple) compounds

This similarity in Raman spectra of $(\text{NH}_4)\text{Zn}(\text{BH}_4)_3$ and $\text{NaZn}(\text{BH}_4)_3$ is due to the presence of $[\text{Zn}(\text{BH}_4)_3]^-$ complex anion in both compounds. In fact, large split in B-H stretching modes indicates bidentate bonding of borohydride anion to zinc cation. Higher frequency peak corresponds to outward B-H stretching while lower frequency peak is ascribed to inward stretching modes of B-H bonds. Small three peaks in $1000\text{--}1400\text{ cm}^{-1}$ region are also indication of bidentate B-H-Zn bending modes [137]. The peak in $1150\text{--}1300\text{ cm}^{-1}$ range corresponds to BH_3 deformation mode which only observed in ammonia borane. While both ammonia borane and $\text{NaZn}(\text{BH}_4)_3(\text{NH}_3)_2$ has NH_3 deformation mode visible in $1550\text{--}1650\text{ cm}^{-1}$ range it is absent in $(\text{NH}_4)\text{Zn}(\text{BH}_4)_3$ [157]. Together with the absence of B-N stretching mode ($750\text{--}850\text{ cm}^{-1}$), it is safe to assume that no partial dehydrogenation happened during synthesis of $(\text{NH}_4)\text{Zn}(\text{BH}_4)_3$, it is not contaminated by ammonia borane like phases and all borohydride species are intact. As a reference compound $\text{NaZn}(\text{BH}_4)_3$ was synthesized with exactly the same mechanochemical synthesis recipe to compare with $(\text{NH}_4)\text{Zn}(\text{BH}_4)_3$ in subsequent characterization techniques.

IV.2.1.3. Thermodynamic analysis

Within a day of being left in inert atmosphere of glovebox $\text{NH}_4\text{Zn}(\text{BH}_4)_3$ turns into grey powder indicating partial decomposition and reduction of zinc. In contact with the air, the compound is pyrophoric.

DCS-TG analysis was performed for both $\text{NH}_4\text{Zn}(\text{BH}_4)_3$ and $\text{NaZn}(\text{BH}_4)_3$ at 2 K/min heating rate (Figure IV-4). $\text{NaZn}(\text{BH}_4)_3$ has slight broad exothermal peak around 50 °C; however, no corresponding mass loss. Conversely, around 100 °C it decomposes sharply with corresponding endothermal peak. On the other hand, $\text{NH}_4\text{Zn}(\text{BH}_4)_3$ has exactly opposite heat profile with small endothermal peak around 30-40 °C corresponding to first mass loss. The main loss is triggered by a broad exothermal peak at 90°C. The exothermal peak indicates formation of BNH_x type decomposition byproducts. However, unlike $\text{NaZn}(\text{BH}_4)_3$, the existence of N-H...H-B bonds represents an opportunity for suppressing the release of diborane or borazine impurity gases. Hence the gaseous decomposition byproducts were analyzed by MS.

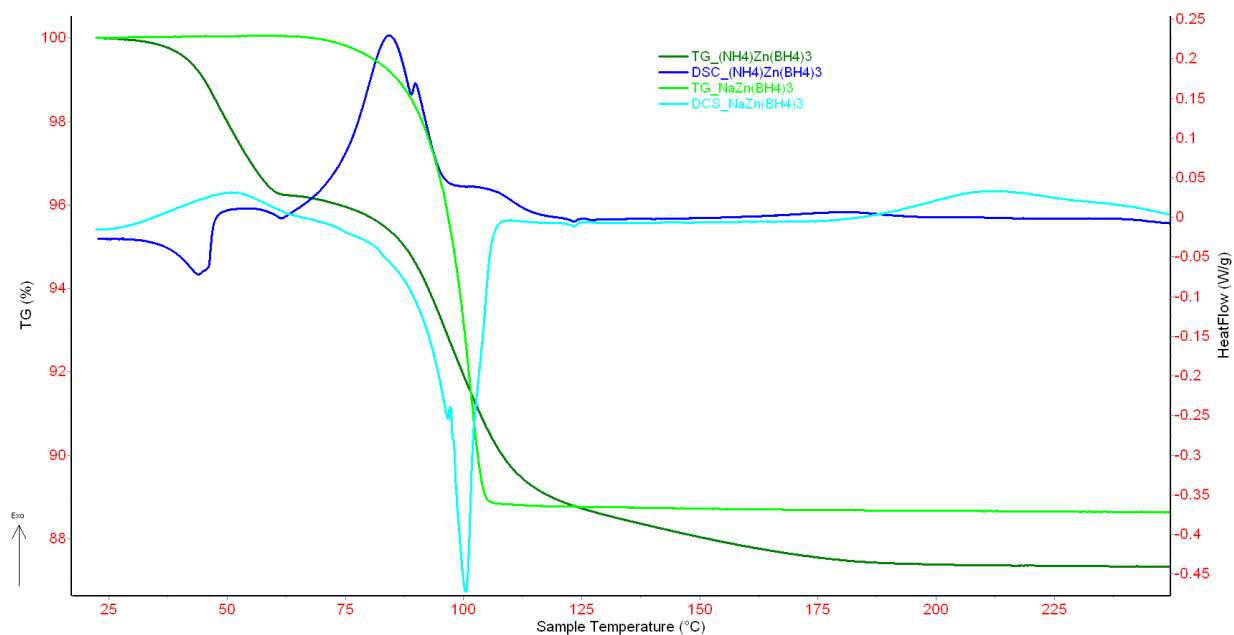
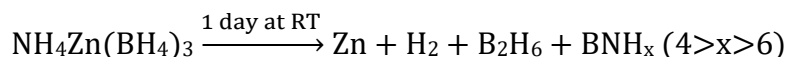


Figure IV-4: DSC data of $\text{NaZn}(\text{BH}_4)_3$ (light blue) and $\text{NH}_4\text{Zn}(\text{BH}_4)_3$ (dark blue), TG data of $\text{NaZn}(\text{BH}_4)_3$ (light green) and $\text{NH}_4\text{Zn}(\text{BH}_4)_3$ (dark green). The heating rate is 2 K/min. Important to note $\text{NaZn}(\text{BH}_4)_3$ has 2 mole of NaCl byproduct while $\text{NH}_4\text{Zn}(\text{BH}_4)_3$ has 3.

As can be seen from Figure V-5, freshly synthesized $\text{NH}_4\text{Zn}(\text{BH}_4)_3$ compound upon heating decomposes releasing hydrogen and diborane in two steps (endothermal peak followed by exothermal one). TPD measurements were performed for both $\text{NaZn}(\text{BH}_4)_3$ and $\text{NH}_4\text{Zn}(\text{BH}_4)_3$. Assuming only release of hydrogen and diborane from both compounds, by replacing Na^+ cation with $[\text{NH}_4]^+$ cation the hydrogen capacity of the compounds for pure phases was increased from 2.6 wt% to 6.7 wt% while the hydrogen purity improved from 12 wt% to 22.5 wt%. Despite the considerable improvement in dehydrogenation properties, $\text{NH}_4\text{Zn}(\text{BH}_4)_3$ still releases too much diborane and more critically is not stable at RT. A day after being kept in glovebox at RT, only the exothermal decomposition step can be observed in TG-MS, releasing mostly hydrogen and diborane and traces of ammonia as well (Figure IV-6). Most likely all the zinc phase is reduced leaving behind an ammonia borane like phase:



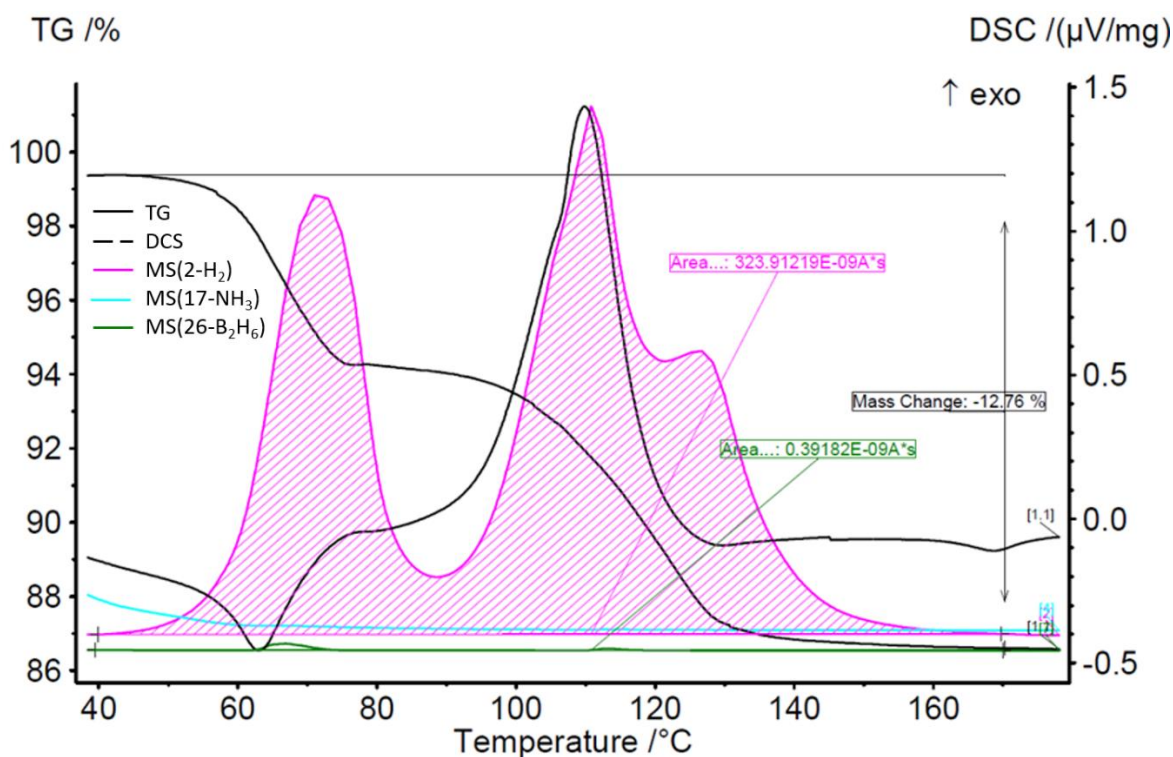


Figure IV-5: $\text{NH}_4\text{Zn}(\text{BH}_4)_3$ right after synthesis, MS m/e signal H_2 (2, pink), ammonia (17, blue), diborane (26, green)

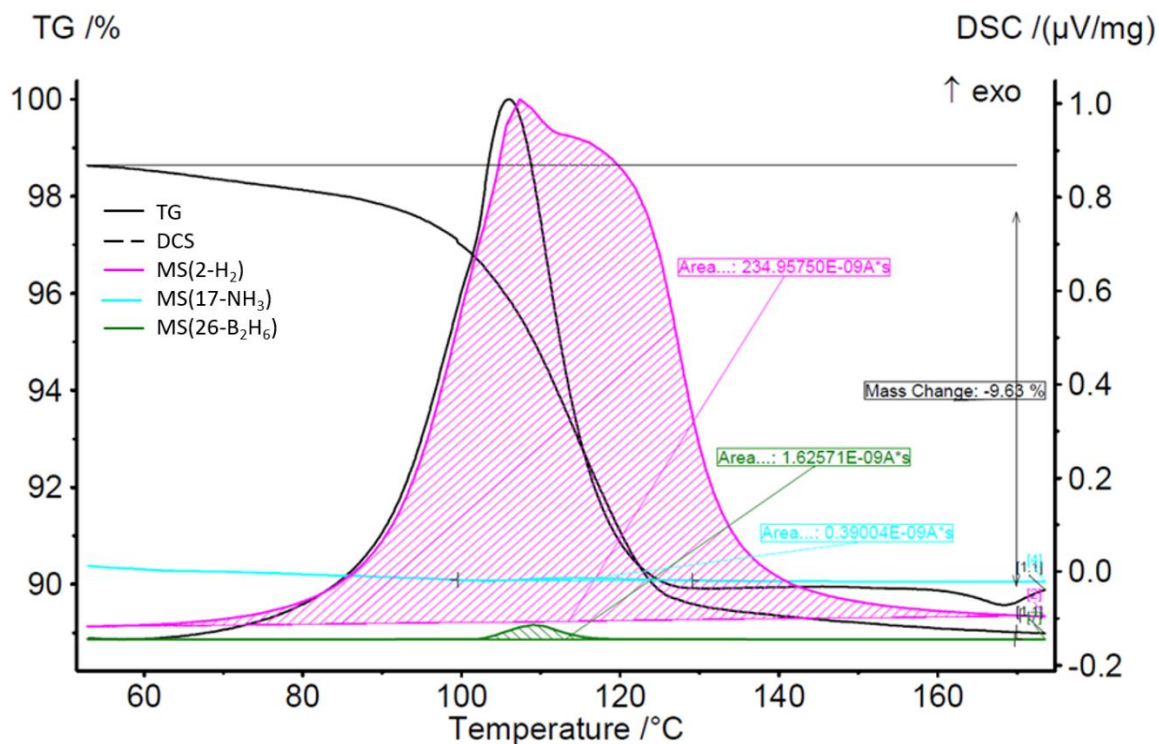


Figure IV-6: $\text{NH}_4\text{Zn}(\text{BH}_4)_3$ one day after synthesis, MS m/e signal H_2 (2, pink), ammonia (17, blue), diborane (26, green)

Raman spectroscopy did not provide the confirmation of B-N bond formation. Hence ^{11}B MAS NMR was performed on this powder with continuous proton decoupling to identify the partial decomposition byproducts. The analysis of the obtained NMR spectrum is shown in Figure IV-7. The main decomposition byproduct is probably the diammoniate of diborane (DADB), $[(\text{NH}_3)_2\text{BH}_2]^+[\text{BH}_4]^-$. This is deduced from the main peaks corresponding to BH_2 and BH_4 environments of boron. It was shown that DADB is the main intermediate for the dehydrogenation of ammonia borane in liquid solvents [158] and liquid ammonia [159]. However, during in situ NMR study of ammonia borane at 88°C after the induction phase DADB is formed during hydrogen release from ammonia borane. Possible other phases observable in Figure IV-7 are the one corresponding to the peak at $\delta = -11\text{ppm}$ which is $\text{NH}_3\text{BH}_2\text{NH}_2\text{BH}_3$ referred as the linear dimer [99]. Additionally, we can also observe small peak at -22ppm possibly best direct observation of NH_3BH_3 . However, since $\text{NH}_4\text{Zn}(\text{BH}_4)_3$ compound was kept at RT not close to melting temperature of ammonia borane, the only explanation is the Zn^{2+} cations that acted as catalyst sites and enhanced the decomposition process of the ammonia borane. In fact, ZnCl_2 is used as catalyst for lowering the dehydrogenation temperature of ammonia borane however not down to RT.

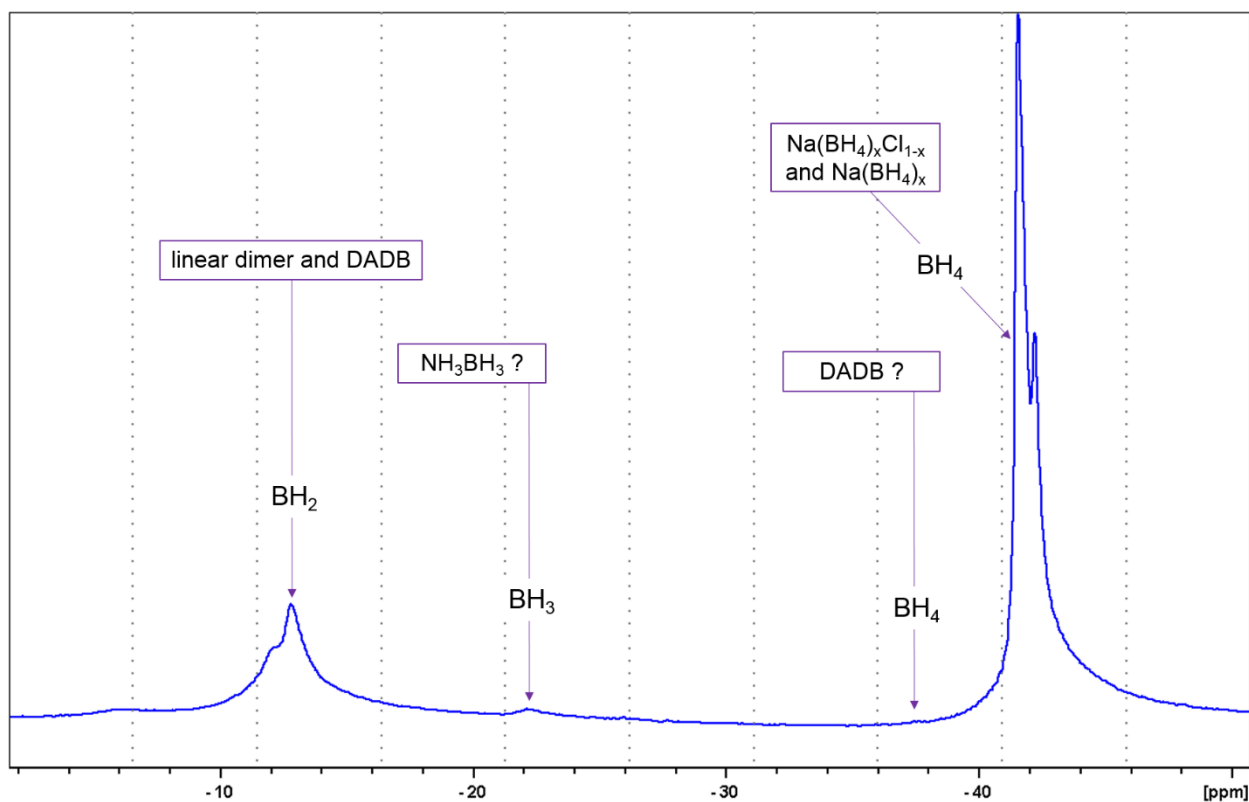
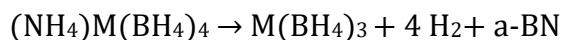


Figure IV-7: $^{11}\text{B}\{-^1\text{H}\}$ MAS NMR spectrum of $\text{Zn}+\text{BNH}_x$ decomposition phase of $(\text{NH}_4)\text{Zn}(\text{BH}_4)_3$

IV.2.2. Overview of ammonium metal borohydrides

There are not many ammonium metal borohydride compounds reported in literature. Dovgaliuk et al synthesized $(\text{NH}_4)\text{Al}(\text{BH}_4)_4$ at -35°C in glovebox by reacting $\text{Al}(\text{BH}_4)_3$ with

NH_4BH_4 [160]. It is reported to decompose similar to $\text{Al}(\text{BH}_4)_3 \cdot \text{NH}_3\text{BH}_3$ with main decomposition byproduct being $\text{Al}(\text{BH}_4)_3 \cdot \text{NHBH}$. Same compound was also reported by Starobrat et al and they also added new members to the ammonium metal borohydride family, namely $(\text{NH}_4)\text{Y}(\text{BH}_4)_4$ and $(\text{NH}_4)\text{Sc}(\text{BH}_4)_4$ [161]. These compounds were synthesized by mechanochemical approach while cooling the ball-mill jar with liquid nitrogen in-between 3 min pauses of the synthesis recipe. For $M = \text{Y}$ and Sc , they reported following decomposition reaction:



Hence, low electronegativity ammonium metal borohydrides will decompose into stable metal borohydride while ammonia borane phase releases hydrogen at low temperatures. $(\text{NH}_4)\text{Al}(\text{BH}_4)_4$ is slightly different with $\text{Al}(\text{BH}_4)_3 \cdot \text{NH}_3\text{BH}_3$ intermediate phase similar to $(\text{NH}_4)\text{Ca}(\text{BH}_4)_3$ which also forms $\text{Ca}(\text{BH}_4)_3 \cdot \text{NH}_3\text{BH}_3$ intermediate phase. A short-lived transient $\text{Zn}(\text{BH}_4)_3 \cdot \text{NH}_3\text{BH}_3$ intermediate might exist; however, the major difference between $(\text{NH}_4)\text{Zn}(\text{BH}_4)_3$ and all the reported compounds is the initial decomposition of $\text{Zn}(\text{BH}_4)_2$ part and reduction of zinc. Unlike all the reported ammonium metal borohydride compounds, corresponding $(\text{NH}_4)\text{Zn}(\text{BH}_4)_2$ is the most unstable and clearly demonstrates exothermal decomposition of ammonia borane like phase at higher temperatures. We have compiled the data from references discussed in this section and plotted decomposition temperature of metal borohydride and corresponding ammonium metal borohydride in Figure IV-8. The figure template is inspired from reference [50].

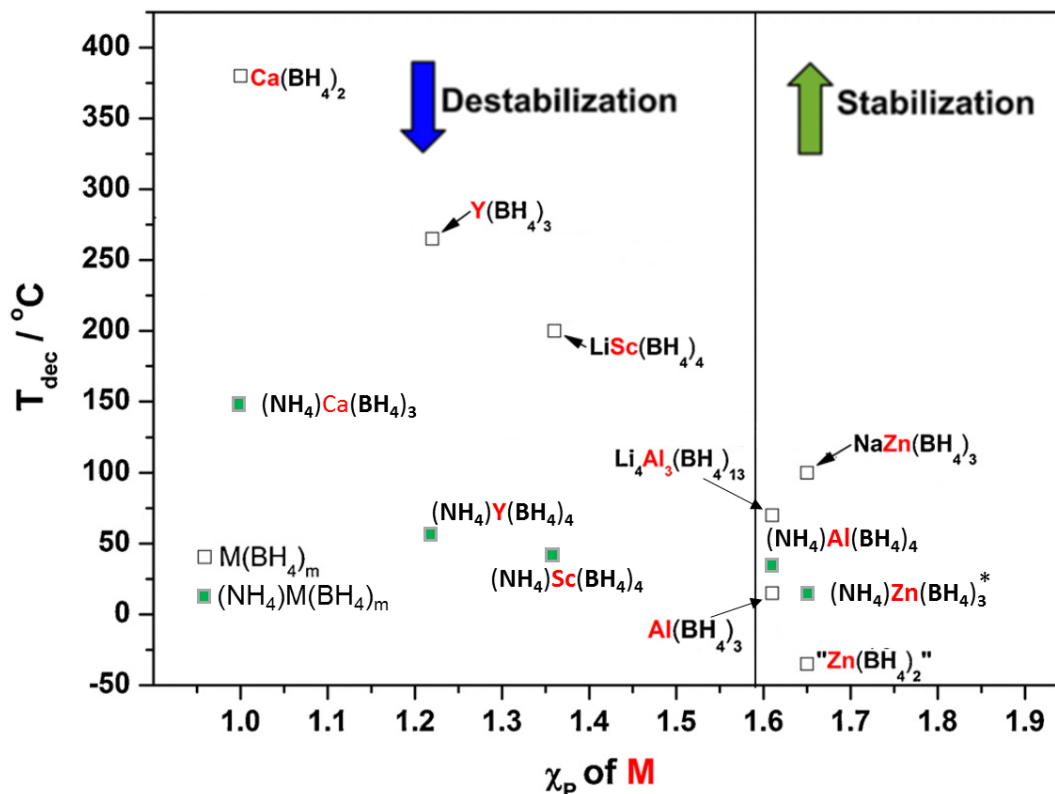


Figure IV-8: Stabilization and destabilization of metal borohydride with ammonium cation

Similar to alkali cation in bimetallic borohydrides or ammonia adduct in ammine metal borohydrides, the low electronegativity metal borohydrides are destabilized by ammonium cation while the high electronegativity metal borohydrides are stabilized. Nevertheless, in terms of their hydrogen storage properties these compounds are not very interesting due to multistep decomposition, poor stability at RT and overall low hydrogen purity.

IV.3. Ammonia borane destabilization

Decomposition of $(\text{NH}_4)\text{Zn}(\text{BH}_4)_3$ at RT into more dehydrogenated phase than ammonia borane is very similar to the catalytic decomposition of ammonia borane by metal chloride additives. Recent study by Nakagawa et al demonstrated that 10 mol% MCl_m added to ammonia borane will decrease its dehydrogenation temperature with increasing electronegativity of metal cation [46]. The catalytic effect is not observed for metal chlorides with $\chi_M < 1.6$. A similar trend was also observed for the amount of released impurity gases like ammonia, diborane and borazine compared to pure ammonia borane. Though, the electronegativity cut-off is much lower at $\chi_M < 1.1$. Meanwhile pure metal additives did not participate in the dehydrogenation of ammonia borane at all. This is in line with previously provided explanation for catalytic effect of metal chlorides. The proposed mechanism describes partial reduction of M^{2+} to $\text{M}^{\alpha+}$ species and involves the formation of the germ $\text{M}^{\alpha+} \cdots \text{NH}_2-(\text{B}^{\gamma+})\text{H}_2$ (where $\alpha \approx 1$). This germ prevents the ring closing reaction of ammonia borane trimers $(\text{NH}_3\text{BH}_2\text{NH}_2\text{BH}_2\text{NH}_2\text{BH}_3)$ hence blocking the formation of borazine ($\text{B}_3\text{H}_6\text{N}_3$) [47]. Therefore, fully reduced metal will not participate in the dehydrogenation of ammonia borane. In case of mortar mixing of MCl_m and NH_3BH_3 , about 5-10 mol% range is necessary to observe kinetic enhancements. However, to minimize the penalty on hydrogen capacity metal chloride amount of as small as 2 mol% can be efficiently utilized with similar enhancement of dehydrogenation kinetics. This was achieved by THF assisted homogeneous mixing of nanosized MCl_2 (where $\text{M}=\text{Ni}; \text{Cu}$) and NH_3BH_3 powders [162].

The electronegativity of the metal cation cannot fully explain the degree of catalytic activity since 5 mol% CuCl_2 has similar improvement as 10 mol% AgCl [46]. Since copper and silver have exactly same electronegativity, we need to consider the difference between their polarizing powers. Although Cu^{2+} has polarizing power of 3.8 assuming that it will be partially reduced to Cu^+ to form a stable germ $\text{M}^{\alpha+} \cdots \text{NH}_2-(\text{B}^{\gamma+})\text{H}_2$, the new polarizing power of Cu^+ becomes almost exactly twice of Ag^+ (1.7 vs 0.8). However the explanation provided in this reference [46] is hinted to same number of chloride anions for 5 mol% CuCl_2 and 10 mol% AgCl additive in ammonia borane. The effect of halides were studied using CoX_2 salt where $\text{X}=\text{F}, \text{Cl}, \text{Br}, \text{I}$ [163]. However, the salt loading was fixed for 20wt% for all mixtures meaning molar ratio of Co^{2+} in this mixture would change as 8, 6, 3.5, 2.5 mol%. The catalytic activity was defined as mass loss from $\text{NH}_3\text{BH}_3-x\text{CoX}_2$ mixture at 100°C and the values were compared to electronegativity and ionic radii of the halides. CoCl_2 and CoBr_2 shared the top of the volcano pattern with lowest activity being observed for CoF_2 and CoI_2 . Nevertheless, using the mass loss values from this article, we can renormalize the mass loss per Co atom and replot the graphs:

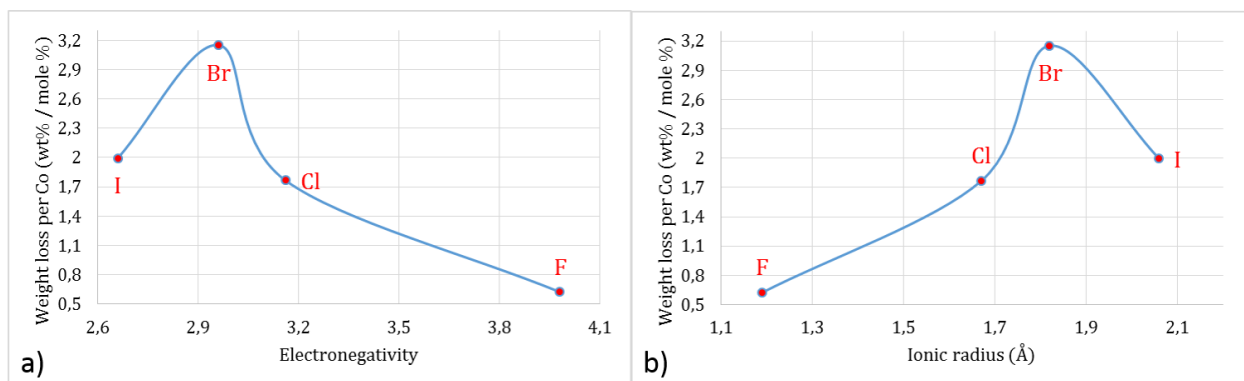


Figure IV-9: Renormalized mass loss percentage from $\text{NH}_3\text{BH}_3-x\text{CoX}_2$ mixture per Co atom (mol%) plotted versus a) electronegativity of halide b) ionic radius of halide in CoX . Data from reference [163]

Hence, we can see that for the same molar ratio of $\text{Co}^{\alpha+}$ cations in ammonia borane, Br^- anions bonded to cobalt provided the highest boost to its catalytic activity. Original explanation of both electronic and steric effects playing a role in modifying the catalytic performance of a given cation remains true due to lower performance of CoI_2 [163]. Since $[\text{BH}_4]^-$ has ionic radius between Br^- and I^- anions we can assume that its contribution to catalytic activity of a chosen metal cation maybe better that of Cl^- [164].

Similar to metal chlorides, metal borohydrides were used to enhance dehydrogenation properties of ammonia borane. $\text{Ca}(\text{BH}_4)_2 \cdot (\text{NH}_3\text{BH}_3)_2$ and $[\text{Li}(\text{BH}_4)]_n \cdot \text{NH}_3\text{BH}_3$ with $n=1, 2$ were synthesized as single phase crystalline samples by ball-milling the metal borohydride and ammonia borane. However, upon heating they dissociate back into metal borohydride and ammonia borane phases. Decomposition then proceeds with first ammonia borane around 100 °C then with metal borohydride at higher temperatures [65]. $\text{Mg}(\text{BH}_4)_2-x\text{NH}_3\text{BH}_3$ mixtures with $x=1,2,3$ were prepared by ball-milling and mortar mixing. Only $\text{Mg}(\text{BH}_4)_2 \cdot (\text{NH}_3\text{BH}_3)_2$ crystalline phase was observed. Interestingly this compound melts at 48°C while the decomposition starts as low as 70-80 °C and finishes before 125 °C. Systematic comparison of various molar ratio mixtures was not provided but the decomposition of $\text{Mg}(\text{BH}_4)_2$ phase was not observed at higher temperatures. Similar to calcium and lithium compounds, for the mixtures of $\text{MBH}_4-2\text{NH}_3\text{BH}_3$ where $\text{M}=\text{Na}, \text{K}, \text{Cs}, \text{Rb}$ no interaction was observed between the components during decomposition. This is explained by the lower polarization power of those cations and consequent negligible effect on dihydrogen elimination reactions [66]. Ammonia borane was introduced to excess liquid $\text{Al}(\text{BH}_4)_3$ to form crystalline $\text{Al}(\text{BH}_4)_3 \cdot (\text{NH}_3\text{BH}_3)$. This compound melts around 46 °C, then the decomposition proceeds in two steps between 60-100 °C [67]. Aluminum is the cation with highest electronegativity and polarizing power reported in $\text{M}(\text{BH}_4)_m \cdot (\text{NH}_3\text{BH}_3)_n$ compounds. Nevertheless, all of these compounds release ammonia, diborane and borazine impurities alongside hydrogen. Molar ratio of metal to ammonia borane in these compounds are mostly fixed with crystalline structure at RT. Despite their decomposition in melted state the effect of various molar ratios is not reported.

LiBH_4NH_3 only desorbs ammonia upon heating up to 250°C ; by mixing this compound with ammonia borane, an eutectic is obtained that melts below RT. Below 0°C , individual components were observed indicating absence of single crystalline phase. Dehydrogenation properties of $\text{LiBH}_4\text{NH}_3-x\text{NH}_3\text{BH}_3$ mixture where $x=1-5$ were analyzed. Although improvements in kinetics of dehydrogenation were observed, the released gases contained ammonia, diborane and borazine contaminations [165].

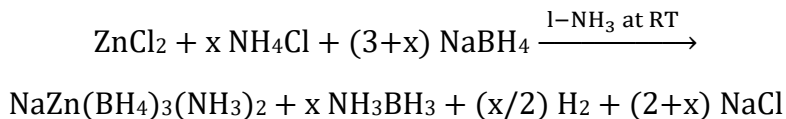
Another interesting mixture is $\text{Zr}(\text{BH}_4)_4(\text{NH}_3)_8-x\text{NH}_3\text{BH}_3$ where $x=2-5$. $\text{Zr}(\text{BH}_4)_4(\text{NH}_3)_8$ was synthesized by ball-milling ZrCl_4 and LiBH_4 resulting $\text{Zr}(\text{BH}_4)_4$ which is similar to aluminum borohydride in its volatility and can be distilled away from LiCl byproduct then reacted with ammonia gas. Pure compounds can release 8.5 wt% hydrogen with similar amount of ammonia impurity (calculated from ~ 90 mol% hydrogen purity) [69]. All the composites decompose between $60-200^\circ\text{C}$ temperature range. By adding up to 5 moles of NH_3BH_3 into $\text{Zr}(\text{BH}_4)_4(\text{NH}_3)_8$ ammonia impurity amount is decreased. However, no diborane or borazine species were observed. Therefore, $\text{Zr}(\text{BH}_4)_4(\text{NH}_3)_8-4\text{NH}_3\text{BH}_3$ mixture reaches 96 mol% hydrogen purity. This results in 12 wt% hydrogen capacity and 4 wt% ammonia release [166]. Another study investigated $\text{Li}_n\text{Al}(\text{BH}_4)_{3+n}(\text{NH}_3)_6-x\text{NH}_3\text{BH}_3$ ball-milled mixtures where $n=0, 2$ $x=1-6$. Among them only $\text{Al}(\text{BH}_4)_3(\text{NH}_3)_6-4\text{NH}_3\text{BH}_3$ which is a simple mixture and $\text{Li}_2\text{Al}(\text{BH}_4)_5(\text{NH}_3)_6(\text{NH}_3\text{BH}_3)_3$ which is a single crystalline phase were discussed. For both compounds, their decomposition happens between on-set of ammonia borane decomposition temperature and off-set temperature of neat $\text{Li}_n\text{Al}(\text{BH}_4)_{3+n}(\text{NH}_3)_6$ phase ($n=0, 2$). Both composites are reported to decompose by 250°C with 16 wt% hydrogen capacity and 3 wt% ammonia impurity (calculated from 19 wt% TG result and 98 mol% hydrogen purity) [167].

Ball-milling of $\text{Mg}(\text{BH}_4)_2(\text{NH}_3)_6-x\text{NH}_3\text{BH}_3$ mixtures for $x=1,2,5,6$ did not also produce any crystalline phases. Pure $\text{Mg}(\text{BH}_4)_2(\text{NH}_3)_6$ first releases only ammonia up to 150°C turning into $\text{Mg}(\text{BH}_4)_2(\text{NH}_3)_2$, as heating continues, the hydrogen is also released which concludes its decomposition process by 250°C . The composite with ammonia borane displays some improved dehydrogenation compared to neat ammonia borane in $100-150^\circ\text{C}$ range. However, the two phases have drastically different thermodynamic stability resulting in mostly independent decomposition of each phase [152]. In $\text{Mg}(\text{BH}_4)_2(\text{NH}_3)_6-x\text{NH}_3\text{BH}_3$ mixture, the coordination sphere of Mg^{2+} is fully saturated by ammonia molecules; hence, ammonia borane species cannot access this cation and benefit from its catalytic properties. $[\text{Mg}(\text{NH}_3)_6]^{2+}$ has effectively much lower polarization power compared to Mg^{2+} . Nevertheless, we can look at $\text{Mg}(\text{BH}_4)_2(\text{NH}_3)_2(\text{NH}_3\text{BH}_3)$ phase which is synthesized by ball-milling as a single crystalline phase. Magnesium cation sits in the center of tetrahedra with two ammonia molecules and two borohydride anions constituting its corners. NH_3 of ammonia borane adduct links the $[\text{BH}_4]-[\text{BH}_4]$ edge of one tetrahedra to the $[\text{NH}_3]-[\text{NH}_3]$ edge of another via its BH_3 end. Despite decomposing as two individual compounds in $100-150^\circ\text{C}$ range and $200-250^\circ\text{C}$ range, due to close proximity and improved access of ammonia borane to Mg^{2+} cation, $\text{Mg}(\text{BH}_4)_2(\text{NH}_3)_2(\text{NH}_3\text{BH}_3)$ releases almost pure hydrogen as opposed to $\text{Mg}(\text{BH}_4)_2(\text{NH}_3)_6-x\text{NH}_3\text{BH}_3$ [168].

ZnCl₂ was also used as additive to improve Mg(BH₄)₂(NH₃)₆–6NH₃BH₃ mixture. In 75-150 °C range with 2-10 mol% ZnCl₂ (recalculated for 1 mole NH₃BH₃ in the original mixture), the release of diborane and borazine was completely suppressed, while ammonia amount was significantly reduced. Curiously, the decomposition peaks corresponding to Mg(BH₄)₂(NH₃)_n (where n<6) at 200-250 °C are also not observable. Since Mg(BH₄)₂(NH₃)₆–6NH₃BH₃–xZnCl₂ mixture is prepared by ball-milling, it is important to ask if any new zinc compounds formed during synthesis. Unfortunately, XRD analysis only proved the existence of NH₃BH₃ phase and possible small amount of Zn(NH₃)₂Cl₂. Nevertheless, the authors speculated possible formation of amorphous ammine zinc borohydride type phases [152].

IV.4. Ammine zinc borohydride – Ammonia borane complex

Liquid ammonia synthesis allowed us to synthesize one-pot synthesis of homogeneous mixtures of ammine zinc borohydride compounds with ammonia borane in any molar ratio. Typical synthesis reaction is:



The main goal with this synthesis was to obtain homogeneous mixture with any ratio of boron and nitrogen species. This enables a study similar to the effect of ammonia to borohydride ratio of $\text{A}_x\text{M}(\text{BH}_4)_{m+x}(\text{NH}_3)_n$ on its dehydrogenation properties [78]. In literature, the reported ZnCl_2 amount used for enhancing dehydrogenation of ammonia borane ranges from 1.5 mol% [169] to 6 mol% [47]. In our $\text{NaZn}(\text{BH}_4)_3(\text{NH}_3)_2-x\text{NH}_3\text{BH}_3$ mixtures, the concentration of zinc cations ranges in 10 to 500 mol%.

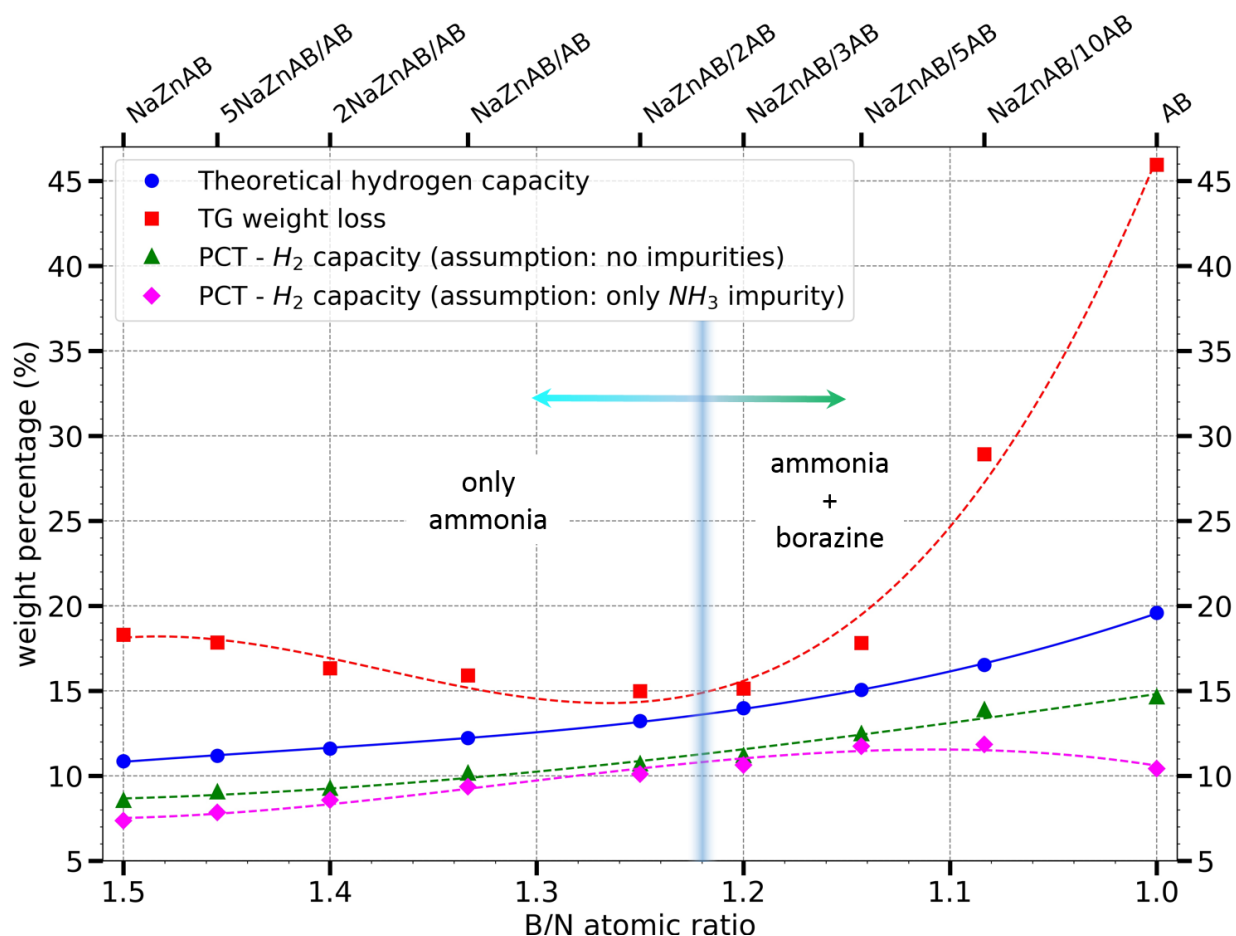


Figure IV-10: Mass loss measured by TG and TPD measurements at 250°C and theoretical hydrogen capacity of various $\text{NaZn}(\text{BH}_4)_3(\text{NH}_3)_2-x\text{NH}_3\text{BH}_3$ ratios (referred as $\text{NaZnAB}/x\text{AB}$)

Hence, $\text{NaZn}(\text{BH}_4)_3(\text{NH}_3)_2-x\text{NH}_3\text{BH}_3$ mixtures were synthesized directly in liquid ammonia in various molar ratios and their thermodynamic properties were characterized by DSC-TG-MS-TPD equipment ensemble. In Figure IV-10, mass loss calculated from TG and TPD measurements are plotted and compared to theoretical hydrogen capacity of various $\text{NaZn}(\text{BH}_4)_3(\text{NH}_3)_2-x\text{NH}_3\text{BH}_3$ mixtures. Calculations from TPD measurements were carried out for both assumptions where released gases are pure hydrogen or contaminated only by ammonia gas. TG results (red ■) always remain above theoretical hydrogen capacity (blue ●) due to release of heavier than hydrogen impurity gases. On the contrary, TPD results (pink ◆) show lower capacity than the theoretical one for the same reason. For $x=2-3$ range, even if the gap between TG and TPD results is minimized, the difference still remains. This means that the pure hydrogen release cannot be achieved in any molar ratio. MS analysis indicates that at and below $x=2-3$ molar ratio only ammonia impurity gas is released. However, above this ratio borazine also starts to be released (Figure IV-S1).

If we look at the DSC curves (Figure IV-11), it becomes more obvious that the two compounds do not decompose in isolation. Pure $\text{NaZn}(\text{BH}_4)_3(\text{NH}_3)_2$ decomposes with single

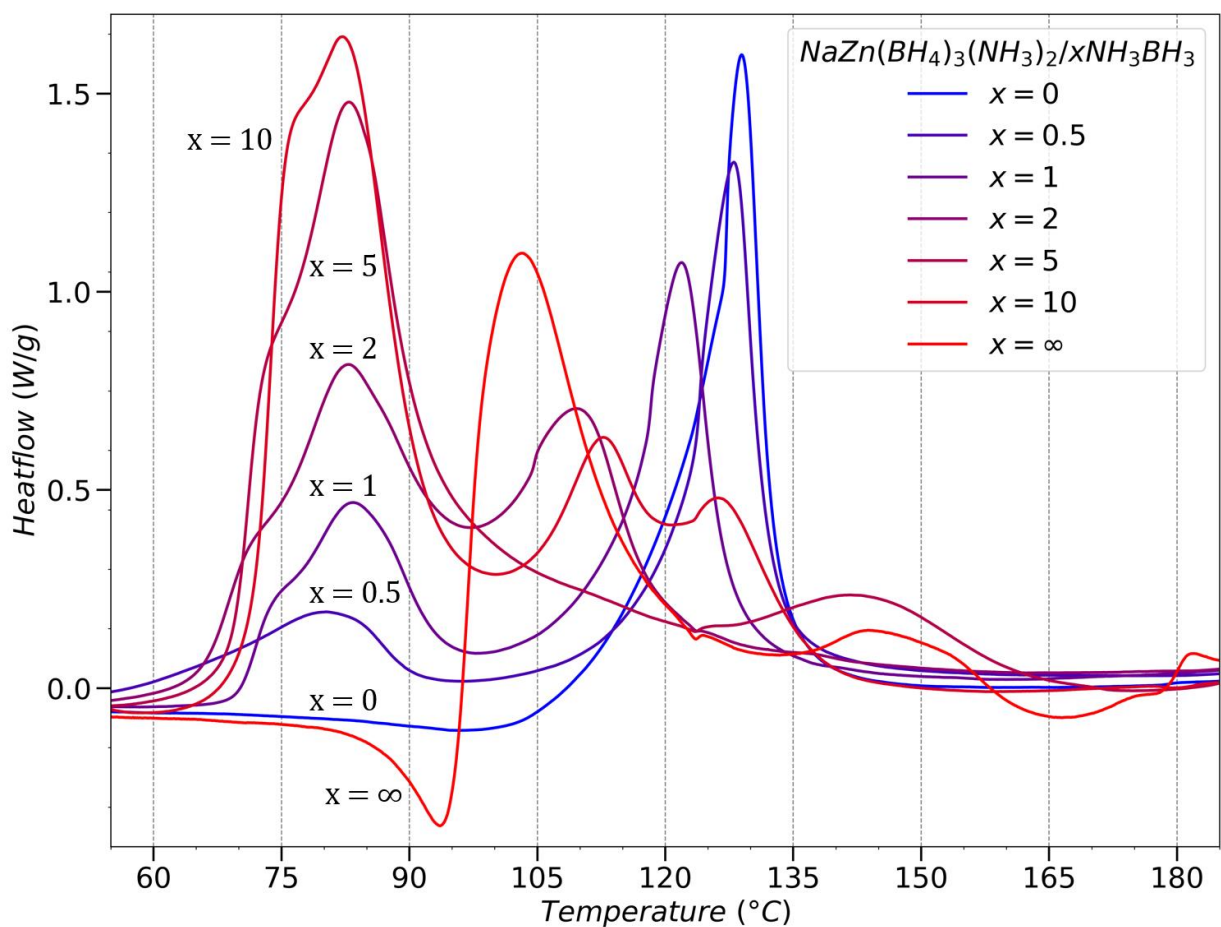


Figure IV-11: DSC curves of various $\text{NaZn}(\text{BH}_4)_3(\text{NH}_3)_2-x\text{NH}_3\text{BH}_3$ mixtures ($2^\circ\text{C}/\text{min}$ heating rate). The heat flow values were calculated by considering the mass percentage of NaCl byproduct phase.

peak in 120-135 °C range (blue line) , while NH_3BH_3 has the main exothermal peak in 95-110 °C range with second smaller one in 135-160 °C range (red line). As the amount of NH_3BH_3 in the mixture increases (increasing x , represented by linear color mixture between blue and red), a new decomposition peak starts to appear in 70-90 °C temperature range. Its intensity also increases with increasing molar ratio of ammonia borane in the mixture. This trend is observed in the presence of concurrent decrease of zinc cations in the mixture from 200 to 10 mol%. Hence, it is safe to assume that release of borazine impurities for $\text{NaZn}(\text{BH}_4)_3(\text{NH}_3)_2-x\text{NH}_3\text{BH}_3$ mixtures with $x>3$ is mainly caused by the fuel mixture, namely the ratio of hydrogenated boron and nitrogen species. Lower x-axis in Figure IV-10, shows the ratio of boron and nitrogen species in the compound. We see that below B/N ratio of ~ 1.2 , the mixture releases borazine gas. This hypothesis is further evidenced by $\text{Zn}(\text{BH}_4)_2(\text{NH}_3)_2-x\text{NH}_3\text{BH}_3$ mixtures (B/N ratio remains 1 regardless of x value). Pure $\text{Zn}(\text{BH}_4)_2(\text{NH}_3)_2$ releases only hydrogen and no impurity gases. However, any amount of added ammonia borane, although it decomposes at lower temperature, it still releases borazine and no ammonia (Figure IV-S2).

To further understand the decomposition process, ^{11}B NMR measurements were performed on $\text{NaZn}(\text{BH}_4)_3(\text{NH}_3)_2-x\text{NH}_3\text{BH}_3$ ($x= 1, 9$) mixtures after isothermal heat-treatments (2-3 hours) at various temperatures in closed steel reactors under inert Ar atmosphere:

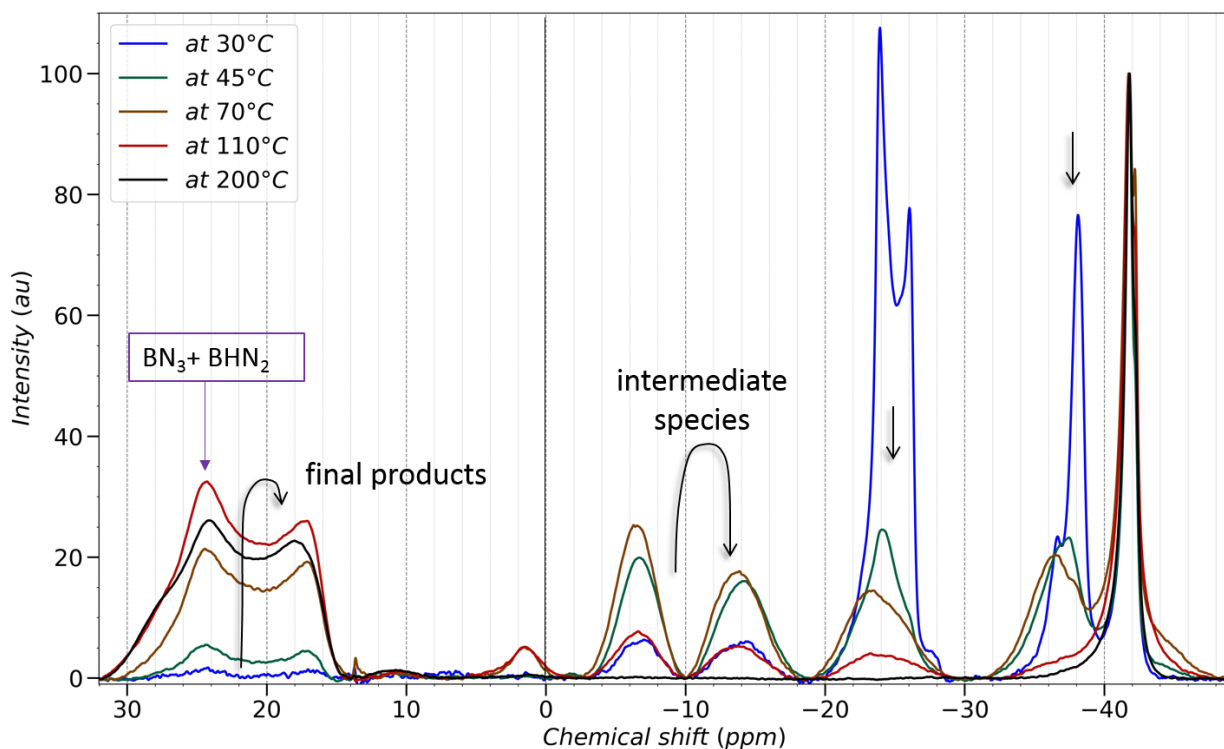


Figure IV-12: Ex-situ $^{11}\text{B}\{-^1\text{H}\}$ NMR analysis of heat-treated $\text{NaZn}(\text{BH}_4)_3(\text{NH}_3)_2-9\text{NH}_3\text{BH}_3$ at various temperatures. Pure NaBH_4 is used as reference for chemical shift at -42.0 ppm.

Since different sample mass is used to fill NMR rotors after heat treatment at each temperature, for quantitative comparison of ex-situ measurements the precise mass

measurements are necessary. The rotors are filled in glovebox and typically can be filled with 10-15 mg of powder. However, with ± 0.5 mg precision of the balance in glovebox a better alternative was found in the NMR spectra of the sample. Since no NaBH_4 contamination of $\text{NaZn}(\text{BH}_4)_3(\text{NH}_3)_2-x\text{NH}_3\text{BH}_3$ could be observed in XRD measurements, the only explanation for the NMR peak at -41.8 ppm (Figure IV-12) are the $[\text{BH}_4]^-$ species in $\text{Na}(\text{BH}_4)_x\text{Cl}_{1-x}$ byproduct of the synthesis process. Hence this peak is used as a reference to renormalize the NMR spectra of different samples. As expected with increasing temperature, both $\text{NaZn}(\text{BH}_4)_3(\text{NH}_3)_2$ and ammonia borane phases disappear in unison. This can be seen by decreasing intensity (black arrows in Figure IV-12) of the peaks in -32–(-40) ppm range corresponding to $\text{NaZn}(\text{BH}_4)_3(\text{NH}_3)_2$ phase and quadrupolar broadening of peaks in -22–(-27) ppm range corresponding to NH_3BH_3 . Simultaneously, in 30–15 ppm range we have the built up of the final decomposition byproducts, tri-coordinated BN_3 or BN_2H type species forming even below 45 °C [100]. The intermediate decomposition species reaches the highest intensity at 70 °C. These species include, BH_2N_2 observable in -10–(-18) ppm range and BHN_3 in -4–(-10) ppm range. A higher temperature intermediate species BN_4 reaches its highest intensity in 3–1 ppm range between 70-110 °C temperature [170].

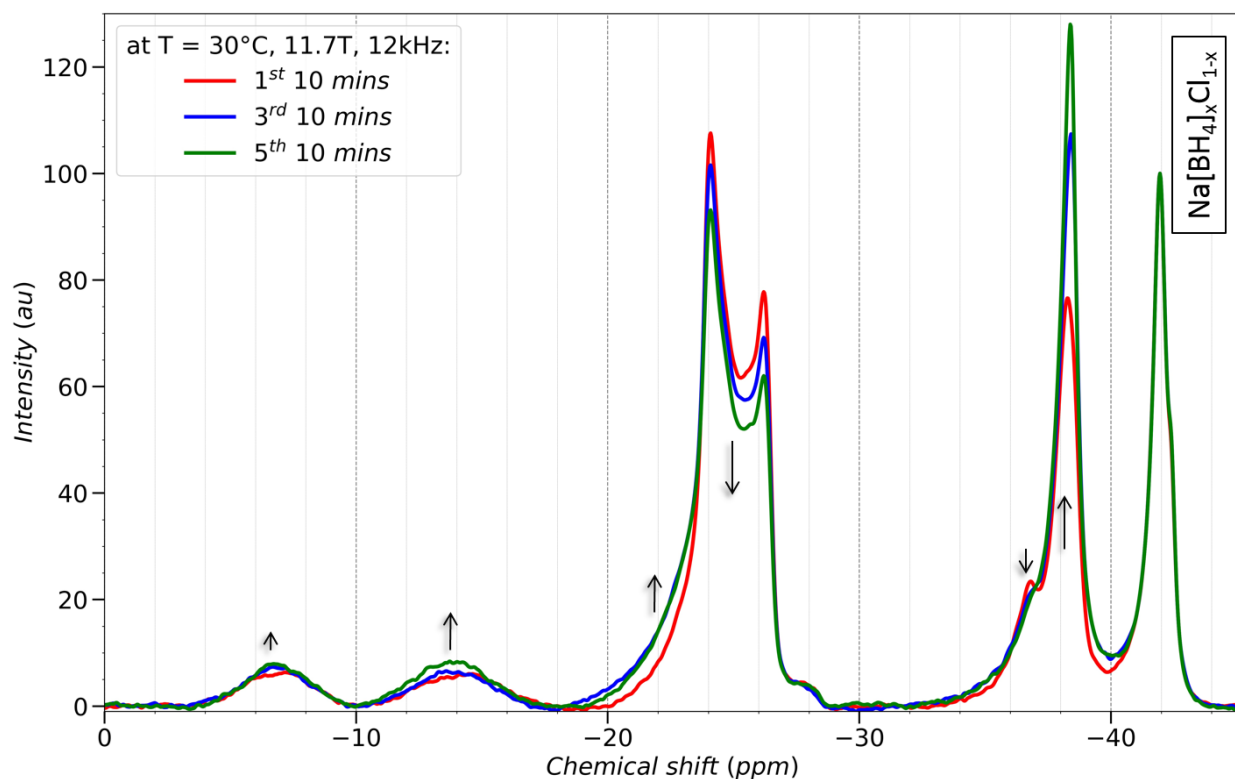


Figure IV-13: In-situ $^{11}\text{B}\{-^1\text{H}\}$ NMR analysis of $\text{NaZn}(\text{BH}_4)_3(\text{NH}_3)_2-9\text{NH}_3\text{BH}_3$ at 30°C

Despite the onset of decomposition temperature for $\text{NaZn}(\text{BH}_4)_3(\text{NH}_3)_2-x\text{NH}_3\text{BH}_3$ mixtures being in 60-70 °C range, under 12 kHz rotation of zirconia rotor at 30 °C, we can observe the decomposition process in action (Figure IV-13). The rotation induced decomposition might be due to the local heating as well as centrifugal force induced compression of powder in the rotor that might improve the access of boron nitrogen species to zinc cations. In Figure IV-

13, ten minutes long accumulation signal were repeated 5 times and 1st, 3rd and 5th spectra are compared. The experiment was not run any longer than 50 mins (5x10mins) to avoid pressure build-up in closed zirconia rotor since it is not designed for in-situ measurements. Similar to ex-situ study, the peak in -41–(-43) ppm due to BH₄ species in Na(BH₄)_xCl_{1-x} byproduct phase is used as the reference to renormalize the spectra. Peaks corresponding to ammonia borane phase decrease as expected while BH₂N₂ and BHN₃ species start to form indicating dehydrogenation process. The unexpected result is increase of intensity for NaZn(BH₄)₃(NH₃)₂ phase. Initial analysis indicate the decrease of BH₄ concentration in B1 site while simultaneously increasing in B2 and B3 sites (Figure III-S8) of NaZn(BH₄)₃(NH₃)₂ phase. However, it is difficult to justify this hypothesis due to limited space for BH₄ species that can maintain certain distance from both Zn²⁺ and Na⁺ cations. A more likely explanation for increase in peak intensity at -38 ppm is the formation of BH₄ species in [(NH₃)₂BH₂⁺][BH₄⁻] (DADB). The mismatch in rate of intensity increase in peaks corresponding to BH₂ species (-10 to -18 ppm) to those of BH₄ species (-38 ppm) in DADB was previously explained by quadrupolar coupling as well as polymerization (of BH₂ species) induced peak broadening [99]. As seen from Figure IV-12 for heat treated sample at 45 °C, the sharp peaks corresponding to BH₄ species is already replaced by single broad low intensity peak. In depth analysis of these peaks is not possible due to lack of temperature control in NMR setup. Low temperature ¹¹B NMR measurements are necessary to perform this analysis. Nevertheless, we wanted to see if sodium cations are involved in destabilization of ammonia borane phase or zinc cations are responsible alone for formation of DADB phase

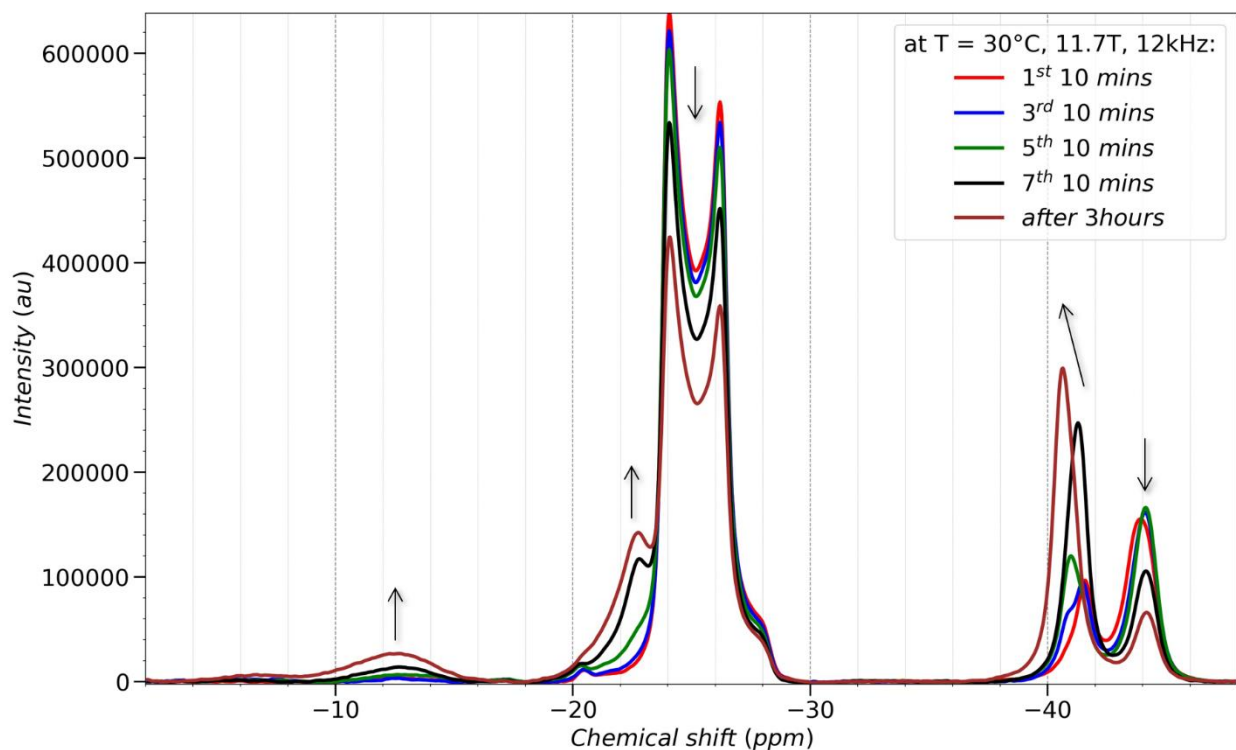


Figure IV-14: In-situ ¹¹B-{¹H} NMR analysis of mortar-mixed Zn(BH₄)₂(NH₃)₂-9NH₃BH₃ at 30°C

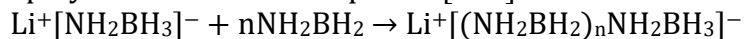
at RT. Hence, a similar in-situ ^{11}B NMR analysis was done on $\text{Zn}(\text{BH}_4)_2(\text{NH}_3)_2-9\text{NH}_3\text{BH}_3$ mixture (Figure IV-14). This mixture was prepared by mortar mixing before the NMR experiment, during preparation noticeable color change to light grey was observed. In-situ NMR decomposition study was performed on $\text{Zn}(\text{BH}_4)_2(\text{NH}_3)_2-9\text{NH}_3\text{BH}_3$ mixture by repeating the same 10 minutes long NMR measurements 7 times. Then it was transferred into glovebox and kept there for 3 hours before performing the same NMR measurement to determine if the decomposition was continuing without rotation. By this time, the powder is black indicating most of the zinc in the powder is reduced. As can be seen from Figure IV-14, the single peak corresponding to $\text{Zn}(\text{BH}_4)_2(\text{NH}_3)_2$ at -44 ppm and the quadrupolar peaks at (-23)–(-27) ppm range corresponding to ammonia borane decrease, while simultaneously new peaks at -12.5 ppm, -22.5 ppm and -41 ppm appear and continue to increase intensity. The peaks at -12.5 ppm and -22.5 ppm correspond to BH_2 and BH_3 species respectively. The peak in (-40)–(-42) ppm range correspond to BH_4 species and continues to upshift while its intensity increases. This is the major difference from in-situ NMR analysis of $\text{NaZn}(\text{BH}_4)_3(\text{NH}_3)_2-9\text{NH}_3\text{BH}_3$ mixture at RT (Figure IV-13). If DADB is the main decomposition phase in both mixtures, the chemical shift from its BH_4 species ranges from -42 ppm to -38 ppm. The presence of BH_3 species (Figure IV-14) is surprising since it does not exist in $[(\text{NH}_3)_2\text{BH}_2]^+[\text{BH}_4]^-$.

Direct observation of $\text{Zn}^{\alpha+}\cdots\text{NH}_2-(\text{B}^{\gamma+})\text{H}_2$ type germ that catalyzes the polymerization of ammonia borane was not possible with ^{11}B NMR. However, direct evidence to formation of DADB at RT in the presence of ammine zinc borohydride species explains the reduced induction time and dehydrogenation at lower temperatures. Experimental evidence to the formation of $\text{Zn}^{\alpha+}\cdots\text{NH}_2-(\text{B}^{\gamma+})\text{H}_2$ type germ might require in-situ decomposition study using ^{15}N NMR. In-situ XPS study might also help to observe the change in oxidation state of zinc cation $2 \rightarrow \alpha \rightarrow 0$ to identify the intermediate species.

IV.4.1. Metal Amidoboranes

A family of materials resembling $\text{M}^{\alpha+}\cdots\text{NH}_2-(\text{B}^{\gamma+})\text{H}_2$ type germ is metal amidoboranes $\text{M}(\text{NH}_2\text{BH}_3)_m$. The presence of BH_3 species (Figure IV-14) during decomposition of $\text{Zn}(\text{BH}_4)_2(\text{NH}_3)_2-9\text{NH}_3\text{BH}_3$ mixture allows us to speculate possible existence of $\text{Zn}(\text{NH}_2\text{BH}_3)_2$ type intermediate phase. Most metal amidoboranes were synthesized by ball-milling MH_m with NH_3BH_3 ($\text{M}=\text{Li}, \text{Na}, \text{K}, \text{Ca}, \text{Sr}$) and similar to the reaction of $\text{L}\cdot\text{BH}_3$ solution with the hydride, it has to be ionic or polar covalent type hydride for successful nucleophilic addition reaction (Chapter 2). The main advantage of amidoboranes is the absence of diborane and borazine type gases during dehydrogenation. Despite significant amount of ammonia being released in some compounds, it can be minimized by adjusting the chemical composition. By combining ^{11}B and ^{23}Na NMR thermal decomposition of NaNH_2BH_3 was studied and it was shown that unlike pure ammonia borane NaNH_2BH_3 does not have DADB or $[-\text{BH}_2-\text{NH}_2-]_n$ type intermediates. Rather, at 115 °C the main decomposition products are NaH and amorphous $\text{Na}_{0.7}\text{NBH}_{1.9}$ [171]. Similarly, an ab-initio computational study on LiNH_2BH_3 showed that energetically more favorable decomposition pathway involves the transfer of a hydride from NH_2BH_3^- to Li^+ and subsequent formation of LiH species. Then LiH facilitates the dihydrogen elimination reaction with proton bonded to nitrogen species

Li-H δ^- ... δ^+ H-N, similar to initial synthesis process. Additionally this reaction lower the energetic barrier to polymerization of B-N species [172]:



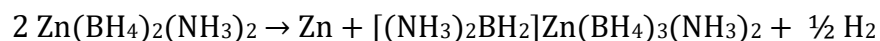
There are not many metal amidoboranes with high electronegativity metal. Unlike most amidoboranes mentioned above, synthesis of magnesium amidoboranes was not possible by direct ball-milling of MgH₂ and ammonia borane. In THF, the mixture releases more than 1 mole of hydrogen (per mole of ammonia borane) meaning Mg(NH₂BH₃)₂ phase is not stable, possibly due to high polarization of the cation. Alternatively, ball-milling of Mg(NH₂)₂ and NH₃BH₃ forms an eutectic and after desorption of 1 mole ammonia crystallizes into Mg(NH₂BH₃)₂·NH₃. The same phase can be synthesized with MgNH phase directly without the need for ammonia desorption [173]. Nevertheless, bimetallic Na₂Mg(NH₃BH₃)₄ can be synthesized directly from MgH₂-2NaH hydride mixture [174]. Similarly, Al(NH₂BH₃)₃ and LiAl(NH₂BH₃)₄ compounds are interesting due to very high polarization power of aluminum cation. These compounds were synthesized by reacting AlCl₃ and LiAlH₄ with NH₃BH₃ at low temperatures. They were heated in glyme at 80 °C and their ¹¹B NMR spectra were recorded every 30 mins. Ionic BH₄ species were observed at (-39)-(-41) ppm at temperature up to 120°C. However, this BH₄ are not accompanied by BH₂ species around -13 ppm to confirm the existence of DADB [175]. The result is not surprising since decomposition of pure NH₃BH₃ in glyme is also very different from solid-state decomposition. In glyme, rapid ring closing reactions of DADB form borazine, cyclodiborazane and cyclotriborazane type intermediate species that does not contain [BH₄]⁻ anion [158]. Even in the presence of glyme-soluble Ni-catalyst at RT ammonia borane decomposes to borazine and polyborazylene type species [176].

Another study reported ball-milling and even hand-milling of LiAlH₄ with ammonia borane resulting in rapid decomposition while releasing diborane and borazine type gases. The final solid byproducts were metallic Al and an amorphous phase. This result conflicts with previous study since it reports LiAl(NH₂BH₃)₄ being more thermodynamically stable than Al(NH₂BH₃)₃ and decomposing around 80°C. Nevertheless, incorporation of extra 2 mole of LiH into LiAlH₄ helped to form a stable crystalline phase upon reaction with ammonia borane. Li₃AlH_{6-x}AB (where x = 4, 5, and 6) mixtures were characterized with ¹¹B NMR after decomposition at 350°C and BH₄ species were observed at -41 ppm similar to decomposition of LiNH₂BH₃ [177]. However, this is some other unidentified amorphous phase since DADB cannot remain stable at 350°C.

IV.4.2. Zinc amidoborane

To identify if Zn(NH₂BH₃)₂ phase exists or not, we set out to synthesize it. Similar to reaction of AlCl₃ with NaNH₂BH₃ at low temperature which yielded Al(NH₂BH₃)₃ [175], sodium amidoboranes was first synthesized by reacting NaH and NH₃BH₃ in THF and liquid ammonia solution. XRD pattern and the reaction yield confirmed a pure phase. Then ZnCl₂ and NaNH₂BH₃ was transferred into ball-mill jar and precooled to 10°C before the synthesis process is started. The synthesis conditions were 500 rpm, ball-to-powder ratio of 305, 2 minutes synthesis followed by 2 minutes of pause while actively cooling the ball-mill jar to 10°C. Due to higher (than usual 155) ball-to-powder ratio, the synthesis process was decided to be monitored every 16 minutes of total synthesis duration. Within the first 16 minutes, the powder turned completely dark. XRD analysis confirmed the existence of only Zn and

NaCl phases. No pressure buildup was detected in ball-mill jar and recovered powder mass close to the expected value. Nevertheless, DSC-TG analysis indicated only 1.5 wt% mass loss at 200°C considering theoretical hydrogen capacity of the system being ~2.5 wt%. Hence, it is safe to conclude that $\text{Zn}(\text{NH}_2\text{BH}_3)_2$ phase is not stable at RT and it accelerated partial decomposition of NaNH_2BH_3 . However, since intermediate decomposition products of NaNH_2BH_3 also contains NaH [171], it could be responsible for reduction of ZnCl_2 . Therefore, direct reaction of ammonia borane with zinc hydride or dimethyl zinc might still yield stable $\text{Zn}(\text{NH}_2\text{BH}_3)_2$ at low temperatures. TG-MS study of mortar mixed ZnCl_2 – $2\text{NaNH}_2\text{BH}_3$ mixture showed main dehydrogenation peak in 50-100°C and second broad peak lasting up to 250°C. Unlike NaNH_2BH_3 this mixture releases no ammonia only pure hydrogen. Hence, assuming $\text{Zn}(\text{NH}_2\text{BH}_3)_2$ is not stable at RT it could be an intermediate phase to decomposition process of $\text{Zn}(\text{BH}_4)_2(\text{NH}_3)_2$. However, ^{11}B NMR analysis of $\text{Zn}(\text{BH}_4)_2(\text{NH}_3)_2$ after heat-treatment at 60°C for 3 hours (Figure IV-15) shows that without any presence of ammonia borane in it at RT, DADB like phase formation occurs after heat-treatment. The chemical shift of BH_4 species at -42.2 ppm is much closer to those in $\text{Zn}(\text{BH}_4)_2(\text{NH}_3)_2$ – $9\text{NH}_3\text{BH}_3$ mixture. Based on the information obtained so far, we can speculate that following initial decomposition pathway is possible:



Hence, $[(\text{NH}_3)_2\text{BH}_2]\text{Zn}(\text{BH}_4)_3(\text{NH}_3)_2$ type intermediate phase could explain the upshift in NMR spectrum (Figure IV-14) with decreasing concentration of zinc in the phase.

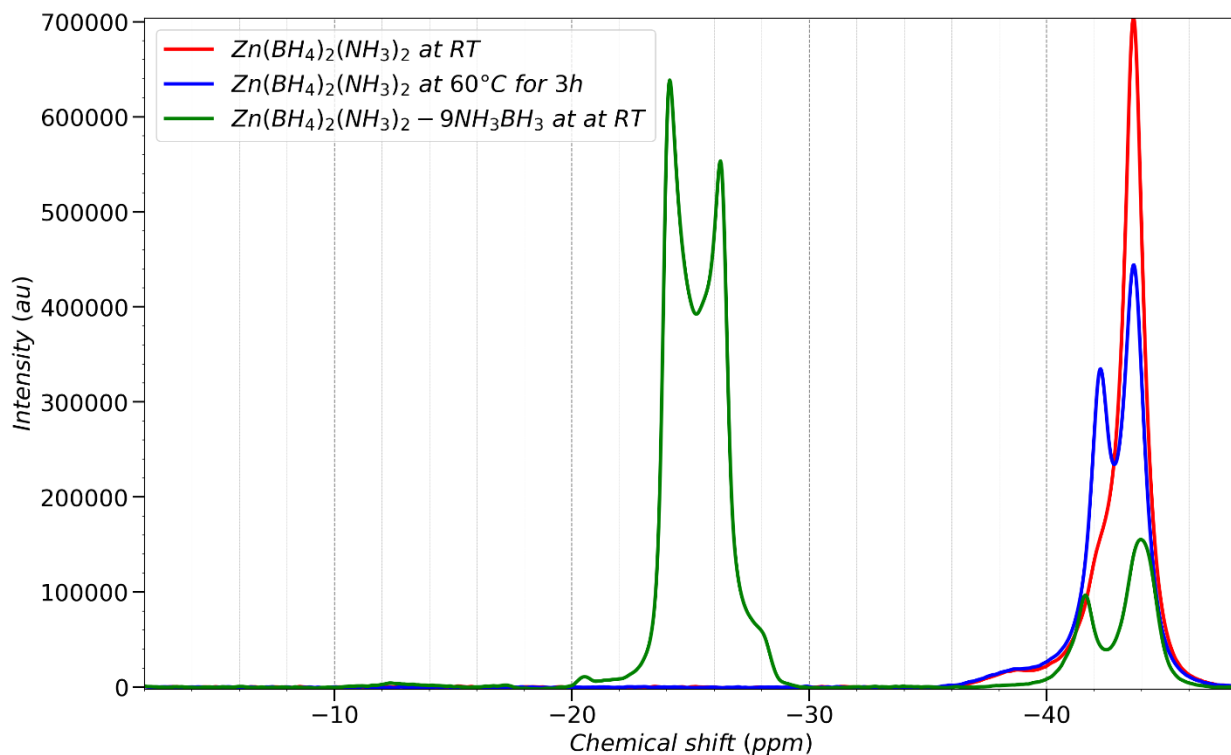


Figure IV-15: ^{11}B NMR spectrum of heat-treated $\text{Zn}(\text{BH}_4)_2(\text{NH}_3)_2$ at 60°C for 3 hours compared to neat $\text{Zn}(\text{BH}_4)_2(\text{NH}_3)_2$ and its ammonia borane mixture at RT.

IV.5. Hydrogen storage capacity of Zn-B-N-H system

Following the 1969 article reporting synthesis of $\text{Zn}(\text{BH}_4)_2 \cdot 4\text{NH}_3$ by reacting THF solution of $\text{Zn}(\text{BH}_4)_2$ with aqueous ammonia solution [133], we wanted to see if this can be applied to $\text{NaZn}(\text{BH}_4)_3(\text{NH}_3)_2$ as well. Hence, by reacting ZnCl_2 (0.3g) and NaBH_4 (0.25g) in THF (7ml) filtrating the NaCl precipitate by centrifuge, chloride-free THF solution of $\text{NaZn}(\text{BH}_4)_3$ is obtained. Crystalline $\text{NaZn}(\text{BH}_4)_3(\text{NH}_3)_2$ can be synthesized by cooling this solution below 0°C and adding aqueous ammonia solution (1ml) to it. Immediately the white precipitate forms and without any delay the solvent extraction can be started. The solvent evaporation was also performed at lowest possible temperature and white powder was recovered. Unwanted hydrolysis of BH_4 species are avoided by keeping the solution below 0°C and high basicity of ammonia solution. XRD analysis showed some NaBH_4 contamination similar to THF assisted ball-milling. This contamination can be avoided by decreasing the molar ratio from 3 to 2.5 in the expense of increased $[\text{BH}_4]^- \rightarrow \text{Cl}^-$ anion substitution. Fixing all the other experimental conditions, $\text{NaZn}(\text{BH}_4)_3(\text{NH}_3)_2$ synthesized by aqueous ammonia and liquid ammonia approaches have hydrogen capacity of 6.6 and 7.3 wt% respectively. Slight hydrogen capacity loss can be attributed to unwanted hydrolysis during solvent evaporation. However, compared to literature, no ball-milling required to obtain THF solution of $\text{NaZn}(\text{BH}_4)_3$ and delivery of ammonia precursor as aqueous solution makes this synthesis technique very cheap and quantitative. Nevertheless, MS study revealed possibly some

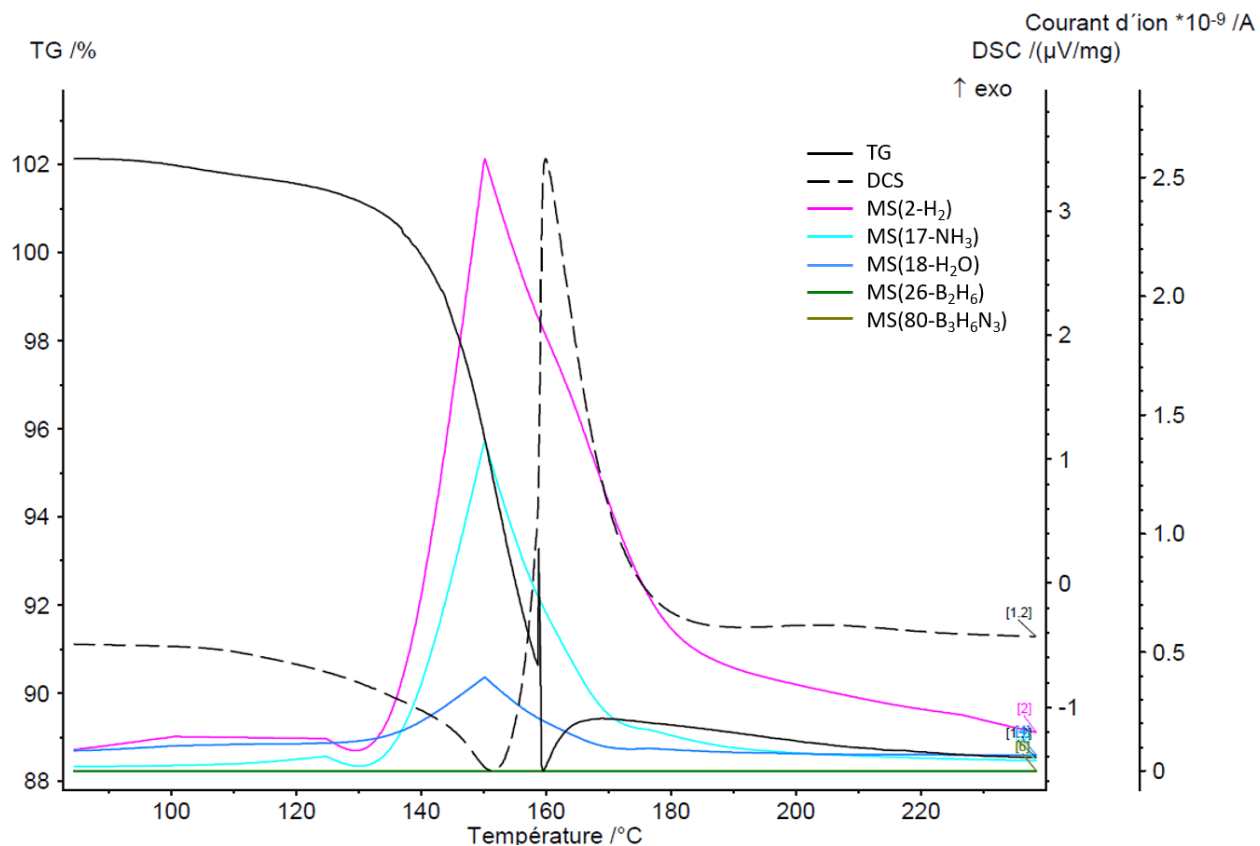


Figure IV-16: DSC-TG-MS result of $\text{NaZn}(\text{BH}_4)_3(\text{NH}_3)_2$ synthesized by THF and aqueous ammonia solution

amount of water (the $m/e=18$ signal) is also released from this compound (Figure IV-16), possibly occupying ammonia sites in the crystalline structure. This result can be optimized for $\text{NaZn}(\text{BH}_4)_3(\text{NH}_3)_2$ however is not applicable to other metal borohydrides due to their limited stability in aqueous solutions. Hence, a better alternative is exposure to dry ammonia atmosphere or direct synthesis in liquid ammonia. As shown in Figure IV-10, $\text{NaZn}(\text{BH}_4)_3(\text{NH}_3)_2-x\text{NH}_3\text{BH}_3$ (where $x=2-3$) has the highest hydrogen purity and capacity. The mixture can be synthesized from both chloride and fluoride precursors. Fluoride precursors enable filtration of NaF precipitate from ammonia soluble $\text{NaZn}(\text{BH}_4)_3(\text{NH}_3)_2-x\text{NH}_3\text{BH}_3$ mixture. This mixture release at least 10 wt% hydrogen and ~ 4.5 wt% ammonia. $\text{NaZn}(\text{BH}_4)_3(\text{NH}_3)_2-3\text{NH}_3\text{BH}_3$ mixture releases three times less ammonia compared to neat $\text{NaZn}(\text{BH}_4)_3(\text{NH}_3)_2$. Assuming amount of ZnCl_2 necessary to suppress the ammonia impurity is linearly correlated by the amount of released ammonia, $\sim 1/8$ mole ZnCl_2 additive should be enough to remove ammonia impurity completely from $\text{NaZn}(\text{BH}_4)_3(\text{NH}_3)_2-3\text{NH}_3\text{BH}_3$ mixture ($\sim 1/3$ needed for neat $\text{NaZn}(\text{BH}_4)_3(\text{NH}_3)_2$). Hence $\text{ZnCl}_2-8\text{NaZn}(\text{BH}_4)_3(\text{NH}_3)_2-20\text{NH}_3\text{BH}_3$ mixture was prepared by mortar mixing and its dehydrogenation properties analyzed by TG-MS-TPD measurements:

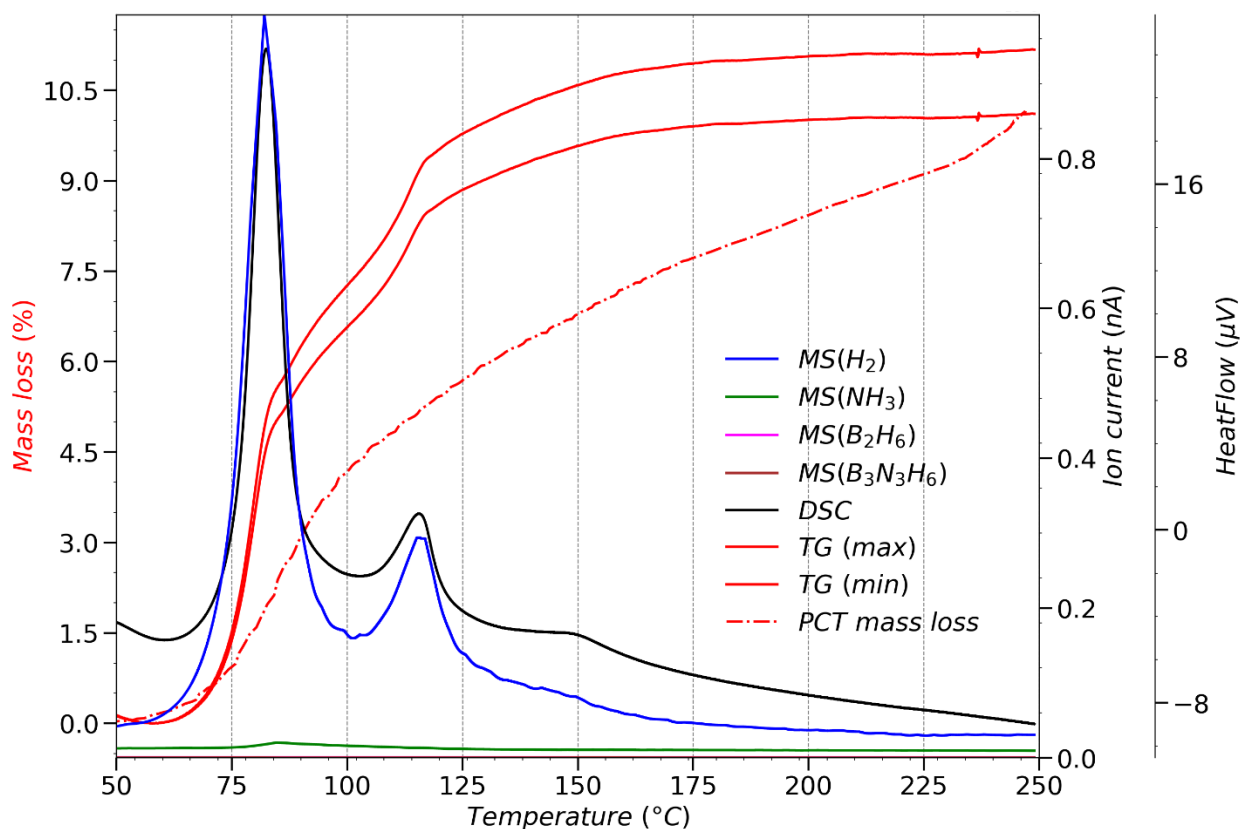


Figure IV-17: TG-DSC-MS-TPD analysis of $\text{ZnCl}_2-8\text{NaZn}(\text{BH}_4)_3(\text{NH}_3)_2-20\text{NH}_3\text{BH}_3$ mixture. Mass loss values are calculated accounting for the weight of NaF byproduct in the mixture.

The biggest source of experimental error for ammonia mole impurity calculations comes from the mass accuracy of TG samples (± 0.5 mg accuracy of the balance in glovebox). Hence,

in Figure IV-17 the range for mass loss percentage measured by TG is given as a range (minimum and maximum values). $\text{ZnCl}_2-8\text{NaZn}(\text{BH}_4)_3(\text{NH}_3)_2-20\text{NH}_3\text{BH}_3$ mixture might release 0.5 ± 0.5 wt% ammonia; however, it releases at least ~ 10 wt% hydrogen. More precise characterization techniques are needed to quantify the impurity gases on ppm level.

There are 108 protic hydrogens and 156 hydridic hydrogens in this mixture. If we assume perfect dihydrogen elimination reaction as the only decomposition mechanism, 108 mole of hydrogen gas will be released which corresponds exactly to 9.8 wt%. This means final solid byproduct contain 48 hydridic hydrogens. However, looking at ^1H NMR spectra of $\text{NaZn}(\text{BH}_4)_3(\text{NH}_3)_2-x\text{NH}_3\text{BH}_3$ mixture for $x=0, 1, 9$ we can see in Figure IV-18a, four peaks corresponding to hydrogens in the mixture. As discussed in Chapter 3, in ^1H NMR $\text{NaZn}(\text{BH}_4)_3(\text{NH}_3)_2$ phase has two peaks at 0 ppm and 3.8 ppm corresponding to hydrogens bonded to nitrogen and boron atoms. Similar pattern is observed for the hydrogens of NH_3BH_3 phase, peaks at 1.4 and 4.2 ppm which increase as x increases from 1 to 9. They can be similarly attributed to hydrogens bonded to nitrogen and boron atoms in ammonia borane phase. Upon heating $\text{NaZn}(\text{BH}_4)_3(\text{NH}_3)_2-\text{NH}_3\text{BH}_3$ mixture at 70°C hydrogens corresponding to ammonia borane phase disappear while $\text{NaZn}(\text{BH}_4)_3(\text{NH}_3)_2$ phase remain intact (Figure IV-18b). On the other hand, $\text{NaZn}(\text{BH}_4)_3(\text{NH}_3)_2-9\text{NH}_3\text{BH}_3$ even at 45°C loses all the peaks corresponding to both phases (Figure IV-18c). At higher temperatures, both mixtures display a broad ^1H NMR spectra with two distinct peaks at 0 ppm and 1.2 ppm. Due to the lack of literature on these hydride phases, we cannot identify the chemical environment of the hydrogens left in the compound. Nevertheless, we can speculate that possible decomposition byproducts are of $\text{ZnCl}_2-8\text{NaZn}(\text{BH}_4)_3(\text{NH}_3)_2-20\text{NH}_3\text{BH}_3$ mixture are $9\text{Zn} + 2\text{NaCl} + 6\text{NaH} + 2\text{B}_{22}\text{N}_{18}\text{H}_{22}$. At 250°C $\text{B}_{22}\text{N}_{18}\text{H}_{22}\approx\text{BNH}$ cannot be completely decomposed to BN, hence solid byproduct of M-B-N-H system will always contain some hydrogen atoms that cannot be removed.

$\text{Zn}(\text{BH}_4)_2(\text{NH}_3)_2$ although releases only pure hydrogen its experimental hydrogen capacity is ~ 8.5 wt%. However, it cannot be synthesized in liquid ammonia with fluoride precursors, leaving only option to expensive organozinc precursors. Hence, by conventional metathesis reaction removal of alkali halide byproduct from $\text{Zn}(\text{BH}_4)_2(\text{NH}_3)_2$ is not possible. Additionally, its mixture with ammonia borane does not improve its hydrogen capacity instead releasing borazine alongside hydrogen.

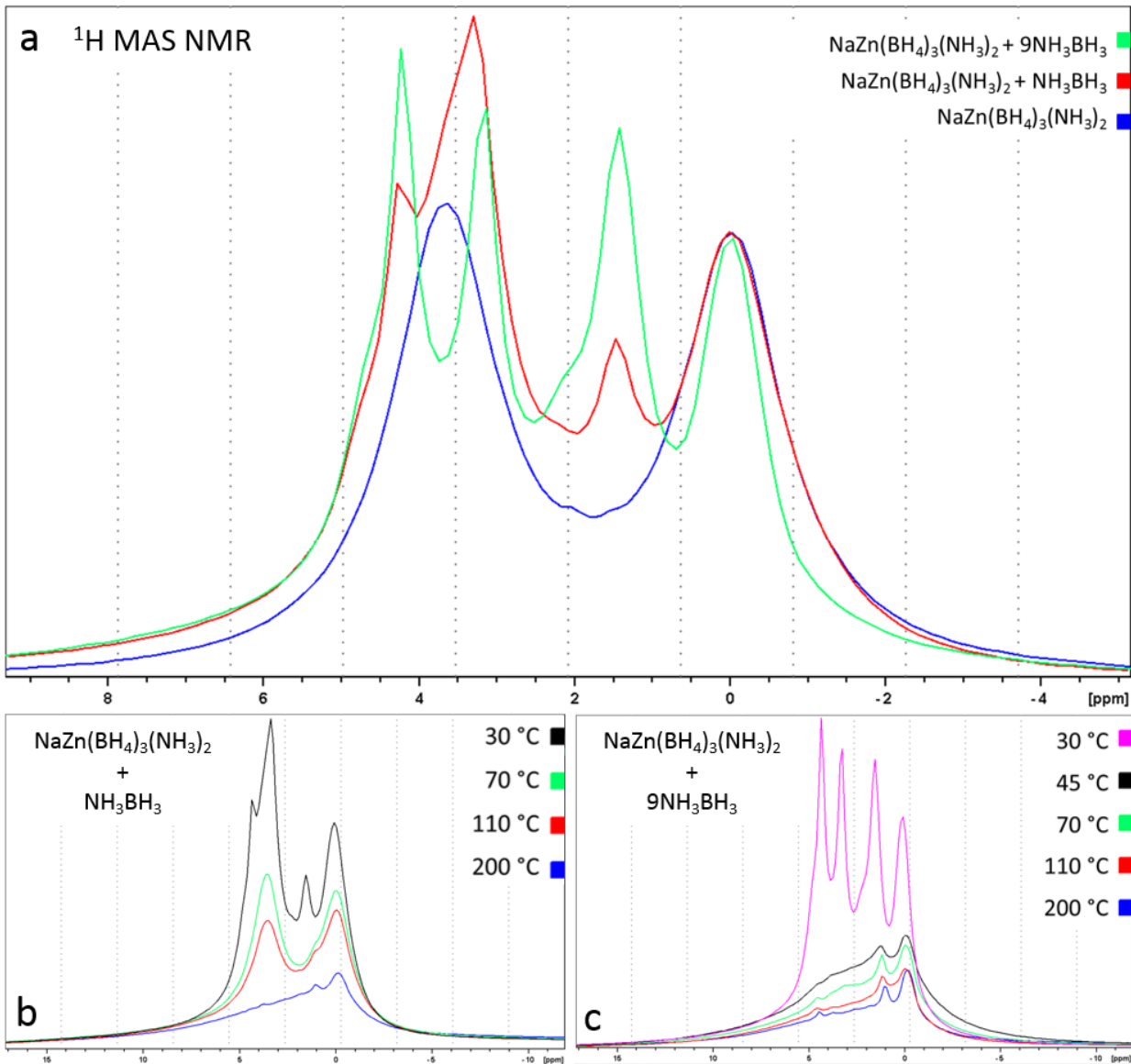


Figure IV-18: ^1H MAS NMR result of a) $\text{NaZn}(\text{BH}_4)_3(\text{NH}_3)_2-x\text{NH}_3\text{BH}_3$ mixture where $x = 0, 1, 9$ at RT b) heat treated $\text{NaZn}(\text{BH}_4)_3(\text{NH}_3)_2-\text{NH}_3\text{BH}_3$ c) $\text{NaZn}(\text{BH}_4)_3(\text{NH}_3)_2-9\text{NH}_3\text{BH}_3$ mixture at various temperature

IV.6. Conclusions

In this chapter, we explored various types of compounds based on Zn-B-N-H system. We synthesized $(\text{NH}_4)\text{Zn}(\text{BH}_4)_3$ for the first time and investigated the potential of ammonium metal borohydrides as hydrogen storage materials. Based on our results and the literature review of limited number of publications on the ammonium metal borohydride compounds, we concluded that ammonium cations despite enabling ‘dihydrogen elimination’ pathway cannot form a thermodynamically stable phase at ambient temperatures. Mechanochemical synthesis is known to produce kinetically stabilized phases. This is further verified when the reaction medium is replaced with liquid ammonia. Despite the use of same precursor (same

stoichiometry), $\text{NaZn}(\text{BH}_4)_3(\text{NH}_3)_2-x\text{NH}_3\text{BH}_3$ mixture was obtained instead of ammonium zinc borohydride.

The co-synthesized $\text{NaZn}(\text{BH}_4)_3(\text{NH}_3)_2$ and NH_3BH_3 phases provided very homogeneous mixture and upon dehydrogenation delivered better hydrogen purity compared to both phases. Using in-situ ^{11}B NMR measurements it was possible to examine the role of metal cation in $\text{NaZn}(\text{BH}_4)_3(\text{NH}_3)_2-x\text{NH}_3\text{BH}_3$ and $\text{Zn}(\text{BH}_4)_2(\text{NH}_3)_2-x\text{NH}_3\text{BH}_3$ systems. We drew the parallels with metal cation assisted catalytic dehydrogenation mechanism of ammonia borane from the literature and demonstrated that the formation of diammoniate of diborane is the main reason for lower dehydrogenation temperature and higher hydrogen purity.

Based on our understanding, we demonstrated that alkali halide free $\text{ZnCl}_2-8\text{NaZn}(\text{BH}_4)_3(\text{NH}_3)_2-20\text{NH}_3\text{BH}_3$ mixture can release at least 10 wt% pure hydrogen which is the highest performance for zinc (Zn-B-N-H) system.

IV.7. Appendix

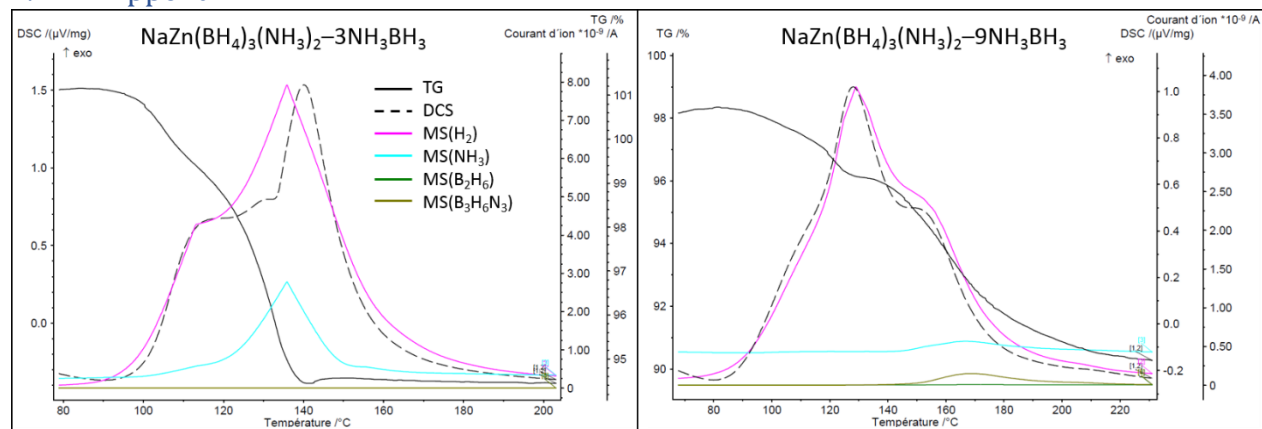


Figure IV-S1: DCS-TG-MS analysis ($10^\circ\text{C}/\text{min}$ heating rate) of $\text{NaZn}(\text{BH}_4)_3(\text{NH}_3)_2-x\text{NH}_3\text{BH}_3$ where a) $x=2$ b) $x=9$

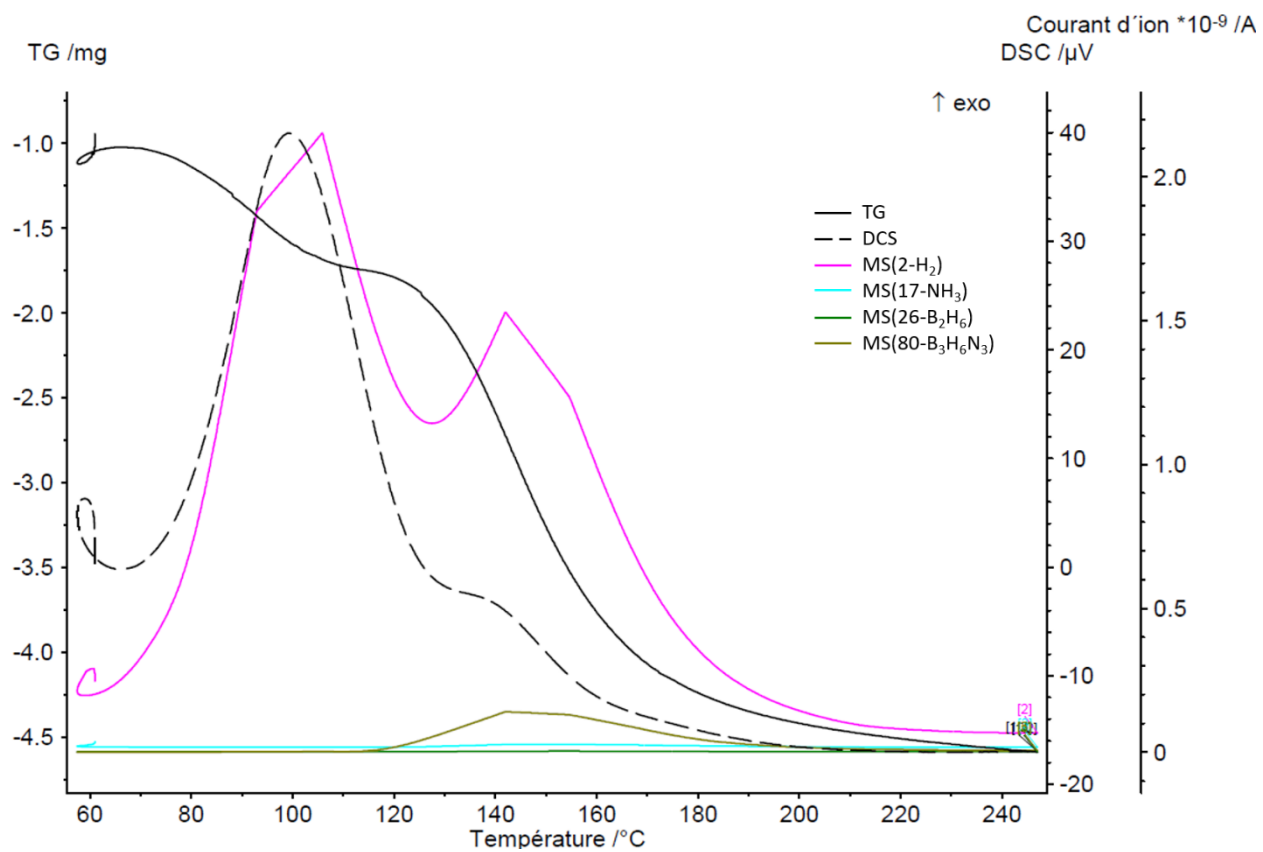


Figure IV-S2: DCS-TG-MS analysis ($10^{\circ}C/min$ heating rate) of $Zn(BH_4)_2(NH_3)_2-3NH_3BH_3$ mixture (mortar mixed)



Chapter V

Mg-B-N-H system and exploration of
reversibility



V. Mg-B-N-H system and exploration of reversibility

V.1. Drawback of Zn-B-N-H system as practical hydrogen storage system

In previous chapters, we explored all the possible combinations of Zn-B-N-H system and achieved a pure hydrogen capacity of 10 wt% with $\text{ZnCl}_2-8\text{NaZn}(\text{BH}_4)_3(\text{NH}_3)_2-20\text{NH}_3\text{BH}_3$ mixture. To achieve this, continued compromises must be done between the ease of synthesis, the dehydrogenation temperature, the hydrogen purity and the experimental hydrogen capacity. In literature, a lot of effort has been focused on destabilization of ammonia borane while retaining its practical hydrogen capacity and improving its hydrogen purity. The trend in most of these approaches as well as in our results is lowered dehydrogenation temperature for improved hydrogen purity. Although high capacity to release pure hydrogen at low temperature is attractive on laboratory scale, designing a practical hydrogen storage system based on these compounds requires the consideration of two major shortcomings: long-term stability at low temperatures and irreversibility of spent fuel.

Highly exothermal decomposition behavior of M-B-N-H compounds enables high kinetics of dehydrogenation while remaining a security risk for unintentional spontaneous release of hydrogen. A system designed around these materials needs to consider eventualities of unusually hot environments and breakdown of heat managements system. Another issue is shelf-life of these compounds. Unlike metal borohydrides or other hydrides, ammine metal borohydrides are much less air sensitive [69] and can remain for long time without degradation in dry air. Even in contact with water, the released ammonia turns the aqueous solution strongly basic and limits the self-hydrolysis reaction. However, the compound that decomposes exothermally at 100°C, even if its kinetics at RT is infinitesimal it is not zero, with enough shelf-time, the degradation of the hydrogen storage capacity will happen. Ammine zinc borohydride compounds are synthesized as white powders and any decomposition at RT easily reflects in its color change. These is due to formation of metallic zinc unlike other ammine metal borohydrides, which form amorphous $\text{M}(\text{BNH}_x)_m$ that remain colorless. Hence, tracking the stability of ammine zinc borohydride compounds in glovebox is much easier. As an example, $\text{KZn}(\text{BH}_4)_3(\text{NH}_3)_2$ compounds, synthesized both from ZnCl_2 and ZnF_2 precursors, are stable in glovebox for months. Their colors remain white and have no detectable change in XRD pattern. This can be explained by their larger endothermal melting peak which acts as a barrier to exothermal dehydrogenation process (Figure III-S12-14). $\text{Zn}(\text{BH}_4)_2(\text{NH}_3)_2$ is the least stable compound turning noticeably grey within a day, it is followed by $\text{LiZn}(\text{BH}_4)_3(\text{NH}_3)_2$ with few days. $\text{NaZn}(\text{BH}_4)_3(\text{NH}_3)_2$ synthesized with ZnCl_2 precursor has noticeable color change within a week, while ZnF_2 precursor improves its stability up to several weeks and months. Although chloride substitution increases the peak temperature of exothermal dehydrogenation process, it has adverse effect on its stability at RT. Alternatively, all of these compounds remain white for months in refrigerator at 10°C.

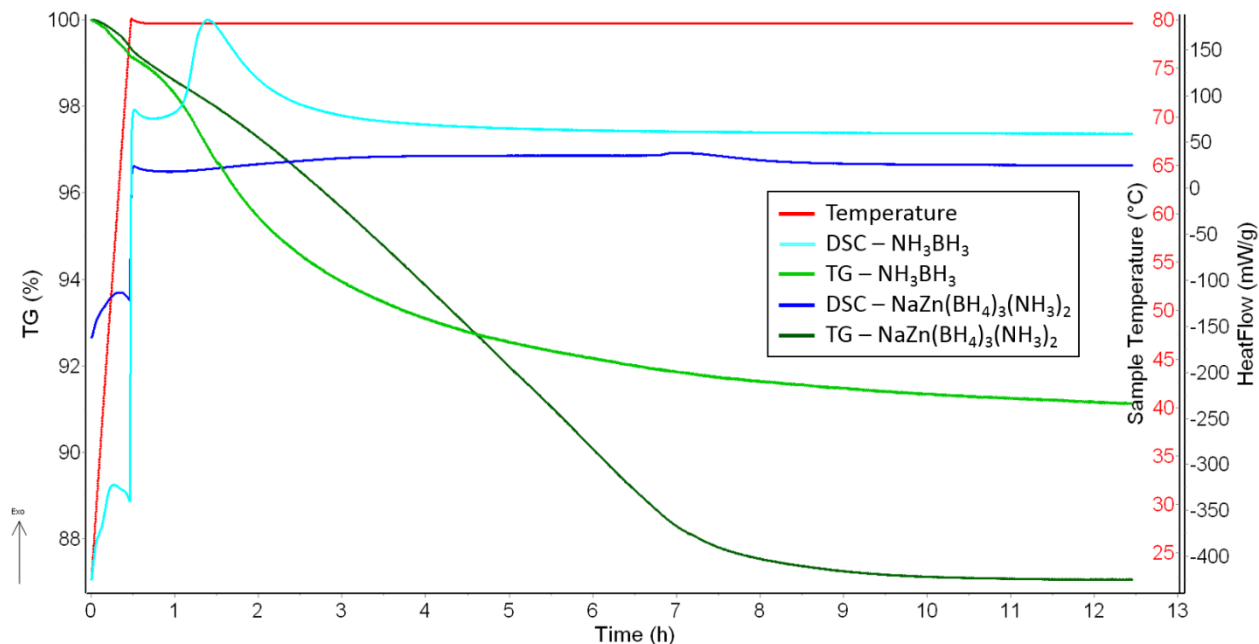


Figure V-1: Isothermal heat treatment of $\text{NaZn}(\text{BH}_4)_3(\text{NH}_3)_2$ (synthesized with ZnF_2 precursor) and NH_3BH_3 at 80°C . Both compounds are synthesized in liquid ammonia.

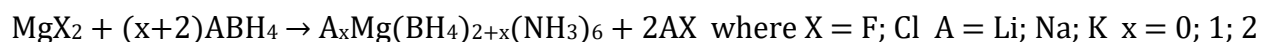
In Figure V-1 the DSC-TG data of isothermal heat treatment at 80°C of NH_3BH_3 and $\text{NaZn}(\text{BH}_4)_3(\text{NH}_3)_2$ synthesized with ZnF_2 precursors is plotted. By 10 hours mark, ammonia borane has lost ~ 9 wt% and $\text{NaZn}(\text{BH}_4)_3(\text{NH}_3)_2$ about ~ 13 wt% of its initial mass. These values mean almost complete decomposition of $\text{NaZn}(\text{BH}_4)_3(\text{NH}_3)_2$ and partial decomposition of ammonia borane to BNH_x where $x < 3$. Although both compounds are stable at RT for considerably long durations their mixtures display detectable color change within hours. Hence, ideally $\text{ZnCl}_2-8\text{NaZn}(\text{BH}_4)_3(\text{NH}_3)_2-20\text{NH}_3\text{BH}_3$ mixture needs to be prepared right before utilization which makes this unacceptable for practical applications.

V.2. Objective

The objective in this chapter is to replace Zn with lower electronegativity Mg in M-B-N-H system, to have a compound that is stable at 85°C for long duration. At the same time to deliver an experimental hydrogen capacity of at least 10 wt% below 250°C with high hydrogen purity. Another goal of the activities described in this chapter is to explore rehydrogenation, reversibility and regeneration possibilities for the spent fuel.

V.3. Synthesis of Mg-B-N-H compounds

Liquid ammonia synthesis through metathesis reaction was explored for identifying possible crystalline $\text{A}_x\text{Mg}(\text{BH}_4)_{2+x}(\text{NH}_3)_n$ type compounds:



With chloride precursors, the only crystalline phases were $\text{Mg}(\text{BH}_4)_2(\text{NH}_3)_6$ and $\text{Li}_2\text{Mg}(\text{BH}_4)_4(\text{NH}_3)_6$. All the other combinations delivered a mixture of these phases with excess alkali borohydride. Contrary to our expectations, $\text{Na}_2\text{Mg}(\text{BH}_4)_4(\text{NH}_3)_6$ phase could

not be synthesized. For $\text{MgCl}_2\text{:NaBH}_4$ precursors with 1:2 stoichiometry at RT, a week later in liquid ammonia considerable chloride anion substitution could be observed in XRD analysis of the obtained powders. This can be improved by either increasing the NaBH_4 stoichiometry or raising the synthesis temperature. Hence, all subsequent synthesis processes were conducted at 60 °C. At this temperature 48 hours is enough to obtain a crystalline phase with negligible anion substitution.

Unfortunately, no reaction could be observed with MgF_2 precursors. This is possibly due to extremely low solubility of MgF_2 in liquid ammonia (even in water). Ammonia does not interact with metal fluorides. However, by treating the ammine metal chlorides with HF or AgF, ammonia soluble $\text{M}(\text{NH}_3)_n\text{F}_m$ type compounds can be synthesized [118]. However, this approach was not tried in our studies. Hence, due to the presence of ammonia soluble alkali chloride byproducts, liquid ammonia filtration of the main phase will not be possible with MgCl_2 precursors. Therefore, it was necessary to develop an alternative approach.

First approach was based on the fact that compared to metal borohydrides, their ammoniates are much less reactive towards air [69]. Hence, the challenge was to find a solvent that can solubilize alkali chloride byproduct while the main phase remaining insoluble. The main selection criteria for the possible solvents included the boiling point, viscosity and safety. To that end, several solvents including dimethyl formamide, ethylene diamine, acetonitrile and chloroform were tried which have certain (decreasing order) solubility for LiCl byproduct. However, the main phase lost its crystallinity in all of the tried solvents except chloroform. Additionally, due to low LiCl solubility, the necessity of using Soxhlet extractor complicated the process. Overall, this strategy was not successful at all, mainly due to higher than expected reactivity of the main phase towards the selected solvents. Moreover, this approach would have failed anyway due to intergrown particulates of $\text{Mg}(\text{BH}_4)_2(\text{NH}_3)_6$ and AlCl phases that formed larger agglomerate particles. This was confirmed by our attempts to perform a density separation. The idea here is that NaCl (or LiCl) having a density of 2.15 g/ml (or 2.07), and the main phase in the range of 0.8-1 g/ml depending on the level of the chloride substitution. Chloroform alongside being able to solubilize LiCl slightly and inert towards the main phase, also has density of 1.48 g/ml that should be able to separate the two phases. However, we observed that almost all the powder floated on the surface of chloroform. Possibly chloroform assisted ball-milling might help to break the agglomerate particles and separate the phases, however we did not try this approach.

Instead, we tried to design a synthesis set-up where formation of intergrown agglomerates particles are prevented. We solubilized LiBH_4 in diethyl ether and added on top $\text{Mg}(\text{NH}_3)_6\text{Cl}_2$ and chloroform. The idea was that $\text{Mg}(\text{NH}_3)_6\text{Cl}_2$ with 1.23 g/ml density would float in the boundary between chloroform and diethyl ether solution since two solvents are not miscible. As soon as the LiCl byproduct forms it would be the only compound heavy enough to precipitate in chloroform. However, in practice it was difficult to apply the procedure while mixing the solvents. Additionally, the chosen solvents were too volatile at RT and required constant replenishment. Diethyl ether was not the ideal solvents since it can solubilize some

LiCl as well. Eventually, switch to amine solvents would have been appropriate (Chapter 2). Hence, for our trial with diethyl ether the separation was not possible but after several days of mixing at RT, the XRD analysis of the powder showed no indication of successful reaction between the precursors. Recovered powder was heavier than expected and amorphous indicated possible side reaction with chloroform. Further work needs to be done to explore the feasibility of this approach.

Synthesis of $\text{Mg}(\text{BH}_4)_2(\text{NH}_3)_6$ can also be achieved by first synthesizing the $\text{Mg}(\text{BH}_4)_2$ phase in pure form and then react it with ammonia gas. However, as discussed in detail in Chapter 2 for high yield metathesis reaction $\text{Mg}(\text{BH}_4)_2$ synthesis requires solvent assisted ball-milling. A more scalable approach is direct reaction between MgH_2 and $\text{L}\cdot\text{BH}_3$, where L is a solvent that can form stable diborane complex. In our experimental attempts to replicate this approach, we tried $\text{L}\cdot\text{BH}_3$ complexes where $\text{L}=\text{DMS}$, THF, TMA, TEA. Desolvation of the solvents ligand from $\text{Mg}(\text{BH}_4)_2\cdot\text{L}$ is reported to be only possible for DMS. However, for our purposes this is not necessary as long as the solvents adduct can be displaced with ammonia molecule. It was reported that direct reaction between metal hydride and diborane gas is limited due to formation of metal borohydride phase on the surface of metal hydride particle that eventually passivates it and prevents the completion of the reaction. This problem is alleviated by continuously ball-milling the powder under diborane gas in order to break the passivation layer and expose the fresh hydride layer [178]. Therefore, even for solvothermal synthesis approach, initial mechanochemical activation of metal hydride precursor and the reduction of particle size below certain limits is very important. Additionally, once reaction takes place, soluble metal borohydride solvates are extracted from unreacted insoluble metal hydride precursors [112].

For our synthesis approach, we used MgH_2 purchased from Alfa Aesar at 98% purity, $\text{L}\cdot\text{BH}_3$ complexes where $\text{L}=\text{DMS}$, TMA, TEA were purchased from Sigma Aldrich with 97% purity. The precursors are used as purchased without any additional treatment. Since $\text{Me}_3\text{N}\cdot\text{BH}_3$ is a solid, THF solvent is used as a reaction medium. All reactions were carried out in 2-3 times the excess of $\text{L}\cdot\text{BH}_3$ in Schlenk reactor under Argon flow up to 2 weeks. The yield of the reactions was very low with unreacted MgH_2 being the main product. This proves that pre-milling is very crucial step.

In liquid ammonia, the completion of the reaction was not a problem; rather the challenge was shifted to obtaining the desired compound. All reactions were carried at 60°C for faster kinetics of the synthesis process. The weight of the recovered product, the generated hydrogen gas and the consumed ammonia amount were measured in the end of the synthesis process to judge the yield of the reaction. The reaction of MgH_2 with quantitative amount of $\text{TMA}\cdot\text{BH}_3$ yielded pure $\text{Mg}(\text{NH}_2\text{BH}_3)_2(\text{NH}_3)_3$ (Figure V-2). To the best our knowledge, this compound has been previously only synthesized by mechanochemical approach by reacting MgH_2 precursors with ammonia borane under ammonia atmosphere [179]. Previously mono-ammoniate version was synthesized by ball-milling MgNH_2 or MgNH precursor with ammonia borane since $\text{Mg}(\text{NH}_2\text{BH}_3)_2$ is not a stable phase without ammonia adducts [173].

To repeat this result, we also performed liquid ammonia synthesis using MgH_2 and NH_3BH_3 which also yielded pure $\text{Mg}(\text{NH}_2\text{BH}_3)_2(\text{NH}_3)_3$ (Figure V-3).

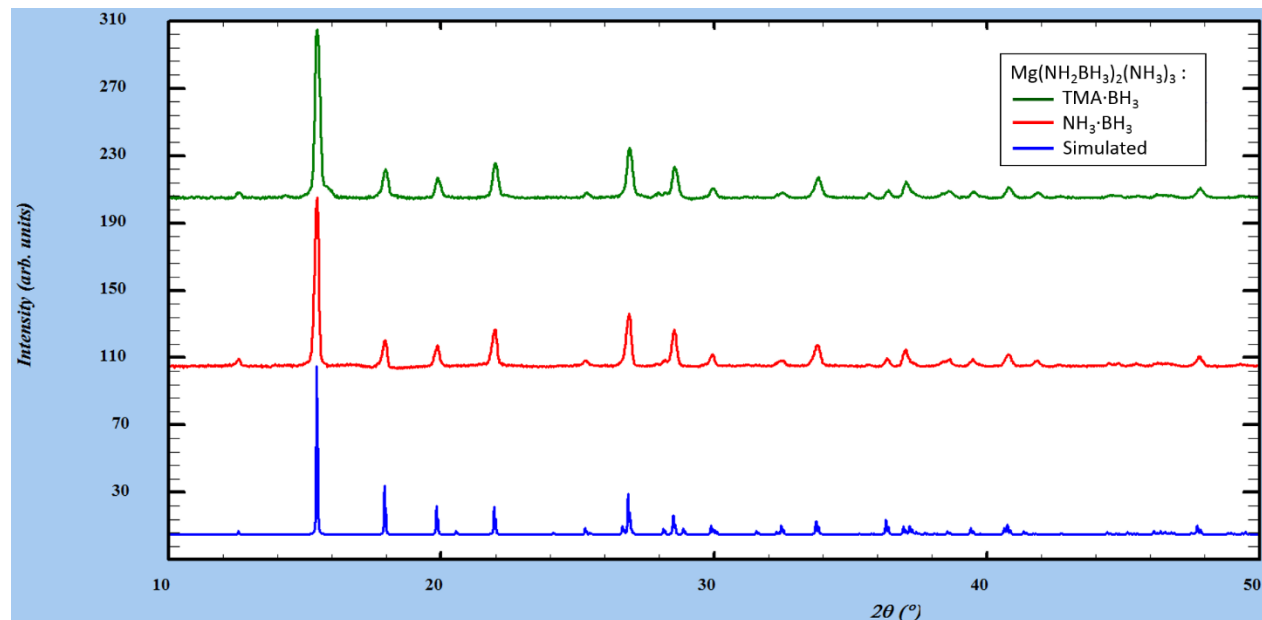


Figure V-2: XRD diffractogram of synthesized $\text{Mg}(\text{NH}_2\text{BH}_3)_2(\text{NH}_3)_3$ with $\text{TMA}\cdot\text{BH}_3$ and NH_3BH_3 (this work) compared to simulated pattern (cif file from reference [5])

Quantitative amount of $\text{DMS}\cdot\text{BH}_3$ and $\text{TEA}\cdot\text{BH}_3$ was difficult to transfer to the reactor (required micro-syringe), so initially excess amount was used compared to the hydride precursor. As expected, the reaction generated a lot of hydrogen and the recovered mass indicated the formation of excess ammonia borane phase. However, the XRD analysis of the

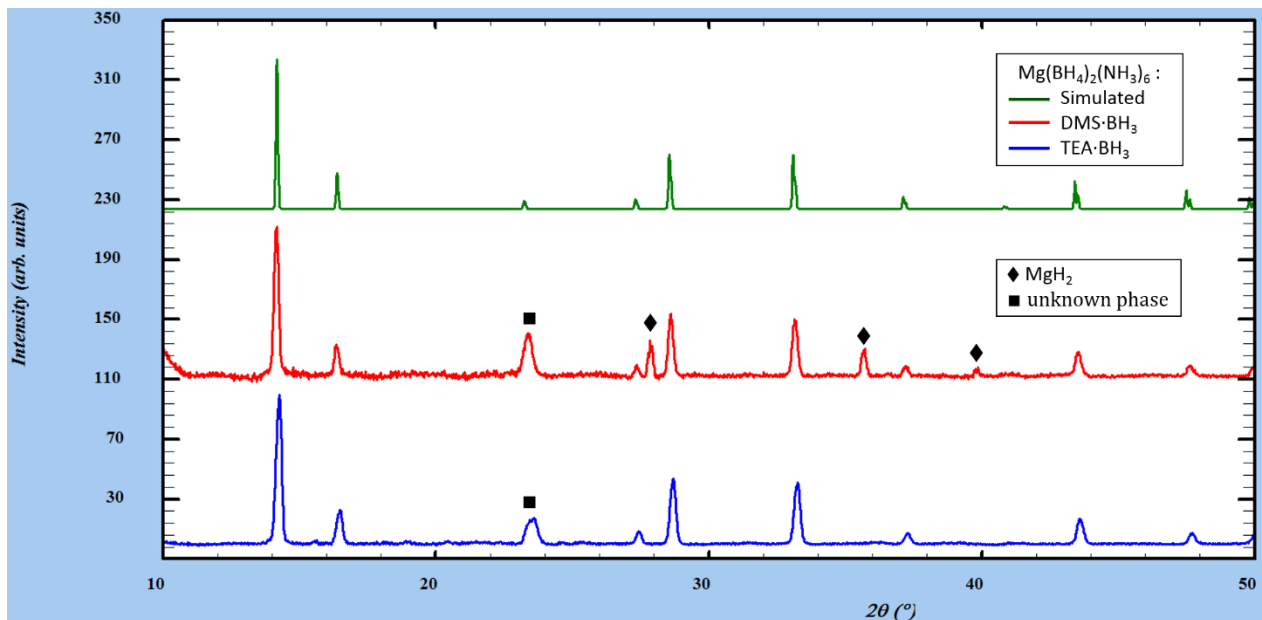


Figure V-3: XRD diffractogram of $\text{Mg}(\text{BH}_4)_2(\text{NH}_3)_6$ synthesized with excess $\text{DMS}\cdot\text{BH}_3$ and $\text{TEA}\cdot\text{BH}_3$ precursors with MgH_2 at 60°C in liquid ammonia compared to simulated pattern.

powder obtained from TEA·BH₃ precursor surprisingly only showed the presence of Mg(BH₄)₂(NH₃)₆ phase (blue line in Figure V-3). The reaction products from both precursors did not show any crystalline ammonia borane phase, instead the higher than expected intensity of the single peak at 2θ = 23.8° was possibly the only sign for the presence of an unknown phase. The reaction with DMS·BH₃ was left with some unreacted MgH₂ indicating preferential reaction for ammonia borane type phase formation compared to Mg(BH₄)₂(NH₃)₆ formation (red line in Figure V-3).

MgH₂ itself does not react well with ammonia and although slow formation of Mg(NH₂)₂ is possible, this approach is reported to yield amorphous phase [33]. On the other hand, TEA·BH₃ reaction with MgH₂ shows complete conversion of hydride phase to Mg(BH₄)₂(NH₃)₆. Nevertheless, the recovered powder mass and generated hydrogen gas indicated presence of amorphous ammonia borane type phase. To observe this amorphous phase, ¹¹B NMR analysis was performed on compound synthesized with TEA·BH₃. As can be seen from Figure V-4, sharp peak observed at -37 ppm corresponds exactly to Mg(BH₄)₂(NH₃)₆ [180]. More importantly, the presence of ammonia borane like phase is clearly observed. BH₃ peak is broad and the slight downshift was previously associated for amidoborane type modification of ammonia borane [179]. Hence, this ammonia borane type phase might include some magnesium as well, however as known from the other synthesis

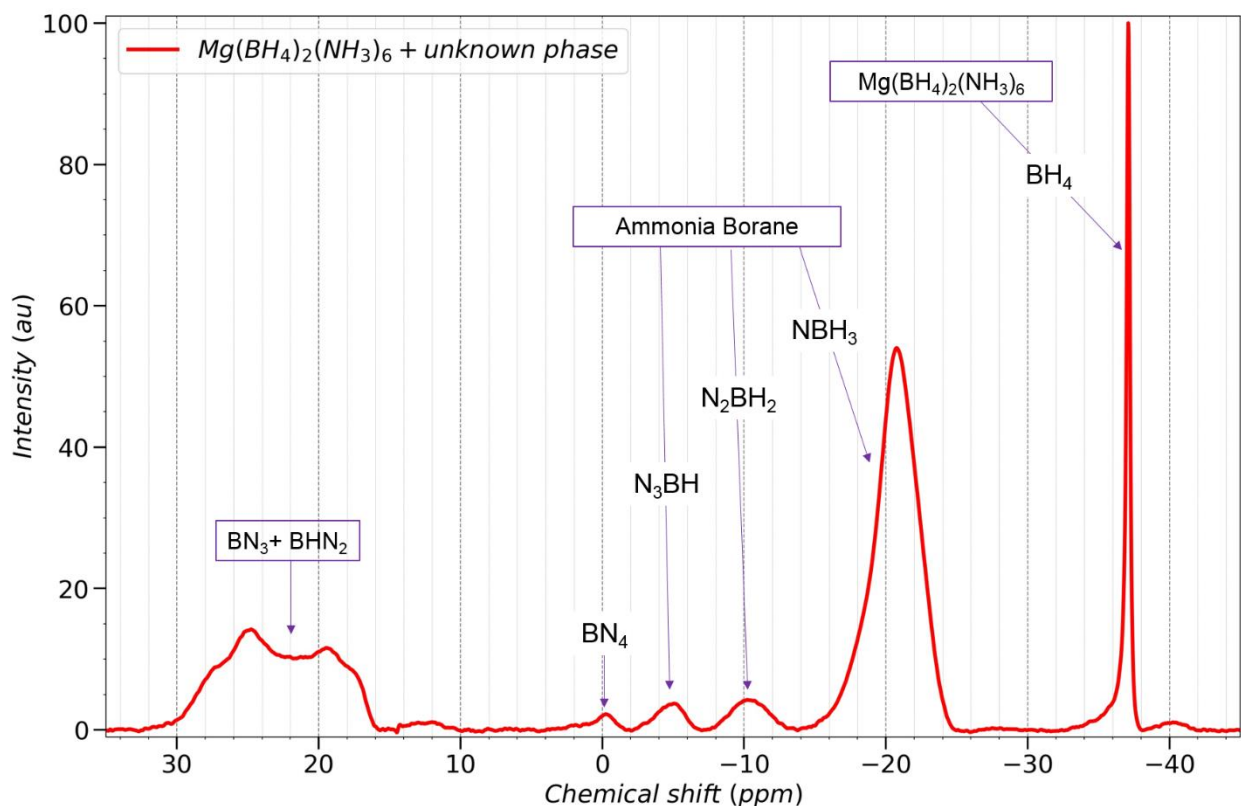


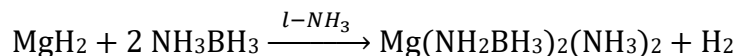
Figure V-4: ¹¹B-¹H MAS NMR analysis of Mg(BH₄)₂(NH₃)₆ synthesized with MgH₂ and excess TEA·BH₃ precursors in liquid ammonia at 60°C. NaBH₄ is used as reference at -42 ppm.

processes, magnesium amidoboranes are stable at 60 °C synthesis temperature. Nevertheless, we can observe that intermediate decomposition byproducts are visible in 0 to -15 ppm (tetra-coordinated boron sites N_xBH_{4-x}) range, while fully dehydrogenated byproducts can be observed in 15-30 ppm range (tri-coordinated N_xBH_{3-x}). This means that the amorphous phase is most likely partially decomposed ammonia borane.

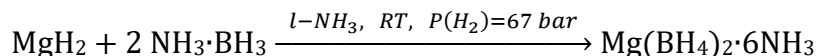
Unlike DMS, THF and TMA, at RT ammonia cannot easily displace TEA in $TEA \cdot BH_3$ to form ammonia borane. However, this displacement can be easily facilitated by increasing the temperature [41]. Hence, almost pure $Mg(BH_4)_2(NH_3)_6$ can be synthesized with $TEA \cdot BH_3$ in liquid ammonia at low temperatures to form $Mg(BH_4)_2(TEA)_n$ followed by temperature increase to 60°C to displace all the TEA adducts. This means during the reaction of MgH_2 with $L \cdot BH_3$ in liquid ammonia, there is a competition between:

- nucleophilic addition reaction, $MgH_2 + 2 L \cdot BH_3 \xrightarrow{l-NH_3} Mg(BH_4)_2 \cdot L_n$
- and ammonia displacement reaction, $L \cdot BH_3 + NH_3 \xrightarrow{l-NH_3} NH_3BH_3$

Therefore, at 60°C, $TMA \cdot BH_3$ reaction with MgH_2 in quantitative amount first results in formation of ammonia borane, then protons of ammonia borane (bonded to nitrogen) react with the hydrides of MgH_2 similar to dihydrogen elimination reaction to yield magnesium amidoboranes:



Since solubility of ammonia borane is 259.7g in 100g of liquid ammonia [37], we wanted to explore if increasing the hydrogen pressure would suppress this reaction and allow the formation of borohydride phase instead:



Hence, this reaction was conducted in liquid ammonia under ~67 bar of hydrogen pressure (steel reactor was filled with 45 bar hydrogen at -73 °C to keep the ammonia frozen and closed to heat up to RT). XRD analysis shows that although $Mg(NH_2BH_3)_2(NH_3)_3$ is the main phase, there is a small crystalline unknown phase (blue line in Figure V-5). However, contrary to our expectations it does not correspond to any known borohydride phase.

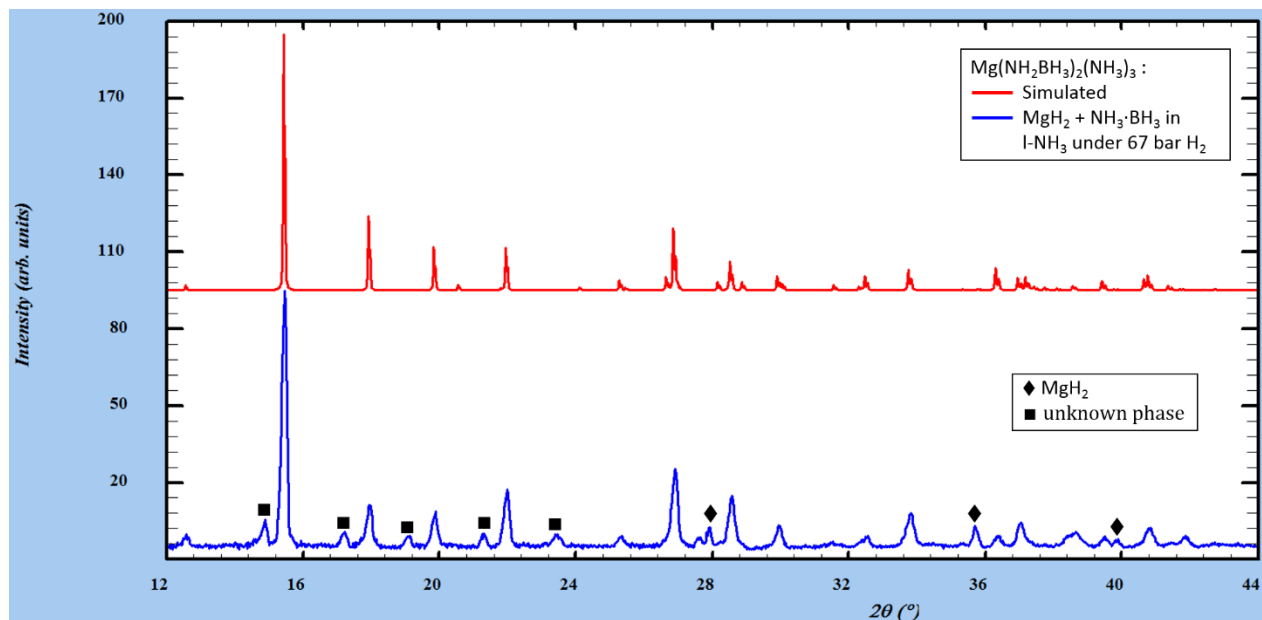


Figure V-5: XRD diffractogram of $\text{Mg}(\text{NH}_2\text{BH}_3)_2(\text{NH}_3)_3$ synthesized at RT with $\text{MgH}_2-2\text{NH}_3\text{BH}_3$ mixture in liquid ammonia under 67 bar hydrogen pressure compared to simulated pattern.

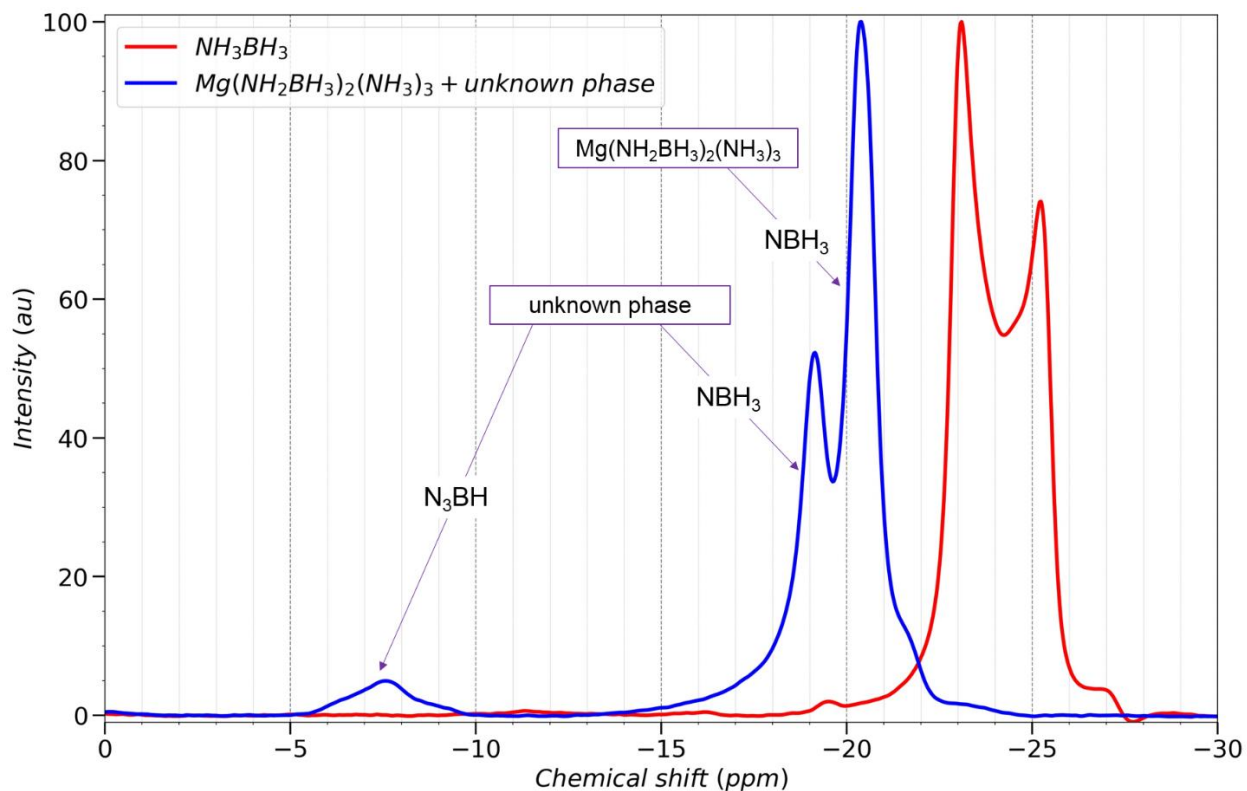


Figure V-6: $^{11}\text{B}\{-^1\text{H}\}$ MAS NMR spectrum of neat ammonia borane is compared to that of $\text{Mg}(\text{NH}_2\text{BH}_3)_2(\text{NH}_3)_3$ synthesized at RT with $\text{MgH}_2+\text{NH}_3\text{BH}_3$ in liquid ammonia under 67 bar hydrogen pressure. NaBH_4 is used as a reference at -42 ppm.

^{11}B NMR analysis was performed to determine whether this unknown phase includes any boron sites as well as to observe potentially amorphous phases. As can be seen from Figure V-6, ^{11}B NMR spectrum of $\text{Mg}(\text{NH}_2\text{BH}_3)_2(\text{NH}_3)_3$ and unknown phase mixture is compared to neat ammonia borane. Previously ^{11}B NMR spectrum of $\text{Mg}(\text{NH}_2\text{BH}_3)_2(\text{NH}_3)_3$ was reported as a single peak at -20.7 ppm [179]. The boron has single atomic site in $\text{Mg}(\text{NH}_2\text{BH}_3)_2(\text{NH}_3)_3$ and its environment is far from cubic symmetry. Despite being a type of modification of ammonia borane, no explanation can be found in the literature for the apparent absence of quadrupole interaction in metal amidoboranes compared to ammonia borane [181],[177]. Nevertheless, the main peak at -20.4 ppm in our results (Figure V-6) aligns perfectly with previous reports. The two peaks at -19.1 ppm and -7.5 ppm are most likely from the unknown phase that might include N_3BH and NBH_3 type bonding environment for the boron atoms. Since this synthesis was done at RT, it is less likely that these peaks correspond to decomposition byproducts of ammonia borane. Since small amount of MgH_2 was left unreacted (blue line in Figure V-5), we can assume that unknown boron phase is type of modification of unreacted ammonia borane precursor.

The main problem with MgH_2 precursors is that it is not widely available for purchase and very difficult to synthesize by direct hydrogenation of magnesium metal powder. Additionally, compared to magnesium hydride synthesized by organometallic precursors which is pyrophoric in contact with air, direct hydrogenation of magnesium powder delivers rather chemically passive MgH_2 . Magnesium has strong affinity for oxygen and form MgO layer on the surface of the particles that limit the diffusion of hydrogen. This layer can be broken by annealing above 400 °C or milling to expose the fresh metal surface to hydrogen gas. Nevertheless, MgH_2 phase formed on the surface acts as passivation layer and prevent further diffusion of hydrogen into the bulk of the particles. Hence, direct hydrogenation of magnesium powder under 200 bar at 570 °C with the help of MgI_2 catalyst can deliver only 60 % yield. Reactive milling is the most efficient approach where surface passivation layer is constantly broken to expose more fresh metal to hydrogen gas. Nevertheless, with ball-milling under 200 bar of hydrogen gas at 350-400 °C, the yield of the reaction is 75 % which can be improved to 97% with the help of catalyst [182].

Hence, by utilizing the power of liquid ammonia to solubilize alkali and alkali earth metals, direct synthesis between Mg metal pieces and ammonia borane was conducted in liquid ammonia. The reaction of ammonia borane with magnesium metal was slower than MgH_2 precursor due to the solubility of metal pieces, which could be improved a lot by using metal powder. As expected, the main product of this synthesis process was $\text{Mg}(\text{NH}_2\text{BH}_3)_2(\text{NH}_3)_3$. Hence, this approach can be applied to synthesis of amidoboranes of any alkali and alkali earth metal since magnesium among them is known to be least soluble in liquid ammonia:



The main problem with this approach is that during solubilization of magnesium metal, electron solution would attack the PTFE magnetic stirring bar and partially reduce it. This

problem would be more severe with alkali metals. Stirring of the solution can be omitted to avoid contamination of the main phase with carbon and alkali fluoride phases.

V.4. Hydrogen storage properties of Mg-B-N-H system

TG-TPD analysis showed that $\text{Mg}(\text{NH}_2\text{BH}_3)_2(\text{NH}_3)_3$ compound releases about 7.5 wt% hydrogen and at least 11 wt% ammonia at 250 °C. It was reported that released ammonia amount from metal amidoboranes decreases if the compound decomposes in closed system compared to under Ar flow. Hence, the reported hydrogen capacity of the compound in a closed system is ~9 wt% (calculated by taking into account 2 mol% ammonia in 10.6 wt% reported in the article) at 300°C [179]. Since our TG measurement is an open system compared to TPD measurements that are closed system, this might affect the precision of hydrogen capacity calculations. This is precisely why we chose to perform our TPD measurements under 1 bar atmosphere not under vacuum to minimize the differences between TG and TPD measurements. Ideally, this 1 bar atmosphere is provided by an inert gas; however, in our case, the only option was hydrogen for TPD measurements. On the other hand, depending on the synthesis reaction, our typical liquid ammonia synthesis can generate its hydrogen atmosphere up to 5 bar and as we saw from magnesium amidoboranes synthesis under 67 bar, the synthesis and decomposition reactions are not too sensitive to hydrogen pressure.

Besides having hydrogen capacity below 10 wt% and releasing too much ammonia, $\text{Mg}(\text{NH}_2\text{BH}_3)_2(\text{NH}_3)_3$ is a type of destabilized ammonia borane, which means its stability at 85 °C for long duration is worse than that of neat ammonia borane. As can be seen from Figure V-7, melting process starts below 40 °C while decomposition at around 70 °C.

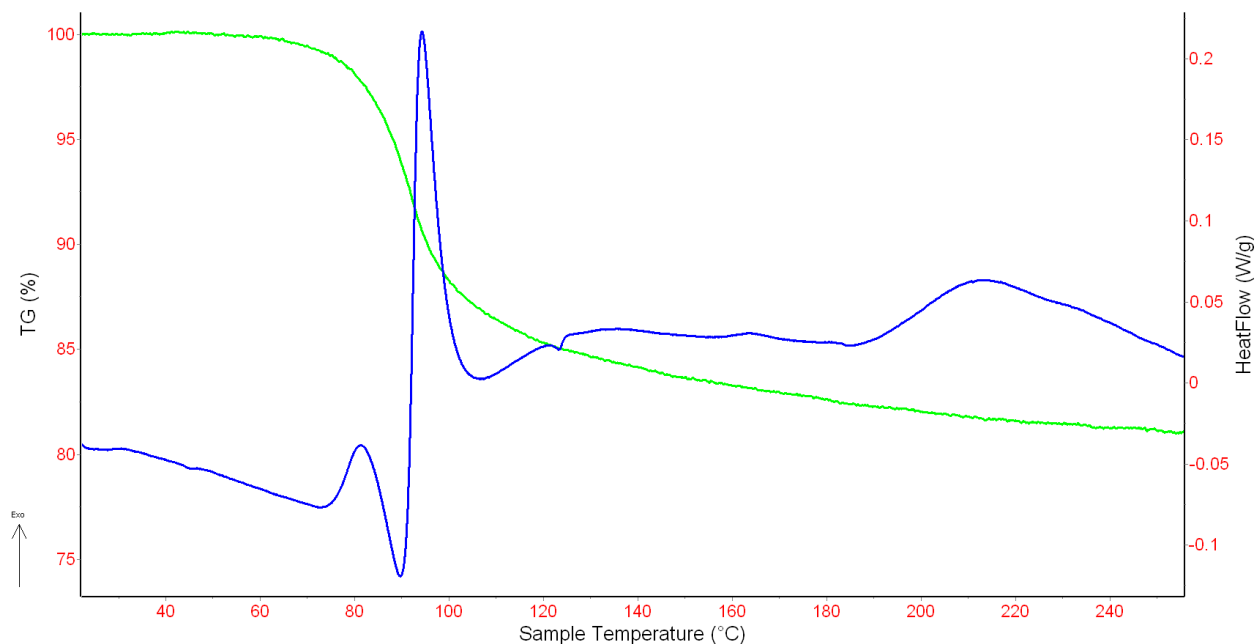


Figure V-7: DSC-TG analysis of $\text{Mg}(\text{NH}_2\text{BH}_3)_2(\text{NH}_3)_3$ synthesized with $\text{MgH}_2\text{-}2\text{NH}_3\text{BH}_3$ mixture in liquid ammonia at 60°C. The heating rate is 2°C/min.

Therefore, we focused on $\text{Mg}(\text{BH}_4)_2(\text{NH}_3)_6$ compounds to deliver a hydrogen storage compound that is stable at 85 °C for long duration.

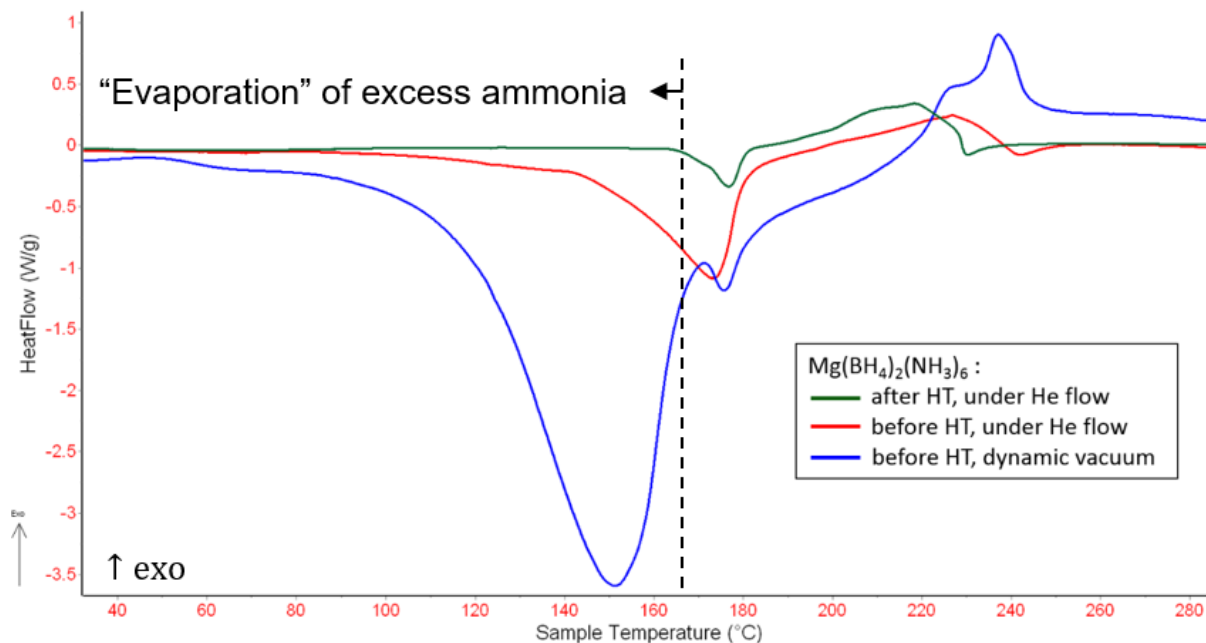


Figure V-8: DCS result under dynamic vacuum (blue), under He flow (red) and under He flow after heat-treatment (HT) at 100 °C under dynamic vacuum for 6 hours (green). $\text{Mg}(\text{BH}_4)_2(\text{NH}_3)_6$ samples were synthesized at 60 °C in liquid ammonia with $\text{MgCl}_2-2\text{NaBH}_4$ mixture and DCS analysis performed at 2°C/min heating rate.

If we look at the DSC result of $\text{Mg}(\text{BH}_4)_2(\text{NH}_3)_6$ measured under He flow (red curve in Figure V-8) we can see an endothermal peak between 140-180°C temperature range. This peak corresponds to melting and ammonia evaporation from the compound. When same experiment is performed under dynamic vacuum the same endothermal peak increases in intensity and its on-set temperature shifts down to 100 °C. Previously heat treatment of $\text{Mg}(\text{BH}_4)_2(\text{NH}_3)_6$ at 118 °C for 4 hours was claimed to release 4 mole of ammonia which results in formation of $\text{Mg}(\text{BH}_4)_2(\text{NH}_3)_2$. In our studies, we determined that heat-treatment can be performed as low as 80 °C, however no crystalline sample can be recovered from de-ammoniated samples at any temperature. Only by accurate mass measurements of the powder before and after heat treatment we inferred that the remaining phase is $\text{Mg}(\text{BH}_4)_2(\text{NH}_3)_2$. After the heat treatment, the DSC profile of the sample shows that endothermal peak is substantially decreased (Figure V-). Exothermal peak observed for all the sample is in 200-250°C range corresponds to main dehydrogenation step, while heat treated samples seem to dehydrogenate at lower temperatures.

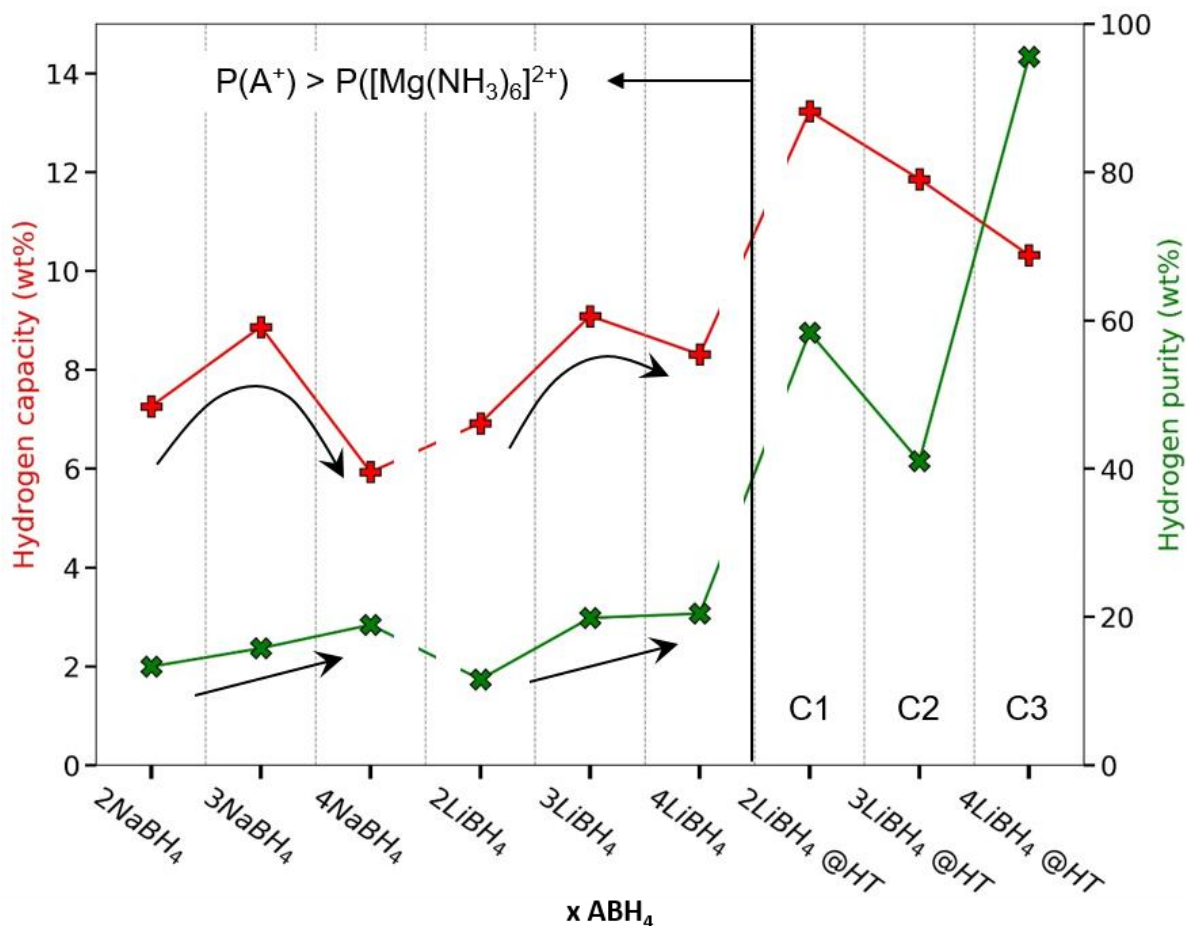
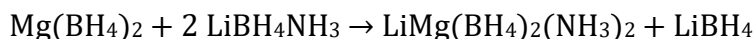


Figure V-9: Calculated hydrogen capacity (red) and hydrogen purity (green) of $MgCl_2 + xABH_4$ synthesized in liquid ammonia at $60^\circ C$. @HT refers to samples that are heat-treated at $100^\circ C$ under dynamic vacuum for 6 hours. The values are calculated by considering the mass percentage of $xAlCl$ salt byproduct in each sample.

As mentioned previously, excess $NaBH_4$ (more than molar ratio 1:2 in $MgCl_2:NaBH_4$ mixture) remained as dead weight in the final product. While $LiBH_4$ resulted in competition between $Mg(BH_4)_2(NH_3)_6$ and $Li_2Mg(BH_4)_4(NH_3)_6$ phases. As we discussed in detail in Chapter 3 and 4, in fact excess alkali borohydride homogeneously mixed with $Mg(BH_4)_2(NH_3)_6$ improves its hydrogen capacity and the hydrogen purity (defined as weight percentage of hydrogen in total weight of released gasses). This is enabled by polarization of BH_4 anions in the vicinity of Li^+ and Na^+ cations, subsequent increase of Brader charge of hydrides that are more readily react with the protons of Mg^{2+} coordinated ammonia molecules. We can see this trend clearly as well for hydrogen capacity and purity values of our ammine magnesium borohydride compounds shown in Figure V-9. By adding an additional 1mole of $LiBH_4$ or $NaBH_4$ to $Mg(BH_4)_2(NH_3)_6$ both hydrogen capacity and the purity increases. For the extra 2 mole addition, hydrogen purity increases further while hydrogen capacity seems to decrease. In fact, as mole percentage of the active material the released mole of hydrogen still increases, however the mass of the active material increases faster. So there is an

optimum amount of alkali borohydride that can be added to a $M(\text{BH}_4)_m(\text{NH}_3)_6$ type compound to improve its hydrogen purity without imposing penalty on its hydrogen capacity.

For heat-treated sample, hydrogen capacity breaches the 10 wt% barrier. While the hydrogen purity is also improved. However, the amount of released ammonia is very sensitive to heat-treatment conditions. Lower temperature and longer duration (low T – long t) is preferred to higher temperature short duration (high T – short t) procedure for higher reproducibility. Nevertheless, some of the samples can reach above 95 wt% hydrogen purity while delivering higher than 10 wt% hydrogen capacity. To understand this result we look at previously reported $\text{LiMg}(\text{BH}_4)_2(\text{NH}_3)_2$ compound that was synthesized by ball-milling through following reaction:



An extra mole of LiBH_4 is left in the main phase as a byproduct of the reaction [75]. To the best of my knowledge synthesis of pure $\text{LiMg}(\text{BH}_4)_2(\text{NH}_3)_2$ has not been reported in the literature. Hence, $\text{LiMg}(\text{BH}_4)_2(\text{NH}_3)_2\text{--LiBH}_4$ mixture reported to release only pure hydrogen and exactly 10 wt% by 250°C [75]. This report corresponds well with our result as well (Figure V-), heat treatment of $\text{Li}_2\text{Mg}(\text{BH}_4)_4(\text{NH}_3)_6$ can turn it into amorphous $\text{LiMg}(\text{BH}_4)_2(\text{NH}_3)_2\text{--LiBH}_4$ mixture.

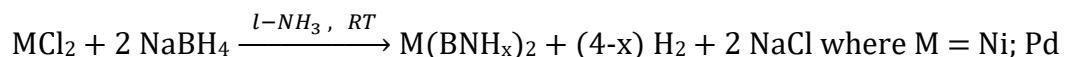
V.5. Regeneration of spent $M(\text{BNH}_x)_m$ fuel

Ammine metal borohydride compounds upon decomposition form an amorphous $M(\text{BNH}_x)_m$ type phase. The ideal approach would be direct hydrogenation; however, this approach has been unsuccessful. This leaves the only approach for chemical regeneration of the spent fuel. The most expensive component of this spent fuel is metal part. Hence, first degree of regeneration process is recovery of metal from $M(\text{BNH}_x)_m$ compound. Second approach of regeneration suggested in literature is the use of hydrazine in liquid ammonia. However, this approach as discussed in Chapter 1 is very costly due to consumption of expensive and hazardous hydrazine while only being capable to regenerate selectively and partially dehydrogenated polyborazylene back to ammonia borane. In fact, it has been applied to M-B-N-H system without any success [177]. The third approach is digestion with strong acid to achieve cleavage of B-N bonds and replace it with B-X, followed by reduction to form B-H bond and displacement of solvent used in previous steps with ammonia. However, this technique has only been applied to regeneration of ammonia borane. We will explore all these approaches in the context of M-B-N-H compounds.

V.5.1. Direct hydrogenation of $M(\text{BNH}_x)_m$

Dehydrogenation of the M-B-N-H compounds is very exothermal which means theoretical rehydrogenation is equally very endothermal. Since dehydrogenation of the compounds is achieved by heating, this means the energy required for rehydrogenation cannot be delivered by thermal means. Instead the only option is higher hydrogen pressure. Hence, direct hydrogenation of spent $M(\text{BNH}_x)_2$ fuel is not possible, at least within reasonable hydrogen pressures. However, part of this energy can be delivered if a solvent can solubilize or modify the bonding energies in $M(\text{BNH}_x)_2$. Additionally, as discussed in Chapter 1, the solvent adducts in $\text{Mg}(\text{BH}_4)_2 \cdot n\text{L}$ are believed to modify the coordination environment as well as electron density distribution around Mg^{2+} leading to modification of the activation energy to dehydrogenation [58]. Similarly, it was proposed that N-CH₂ groups of NEt_3 plays an important role as the activation of hydrogen molecule on Ni_3B catalyst surface [44]. Hence, the synergetic solvent-catalyst mediated hydrogenation was an interesting prospect to explore.

Since Ni and Pd metals are known for their ability to cleave hydrogen molecule very easily, instead of synthesizing nickel or palladium boride catalysts we decided to first synthesize $\text{Ni}(\text{BNH}_x)_2$ and $\text{Pd}(\text{BNH}_x)_2$ in order to ascertain their ability to hydrogenate B-N bonds in close proximity of these metal atoms. The proposed synthesis process was:



The proposed procedure was to fully decompose the obtained compound at 250°C and then attempt the hydrogenation at 30-60°C temperature range under 50 bar of hydrogen pressure. Palladium compound, as expected, released a lot of hydrogen during synthesis and formed black amorphous compound. To our surprise, nickel compound was crystalline ammine nickel borohydride (Figure V-S1). With 1.91 Pauling electronegativity of nickel we did not expect this compound to be stable at RT. Nevertheless, we believe it was stabilized by incorporating of chloride anions into the structure. Similar behavior was also observed for $\text{KZn}(\text{BH}_4)_3(\text{NH}_3)_2$ compound when synthesized at 70°C. The $\text{Ni}(\text{BH}_4)_2(\text{NH}_3)_6$ compound is isostructural with $\text{Ni}(\text{NH}_3)_6\text{Cl}_2$ (Fm-3m space group), obtained product had two phases with different degree of anion substitution as evidenced from their unit cell parameters (10.43Å and 10.67Å) being bigger than that of neat $\text{Ni}(\text{NH}_3)_6\text{Cl}_2$ (10.03Å). Determining the degree of anion substitution was not possible from Rietveld analysis, however almost all the NaBH_4 precursor was consumed during the synthesis meaning that anion substitution is well below 50%. The $\text{Ni}(\text{BH}_4)_2(\text{NH}_3)_6$ compound decomposes between 100-200 °C range in two steps releasing mostly ammonia but also some hydrogen in each step (Figure V-S2). Both palladium and nickel compound were separately decomposed at 250°C and the obtained byproducts were amorphous $M(\text{BNH}_x)_2$. Additionally, amorphous Ni_3B was also synthesized by reacting anhydrous NiCl_2 with NaBH_4 in THF. Alkali halide byproduct were not filtered from all the discussed phases.

For the direct hydrogenation attempts, the mass change of the sample $M(\text{BNH}_x)_2$ was tracked before and after hydrogenation, followed by XRD and TG-MS analysis afterwards to confirm

any changes in the “hydrogenated” compounds. Following hydrogenation attempts were done at 60 °C under 45 bar of hydrogen pressure for 12 hours:

Sample	Solvent	Catalyst	Result
Mg(BNH _x) ₂	None; TEA; THF	None	No change
Mg(BNH _x) ₂	None; TEA; THF	Pd(BNH _x) ₂ , 33 wt% loading	No change
Mg(BNH _x) ₂	None	Ni(BNH _x) ₂ , 33 wt% loading	No change
Mg(BNH _x) ₂	TEA	Ni(BNH _x) ₂ , 33 wt% loading	300% weight increase
Mg(BNH _x) ₂	TEA	Ni ₃ B, 33 wt% loading	5% weight increase
Mg(BNH _x) ₂	Liquid ammonia	None	50% weight increase

The sample and the catalyst powder were mixed in mortar, typically less than half a milliliter of solvents were added on top of 50-100 mg total powder. All the solvents have sufficient hydrogen gas solubility [183]. Despite 5 % mass increase in TEA+Ni₃B system, MS analysis showed only release of TEA from the powder. This system was shown to successfully work together for hydrodechlorination of TEA·BCl₃ sample [44]. TEA+Ni(BNH_x)₂ system gained 300% mass and MS analysis showed 4 wt% release of only ammonia and no TEA (Figure V-S3). As the powder remained amorphous and considering the release of ammonia from the samples, a possible explanation is reaction of Ni(BNH_x)₂ with carbon groups of TEA that left behind ammonia. Hydrogenation in liquid ammonia was done under 70 bar since the reactor was filled with 45 bar at -80°C. Hydrogenation resulted in 50 % mass gain and small unknown crystalline phase formation, subsequent MS analysis released 11 wt% ammonia and some hydrogen by 250 °C (Figure V-S4). As a conclusion, rather unsurprisingly direct hydrogenation at 45 bar is not possible for Mg(BNH_x)₂ samples; however, its interaction with liquid ammonia is worthy of further attention.

V.5.2. Metal recovery from M(BNH_x)_m

All ammine metal borohydrides decompose into amorphous M(BNH_x)₂ phase. Hence, as the most expensive component of the spent fuel, its recyclability is important. Major exception to decomposition process M-B-N-H system is zinc compound. Recently, hydrolysis properties of NaZn(BH₄)₃ and NaZn(BH₄)₃(NH₃)₂ were investigated. NaZn(BH₄)₃ hydrolysis is too fast and difficult to control. Its main hydrolysis byproducts are zinc and sodium metaborate. NaZn(BH₄)₃(NH₃)₂, on the other hand, releases some ammonia during hydrolysis and the rest of the ammonia raises the pH of the solution and inhibits further hydrolysis of the compound. In basic solution, ZnO formation is possible [184]. However, with the use of excess amount of water, the main decomposition product we obtained was metallic zinc. Upon dehydrogenation most ammine metal borohydrides decompose into amorphous M(BNH_x)_m phase, zinc compounds are the exception forming zinc metal which is completely stable in air and even in water. By solubilizing BNH_x part in water, zinc can be easily separated. Its reaction with HF solution gives us a pathway to recycle the most expensive component of Zn-B-N-H system. Alternatively, direct digestion with NH₄F at 100-150 °C is the easiest approach to obtain anhydrous ZnF₂.

Mg(BNH_x)₂, on the other hand, requires a different approach. Water insoluble magnesium phases are Mg(OH)₂ and MgF₂. Fluoride precursor is not interesting due to its inability to react with alkali borohydride compounds. Instead, Mg(BNH_x)₂ in water precipitates as amorphous Mg(OH)₂, it can be subsequently filtrated and treated with NH₄Cl solution that form crystalline NH₄MgCl₃·6H₂O. Preparation of anhydrous magnesium chloride from this compound is a known procedure [185].

V.5.3. Full regeneration of Mg(BNH_x)₂

Part of the motivation for our attempts to synthesize Mg(BH₄)₃(NH₃)₆ directly from MgH₂+NH₃BH₃ mixture was that full regeneration of ammonia borane is more or less known [40]. As discussed in detail in Chapter 1, this process has three steps: digestion, reduction and ammonia displacement. First step can achieve 90 % conversion yield from BNH_x to TEA·BCl₃ species with the help of AlCl₃-HCl-CS₂ superacid/solvent mixture under 40 bar of anhydrous HCl pressure at 80 °C [41]. Reduction step turn TEA·BCl₃ to TEA·BH₂Cl/TEA·BH₃ mixture with 70%/30% ratio with help of TEA+Ni₃B catalyst system, at 160 °C under 60 bar hydrogen pressure after 48 hours [41]. Finally, at 80°C TEA·BH₃ is displaced with ammonia to obtain NH₃BH₃. As we can see, although experimental conditions required for each step of this process are not typical, the process is well understood. Nevertheless, further work is needed to improve the yield and the cost of full regeneration process.

Despite the fact that the direct synthesis of Mg(BH₄)₃(NH₃)₆ from MgH₂+NH₃BH₃ mixture was not successful, pure compound can be synthesized with MgH₂+TEA·BH₃ in liquid ammonia at RT. After a week, the reaction is heated above 60°C to enable ammonia displacement of TEA adducts in Mg(BH₄)₂(TEA)_n. Essentially, the third step of the ammonia borane regeneration process can be integrated into Mg(BH₄)₃(NH₃)₆ synthesis process.

V.5.3.1. B-N bond cleavage

The reactivity of hydrogen halide acid HX with the monomers of RN-BR' depends on the nature of R'. For B(NR₂)₃ where R=H, CH₃ or C₂H₅ groups react quantitatively with HCl creating protonated nitrogen bonds and B-Cl bonds. However, formation of dimers prevents the reaction completely [186]. Digestion of BN compared to other ceramics (Al₂O₃, AlN, Si₃N₄) is more difficult with conventional strong acids like HCl, H₂SO₄ or HNO₃ instead most literature work relies in hydrofluoric acid used in closed digestion vessel ("Teflon bomb") at high temperatures. While chlorine gas reacts with BN upon heating up to 700°C and forms BCl₃ and N₂ gasses. On the other hand, BN burns completely and rapidly at RT in 130 mbar of F₂ gas (dilution of the gas is necessary due to very exothermal nature of the reaction) turning into BF₃ and N₂ gasses [186]. Easiest way of converting BF₃ to other boron halides with high yield is by reaction with appropriate AlX₃. Additionally, BN is easily converted to NH₄BF₄ by HF treatment [187]. HF is generally avoided in laboratory synthesis procedures due to strict safety requirements for handling HF solutions. However, on the industrial scale it is the cheapest and most widely used hydrogen halide [186]. The use of "Teflon bomb" closed vessel is advantageous for preventing leakage and loss of the material; however, it is costly due to heating requirement for long duration (several hours to days). By using microwave excitation source, the reaction time can be shorted up to 80-99% [188]. Since

pure BN cannot be solvated in acid solutions, a well-known technique is alkali carbonate/metaborate fusion. In eutectic melt of NaKCO_3 boron nitride easily solubilizes [189]. Once cooled, its digestion in dilute HCl or HNO_3 is possible [190], [191]. It is also known that, in metal containing boron nitride compounds during the reaction with halogen gases, M-B bond is broken in preference to B-N bond [186]. The main extract from all these discussions is that the presence of metal cation bonded directly to boron nitrogen atoms in $\text{M}(\text{BNH}_x)_m$ compound might be an advantage that facilitates easier acid digestion compared to pure BNH_x . Microwave heating can be used to minimize the energy cost and improve the overall yield of the digestion process. However, non-aqueous acid solutions need to be used to prevent the formation of boric acid species, a microwave assisted CO_2 capture in non-aqueous amine solvents have also been demonstrated [192].

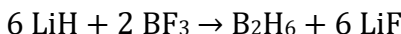
Since we did not have any high pressure anhydrous HCl source, the digestion by this approach was not possible. However, we tried to use NH_4Cl as an alternative that would decompose into ammonia and HCl gas. In an open reactor above 200°C , ammonium chloride simply sublimates. Hence, $\text{Mg}(\text{BNH}_x)_2-8\text{NH}_4\text{Cl}$ mixtures were heated in a closed stainless steel reactor at 300°C for 3 hours. Although ammonium chloride decomposition is a reversible reaction, its amount was limited to not generate more than 5 bars in the reactor if fully decomposed into HCl and NH_3 gases. Some unknown crystalline phases did appear after this digestion experiment, however most of the ammonium chloride remained unreacted (Figure V-S5). Since the stainless-steel reactor was not designed for higher temperature digestion experiments for longer duration, we abandoned this approach. Identification of the unknown peak was not possible, contrary to our expectation they did not correspond to $\text{Mg}(\text{NH}_3)_6\text{Cl}_2$ or NH_3BCl_3 phases.

Similarly, due to dangers associated with handling anhydrous HF , we decided to use NH_4F as an alternative. $\text{Mg}(\text{BNH}_x)_2-10\text{NH}_4\text{F}$ mixtures were heated in Teflon cup inside a steel reactor under open Ar flow. Heating to 100°C for 6 hours is enough to obtain pure $\text{MgF}_2-\text{NH}_4\text{BF}_4$ mixtures (Figure V-S6). Density separation of these phases (3.13 vs 1.85 g/ml) should be possible, however as we discussed previously, MgF_2 is not a useful precursor for synthesis of ammine magnesium borohydride compounds. Heating $\text{Mg}(\text{BH}_4)_2(\text{NH}_3)_6$ to 600°C results in dissociation of Mg and BN phases [180]. In fact, this could be the most efficient way to separate metal component from low temperature decomposition phase $\text{M}(\text{BNH}_x)_m$, since sublimation temperature of pure boron nitride of 3000°C is much higher than the melting temperature of metals [193]. However, further studies must be done on this approach since BN is also soluble in molten nitrides such as Li_3N , Li_3BN_2 and Mg_3N_2 [189].

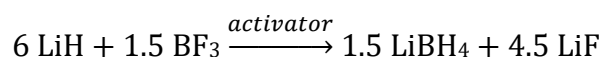
Unlike solid-state digestion reaction in Teflon reactor, by attempting digestion of $\text{Mg}(\text{BNH}_x)_2$ by NH_4F in liquid ammonia, we expected to obtain a $\text{Mg}(\text{BF}_4)_2$ type phase, but unfortunately, MgF_2 was still the main product (Figure V-S6). Reduction of B-F bonds in $\text{Mg}(\text{BF}_4)_2$ into $\text{Mg}(\text{BH}_4)_2$ was the original goal; however, we decided to continue with only NH_4BF_4 phase for testing our reduction approach.

V.5.3.2. B-F bond reduction

Ammonia borane digestion with NH_4F at 100°C for 6 hours gives pure NH_4BF_4 . Upon heating, this compound decomposes into HF, NH_3 and BF_3 gasses [194]. B-F bond in NH_4BF_4 is longer than in NH_3BF_3 . Due to change in hybridization from sp^2 to sp^3 , the B-F bond length increases from 130.7 pm to 139.6 pm [4]. This might make the reduction process of B-F bonds in BF_4 species easier compared to bonds in BF_3 species. The easiest way of converting boron difluoride gas to diborane is reaction with LiH, NaH and LiAlH_4 . Dilute $\text{Et}_2\text{O}\cdot\text{BF}_3$ solution is reported to react with LiH producing almost pure diborane gas except diethyl ether vapor:

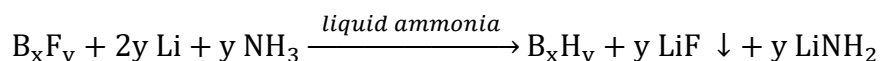


However, the presence of LiBH_4 activator in the solution as well as the use of THF solvent that can solubilize more diborane results in formation of LiBH_4 and LiF byproduct:



Nevertheless, this reaction is strongly inhibited by the formation of oxide layer on the surface of LiH particles due to the presence of water in the solution which prolongs the induction period and delivers non-reproducible reaction yield in 20-90% range [196]. However, as we mentioned in Chapter 1, reduction of B-X bonds by metal hydrides is expensive and only transfers the rehydrogenation problem onto even more stable LiF compound.

Inspired from the reduction of C-F bonds by lithium metal in liquid ammonia [121], we wanted to see if the reduction of B-F can be done by electron solution as well. This approach would still use two lithium atoms per fluorine atom; however, it would bypass the hydrogenation of alkali metal (formation of LiH) and instead ammonia would be used as a hydrogenation source:



$\text{NH}_4\text{BF}_4\text{-}8\text{Li}$ mixture (lithium used as metal pieces) was left in liquid ammonia at 60°C for 2 days. No stirring of the solution was possible since C-F bonds Teflon magnetic bar is reduced instead of B-F bonds. After this reduction process, XRD analysis of the powder showed that the main crystalline phase unsurprisingly is LiNH_2 (Figure V-10). More importantly, the presence of LiF phase proves partial reduction of B-F bonds which is either poorly crystalline or has very small nano-crystallites.

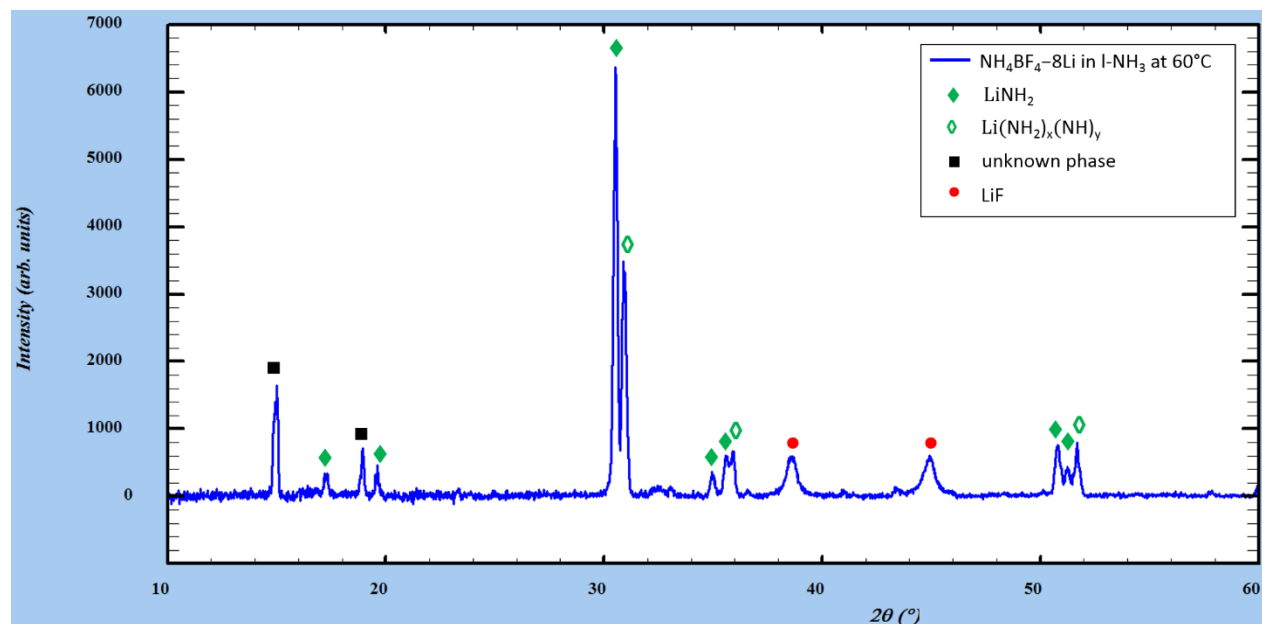
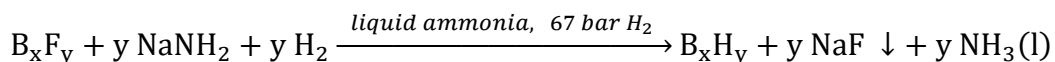


Figure V-10: XRD analysis of $\text{NH}_4\text{BF}_4\text{-8Li}$ mixture left in liquid ammonia for 2 days at 60°C .

This approach was not very efficient and consumed a lot of ammonia, turning most of the lithium metal into LiNH_2 . Lithium amide formation is essentially competing with B-F bond reduction and apparently it is the dominant reaction. We took another inspiration from reversibility of alkali amide [122] (discussed in Chapter 2) reaction to improve our process. Instead of using Na metal we chose to use NaNH_2 . The idea relies upon the assumption that by applying hydrogen pressure, a mole of hydrogen would be consumed to make a mole of ammonia while generate a mole of $\text{Na}^+ + \text{e}^-$ pair soluble in liquid ammonia:



Another potential advantage of this approach is that number of Na atoms needed for reduction of one B-F bonds decreases to half. Number of alkali fluoride byproduct per B-H bond formation still remains 1. Enthalpy and Gibbs free energy calculations show (Figure V-S7a) that if a single electron in liquid ammonia can attack more than one B-F bond, the formation of ammonia insoluble NH_4F can be possible. Consequently, the formation of NaF byproduct can be decreased from 4 to 1.8 moles while $\Delta G < 0$. In fact the formation of NH_4F would be an equivalent of $\text{TEA} \cdot \text{BCl}_3$ reduction under hydrogen pressure which was only possible due to formation of $\text{TEA} \cdot \text{HCl}$ byproduct (Chapter 1) [44]. However, the full reduction of NaBF_4 into NaBH_4 without the any formation of NaF (only NH_4F) is not thermodynamically allowed ($\Delta G = 300 \text{ kJ/mol}$).

To perform this reduction experiment, $\text{NH}_4\text{BF}_4\text{-4NaNH}_2$ mixture was transferred to a reactor where ammonia gas was condensed into and cooled further down to -70°C before the 45 bar of hydrogen pressure was applied to it. Then the reactor was closed and was to let to heat up to RT. Due to heating, the frozen ammonia in the reactor thawed and the hydrogen pressure increased to ~ 67 bar. After 12 hours, the reactor was evacuated and XRD

analysis was performed. As we can see from Figure V-11, most of the NaNH₂ remained unreacted. However, as a proof of our idea, the broad peaks corresponding to NaF phase were observed.

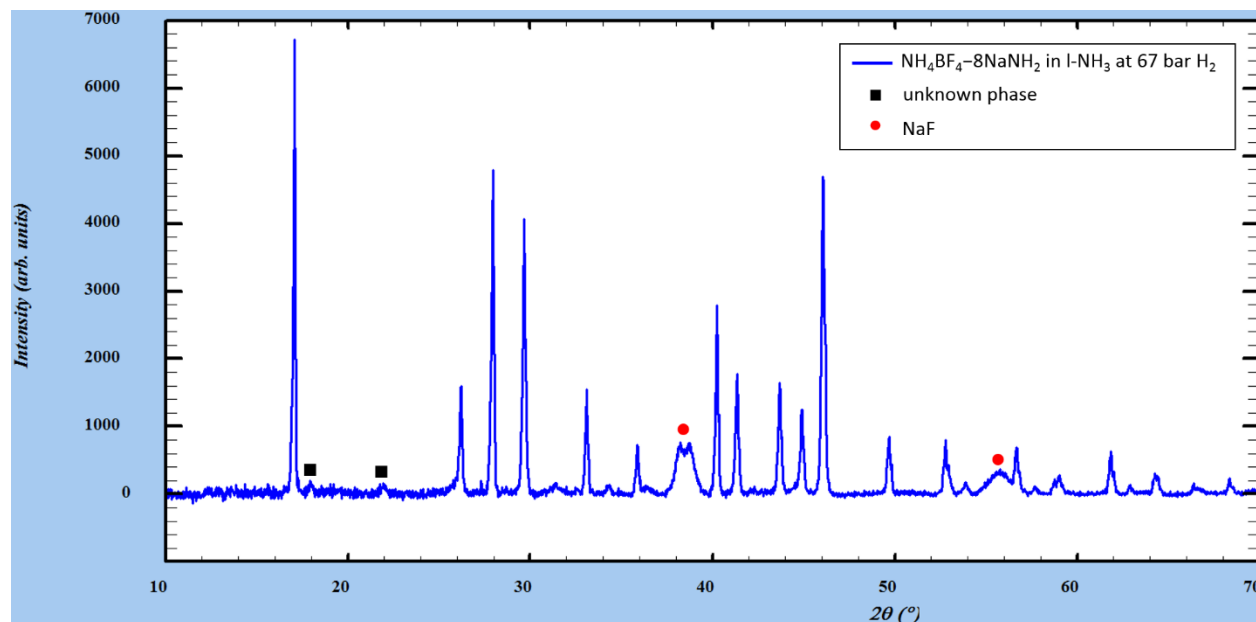
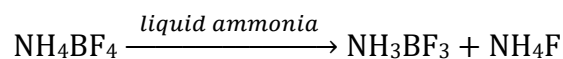


Figure V-11: XRD analysis of NH₄BF₄–8NaNH₂ mixture in liquid ammonia under 67 bar of hydrogen pressure. All the unmarked peaks correspond to only NaNH₂ phase.

An interesting point is that NH₄BF₄ after exposure to liquid ammonia becomes undetectable in XRD analysis. Currently, we do not have any explanation for this observation. Hence, in both Figure V-10 and Figure V-11, due to the loss of crystallinity in NH₄BF₄ phase, we cannot not observe the changes after reduction attempts. Additionally, following decomposition of NH₄BF₄ in liquid ammonia is possible:



Although we did observe two peaks corresponding to some unknown phase in both Figure V- and Figure V-, they do match to NH₃BF₃ or any other known phase. Additionally, if the described decomposition reaction is present that would explain the formation of LiF and NaF species without any reduction of the B-F bonds in NH₃BF₃ phase. To shed light to this situation we performed ¹¹B NMR analysis:

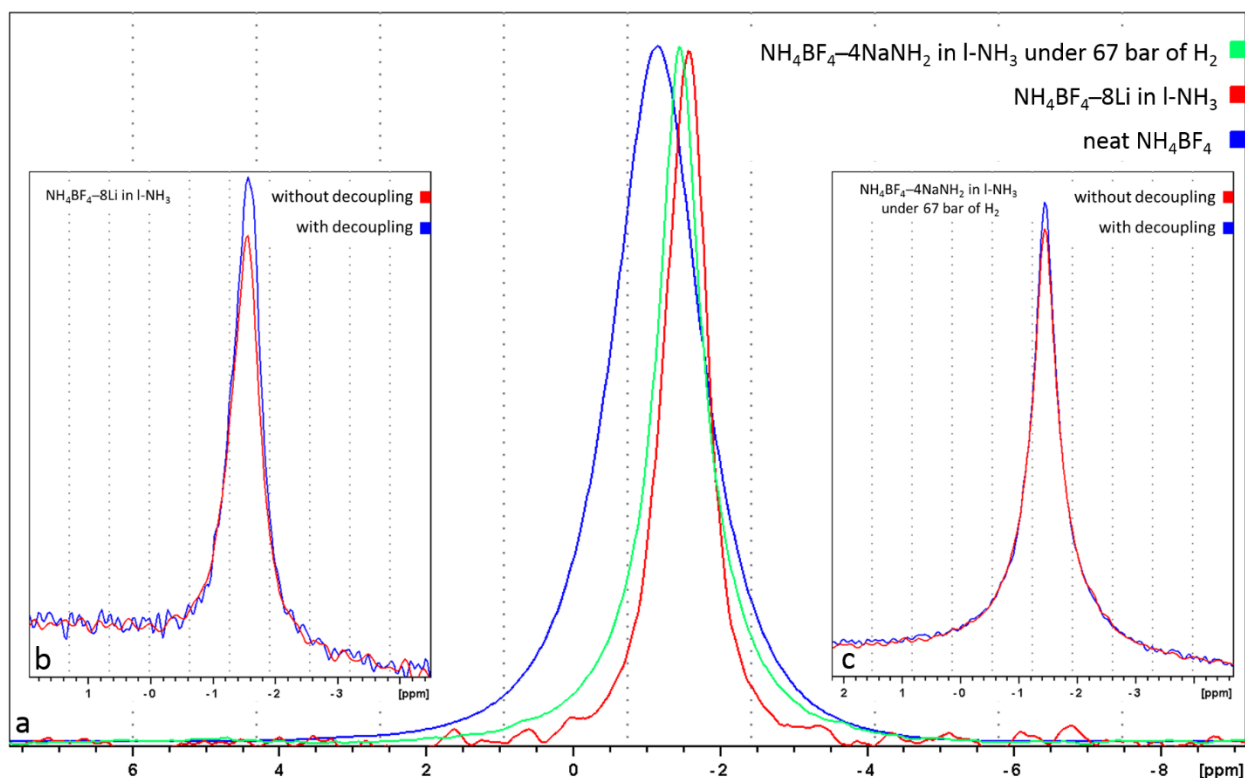


Figure V-12: ^{11}B NMR was performed a) on neat NH_4BF_4 and two partially reduced samples b) effect of proton decoupling on samples reduced by ammonia solution of lithium c) effect of proton decoupling on sample reduced by ammonia solution of sodium amide under 67 bar of hydrogen pressure. NaBH_4 peak was at -42 ppm as the reference.

If full reduction of B-F bonds would have been possible, the main hydrogenated phase would have been either NH_4BH_4 or NaBH_4 . No ^{11}B NMR peaks corresponding to sodium borohydride or ammonia borane was observed (Figure V-12a). In literature, ball-milled $\text{NaBF}_4\text{-NaBH}_4$ samples resulted in formation of $\text{NaBH}_x\text{F}_{4-x}$ compound. NaBF_4 has chemical shift of -1.7 ppm and it was claimed that calculations indicated NaBF_2H_2 would only have 3ppm chemical shift compared to NaBF_4 [35]. However, another similar study performed on ball-milled $\text{KBH}_4\text{-KBF}_4$ mixtures claimed $\text{KBH}_x\text{F}_{4-x}$ would have several peaks with chemical shift values very close to that of KBH_4 (-38 ppm) for $x = 1-3$ [107]. Although, it seems that the consensus does not exist for the degree of chemical shift for partial substitution of H-sites with F^- in borohydride anions, both articles agree that the range of chemical shift is small. Neat NH_4BF_4 has a chemical shift of -1.35 ppm, while after treatment in liquid ammonia solution of lithium metal this chemical shift is -1.80 ppm. NH_4BF_4 reduced by liquid ammonia solution of sodium amide under 67 bar of hydrogen pressure has a chemical shift of -1.70 ppm. Hence, we do have a clear chemical shift towards BH_4 sites in samples after reduction attempts (Figure V-12a). However, considering the resolution of the spectrometer and the small scale of chemical shifts, a better evidence would be in proton decoupling analysis. Proton decoupling should not affect the intensity of the ^{11}B NMR if there are no hydrogens around the boron atoms. To that end NMR spectra was measured with and

without proton decoupling while keeping all the experimental parameters same. As shown in Figure V-12b and c, the effect of proton decoupling on signal intensity is negligible. This means that the reduction process by lithium metal is higher compared to reduction by sodium amide solution under hydrogen pressure which is also confirmed the degree of chemical shift. However, both processes achieved negligible reduction and have very low overall yield.

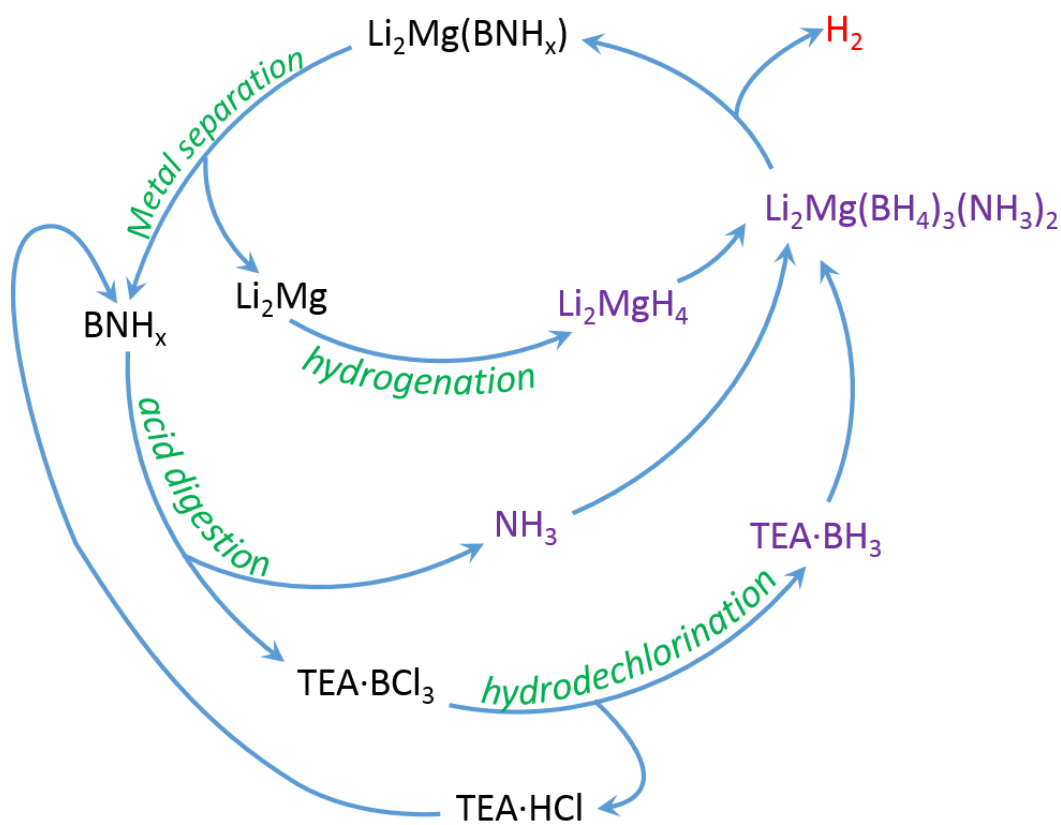
As a summary, the digestion of BNH_x spent fuel is much easier with NH_4F compared to anhydrous HCl where a high-pressure anhydrous acid system is necessary. The yield of NH_4F digestion process is close to 100%. However, reduction of $\text{L}\cdot\text{BX}_3$ species where $\text{X}=\text{F}$ is much harder than $\text{X}=\text{Cl}$. Successful hydrodechlorination process with high yield has been shown in the presence of synergetic interaction of TEA and Ni_3B catalyst. However, the stability of Ni_3B catalyst in the presence of $\text{TEA}\cdot\text{HF}$ is less likely. Therefore, we approached this process by employing reduction power of liquid ammonia solution of alkali metals. Experimental evidence shows the feasibility of the idea; however, the yield of the reduction process is very low and full reduction of B-F bonds might be unattainable. This could be due the fact that B-F bond has the highest formation energy of all the bonds discussed in this chapter including B-Cl and C-H bonds (Figure V-S7b).

V.6. Conclusion

In this chapter, due to the thermal stability limitation of Zn-B-N-H system we focused on Mg-B-N-H compounds. We successfully demonstrated the ability to synthesize magnesium amidoborane compounds using magnesium metal and ammonia borane precursors. However, thermal stability of this compound is very similar to that of Zn-B-N-H system. Hence, we focused our efforts on $\text{A}_x\text{Mg}(\text{BH}_4)_{2+x}(\text{NH}_3)_n$ compounds. In liquid ammonia, 67 bar of hydrogen pressure was not enough to suppress the dihydrogen elimination reaction between hydride of the hydride MgH_2 and the proton of ammonia borane to force the formation of magnesium borohydride. The same result was obtained for $\text{L}\cdot\text{BH}_3$ precursors with solvents that are softer Lewis base than ammonia. However, by choosing L that is a harder Lewis base than ammonia at RT, successful formation of $\text{Mg}(\text{BH}_4)_2\cdot n\text{L}$ in liquid ammonia is possible. Base exchange reaction was then achieved by increasing the temperature of the liquid ammonia solution resulting in formation of $\text{Mg}(\text{BH}_4)_2(\text{NH}_3)_6$. For $\text{L}=\text{TEA}$ this temperature is above 60 °C. The hydrogen capacity of at least 10 wt% was shown with at least 65 wt% hydrogen purity for $\text{Li}_2\text{Mg}(\text{BH}_4)_4(\text{NH}_3)_2$ samples after heat treatment at 100 °C for 6 hours.

We verified the impossible direct hydrogenation $\text{Mg}(\text{BNH}_x)_2$ spent fuel. However, the search for modification of this process by solvent adducts and hydrogenation catalysts led us to synthesize $\text{Ni}(\text{BH}_4)_2(\text{NH}_3)_6$ compound for the first time. This is the known highest electronegativity amine metal borohydride compound stabilized at RT by chloride anion substitution of borohydride sites. We explored chemical regeneration of spent $\text{Mg}(\text{BNH}_x)_2$ fuel. Digestion with NH_4F was shown to be very easy and quantitative. Due to very stable nature of B-F bonds in obtained NH_4BF_4 compounds, compared to direct reduction with alkali hydrides we sought the power of liquid ammonia solution of alkali metal as a way of

bypassing hydride formation from alkali metals as well as possible reduction of alkali fluoride byproducts. Limited success was observed in these reduction efforts. Hence, high pressure anhydrous HCl digestion followed by hydrodechlorination under high hydrogen pressure in the presence of synergetic interaction of TEA solvent and Ni₃B catalyst seems to be the best regeneration approach to BNH_x spent fuel of ammonia borane. In case of ammine metal borohydrides, the presence of metal in M(BNH_x)_m spent fuel might be advantages for improving the conditions necessary for digestion process together with microwave assistance. However, dissociation of M(BNH_x)_m into metal and BNH_x before the digestion process might be necessary since formation of metal halides is not desired for full regeneration cycle. Dissociation can be achieved by simply heating to high enough temperature (600 °C for magnesium compounds) where the only stable phase is boron nitride. For zinc compounds this dissociation process happens at RT. For the full regeneration process, obtained metals must be hydrogenated in order to react them with TEA·BH₃ at RT and then at T > 60 °C to obtain M(BH₄)_m(NH₃)_n compounds. Unfortunately, direct hydrogenation of zinc metal is not possible and require only chemical routes which involve organometallic precursors as well as other hydride such as LiH and LiAlH₄ [132]. Hence, potential rough diagram of full regeneration cycle where no LiF byproduct is generated in any step might look like this:



Further research and optimization of each step is necessary to determine the yield and the cost of the overall regeneration cycle.

V.7. Appendix

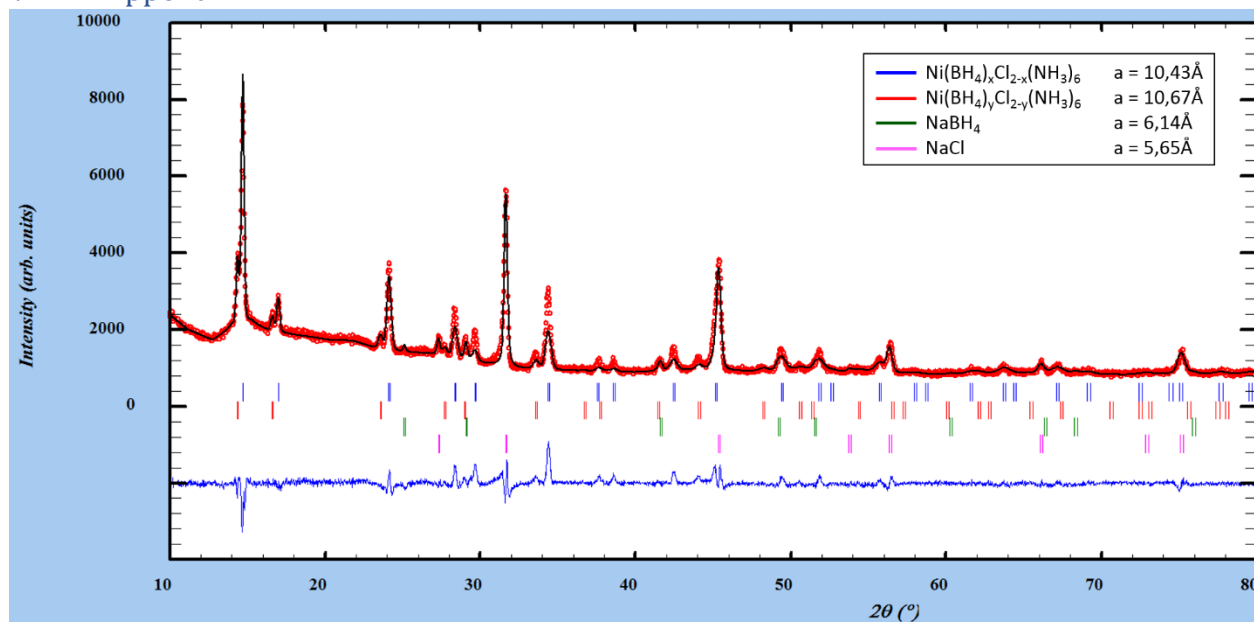


Figure V-S1: Rietveld analysis of $\text{Ni}(\text{BH}_4)_x\text{Cl}_{2-x}(\text{NH}_3)_6$ compound. All phases have cubic crystalline structure ($Fm\text{-}3m$ space group)

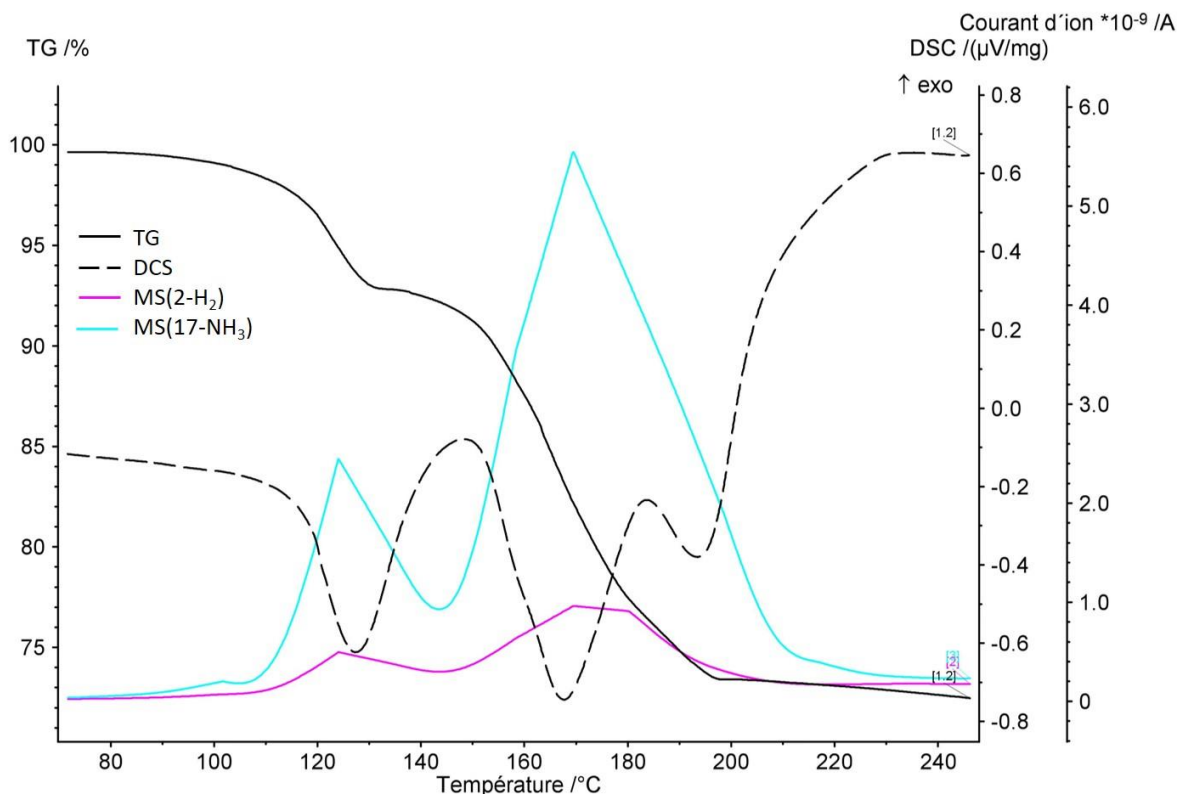


Figure V-S2: DCS-TG-MS analysis of $\text{Ni}(\text{BH}_4)_x\text{Cl}_{2-x}(\text{NH}_3)_6$ compound. Heating rate is $10^\circ\text{C}/\text{min}$.

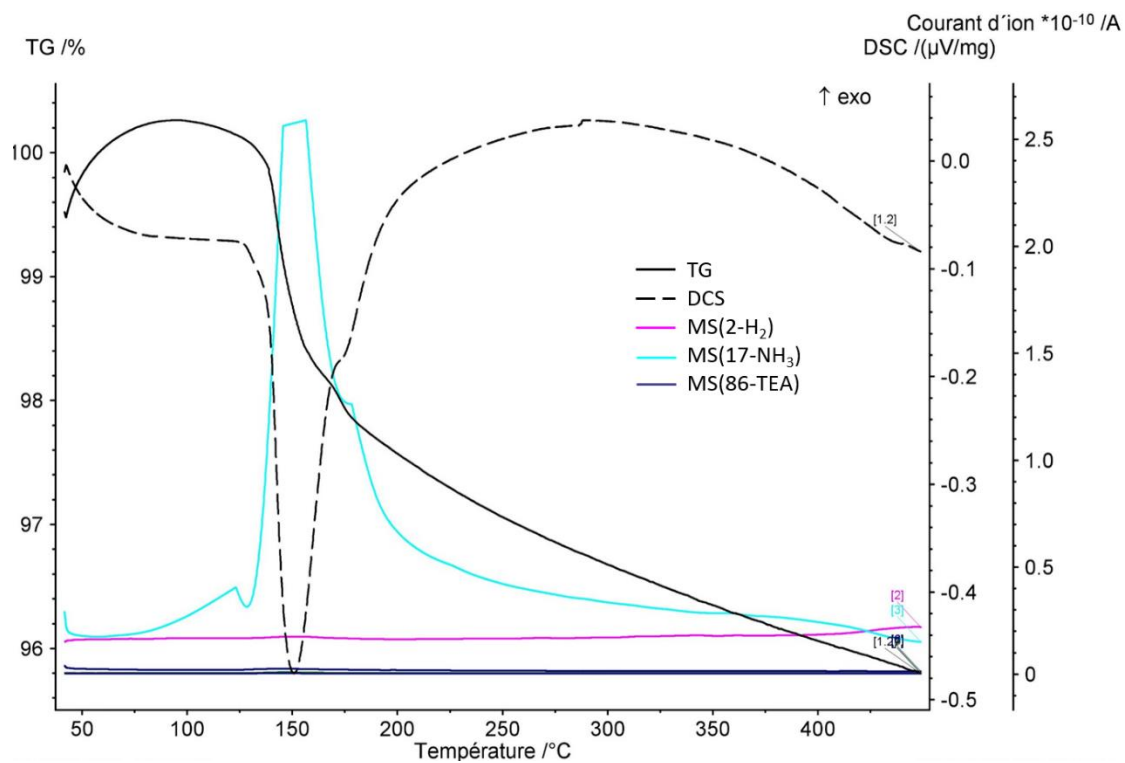


Figure V-S3: Hydrogenation of $2\text{Mg}(\text{BNH}_x)_2\text{-Ni}(\text{BNH}_x)_2$ mixture in TEA under 50 bar hydrogen pressure

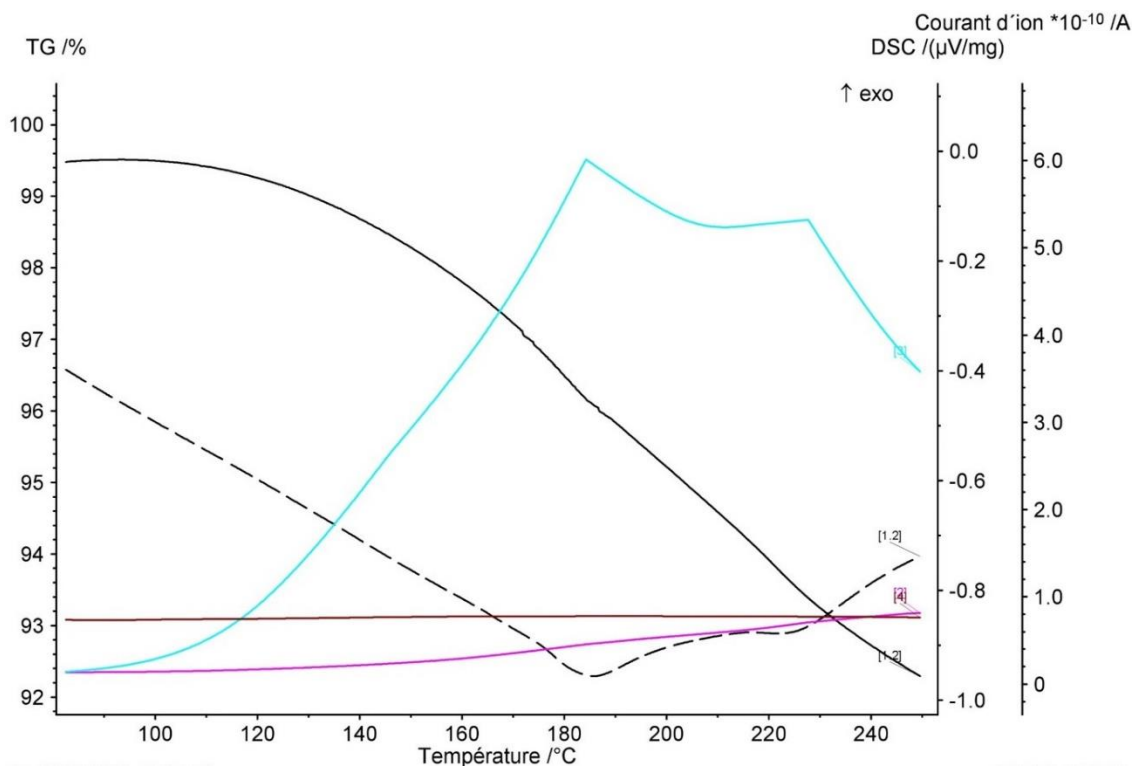


Figure V-S4: Hydrogenation of $Mg(BNH_x)_2$ in liquid ammonia under 70 bar hydrogen pressure

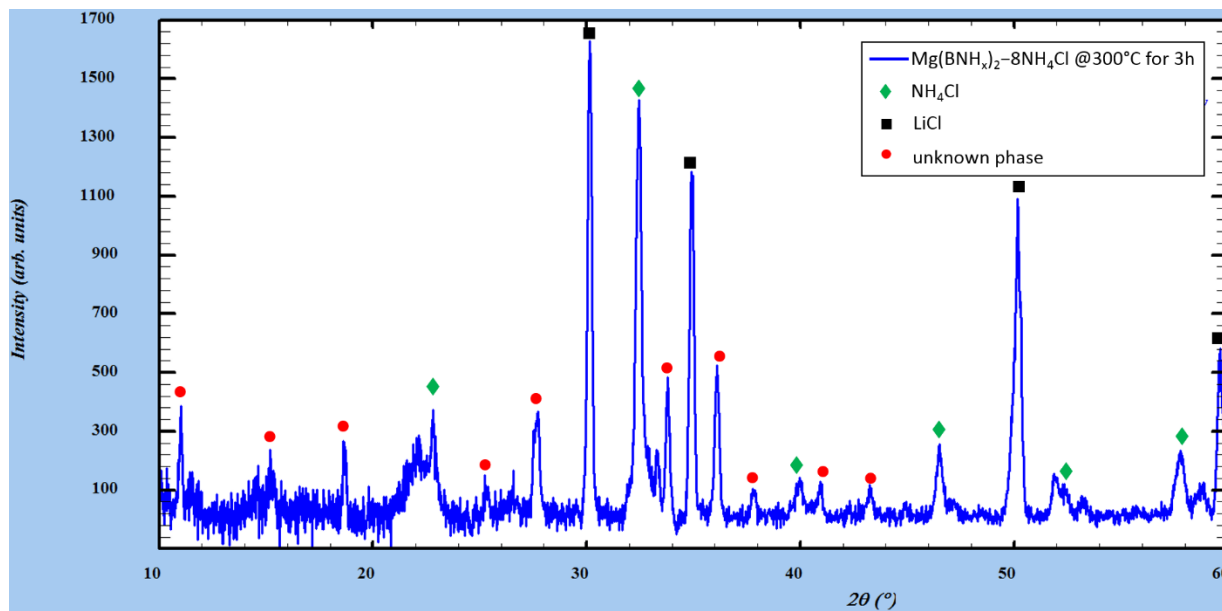


Figure V-S5: XRD analysis of $Mg(BNH_x)_2$ after digestion attempt with NH_4Cl at $300^\circ C$

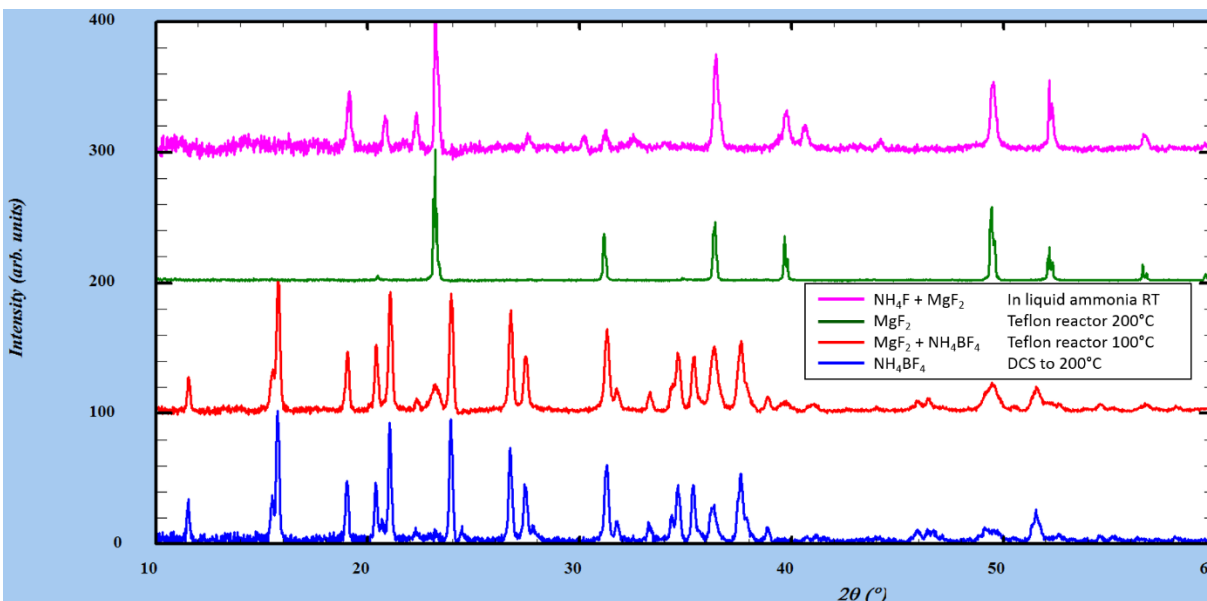


Figure V-S6: XRD analysis of $Mg(BNH_x)_2$ after digestion NH_4F in a) liquid ammonia at RT b) in a Teflon reactor at $200^\circ C$ (NH_4BF_4 decomposed completely) c) in Teflon reactor at $100^\circ C$ d) in aluminium crucible of DCS (MgF_2 reacted with the crucible)

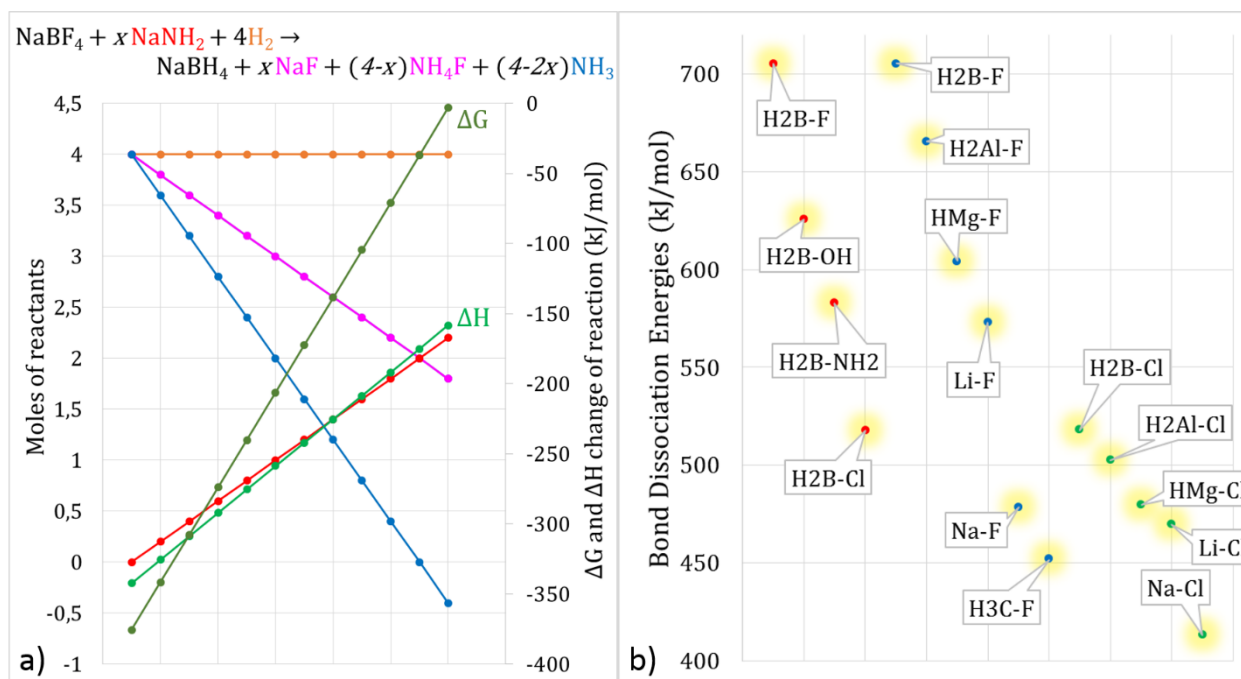


Figure V-S7 a) Enthalpy and Gibbs free energy of a $NaBF_4$ reduction to $NaBH_4$, assuming NH_4F byproduct can be formed the reaction remains exothermal and spontaneous when NaF byproduct decreased from 4 to 2 mole b) comparison of dissociation energies of chemical bonds discussed in this chapter

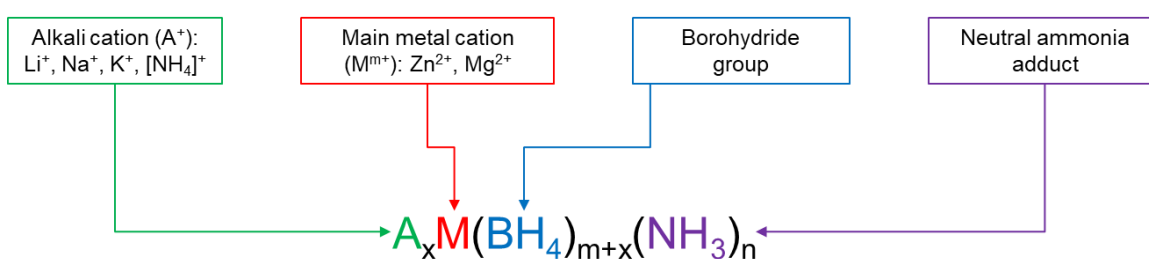


General Conclusions and Perspectives



VI. General Conclusions and Perspectives

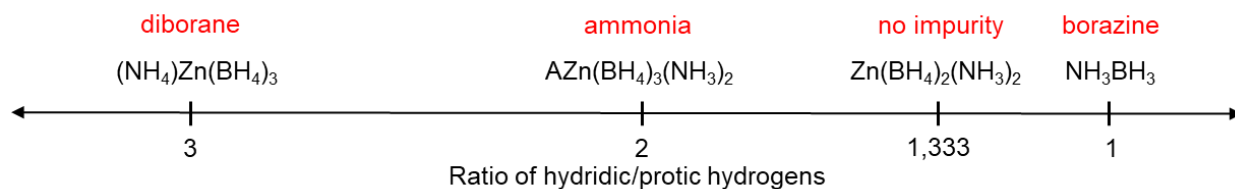
In Chapter I, we explored the literature and state of the art in chemical hydrogen storage approaches. We identified that the M-B-N-H based compounds potentially can deliver high volumetric and gravimetric hydrogen capacity. However, before achieving this performance several drawbacks needed to be overcome and clarified. The role of the main metal cation in ammine metal borohydrides was more or less understood in literature. Higher electronegativity or higher polarization metals lowered the energetic barrier to exothermal reaction between protic and hydridic hydrogens in ammonia and borohydride groups, respectively. Assuming this is the main dehydrogenation process in these compounds we set out to find the role of alkali cations in the structure and the hydridic to protic hydrogen ratio (analogy to fuel-oxidizer ratio).



However before tackling any of these questions we needed to develop a scalable synthesis process that allowed the synthesis of desired ammine metal borohydride compounds. As we discussed in detail in Chapter II and the beginning of Chapter III existing techniques in literature such as ball-milling and solvothermal synthesis using organic solvents has limitations that needed to be improved. Hence, major part of our efforts during this thesis project was devoted to development of high temperature liquid ammonia based synthesis approach. The technique allowed us to swap the alkali cation (A) in $AZn(BH_4)_3(NH_3)_2$ from Li to Na to K. The results helped us to conclude that the role of the alkali cation in dehydrogenation properties of ammine zinc borohydride compounds is significant. The main extract is that the presence of an alkali cation with a polarization power lower than that of the main cation is detrimental to the purity of the released hydrogen. Alternatively, if the coordination sphere of the main metal cation is completely filled with ammonia molecules the effective polarization power of $[M(NH_3)_n]^{m+}$ will be lower than that of a potassium cation. In this case, the presence of an alkali cation improves the dehydrogenation process. We further demonstrated this difference with the dehydrogenation behaviour of $A_x Mg(BH_4)_{2+x}(NH_3)_n$ (where $A=Li; Na, x=0; 1; 2, n=2; 6$) compounds in the first half of Chapter V:



Since most ammine metal borohydride compounds dehydrogenate after melting triggered amorphization step, the role of the crystalline structure becomes less relevant. This also presented an opportunity to explore protic and hydridic hydrogen ratio in the compounds that is not fixed with the chemical formula of the crystalline phase. To that end, we co-synthesized $\text{NaZn}(\text{BH}_4)_3(\text{NH}_3)_2-x\text{NH}_3\text{BH}_3$ (for $x=0$ to ∞) mixture in liquid ammonia which allowed us to obtain very high homogeneity. Our priori understanding of the decomposition process of M-B-N-H systems did not allow for reliable prediction of impurity gasses based on protic/hydridic hydrogen ratio:



In Chapter IV, we explored in detail decomposition mechanism of $\text{NaZn}(\text{BH}_4)_3(\text{NH}_3)_2-x\text{NH}_3\text{BH}_3$ mixture using ex-situ and in-situ solid state ^{11}B NMR technique. These studies provided a unique look into the decomposition process in amorphous state that was not observable by many in-situ XRD measurements performed in literature. The main observation was that the main cation in M-B-N-H systems played a catalytic role in transforming the compound to diammoniate of diborane $(\text{NH}_3)_2\text{BH}_2[\text{BH}_4]$ which enabled a new dehydrogenation pathway that is lower in temperature and higher in hydrogen purity. Based on our in-depth understanding, we were able to design a $\text{ZnCl}_2-8\text{NaZn}(\text{BH}_4)_3(\text{NH}_3)_2-20\text{NH}_3\text{BH}_3$ mixture that released 10 wt% almost pure hydrogen, highest known performance for Zn-B-N-H system.

Although hydrogen storage capacity of M-B-N-H systems is impressive, reversible rehydrogenation of the compounds remains as a major roadblock to potential commercial applications of these compounds. This was further confirmed by our failed attempt in directly hydrogenating $\text{Mg}(\text{NH}_2\text{BH}_3)_2(\text{NH}_3)_3$ to $\text{Mg}(\text{BH}_4)_2(\text{NH}_3)_6$ under 70 bar hydrogen atmosphere (Chapter V). The cleavage of B-N bond requires unreasonable hydrogen pressures. To avoid blind, trial-error based experimental attempts in futility, the computational techniques are necessary to determine whether thermodynamics is in our favour and whether developing catalysts for rehydrogenation process is a fruitful endeavour. Hence, based on current literature we chose a chemical approach to address this problem. By leveraging our liquid ammonia based synthesis approach, we developed a fully contained cycle for chemical rehydrogenation of completely dehydrogenated ammine metal borohydride compounds, $\text{M}(\text{BNH}_x)_m$. Once broken into simpler chemical processes existing thermodynamic data allowed us to perform thermochemical calculations. These calculations show that the anhydrous acid digestion and hydrodehalogenation reactions are thermodynamically allowed. Further work is necessary to develop experimental setups, to synthesize catalysts in order to improve the reaction efficiency and the overall cost of this chemical regeneration approach.



Résumé détaillé des chapitres



VII. Résumé détaillé des chapitres

VII.1. Chapitre I - L'état de l'art

La consommation d'énergie est directement liée à la disparité économique mondiale puisque, par exemple, les 20% les plus riches de la population mondiale consomment plus du double de l'énergie des 80% les plus pauvres. Ce n'est pas un hasard si le produit intérieur brut d'un pays est en corrélation avec son niveau de consommation d'énergie [1]. L'augmentation de la population mondiale et son désir de mener une vie plus aisée augmenteront inévitablement la demande en énergie. Alors que les besoins en énergie du monde augmentent de plus en plus vite, à compter de 2019, les sources d'énergie renouvelables ne représentent plus que 4,5% de la demande mondiale, restant derrière les sources nucléaires et hydrothermales. La bonne nouvelle est que plus de 60% (et en augmentation) de l'apport net d'énergie nouvelle provient de sources renouvelables. Cependant, il s'agit de la source d'énergie brute ; c'est-à-dire qu'à partir du moment où cette énergie est traitée, distribuée, livrée et converti en une forme utilisable comme l'électricité ou le carburant, le processus subit de nombreuses pertes d'efficacité [2].

En ce qui concerne le coût de la production d'électricité, les technologies de production d'énergie renouvelable telles que les panneaux photovoltaïques et les éoliennes sont déjà compétitives par rapport aux sources classiques de combustibles fossiles dans de nombreuses régions du monde. Cependant, le principal obstacle à leur adoption rapide est l'inadéquation entre la demande et l'offre d'électricité. Ce problème a été qualifié de « courbe du canard », illustrant une forme de canard grossière due au déséquilibre quotidien entre la demande d'électricité en période de pointe et la production d'énergie renouvelable [3]. Au-delà de l'échelle quotidienne, ces déséquilibres existent sur des échelles plus longues telles que les périodes mensuelles, saisonnières et annuelles. La solution peut être apportée par les technologies de stockage d'énergie.

Les technologies de supercondensateurs et de batteries ont suffisamment mûri pour devenir économiquement viables pour les applications d'électromobilité et de stockage d'énergie à court terme. Cependant, il existe une limitation fondamentale de la quantité d'énergie pouvant être stockée à l'aide de ces technologies en raison de leur faible capacité d'énergie gravimétrique. Par conséquent, pour le stockage d'énergie à long terme et à grande échelle, les seules options possibles sont l'hydrogène, l'hydroélectricité pompée et l'air comprimé (Figure I-1). Parmi ces technologies, le stockage de l'hydrogène est le seul à ne pas être limité par les caractéristiques géographiques disponibles (montagnes, rivières et grottes souterraines profondes) du pays [4].

Bien que l'hydrogène ait la plus grande capacité énergétique gravimétrique en raison de sa très faible densité, sa capacité volumétrique n'est pas aussi impressionnante (0,12 MJ/L) par rapport aux carburants classiques tels que le diesel (38,6 MJ / L) [6]. Par conséquent, la nécessité de stocker l'hydrogène dans un milieu plus dense est devenue très importante. Actuellement, il existe deux approches principales, le stockage physique et chimique de l'hydrogène.

Dans le stockage physique, l'hydrogène est stocké sous forme de molécules d'hydrogène (H_2). Pour y parvenir, la liquéfaction et la compression de gaz à haute pression sont les deux principales techniques utilisées. Les approches les plus courantes sont l'hydrogène comprimé, l'hydrogène liquéfié et le stockage à basse température en milieu poreux. Chaque technique a ses limites.

Le stockage chimique de l'hydrogène fait référence à tout milieu contenant des atomes d'hydrogène sauf sous sa forme moléculaire. Contrairement à la physisorption, l'énergie d'interaction dans la chimisorption entre l'atome d'hydrogène et le composé hôte est suffisamment élevé pour dissocier la molécule H_2 . Toute molécule chimique qui contient suffisamment d'atomes d'hydrogène et peut le libérer sans apport énergétique important constitue un candidat potentiel.

Dans ce chapitre, nous avons présenté les résultats de l'analyse bibliographique sur les types de matériaux qui permettent le stockage physique et chimique de l'hydrogène. Parmi eux, les composés chimiques de densité supérieure restent des milieux attractifs pour le stockage de l'hydrogène en raison de leurs valeurs de capacité volumétrique et gravimétrique théoriquement élevées. La figure I-9 montre que l'ammoniac liquide, le borazane, les borohydrures de métaux légers et leurs ammoniates sont parmi les composés susceptibles de répondre aux exigences de capacité en hydrogène définies par le US Department of Energy pour une application mobile à base de piles combustible. À l'exception de l'ammoniac liquide, le reste de ces composés est basé sur le système M-B-N-H.

Par conséquent, dans cette thèse, nous nous sommes concentrés sur les composés M-B-N-H afin de comprendre quel type de compromis il faut faire pour que la capacité expérimentale en hydrogène soit aussi proche que possible des valeurs théoriques. Certains de ces compromis dérivent des autres paramètres importants telles que la pureté de l'hydrogène libéré et la température de déshydrogénation. La capacité hydrogène pratique, la pureté et la température de déshydrogénation d'un composé M-B-N-H donné sont interconnectées et cette connexion ne peut être comprise que par la compréhension du rôle de chaque atome dans la structure et de leur interaction au cours du processus de déshydrogénation. Ainsi, en utilisant diverses techniques de caractérisation, nous nous sommes efforcés de comprendre la complexité de ces interactions.

Les autres défis majeurs sont la complexité, le coût élevé et la difficulté de mise à l'échelle industrielle des processus de synthèse nécessaires pour permettre le développement de technologies pratiques basées sur les composés M-B-N-H. Ainsi, nous nous sommes concentrés sur le développement de méthodes de synthèse plus simples et optimisées afin de relever ces défis.

Finalement, il est fortement probable que l'inconvénient majeur empêchant les applications pratiques des composés de type M-B-N-H soit l'absence de réversibilité directe (i.e., la réhydrogénation) ou éventuellement la régénération des produits de réaction. Cette étape est cruciale afin de minimiser les coûts et augmenter la durabilité. Comme il a été déjà

mentionné précédemment, l'hydrogénation directe est improbable et d'autres voies chimiques ont été explorées pour le processus de régénération complet.

VII.2. Chapitre II - Méthodologie

Dans ce chapitre, nous présentons une brève description des conditions expérimentales ainsi que des techniques de caractérisation courantes des composés de type M-B-N-H. Ensuite, un résumé des diverses approches de synthèse de ces composés décrites dans la littérature a été réalisé, suivi par la présentation détaillée des procédures et des équipements utilisés au cours de cette thèse.

VII.3. Chapitre III - Synthèse et caractérisation de borohydrures d'amines de zinc

Dans les composés $M(\text{BH}_4)_m(\text{NH}_3)_n$, le pouvoir de polarisation des cations entraîne la modification de la charge partielle sur les groupements $[\text{BH}_4]^-$ et NH_3 , puis de leurs atomes d'hydrogène. Cela permet d'améliorer ou de supprimer le processus de libération de l'hydrogène. En raison de la plus grande affinité des molécules d'ammoniac pour le cation métallique $[\text{M}(\text{NH}_3)_6]^{m+}$, celui-ci est complètement protégé du pouvoir de réduction des anions $[\text{BH}_4]^-$. Lors du chauffage, les adduits d'ammoniac en excès dans la structure sont généralement libérés sous forme d'impureté d'ammoniac. En ajoutant des cations alcalins à la structure, ceux-ci peuvent polariser les anions $[\text{BH}_4]^-$ et favoriser le processus de libération du dihydrogène, $\text{A-B-H}^{\delta-} \cdots \text{H}^{\delta+}-\text{N-M}$. Cependant, il existe une quantité optimale d' ABH_4 qui peut être ajoutée à la structure $M(\text{BH}_4)_m(\text{NH}_3)_n$ afin d'améliorer la pureté de l'hydrogène sans pénaliser la capacité expérimentale en hydrogène du composé. Une autre approche consiste à réduire les adduits d'ammoniac. L'une des familles de composés qui préfèrent naturellement un nombre limité d'adduits d'ammoniac, a la composition de type $\text{A}_x\text{Zn}(\text{BH}_4)_{2+x}(\text{NH}_3)_2$ (ou $x=0,1$), avec une bonne capacité en hydrogène et une bonne pureté.

L'objectif principal de ce chapitre était d'utiliser des composés apparentés au $\text{Zn}(\text{BH}_4)_2(\text{NH}_3)_2$ comme « banc d'essai » pour l'étude de divers facteurs susceptibles d'affecter le processus de décomposition et les propriétés d'hydrogénation du borohydrure métallique complexé à l'ammoniac. Au lieu de comparer de nombreux composés différents, l'objectif était de se concentrer sur un système capable d'exclure le plus possible les effets de diverses approches de synthèse, de différentes structures cristallines, du nombre d'adduits d'ammoniac, des modifications de l'électronégativité des cations métalliques centraux et d'autres phases d'impuretés.

Une nouvelle technique de synthèse basée sur l'ammoniac liquide en tant que solvant a été développée, permettant la synthèse directe et en une seule étape de divers composés de base de borohydrure de zinc et ammoniac. Les composés synthétisés avec des précurseurs de ZnCl_2 ont montré une substitution partielle des anions borohydrure par des anions chlorure. Lors de l'utilisation de précurseurs de ZnF_2 , cet effet de substitution d'anions a été complètement éliminé. Quatre composés de borohydrure de zinc complexé à l'ammoniac ont été synthétisés. Parmi ceux-ci, deux sont rapportés pour la première fois dans ce travail, à savoir les composés $\text{LiZn}(\text{BH}_4)_3(\text{NH}_3)_2$ et $\text{KZn}(\text{BH}_4)_3(\text{NH}_3)_2$.

Les tétraèdres de zinc avec deux groupements borohydrure et deux ligands d'ammoniac forment la base de tous les composés rapportés. Un composé bimétallique $AZn(BH_4)_3(NH_3)_2$ où $A = Li; Na; K$ au niveau atomique est une combinaison de $Zn(BH_4)_2(NH_3)_2$ (tétraèdres de Zn) monométallique et de ABH_4 . Pour les composés avec substitution partielle des anions chlorures, cet environnement atomique a plus de chances de ressembler à $AZn(BH_4)_{3-x}Cl_x(NH_3)_2 = Zn(BH_4)_2(NH_3)_2 + ACl$ en raison du site de bore préférentiel pour la substitution par les anions chlorure. La présence d'un borohydrure alcalin supplémentaire à proximité de ce tétraèdre et la possibilité de régler finement l'électronégativité du cation alcalin en le remplaçant par le lithium, le sodium ou le potassium, ont fourni un ensemble unique de composés permettant d'étudier le processus de déshydrogénation ainsi que la libération d'impureté ammoniacale indésirable. Par conséquent, l'électronégativité inférieure des cations alcalins et les effets de substitution d'anions chlorures à électronégativité plus élevée, ont comme résultat une plus grande libération d'impuretés d'ammoniac pendant le processus de déshydrogénation.

VII.4. Chapitre IV - Optimiser la capacité d'hydrogène des composés Zn-B-N-H

Dans ce chapitre, nous nous sommes concentrés sur l'amélioration de la capacité de stockage de l'hydrogène du système Zn-B-N-H et nous avons exploré tous les composés et mélanges de stockage de l'hydrogène pouvant être formés à partir de ces atomes : $NH_4Zn(BH_4)_3$, $Zn(BH_4)_2(NH_3)_2$ et $Zn(NH_2BH_3)_2$. En nous basant sur les résultats et la compréhension des matériaux à base de borohydrure de zinc et de leur technique de synthèse potentiellement industrialisable présentés au chapitre 3, nous avons démontré la libération d'hydrogène pur à 10 wt% du mélange $ZnCl_2-8NaZn(BH_4)_3(NH_3)_2-20NH_3BH_3$.

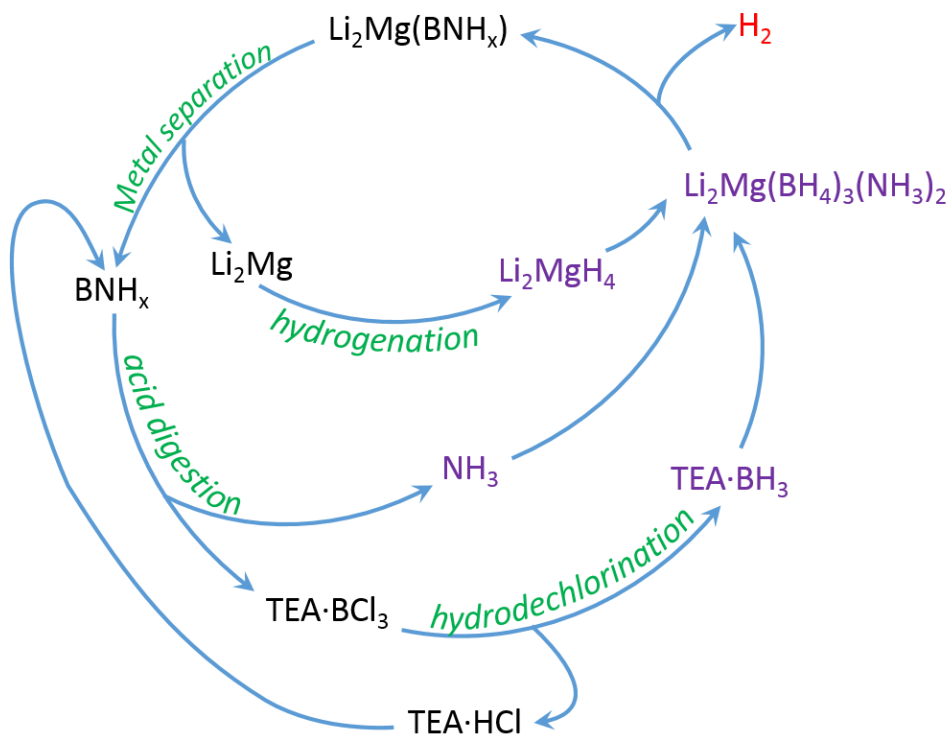
Nous avons effectué des études in-situ de déshydrogénation par RMN ^{11}B de mélanges de $NaZn(BH_4)_3(NH_3)_2-9NH_3BH_3$ et de $Zn(BH_4)_2(NH_3)_2-9NH_3BH_3$ qui offraient une perspective unique en ce qui concerne la déshydrogénation des borohydrures d'ammonium et de borazane.

VII.5. Chapitre V - Système Mg-B-N-H et exploration de la réversibilité

Dans ce chapitre, en raison de la limitation de la stabilité thermique du système Zn-B-N-H, nous nous sommes concentrés sur les composés Mg-B-N-H. Nous avons démontré avec succès notre capacité à synthétiser des composés d'amidoborane de magnésium à l'aide de précurseurs de magnésium métallique et de borazane. Cependant, la stabilité thermique de ce composé est très similaire à celle du système Zn-B-N-H. Par conséquent, nous avons concentré nos efforts sur les composés $A_xMg(BH_4)_{2+x}(NH_3)_n$. Dans l'ammoniac liquide, une pression d'hydrogène de 67 bar n'était pas suffisante pour supprimer la réaction de libération d'hydrogène lors de la réaction entre l'atome H^- de l'hydrure MgH_2 et le proton H^+ du borazane pour forcer la formation de borohydrure de magnésium. Le même résultat a été obtenu pour les précurseurs $L \cdot BH_3$ avec des solvants constitués d'une base de Lewis moins forte que l'ammoniac. Cependant, en choisissant L qui est une base de Lewis plus forte que l'ammoniac à température ambiante, il est possible de former avec succès $Mg(BH_4)_2 \cdot nL$ dans l'ammoniac liquide. La réaction d'échange de base a ensuite été obtenue en augmentant la température de la solution d'ammoniac liquide, ce qui a entraîné la formation de

$\text{Mg}(\text{BH}_4)_2(\text{NH}_3)_6$. Pour $L = \text{TEA}$, cette température est supérieure à $60\text{ }^\circ\text{C}$. La capacité en hydrogène d'au moins $10\text{ wt}\%$ a été mesurée avec une pureté d'hydrogène au moins $65\text{ wt}\%$ pour les composés de type $\text{Li}_2\text{Mg}(\text{BH}_4)_4(\text{NH}_3)_2$ après traitement thermique à $100\text{ }^\circ\text{C}$ pendant 6 heures.

Nous avons constaté l'impossibilité d'hydrogénation directe pour le composé $\text{Mg}(\text{BNH}_x)_2$. Cependant, la recherche d'une modification de ce procédé par des adduits de solvants et des catalyseurs d'hydrogénation nous a conduit à synthétiser pour la première fois le composé $\text{Ni}(\text{BH}_4)_2(\text{NH}_3)_6$. Il s'agit du composé borohydrure métallique complexé à l'ammoniac, dont l'électronégativité du cation est la plus élevée et qui a été stabilisé à température ambiante par substitution des sites borohydrure par les anions chlorure. Nous avons exploré la régénération chimique du composé $\text{Mg}(\text{BNH}_x)_2$. La digestion avec NH_4F s'est avérée très facile et quantifiable. En raison de la nature très stable des liaisons BF dans les composés NH_4BF_4 obtenus, par rapport à la réduction directe avec des hydrures alcalins, nous avons utilisé la puissance de la solution ammoniacale du métal alcalin en tant que moyen de contourner la formation d'hydrure à partir de métaux alcalins, ainsi que de réduire éventuellement les sous-produits de fluorure alcalin. Un succès limité a été observé grâce à ces efforts de réduction directe. Par conséquent, la digestion au HCl anhydre à haute pression suivie d'une hydrodécholoration sous une pression d'hydrogène élevée et en présence d'une interaction combinée du solvant TEA et du catalyseur Ni_3B semble être la meilleure approche de régénération du composé BNH_x à base de borazane. Dans le cas des borohydrures métalliques complexé à l'ammoniac, la présence de métal dans le composé $\text{M}(\text{BNH}_x)_m$ pourrait être un avantage pour améliorer les conditions nécessaires au processus de digestion, en s'appuyant aussi sur la technique par micro-ondes. Cependant, une dissociation de $\text{M}(\text{BNH}_x)_m$ en métal et BNH_x avant le processus de digestion peut être nécessaire, car la formation d'halogénures métalliques n'est pas souhaitée pour un cycle de régénération complet. La dissociation peut être obtenue en chauffant simplement à une température suffisamment élevée ($600\text{ }^\circ\text{C}$ pour les composés de magnésium) où la seule phase stable est le nitrure de bore. Pour les composés de zinc, ce processus de dissociation se produit à température ambiante. Pour le processus de régénération complète, les métaux obtenus doivent être hydrogénés afin de les faire réagir avec $\text{TEA}\cdot\text{BH}_3$ à température ambiante, puis à $T > 60\text{ }^\circ\text{C}$ pour obtenir les composés $\text{M}(\text{BH}_4)_m(\text{NH}_3)_n$. Malheureusement, l'hydrogénation directe du zinc métallique n'est pas possible et nécessite des voies chimiques impliquant des précurseurs organométalliques ainsi que d'autres hydrures tels que LiH et LiAlH_4 [132]. Par conséquent, un possible diagramme approximatif du cycle de régénération complète, dans lequel aucun sous-produit de LiF n'est généré à aucune étape, pourrait ressembler à ceci :



Des recherches supplémentaires et une optimisation de chaque étape sont nécessaires pour déterminer le rendement et le coût du cycle de régénération global.

References

- [1] J. H. Brown *et al.*, 'Energetic Limits to Economic Growth', *BioScience*, vol. 61, no. 1, pp. 19–26, Jan. 2011, doi: 10.1525/bio.2011.61.1.7.
- [2] 'BP Statistical Review of World Energy', BP, 2019.
- [3] B. Kulkarni, D. Patil, and R. G. Suryavanshi, 'IOT Based PV assisted EV Charging Station for Confronting Duck Curve', in *2018 International Conference on Computational Techniques, Electronics and Mechanical Systems (CTEMS)*, 2018, pp. 36–39.
- [4] K. T. Møller, T. R. Jensen, E. Akiba, and H. Li, 'Hydrogen - A sustainable energy carrier', *Prog. Nat. Sci. Mater. Int.*, vol. 27, no. 1, pp. 34–40, Feb. 2017, doi: 10.1016/j.pnsc.2016.12.014.
- [5] 'HYDROGEN FROM RENEWABLE POWER TECHNOLOGY OUTLOOK FOR THE ENERGY TRANSITION', International Renewable Energy Agency, 2018.
- [6] P. P. Edwards, V. L. Kuznetsov, W. I. F. David, and N. P. Brandon, 'Hydrogen and fuel cells: Towards a sustainable energy future', *Energy Policy*, vol. 36, no. 12, pp. 4356–4362, Dec. 2008, doi: 10.1016/j.enpol.2008.09.036.
- [7] B. C. Ong, S. K. Kamarudin, and S. Basri, 'Direct liquid fuel cells: A review', *Int. J. Hydrog. Energy*, vol. 42, no. 15, pp. 10142–10157, Apr. 2017, doi: 10.1016/j.ijhydene.2017.01.117.
- [8] A. Afif, N. Radenahmad, Q. Cheok, S. Shams, J. H. Kim, and A. K. Azad, 'Ammonia-fed fuel cells: a comprehensive review', *Renew. Sustain. Energy Rev.*, vol. 60, pp. 822–835, Jul. 2016, doi: 10.1016/j.rser.2016.01.120.
- [9] F. Jiao and B. Xu, 'Electrochemical Ammonia Synthesis and Ammonia Fuel Cells', *Adv. Mater.*, p. 1805173, Dec. 2018, doi: 10.1002/adma.201805173.
- [10] B. Bensmann, R. Hanke-Rauschenbach, I. K. Peña Arias, and K. Sundmacher, 'Energetic evaluation of high pressure PEM electrolyzer systems for intermediate storage of renewable energies', *Electrochimica Acta*, vol. 110, pp. 570–580, Nov. 2013, doi: 10.1016/j.electacta.2013.05.102.
- [11] S. Metz, 'Linde pioneers hydrogen compression techniques for fuel cell electric vehicles', *Fuel Cells Bull.*, vol. 2014, no. 9, pp. 12–15, 2014.
- [12] H. Barthélémy, 'Hydrogen storage – Industrial perspectives', *Int. J. Hydrog. Energy*, vol. 37, no. 22, pp. 17364–17372, Nov. 2012, doi: 10.1016/j.ijhydene.2012.04.121.
- [13] S. Satyapal, J. Petrovic, C. Read, G. Thomas, and G. Ordaz, 'The U.S. Department of Energy's National Hydrogen Storage Project: Progress towards meeting hydrogen-powered vehicle requirements', *Catal. Today*, vol. 120, no. 3–4, pp. 246–256, Feb. 2007, doi: 10.1016/j.cattod.2006.09.022.
- [14] M. Bracha, G. Lorenz, A. Patzelt, and M. Wanner, 'Large-scale hydrogen liquefaction in Germany', *Int. J. Hydrog. Energy*, vol. 19, no. 1, pp. 53–59, 1994.
- [15] D. Beysens, D. Chatain, V. Nikolayev, and Y. Garrabos, 'MAGNETIC FACILITY GIVES HEAT TRANSFER DATA IN H₂ AT VARIOUS ACCELERATION LEVELS', in *Space Launcher Liquid Propulsion*, Belgium, 2002.
- [16] L. M. Das, 'On-board hydrogen storage systems for automotive application', *Int. J. Hydrog. Energy*, vol. 21, no. 9, pp. 789–800, 1996.
- [17] K. L. Cashdollar, I. A. Zlochower, G. M. Green, R. A. Thomas, and M. Hertzberg, 'Flammability of methane, propane, and hydrogen gases', *J. Loss Prev. Process Ind.*, vol. 13, no. 3–5, pp. 327–340, 2000.
- [18] G. E. Schmauch and A. H. Singleton, 'Technical aspects of ortho-parahydrogen conversion', *Ind. Eng. Chem.*, vol. 56, no. 5, pp. 20–31, 1964.
- [19] H. Frost, T. Düren, and R. Q. Snurr, 'Effects of surface area, free volume, and heat of adsorption on hydrogen uptake in metal-organic frameworks', *J. Phys. Chem. B*, vol. 110, no. 19, pp. 9565–9570, 2006.

- [20] H.-C. Zhou, J. R. Long, and O. M. Yaghi, 'Introduction to Metal–Organic Frameworks', *Chem. Rev.*, vol. 112, no. 2, pp. 673–674, 2012.
- [21] M. P. Suh, H. J. Park, T. K. Prasad, and D.-W. Lim, 'Hydrogen Storage in Metal–Organic Frameworks', *Chem. Rev.*, vol. 112, no. 2, pp. 782–835, Feb. 2012, doi: 10.1021/cr200274s.
- [22] J. Ren, H. W. Langmi, B. C. North, and M. Mathe, 'Review on processing of metal-organic framework (MOF) materials towards system integration for hydrogen storage: Review on processing of MOF materials towards system integration', *Int. J. Energy Res.*, vol. 39, no. 5, pp. 607–620, Apr. 2015, doi: 10.1002/er.3255.
- [23] G. J. Kubas, 'Metal–dihydrogen and σ -bond coordination: the consummate extension of the Dewar–Chatt–Duncanson model for metal–olefin π bonding', *J. Organomet. Chem.*, vol. 635, pp. 37–68, 2001.
- [24] N. Muradov and T. Veziroglu, 'From hydrocarbon to hydrogen? carbon to hydrogen economy', *Int. J. Hydrog. Energy*, vol. 30, no. 3, pp. 225–237, Mar. 2005, doi: 10.1016/j.ijhydene.2004.03.033.
- [25] K. E. Lamb, M. D. Dolan, and D. F. Kennedy, 'Ammonia for hydrogen storage; A review of catalytic ammonia decomposition and hydrogen separation and purification', *Int. J. Hydrog. Energy*, vol. 44, no. 7, pp. 3580–3593, Feb. 2019, doi: 10.1016/j.ijhydene.2018.12.024.
- [26] M. Niermann, S. Drünert, M. Kaltschmitt, and K. Bonhoff, 'Liquid organic hydrogen carriers (LOHCs) – techno-economic analysis of LOHCs in a defined process chain', *Energy Environ. Sci.*, vol. 12, no. 1, pp. 290–307, 2019, doi: 10.1039/C8EE02700E.
- [27] P. T. Aakko-Saksa, C. Cook, J. Kiviaho, and T. Repo, 'Liquid organic hydrogen carriers for transportation and storing of renewable energy – Review and discussion', *J. Power Sources*, vol. 396, pp. 803–823, Aug. 2018, doi: 10.1016/j.jpowsour.2018.04.011.
- [28] Q. Lai *et al.*, 'Hydrogen Storage Materials for Mobile and Stationary Applications: Current State of the Art', *ChemSusChem*, vol. 8, no. 17, pp. 2789–2825, Sep. 2015, doi: 10.1002/cssc.201500231.
- [29] B. Sakintuna, F. Lamaridarkrim, and M. Hirscher, 'Metal hydride materials for solid hydrogen storage: A review☆', *Int. J. Hydrog. Energy*, vol. 32, no. 9, pp. 1121–1140, Jun. 2007, doi: 10.1016/j.ijhydene.2006.11.022.
- [30] G. Sandrock, J. Reilly, J. Graetz, W.-M. Zhou, J. Johnson, and J. Wegrzyn, 'Accelerated thermal decomposition of AlH₃ for hydrogen-fueled vehicles', *Appl. Phys. A*, vol. 80, no. 4, pp. 687–690, Feb. 2005, doi: 10.1007/s00339-004-3105-0.
- [31] S. K. Konovalov and B. M. Bulychev, 'The P, T-State diagram and solid phase synthesis of aluminum hydride', *Inorg. Chem.*, vol. 34, no. 1, pp. 172–175, 1995.
- [32] B. Bogdanović and M. Schwickardi, 'Ti-doped alkali metal aluminium hydrides as potential novel reversible hydrogen storage materials', *J. Alloys Compd.*, vol. 253, pp. 1–9, 1997.
- [33] H. Y. Leng, T. Ichikawa, S. Hino, N. Hanada, S. Isobe, and H. Fujii, 'Synthesis and decomposition reactions of metal amides in metal–N–H hydrogen storage system', *J. Power Sources*, vol. 156, no. 2, pp. 166–170, Jun. 2006, doi: 10.1016/j.jpowsour.2005.03.228.
- [34] P. Chen, Z. Xiong, J. Luo, J. Lin, and K. L. Tan, 'Interaction of hydrogen with metal nitrides and imides', *Nature*, vol. 420, pp. 302–304, Nov. 2002.
- [35] T. Ichikawa, S. Isobe, N. Hanada, and H. Fujii, 'Lithium nitride for reversible hydrogen storage', *J. Alloys Compd.*, vol. 365, no. 1–2, pp. 271–276, Feb. 2004, doi: 10.1016/S0925-8388(03)00637-6.
- [36] H. Miyaoka *et al.*, 'Kinetic Modification on Hydrogen Desorption of Lithium Hydride and Magnesium Amide System', *Materials*, vol. 8, no. 7, pp. 3896–3909, Jun. 2015, doi: 10.3390/ma8073896.
- [37] U. B. Demirci, 'Ammonia borane, a material with exceptional properties for chemical hydrogen storage', *Int. J. Hydrog. Energy*, vol. 42, no. 15, pp. 9978–10013, Apr. 2017, doi: 10.1016/j.ijhydene.2017.01.154.

- [38] 'Low-Cost Precursors to Novel Hydrogen Storage Materials', The Dow Chemical Company, Dec. 2010.
- [39] A. D. Sutton *et al.*, 'Regeneration of Ammonia Borane Spent Fuel by Direct Reaction with Hydrazine and Liquid Ammonia', *Science*, vol. 331, no. 6023, pp. 1423–1426, Mar. 2011, doi: 10.1126/science.1197796.
- [40] O. T. Summerscales and J. C. Gordon, 'Regeneration of ammonia borane from spent fuel materials', *Dalton Trans.*, vol. 42, no. 28, p. 10075, 2013, doi: 10.1039/c3dt50475a.
- [41] C. Reller and F. O. R. L. Mertens, 'A Self-Contained Regeneration Scheme for Spent Ammonia Borane Based on the Catalytic Hydrodechlorination of BCl_3 ', *Angew. Chem. Int. Ed.*, vol. 51, no. 47, pp. 11731–11735, Nov. 2012, doi: 10.1002/anie.201201134.
- [42] S. Hausdorf, 'A procedure for the regeneration of ammonia borane from BNH-waste products', *Int. J. Hydrog. Energy*, vol. 33, no. 2, pp. 608–614, Jan. 2008, doi: 10.1016/j.ijhydene.2007.10.035.
- [43] F. Maurice, T. Dewing, and J. Dewing, 'Production of Boron compounds', 3103417.
- [44] C. Reller and F. O. R. L. Mertens, 'Hydrodechlorination of Et_3NBCl_3 Catalyzed by Amorphous Nickel Boride - A Mechanistic Approach', *Eur. J. Inorg. Chem.*, vol. 2014, no. 3, pp. 450–459, Jan. 2014, doi: 10.1002/ejic.201301253.
- [45] Y. Li *et al.*, 'Enhanced dehydrogenation of ammonia borane by reaction with alkaline earth metal chlorides', *Int. J. Hydrog. Energy*, vol. 37, no. 5, pp. 4274–4279, Mar. 2012, doi: 10.1016/j.ijhydene.2011.11.146.
- [46] Y. Nakagawa *et al.*, 'A Systematic Study of the Effects of Metal Chloride Additives on H_2 Desorption Properties of Ammonia Borane', *J. Chem. Eng. Data*, vol. 61, no. 5, pp. 1924–1929, May 2016, doi: 10.1021/acs.jced.6b00143.
- [47] F. Toche, R. Chiriac, U. B. Demirci, and P. Miele, 'Ammonia borane thermolytic decomposition in the presence of metal (II) chlorides', *Int. J. Hydrog. Energy*, vol. 37, no. 8, pp. 6749–6755, Apr. 2012, doi: 10.1016/j.ijhydene.2012.01.037.
- [48] K. Wang, Z. Pan, and X. Yu, 'Metal B-N-H hydrogen-storage compound: Development and perspectives', *J. Alloys Compd.*, vol. 794, pp. 303–324, Jul. 2019, doi: 10.1016/j.jallcom.2019.04.240.
- [49] Y. Nakamori *et al.*, 'Correlation between thermodynamical stabilities of metal borohydrides and cation electronegativities: First-principles calculations and experiments', *Phys. Rev. B*, vol. 74, no. 4, Jul. 2006, doi: 10.1103/PhysRevB.74.045126.
- [50] L. H. Jepsen *et al.*, 'Boron–nitrogen based hydrides and reactive composites for hydrogen storage', *Mater. Today*, vol. 17, no. 3, pp. 129–135, Apr. 2014, doi: 10.1016/j.mattod.2014.02.015.
- [51] T. Jaroń, P. A. Orłowski, W. Wegner, K. J. Fijałkowski, P. J. Leszczyński, and W. Grochala, 'Hydrogen Storage Materials: Room-Temperature Wet-Chemistry Approach toward Mixed-Metal Borohydrides', *Angew. Chem.*, vol. 127, no. 4, pp. 1252–1255, Jan. 2015, doi: 10.1002/ange.201408456.
- [52] T. Jaroń, W. Wegner, K. J. Fijałkowski, P. J. Leszczyński, and W. Grochala, 'Facile Formation of Thermodynamically Unstable Novel Borohydride Materials by a Wet Chemistry Route', *Chem. - Eur. J.*, vol. 21, no. 15, pp. 5689–5692, Apr. 2015, doi: 10.1002/chem.201404968.
- [53] P. Martelli, R. Caputo, A. Remhof, P. Mauron, A. Borgschulte, and A. Züttel, 'Stability and Decomposition of NaBH_4 ', *J. Phys. Chem. C*, vol. 114, no. 15, pp. 7173–7177, Apr. 2010, doi: 10.1021/jp909341z.
- [54] J.-H. Kim, S.-A. Jin, J.-H. Shim, and Y. W. Cho, 'Thermal decomposition behavior of calcium borohydride $\text{Ca}(\text{BH}_4)_2$ ', *J. Alloys Compd.*, vol. 461, 2008.

- [55] Y. Zhang, E. Majzoub, V. Ozoliņš, and C. Wolverton, 'Theoretical Prediction of Metastable Intermediates in the Decomposition of $\text{Mg}(\text{BH}_4)_2$ ', *J. Phys. Chem. C*, vol. 116, no. 19, pp. 10522–10528, May 2012, doi: 10.1021/jp302303z.
- [56] G. Severa, E. Rönnebro, and C. M. Jensen, 'Direct hydrogenation of magnesium boride to magnesium borohydride: demonstration of >11 weight percent reversible hydrogen storage', *Chem Commun*, vol. 46, no. 3, pp. 421–423, 2010, doi: 10.1039/B921205A.
- [57] M. Chong, M. Matsuo, S. Orimo, T. Autrey, and C. M. Jensen, 'Selective Reversible Hydrogenation of $\text{Mg}(\text{B}_3\text{H}_8)_2/\text{MgH}_2$ to $\text{Mg}(\text{BH}_4)_2$: Pathway to Reversible Borane-Based Hydrogen Storage?', *Inorg. Chem.*, vol. 54, no. 8, pp. 4120–4125, Apr. 2015, doi: 10.1021/acs.inorgchem.5b00373.
- [58] M. Chong, T. Autrey, and C. Jensen, 'Lewis Base Complexes of Magnesium Borohydride: Enhanced Kinetics and Product Selectivity upon Hydrogen Release', *Inorganics*, vol. 5, no. 4, p. 89, Dec. 2017, doi: 10.3390/inorganics5040089.
- [59] C. Sugai *et al.*, 'Kinetic Enhancement of Direct Hydrogenation of MgB_2 to $\text{Mg}(\text{BH}_4)_2$ upon Mechanical Milling with THF, MgH_2 , and/or Mg', *ChemPhysChem*, vol. 20, no. 10, pp. 1301–1304, May 2019, doi: 10.1002/cphc.201801187.
- [60] E. A. Nickels *et al.*, 'Tuning the Decomposition Temperature in Complex Hydrides: Synthesis of a Mixed Alkali Metal Borohydride', *Angew. Chem. Int. Ed.*, vol. 47, no. 15, pp. 2817–2819, Mar. 2008, doi: 10.1002/anie.200704949.
- [61] D. Ravnsbaek *et al.*, 'A Series of Mixed-Metal Borohydrides', *Angew. Chem.*, vol. 121, no. 36, pp. 6787–6791, Aug. 2009, doi: 10.1002/ange.200903030.
- [62] R. Černý *et al.*, 'Trimetallic Borohydride $\text{Li}_3\text{MZn}_5(\text{BH}_4)_{15}$ (M = Mg, Mn) Containing Two Weakly Interconnected Frameworks', *Inorg. Chem.*, vol. 52, no. 17, pp. 9941–9947, Sep. 2013, doi: 10.1021/ic401139k.
- [63] T. He *et al.*, 'Alkali and alkaline-earth metal borohydride hydrazinates: synthesis, structures and dehydrogenation', *Phys. Chem. Chem. Phys.*, vol. 15, no. 25, p. 10487, 2013, doi: 10.1039/c3cp51473k.
- [64] J. Mao, Q. Gu, Z. Guo, and H. K. Liu, 'Sodium borohydride hydrazinates: synthesis, crystal structures, and thermal decomposition behavior', *J. Mater. Chem. A*, vol. 3, no. 21, pp. 11269–11276, 2015, doi: 10.1039/C5TA02276B.
- [65] H. Wu *et al.*, 'A new family of metal borohydride ammonia borane complexes: Synthesis, structures, and hydrogen storage properties', *J. Mater. Chem.*, vol. 20, no. 31, p. 6550, 2010, doi: 10.1039/c0jm01542c.
- [66] L. H. Jepsen *et al.*, 'Synthesis, Crystal Structure, Thermal Decomposition, and ^{11}B MAS NMR Characterization of $\text{Mg}(\text{BH}_4)_2(\text{NH}_3\text{BH}_3)_2$ ', *J. Phys. Chem. C*, vol. 118, no. 23, pp. 12141–12153, Jun. 2014, doi: 10.1021/jp502788j.
- [67] I. Dovgaliuk, C. S. Le Duff, K. Robeyns, M. Devillers, and Y. Filinchuk, 'Mild Dehydrogenation of Ammonia Borane Complexed with Aluminum Borohydride', *Chem. Mater.*, vol. 27, no. 3, pp. 768–777, Feb. 2015, doi: 10.1021/cm503601h.
- [68] S. R. Johnson *et al.*, 'The Monoammoniate of Lithium Borohydride, $\text{Li}(\text{NH}_3)\text{BH}_4$: An Effective Ammonia Storage Compound', *Chem. - Asian J.*, vol. 4, no. 6, pp. 849–854, Jun. 2009, doi: 10.1002/asia.200900051.
- [69] J. Huang *et al.*, 'Synthesis, structure and dehydrogenation of zirconium borohydride octaammoniate', *Chem Commun*, vol. 51, no. 14, pp. 2794–2797, 2015, doi: 10.1039/C4CC09317H.
- [70] R. Z. Sørensen *et al.*, 'Indirect, Reversible High-Density Hydrogen Storage in Compact Metal Ammine Salts', *J. Am. Chem. Soc.*, vol. 130, no. 27, pp. 8660–8668, Jul. 2008, doi: 10.1021/ja076762c.

- [71] E. Roedern and T. R. Jensen, 'Ammine-Stabilized Transition-Metal Borohydrides of Iron, Cobalt, and Chromium: Synthesis and Characterization', *Inorg. Chem.*, vol. 54, no. 21, pp. 10477–10482, Nov. 2015, doi: 10.1021/acs.inorgchem.5b01959.
- [72] Q. Gu *et al.*, 'Structure and decomposition of zinc borohydride ammonia adduct: towards a pure hydrogen release', *Energy Environ. Sci.*, vol. 5, no. 6, p. 7590, 2012, doi: 10.1039/c2ee02485c.
- [73] Y. Guo, Y. Jiang, G. Xia, and X. Yu, 'Ammine aluminium borohydrides: an appealing system releasing over 12 wt% pure H₂ under moderate temperature', *Chem. Commun.*, vol. 48, no. 37, p. 4408, 2012, doi: 10.1039/c2cc30751k.
- [74] Y. Guo, H. Wu, W. Zhou, and X. Yu, 'Dehydrogenation Tuning of Ammine Borohydrides Using Double-Metal Cations', *J. Am. Chem. Soc.*, vol. 133, no. 13, pp. 4690–4693, Apr. 2011, doi: 10.1021/ja1105893.
- [75] W. Sun *et al.*, 'A New Ammine Dual-Cation (Li, Mg) Borohydride: Synthesis, Structure, and Dehydrogenation Enhancement', *Chem. - Eur. J.*, vol. 18, no. 22, pp. 6825–6834, May 2012, doi: 10.1002/chem.201102651.
- [76] F. Yuan, Q. Gu, X. Chen, Y. Tan, Y. Guo, and X. Yu, 'Complex Ammine Titanium(III) Borohydrides as Advanced Solid Hydrogen-Storage Materials with Favorable Dehydrogenation Properties', *Chem. Mater.*, vol. 24, no. 17, pp. 3370–3379, Sep. 2012, doi: 10.1021/cm301387d.
- [77] J. Kollonitsch and O. Fuchs, 'Preparation of Aluminium Borohydride and its Applications in Organic Reductions', *Nature*, vol. 4492, Dec. 1955.
- [78] L. H. Jepsen, M. B. Ley, Y. Filinchuk, F. Besenbacher, and T. R. Jensen, 'Tailoring the Properties of Ammine Metal Borohydrides for Solid-State Hydrogen Storage', *ChemSusChem*, vol. 8, no. 8, pp. 1452–1463, Apr. 2015, doi: 10.1002/cssc.201500029.
- [79] G. Soloveichik *et al.*, 'Ammine Magnesium Borohydride Complex as a New Material for Hydrogen Storage: Structure and Properties of Mg(BH₄)₂·2NH₃', *Inorg. Chem.*, vol. 47, no. 10, pp. 4290–4298, May 2008, doi: 10.1021/ic7023633.
- [80] H. Chu, G. Wu, Z. Xiong, J. Guo, T. He, and P. Chen, 'Structure and Hydrogen Storage Properties of Calcium Borohydride Diammoniate', *Chem. Mater.*, vol. 22, no. 21, pp. 6021–6028, Nov. 2010, doi: 10.1021/cm1023234.
- [81] U. B. Demirci, O. Akdim, J. Andrieux, J. Hannauer, R. Chamoun, and P. Miele, 'Sodium Borohydride Hydrolysis as Hydrogen Generator: Issues, State of the Art and Applicability Upstream from a Fuel Cell', *Fuel Cells*, vol. 10, no. 3, pp. 335–350, Jun. 2010, doi: 10.1002/uce.200800171.
- [82] Y. Kojima and H. Tetsuya, 'Recycling process of sodium metaborate to sodium borohydride', *Int. J. Hydrog. Energy*, vol. 28, pp. 989 – 993, 2003.
- [83] H. Zhong *et al.*, 'An one-step approach towards hydrogen production and storage through regeneration of NaBH₄', *Energy Storage Mater.*, vol. 7, pp. 222–228, Apr. 2017, doi: 10.1016/j.ensm.2017.03.001.
- [84] H. I. Schlesinger, H. C. Brown, and A. E. Finholt, 'The Preparation of Sodium Borohydride by the High Temperature Reaction of Sodium Hydride with Borate Esters', *J. Am. Chem. Soc.*, vol. 75, no. 1, pp. 205–209, 1953.
- [85] H. I. Schlesinger, H. C. Brown, D. L. Mayfield, and J. R. Gilbreath, 'Procedures for the Preparation of Methyl Borate¹', *J. Am. Chem. Soc.*, vol. 75, no. 1, pp. 213–215, 1953.
- [86] C.-H. Liu, B.-H. Chen, D.-J. Lee, J.-R. Ku, and F. Tsau, 'Trimethyl Borate Regenerated from Spent Sodium Borohydride after Hydrogen Production', *Ind. Eng. Chem. Res.*, vol. 49, no. 20, pp. 9864–9869, Oct. 2010, doi: 10.1021/ie101309f.
- [87] G. Moussa, R. Moury, U. B. Demirci, and P. Miele, 'Borates in hydrolysis of ammonia borane', *Int. J. Hydrog. Energy*, vol. 38, no. 19, pp. 7888–7895, Jun. 2013, doi: 10.1016/j.ijhydene.2013.04.121.

- [88] W. C. Conner and J. L. Falconer, 'Spillover in Heterogeneous Catalysis', *Chem. Rev.*, vol. Chemical Reviews, no. 95, pp. 759–788, 1995.
- [89] L. Wang and R. T. Yang, 'New sorbents for hydrogen storage by hydrogen spillover – a review', *Energy Environ. Sci.*, vol. 1, no. 2, p. 268, 2008, doi: 10.1039/b807957a.
- [90] A. J. Du, S. C. Smith, X. D. Yao, and G. Q. Lu, 'Hydrogen Spillover Mechanism on a Pd-Doped Mg Surface as Revealed by ab initio Density Functional Calculation', *J. Am. Chem. Soc.*, vol. 129, no. 33, pp. 10201–10204, Aug. 2007, doi: 10.1021/ja0722776.
- [91] C. W. Gregory, R. S. J. Ronan, D. M. Jason, and W. S. Douglas, 'Reversible, Metal-Free Hydrogen Activation', *Science*, vol. 314, no. 5802, pp. 1124–1126, Nov. 2006, doi: 10.1126/science.1132898.
- [92] D. W. Stephan and G. Erker, 'Frustrated Lewis Pairs: Metal-free Hydrogen Activation and More', *Angew. Chem. Int. Ed.*, vol. 49, no. 1, pp. 46–76, Jan. 2010, doi: 10.1002/anie.200903708.
- [93] V. Sumerin *et al.*, 'Experimental and theoretical treatment of hydrogen splitting and storage in boron–nitrogen systems', *J. Organomet. Chem.*, vol. 694, no. 17, pp. 2654–2660, Aug. 2009, doi: 10.1016/j.jorganchem.2009.03.023.
- [94] D. W. Stephan and G. Erker, 'Frustrated Lewis Pair Chemistry: Development and Perspectives', *Angew. Chem. Int. Ed.*, vol. 54, no. 22, pp. 6400–6441, May 2015, doi: 10.1002/anie.201409800.
- [95] J. Lam, K. M. Szkop, E. Mosaferi, and D. W. Stephan, 'FLP catalysis: main group hydrogenations of organic unsaturated substrates', *Chem. Soc. Rev.*, vol. 48, no. 13, pp. 3592–3612, 2019, doi: 10.1039/C8CS00277K.
- [96] W. T. Klooster, T. F. Koetzle, P. E. M. Siegbahn, T. B. Richardson, and R. H. Crabtree, 'Study of the N–H···H–B Dihydrogen Bond Including the Crystal Structure of BH₃NH₃ by Neutron Diffraction', *J. Am. Chem. Soc.*, vol. 121, no. 27, pp. 6337–6343, Jul. 1999, doi: 10.1021/ja9825332.
- [97] P. K. Pranzas *et al.*, 'Characterization of Hydrogen Storage Materials and Systems with Photons and Neutrons', *Adv. Eng. Mater.*, vol. 13, no. 8, pp. 730–736, Aug. 2011, doi: 10.1002/adem.201000298.
- [98] A. Yadav, N. Bulakh, A. Gupta, N. Sikder, and A. K. Sikder, 'Rapid determination of impurity of boron nitride in amorphous boron powder using inductively coupled plasma-atomic emission spectrometry (ICP-AES) and ion chromatography (IC)', *Anal. Methods*, vol. 9, no. 21, pp. 3141–3150, 2017, doi: 10.1039/C7AY00140A.
- [99] A. C. Stowe, W. J. Shaw, J. C. Linehan, B. Schmid, and T. Autrey, 'In situ solid state 11B MAS-NMR studies of the thermal decomposition of ammonia borane: mechanistic studies of the hydrogen release pathways from a solid state hydrogen storage material', *Phys. Chem. Chem. Phys.*, vol. 9, no. 15, p. 1831, 2007, doi: 10.1039/b617781f.
- [100] C. Gervais and F. Babonneau, 'High resolution solid state NMR investigation of various boron nitride preceramic polymers', *J. Organomet. Chem.*, vol. 657, pp. 75–82, 2002.
- [101] C. F. Burmeister and A. Kwade, 'Process engineering with planetary ball mills', *Chem. Soc. Rev.*, vol. 42, no. 18, p. 7660, 2013, doi: 10.1039/c3cs35455e.
- [102] Y.-S. Kwon, K. B. Gerasimov, and S.-K. Yoon, 'Ball temperatures during mechanical alloying in planetary mills', *J. Alloys Compd.*, vol. 346, no. 1–2, pp. 276–281, 2002.
- [103] M. L. Huber and A. H. Harvey, *Thermal Conductivity of Gases*, vol. CRC Handbook of Chemistry and Physics, 92 vols. CRC-Press, Boca Raton, FL, 2011.
- [104] Z. Z. Fang, L. P. Ma, X. D. Kang, P. J. Wang, P. Wang, and H. M. Cheng, 'In situ formation and rapid decomposition of Ti(BH₄)₃ by mechanical milling LiBH₄ with TiF₃', *Appl. Phys. Lett.*, vol. 94, no. 4, p. 044104, Jan. 2009, doi: 10.1063/1.3076106.
- [105] T. Jaroń and W. Grochala, 'Y(BH₄)₃ — an old–new ternary hydrogen store akalearning from a multitude of failures', *Dalton Trans*, vol. 39, no. 1, pp. 160–166, 2010, doi: 10.1039/B910698G.
- [106] H. Grove *et al.*, 'Halide substitution in Ca(BH₄)₂', *RSC Adv*, vol. 4, no. 9, pp. 4736–4742, 2014, doi: 10.1039/C3RA46226A.

- [107] R. H. Heyn *et al.*, 'Structural and spectroscopic characterization of potassium fluoroborohydrides', *Phys. Chem. Chem. Phys.*, vol. 15, no. 27, p. 11226, 2013, doi: 10.1039/c3cp52070f.
- [108] M. Paskevicius *et al.*, 'Metal borohydrides and derivatives – synthesis, structure and properties', *Chem Soc Rev*, vol. 46, no. 5, pp. 1565–1634, 2017, doi: 10.1039/C6CS00705H.
- [109] H. Hagemann and R. Černý, 'Synthetic approaches to inorganic borohydrides', *Dalton Trans.*, vol. 39, no. 26, p. 6006, 2010, doi: 10.1039/b927002g.
- [110] 'Chemister.ru Database'. [Online]. Available: <http://chemister.ru/Database/search-en.php>.
- [111] G. L. Soloveichik, M. Andrus, Y. Gao, J.-C. Zhao, and S. Kniajanski, 'Magnesium borohydride as a hydrogen storage material: Synthesis of unsolvated $Mg(BH_4)_2$ ', *Int. J. Hydrog. Energy*, vol. 34, no. 5, pp. 2144–2152, Mar. 2009, doi: 10.1016/j.ijhydene.2008.12.053.
- [112] B. Richter, J. B. Grinderslev, K. T. Møller, M. Paskevicius, and T. R. Jensen, 'From Metal Hydrides to Metal Borohydrides', *Inorg. Chem.*, vol. 57, no. 17, pp. 10768–10780, Sep. 2018, doi: 10.1021/acs.inorgchem.8b01398.
- [113] P. Zanella, L. Crociani, N. Masciocchi, and G. Giunchi, 'Facile High-Yield Synthesis of Pure, Crystalline $Mg(BH_4)_2$ ', *Inorg. Chem.*, vol. 46, no. 22, pp. 9039–9041, Oct. 2007, doi: 10.1021/ic701436c.
- [114] N. A. Tumanov *et al.*, 'Challenges in the synthetic routes to $Mn(BH_4)_2$: insight into intermediate compounds', *Dalton Trans*, vol. 44, no. 14, pp. 6571–6580, 2015, doi: 10.1039/C4DT03807J.
- [115] M. B. Ley *et al.*, 'Novel solvates $M(BH_4)_3S(CH_3)_2$ and properties of halide-free $M(BH_4)_3$ ($M = Y$ or Gd)', *Dalton Trans*, vol. 43, no. 35, pp. 13333–13342, 2014, doi: 10.1039/C4DT01125B.
- [116] L. V. Titov, L. A. Gavrilova, E. R. Eremin, S. S. Mishchenchuk, and V. Y. Rosolovski, 'Tetrabutylammonium borohydride with aluminum borohydride', *Russ. Chem. Bull.*, vol. 20, no. 6, pp. 1266–1268, 1971.
- [117] Y. Yang, Y. Liu, Y. Li, M. Gao, and H. Pan, 'Synthesis and Thermal Decomposition Behaviors of Magnesium Borohydride Ammoniates with Controllable Composition as Hydrogen Storage Materials', *Chem. - Asian J.*, vol. 8, no. 2, pp. 476–481, Feb. 2013, doi: 10.1002/asia.201200970.
- [118] W. R. Parry, P. R. Girardot, and D. R. Schultz, 'The Preparation and Properties of Hexamminecobalt (III) Borohydride, Hexamminechromium(III) Borohydride and Ammonium Borohydride', *J. Am. Chem. Soc.*, vol. 80, no. 1, 1958.
- [119] G. F. Huff, F. Chapel, A. D. McElroy, C. Evans, and A. M. Roy, 'Electrochemical method for the preparation of metal borohydrides', 2855353, 1958.
- [120] W. C. Johnson and A. W. Meyer, 'The Properties of Solutions of Metals in Liquid Ammonia', *Chem. Rev.*, vol. 8, no. 2, pp. 273–301, 1931.
- [121] N. Chakrabarti and J. Jacobus, 'The chemical reduction of poly (tetrafluoroethylene)', *Macromolecules*, vol. 21, no. 10, pp. 3011–3014, 1988.
- [122] E. J. Kirschke and W. L. Jolly, 'The reversibility of the reaction of alkali metals with liquid ammonia', *Inorg. Chem.*, vol. 6, no. 5, pp. 855–862, 1967.
- [123] R. Juza, 'Amides of the alkali and the alkaline earth metals', *Angew. Chem. Int. Ed. Engl.*, vol. 3, no. 7, pp. 471–481, 1964.
- [124] J. J. Lagowski, 'Liquid Ammonia', *Synth. React. Inorg. Met.-Org. Nano-Met. Chem.*, vol. 37, no. 2, pp. 115–153, Mar. 2007, doi: 10.1080/15533170601187474.
- [125] F. Kraus, 'Fluorine chemistry meets liquid ammonia', *Bioinorg. React. Mech.*, vol. 8, no. 1–2, Jan. 2012, doi: 10.1515/irm-2012-0003.
- [126] R. W. Parry, D. H. Campbell, D. R. Schultz, P. R. Girardot, and C. R. Taylor, 'Chemistry of boron hydrides and related hydrides', Wright Air Development Center, U.S. Air Force, Project M966, 1952.
- [127] T. Richter and R. Niewa, 'Chemistry of Ammonothermal Synthesis', *Inorganics*, vol. 2, no. 1, pp. 29–78, Feb. 2014, doi: 10.3390/inorganics2010029.

- [128] J. A. Dean and N. A. Lange, Eds., *Lange's handbook of chemistry*, 15. ed. New York, NY: McGraw-Hill, 1999.
- [129] V. D. Makhaev, N. S. Kedrova, and N. N. Mal'tseva, 'The reaction of zinc chloride with borohydrides of the alkali metals in organic solvents', *Bull. Acad. Sci. USSR Div. Chem. Sci.*, vol. 23, no. 12, pp. 482–485, 1974.
- [130] H. Nöth, E. Wiberg, and L. P. Winter, 'Boranatozinkate der Alkalimetalle', *Z. Für Anorg. Allg. Chem.*, vol. 386, pp. 73–86, 1971.
- [131] G. Xia, Q. Gu, Y. Guo, and X. Yu, 'Ammine bimetallic (Na, Zn) borohydride for advanced chemical hydrogen storage', *J. Mater. Chem.*, vol. 22, no. 15, p. 7300, 2012, doi: 10.1039/c2jm16370e.
- [132] G. D. Barbaras, C. Dillard, A. E. Finholt, T. Wartik, K. E. Wilzbach, and H. I. Schlesinger, 'The Preparation of the Hydrides of Zinc, Cadmium, Beryllium, Magnesium and Lithium by the Use of Lithium Aluminum Hydride', *J. Am. Chem. Soc.*, vol. 73, no. 10, pp. 4585–4590, 1951.
- [133] H. Nöth, E. Wiberg, and L. P. Winter, 'Boranate und Boranato-metallate. I. Zur Kenntnis von Solvaten des Zinkboranats', *Z. Für Anorg. Allg. Chem.*, vol. 370, no. 5–6, pp. 209–223, 1969.
- [134] R. Černý *et al.*, 'Potassium Zinc Borohydrides Containing Triangular [Zn(BH₄)₃] – and Tetrahedral [Zn(BH)₄xCl_{4-x}]²⁻ Anions', *J. Phys. Chem. C*, vol. 116, no. 1, pp. 1563–1571, Jan. 2012, doi: 10.1021/jp209848r.
- [135] J. L. Limpo and A. Luis, 'Solubility of zinc chloride in ammoniacal ammonium chloride solutions', *Hydrometallurgy*, vol. 32, no. 2, pp. 247–260, 1993.
- [136] M. Mostajeran, D. J. Wolstenholme, C. Frazee, G. S. McGrady, and R. T. Baker, 'Solution-based routes to ammine metal borohydrides: formation of ammonia-borane', *Chem Commun*, vol. 52, no. 12, pp. 2581–2584, 2016, doi: 10.1039/C5CC10027E.
- [137] R. Černý, K. Chul Kim, N. Penin, V. D'Anna, H. Hagemann, and D. S. Sholl, 'AZn₂(BH₄)₅ (A = Li, Na) and NaZn(BH₄)₃: Structural Studies', *J. Phys. Chem. C*, vol. 114, no. 44, pp. 19127–19133, Nov. 2010, doi: 10.1021/jp105957r.
- [138] D. B. Ravnsbæk *et al.*, 'Structural studies of lithium zinc borohydride by neutron powder diffraction, Raman and NMR spectroscopy', *J. Alloys Compd.*, vol. 509, pp. S698–S704, Sep. 2011, doi: 10.1016/j.jallcom.2010.11.008.
- [139] N. J. Hess *et al.*, 'Spectroscopic studies of the phase transition in ammonia borane: Raman spectroscopy of single crystal NH₃BH₃ as a function of temperature from 88 to 330 K', *J. Chem. Phys.*, vol. 128, no. 3, p. 034508, Jan. 2008, doi: 10.1063/1.2820768.
- [140] R. Černý *et al.*, 'NaSc(BH₄)₄: A Novel Scandium-Based Borohydride', *J. Phys. Chem. C*, vol. 114, no. 2, pp. 1357–1364, Jan. 2010, doi: 10.1021/jp908397w.
- [141] S. F. Parker, 'Spectroscopy and bonding in ternary metal hydride complexes—Potential hydrogen storage media', *Coord. Chem. Rev.*, vol. 254, no. 3–4, pp. 215–234, Feb. 2010, doi: 10.1016/j.ccr.2009.06.016.
- [142] Y. Yang, Y. Liu, H. Wu, W. Zhou, M. Gao, and H. Pan, 'An ammonia-stabilized mixed-cation borohydride: synthesis, structure and thermal decomposition behavior', *Phys Chem Chem Phys*, vol. 16, no. 1, pp. 135–143, 2014, doi: 10.1039/C3CP54099E.
- [143] W. G. Schneider, H. J. Bernstein, and J. A. Pople, 'Proton Magnetic Resonance Chemical Shift of Free (Gaseous) and Associated (Liquid) Hydride Molecules', *J. Chem. Phys.*, vol. 28, no. 4, pp. 601–607, Apr. 1958, doi: 10.1063/1.1744199.
- [144] L. H. Jepsen *et al.*, 'Trends in Syntheses, Structures, and Properties for Three Series of Ammine Rare-Earth Metal Borohydrides, M(BH₄)₃ · n NH₃ (M = Y, Gd, and Dy)', *Inorg. Chem.*, vol. 54, no. 15, pp. 7402–7414, Aug. 2015, doi: 10.1021/acs.inorgchem.5b00951.
- [145] Y. Song, F. Wu, X. Zheng, X. Ma, F. Fang, and Y. Guo, 'Stepwise combination of NH₃ with BH₄⁻ in metal borohydride ammoniate', *Chem Commun*, vol. 51, no. 6, pp. 1104–1107, 2015, doi: 10.1039/C4CC08228A.

- [146] E. Welchman and T. Thonhauser, 'Decomposition mechanisms in metal borohydrides and their ammoniates', *J Mater Chem A*, vol. 5, no. 8, pp. 4084–4092, 2017, doi: 10.1039/C6TA09423F.
- [147] Z. Tang *et al.*, 'Metal cation-promoted hydrogen generation in activated aluminium borohydride ammoniates', *Acta Mater.*, vol. 61, no. 13, pp. 4787–4796, Aug. 2013, doi: 10.1016/j.actamat.2013.05.003.
- [148] M. H. Brooker and Max. A. Bredig, 'Significance of both polarizability and polarizing power of cations in nitrate vibrational spectra', *J. Chem. Phys.*, vol. 58, no. 12, pp. 5319–5321, Jun. 1973, doi: 10.1063/1.1679146.
- [149] K. Li and D. Xue, 'Estimation of Electronegativity Values of Elements in Different Valence States', *J. Phys. Chem. A*, vol. 110, no. 39, pp. 11332–11337, Oct. 2006, doi: 10.1021/jp062886k.
- [150] X. Chen, W. Zou, R. Li, G. Xia, and X. Yu, 'Decomposition Mechanism of Zinc Ammine Borohydride: A First-Principles Calculation', *J. Phys. Chem. C*, Feb. 2018, doi: 10.1021/acs.jpcc.8b00455.
- [151] X. Chen *et al.*, 'First-principles study of decomposition mechanisms of $\text{Mg}(\text{BH}_4)_2 \cdot 2\text{NH}_3$ and $\text{LiMg}(\text{BH}_4)_3 \cdot 2\text{NH}_3$ ', *RSC Adv.*, vol. 7, no. 49, pp. 31027–31032, 2017, doi: 10.1039/C7RA05322C.
- [152] X. Chen *et al.*, 'Improved dehydrogenation properties of the combined $\text{Mg}(\text{BH}_4)_2 \cdot 6\text{NH}_3 - \text{nNH}_3\text{BH}_3$ system', *Int. J. Hydrog. Energy*, vol. 38, no. 36, pp. 16199–16207, Dec. 2013, doi: 10.1016/j.ijhydene.2013.09.123.
- [153] Q. Wang, Y. Guan, W. Gao, J. Guo, and P. Chen, 'Thermodynamic Properties of Ammonia Production from Hydrogenation of Alkali and Alkaline Earth Metal Amides', *ChemPhysChem*, vol. 20, no. 10, pp. 1376–1381, May 2019, doi: 10.1002/cphc.201801090.
- [154] H. Yamamoto, H. Miyaoka, S. Hino, H. Nakanishi, T. Ichikawa, and Y. Kojima, 'Recyclable hydrogen storage system composed of ammonia and alkali metal hydride', *Int. J. Hydrog. Energy*, vol. 34, no. 24, pp. 9760–9764, Dec. 2009, doi: 10.1016/j.ijhydene.2009.10.034.
- [155] P. Schouwink *et al.*, 'Structure and properties of complex hydride perovskite materials', *Nat. Commun.*, vol. 5, p. 5706, Dec. 2014, doi: 10.1038/ncomms6706.
- [156] P. Schouwink, F. Morelle, Y. Sadikin, Y. Filinchuk, and R. Černý, 'Increasing Hydrogen Density with the Cation-Anion Pair $\text{BH}_4^- - \text{NH}_4^+$ in Perovskite-Type $\text{NH}_4\text{Ca}(\text{BH}_4)_3$ ', *Energies*, vol. 8, no. 8, pp. 8286–8299, Aug. 2015, doi: 10.3390/en8088286.
- [157] C. Ziparo, D. Colognesi, A. Giannasi, and M. Zoppi, 'Raman Spectra of Ammonia Borane: Low Frequency Lattice Modes', *J. Phys. Chem. A*, vol. 116, no. 35, pp. 8827–8832, Sep. 2012, doi: 10.1021/jp303968p.
- [158] W. J. Shaw *et al.*, 'In Situ Multinuclear NMR Spectroscopic Studies of the Thermal Decomposition of Ammonia Borane in Solution', *Angew. Chem. Int. Ed.*, vol. 47, no. 39, pp. 7493–7496, Sep. 2008, doi: 10.1002/anie.200802100.
- [159] T. P. Onak and I. Shapiro, 'B¹¹ Nuclear Magnetic Resonance Spectrum of the "Diammoniate of Diborane"', *J. Chem. Phys.*, vol. 32, no. 3, pp. 952–952, Mar. 1960, doi: 10.1063/1.1730834.
- [160] I. Dovgaliuk *et al.*, 'Solid Aluminum Borohydrides for Prospective Hydrogen Storage', *ChemSusChem*, vol. 10, no. 23, pp. 4725–4734, Dec. 2017, doi: 10.1002/cssc.201701629.
- [161] A. Starobrat, T. Jaroń, and W. Grochala, 'New hydrogen-rich ammonium metal borohydrides, $\text{NH}_4[\text{M}(\text{BH}_4)_4]$, M = Y, Sc, Al, as potential H₂ sources', *Dalton Trans.*, 2018, doi: 10.1039/C7DT03926C.
- [162] T. He *et al.*, 'Nanosized Co- and Ni-catalyzed ammonia borane for hydrogen storage', *Chem. Mater.*, vol. 21, no. 11, pp. 2315–2318, 2009.
- [163] R. Chiriac, F. Toche, U. B. Demirci, O. Krol, and P. Miele, 'Ammonia borane decomposition in the presence of cobalt halides', *Int. J. Hydrog. Energy*, vol. 36, no. 20, pp. 12955–12964, Oct. 2011, doi: 10.1016/j.ijhydene.2011.07.040.

- [164] W. H. Stockmayer, D. W. Rice, and C. C. Stephenson, 'Thermodynamic properties of sodium borohydride and aqueous borohydride ion', *J. Am. Chem. Soc.*, vol. 77, no. 7, pp. 1980–1983, 1955.
- [165] Y. Tan *et al.*, 'A liquid-based eutectic system: $\text{LiBH}_4\text{-NH}_3\text{-nNH}_3\text{BH}_3$ with high dehydrogenation capacity at moderate temperature', *J. Mater. Chem.*, vol. 21, no. 38, p. 14509, 2011, doi: 10.1039/c1jm11158b.
- [166] J. Huang, Y. Tan, Q. Gu, L. Ouyang, X. Yu, and M. Zhu, 'Ammonia borane modified zirconium borohydride octaammoniate with enhanced dehydrogenation properties', *J. Mater. Chem. A*, vol. 3, no. 10, pp. 5299–5304, 2015.
- [167] Y. Tan *et al.*, 'A synergistic strategy established by the combination of two H-enriched B–N based hydrides towards superior dehydrogenation', *J. Mater. Chem. A*, vol. 1, no. 35, pp. 10155–10165, 2013.
- [168] X. Chen, F. Yuan, Q. Gu, and X. Yu, 'Synthesis, structures and hydrogen storage properties of two new H-enriched compounds: $\text{Mg}(\text{BH}_4)_2(\text{NH}_3\text{BH}_3)_2$ and $\text{Mg}(\text{BH}_4)_2(\text{NH}_3)_2(\text{NH}_3\text{BH}_3)$ ', *Dalton Trans.*, vol. 42, no. 40, pp. 14365–14368, 2013.
- [169] R.-Q. Zhong *et al.*, 'Improved Hydrogen Release from Ammonia–Borane with ZIF-8', *Inorg. Chem.*, vol. 51, no. 5, pp. 2728–2730, Mar. 2012, doi: 10.1021/ic202562b.
- [170] T. Kobayashi, S. Gupta, M. A. Caporini, V. K. Pecharsky, and M. Pruski, 'Mechanism of Solid-State Thermolysis of Ammonia Borane: A ^{15}N NMR Study Using Fast Magic-Angle Spinning and Dynamic Nuclear Polarization', *J. Phys. Chem. C*, vol. 118, no. 34, pp. 19548–19555, Aug. 2014, doi: 10.1021/jp504328x.
- [171] K. Shimoda, Y. Zhang, T. Ichikawa, H. Miyaoka, and Y. Kojima, 'Solid state NMR study on the thermal decomposition pathway of sodium amidoborane NaNH_2BH_3 ', *J. Mater. Chem.*, vol. 21, no. 8, pp. 2609–2615, 2011.
- [172] D. Y. Kim, N. J. Singh, H. M. Lee, and K. S. Kim, 'Hydrogen-Release Mechanisms in Lithium Amidoboranes', *Chem. - Eur. J.*, vol. 15, no. 22, pp. 5598–5604, May 2009, doi: 10.1002/chem.200900092.
- [173] Y. S. Chua *et al.*, 'Synthesis, structure and dehydrogenation of magnesium amidoborane monoammoniate', *Chem. Commun.*, vol. 46, no. 31, p. 5752, 2010, doi: 10.1039/c0cc01260b.
- [174] H. Wu *et al.*, 'Sodium magnesium amidoborane: the first mixed-metal amidoborane', *Chem. Commun.*, vol. 47, no. 14, pp. 4102–4104, 2011.
- [175] M. F. Hawthorne, S. S. Jalisatgi, A. V. Safronov, H. B. Lee, and J. Wu, 'Chemical hydrogen storage using polyhedral borane anions and aluminum-ammonia-borane complexes', University of Missouri, Columbia, MO, 2010.
- [176] V. Pons *et al.*, 'Coordination of aminoborane, NH_2BH_2 , dictates selectivity and extent of H_2 release in metal-catalysed ammonia borane dehydrogenation', *Chem Commun*, no. 48, pp. 6597–6599, 2008, doi: 10.1039/B809190K.
- [177] G. Xia, Y. Tan, X. Chen, Z. Guo, H. Liu, and X. Yu, 'Mixed-metal (Li, Al) amidoborane: synthesis and enhanced hydrogen storage properties', *J. Mater. Chem. A*, vol. 1, no. 5, pp. 1810–1820, 2013.
- [178] O. Friedrichs, A. Remhof, A. Borgschulte, F. Buchter, S. I. Orimo, and A. Züttel, 'Breaking the passivation—the road to a solvent free borohydride synthesis', *Phys. Chem. Chem. Phys.*, vol. 12, no. 36, p. 10919, 2010, doi: 10.1039/c0cp00022a.
- [179] X. Kang, H. Wu, J. Luo, W. Zhou, and P. Wang, 'A simple and efficient approach to synthesize amidoborane ammoniates: case study for $\text{Mg}(\text{NH}_2\text{BH}_3)_2(\text{NH}_3)_3$ with unusual coordination structure', *J. Mater. Chem.*, vol. 22, no. 26, pp. 13174–13179, 2012.
- [180] Y. Yang, Y. Liu, Y. Li, M. Gao, and H. Pan, 'Heating Rate-Dependent Dehydrogenation in the Thermal Decomposition Process of $\text{Mg}(\text{BH}_4)_2\cdot 6\text{NH}_3$ ', *J. Phys. Chem. C*, vol. 117, no. 32, pp. 16326–16335, Aug. 2013, doi: 10.1021/jp404424m.

- [181] Y. S. Chua, G. Wu, Z. Xiong, T. He, and P. Chen, 'Calcium Amidoborane Ammoniate—Synthesis, Structure, and Hydrogen Storage Properties', *Chem. Mater.*, vol. 21, no. 20, pp. 4899–4904, Oct. 2009, doi: 10.1021/cm9020222.
- [182] V. A. Yartys *et al.*, 'Magnesium based materials for hydrogen based energy storage: Past, present and future', *Int. J. Hydrog. Energy*, vol. 44, no. 15, pp. 7809–7859, Mar. 2019, doi: 10.1016/j.ijhydene.2018.12.212.
- [183] C. L. Young, Ed., *Hydrogen and deuterium*, 1st ed. Oxford ; New York: Pergamon Press, 1981.
- [184] M. Wang *et al.*, 'Synthesis and hydrolysis of $\text{NaZn}(\text{BH}_4)_3$ and its ammoniates', *J. Mater. Chem. A*, vol. 5, no. 32, pp. 17012–17020, 2017, doi: 10.1039/C7TA05082H.
- [185] H.-C. Eom, H. Park, and H.-S. Yoon, 'Preparation of anhydrous magnesium chloride from ammonium magnesium chloride hexahydrate', *Adv. Powder Technol.*, vol. 21, no. 2, pp. 125–130, Mar. 2010, doi: 10.1016/j.apt.2010.01.003.
- [186] J. J. Zuckerman, *Inorganic Reactions and Methods, The Formation of Bonds to Halogens*, vol. 4. John Wiley & Sons, 2009.
- [187] A. Yadav, N. Bulakh, A. Gupta, N. Sikder, and A. K. Sikder, 'Rapid determination of impurity of boron nitride in amorphous boron powder using inductively coupled plasma-atomic emission spectrometry (ICP-AES) and ion chromatography (IC)', *Anal. Methods*, vol. 9, no. 21, pp. 3141–3150, 2017.
- [188] H. Matusiewicz, 'High-pressure microwave dissolution of ceramics prior to trace metal determinations by microwave induced plasma atomic emission spectrometry', *Microchim. Acta*, vol. 111, no. 1–3, pp. 71–82, 1993.
- [189] G. E. Spriggs, '13.5 Properties of diamond and cubic boron nitride', in *Powder Metallurgy Data. Refractory, Hard and Intermetallic Materials*, Springer, 2002, pp. 118–139.
- [190] S. Mann, D. Geilenber, J. A. BROEKAERT, and M. Jansen, 'Digestion methods for advanced ceramic materials and subsequent determination of silicon and boron by inductively coupled plasma atomic emission spectrometry', *J. Anal. At. Spectrom.*, vol. 12, no. 9, pp. 975–979, 1997.
- [191] 'Certificate of analysis Boron nitride'. BAM.
- [192] F. Bougie, D. Pokras, and X. Fan, 'Novel non-aqueous MEA solutions for CO₂ capture', *Int. J. Greenh. Gas Control*, vol. 86, pp. 34–42, Jul. 2019, doi: 10.1016/j.ijggc.2019.04.013.
- [193] L. H. Dreger, V. V. Dadape, and J. L. Margrave, 'Sublimation and decomposition studies on boron nitride and aluminum nitride', *J. Phys. Chem.*, vol. 66, no. 8, pp. 1556–1559, 1962.
- [194] G. K. Friestad and B. P. Branchaud, 'Ammonium Tetrafluoroborate', in *Encyclopedia of Reagents for Organic Synthesis*, American Cancer Society, 2001.
- [195] R. J. Gillespie, 'Covalent and ionic molecules: Why are BeF_2 and AlF_3 high melting point solids whereas BF_3 and SiF_4 are gases?', *J. Chem. Educ.*, vol. 75, no. 7, p. 923, 1998.
- [196] V. I. Mikheeva and E. M. Fedneva, 'Reaction between the ether complex of boron trifluoride and lithium hydride Communication 1. Preparation of pure diborane', *Russ. Chem. Bull.*, vol. 5, no. 8, pp. 925–934, 1956.
- [197] L. H. Rude *et al.*, 'Hydrogen–fluorine exchange in $\text{NaBH}_4\text{--NaBF}_4$ ', *Phys. Chem. Chem. Phys.*, vol. 15, no. 41, p. 18185, 2013, doi: 10.1039/c3cp52815d.